TESIS DE LA UNIVERSIDAD DE ZARAGOZA

2019

106

Cristian Lavieja Belanche

New techniques for the aesthetic and functional marking on polymers using laser technology

Departamento

Instituto Universitario de Ciencia de Materiales de Aragón (ICMA)

Director/es

Peña Latorre, jose Ignacio

Oriol Langa, Luis

ISSN 2254-7606

Prensas de la Universidad Universidad Zaragoza

ISSN 2254-7606

Universidad Zaragoza
1542

Tesis Doctoral

NEW TECHNIQUES FOR THE AESTHETIC AND FUNCTIONAL MARKING ON POLYMERS USING LASER TECHNOLOGY

Autor

Cristian Lavieja Belanche

Director/es

Peña Latorre, jose Ignacio
Oriol Langa, Luis

UNIVERSIDAD DE ZARAGOZA

Instituto Universitario de Ciencia de Materiales de Aragón (ICMA)

2018

New techniques for the aesthetic and functional marking on polymers using laser technology

by
Cristian Lavieja Belanche

Advisors
Dr. José Ignacio Peña Torre
Dr. Luis Oriol Langa

University of Zaragoza
ICMA - Instituto de Ciencia de Materiales de Aragón

A mis padres, por siempre estar ahí

A mis abuelos, por enseñarme a vivir

A mi novia, por su indispensable apoyo

Al atletismo, por enseñarme constancia y humildad

"Walking in a straight line one cannot get very far"

"Caminando en línea recta uno no puede llegar muy lejos"

The Little Prince (El Principito)

Agradecimientos

Resulta difícil resumir casi cinco años de trabajo en los que he compartido experiencias con tanta gente. Durante este tiempo he vivido a mitad camino entre el departamento de materiales del antiguo CPS (ahora EINA) y BSH montañana. De ambos lugares atesoro muy buenas y enriquecedoras experiencias así como el placer de haber trabajado junto a grandísimas personas.

En primer lugar agradecer la inestimable labor de mis dos directores de tesis, José Ignacio y Luis. Juntos hemos compartido innumerables horas de trabajo, ideas y revisiones del trabajo, y sin ellos esta tesis sería impensable. Gracias por vuestra inagotable paciencia y buen humor. Si esta tesis es hoy científica es por vuestra labor, gracias por haber hecho esto posible. Tampoco puedo dejar de acordarme de la labor de la doctora Mariajo Clemente, mi gran apoyo durante toda la tesis y pieza fundamental en este trabajo. Sin ella todavía estaría luchando contra el misterioso mundo de los polímeros y la caracterización química.

En segundo lugar agradecer a todos los compañeros y amigos con los que he compartido la sala de colaboradores y tantas comidas en la biblioteca del departamento, Carlos, María, Hernán, Gabriel, Irene, Guillermo, Sergio, Víctor y en especial a los que me han tenido que aguantar durante la etapa de redacción de la tesis, Álvaro, Lorena, José Antonio y Javi. Vuestro apoyo, ánimos y quejas compartidas han sido fundamentales para mantenerme con buen ánimo durante este periodo final. Cada una de nuestras comidas, charlas matutinas, vespertinas o nocturnas siempre ha despertado en mí inquietudes y "ansias" de conocimiento. También agradecer a todo el personal del departamento, técnicos, secretaría y profesorado.

Por supuesto agradecer a todos mis compañeros en BSH a lo largo de estos años. A Andrés por su grandísima profesionalidad, consejos y amistad, y por supuesto por su ayuda con la preparación de muestras. A los dos hermanos Gimeno, Carlos y Manuel, con ellos he compartido la experiencia completa de BSH, desde becarios hasta "cajas rojas", su humor y compañerismo son inigualables. No me puedo olvidar de Alberto, uno de los mejores profesionales y personas dentro y fuera del trabajo que he tenido la suerte de conocer y aprender de él. De mi "becaria" Sandra, tu buen ánimo y entusiasmo vital hacía que cualquier tedioso experimento pasara volando. A Toni, con el que por desgracia tuve menos tiempo del que desearía para compartir laboratorio y hobbies, por ayudarme en cualquier momento sin pedir nunca nada a cambio mientras fantaseábamos con nuestras frikadas. A Marcos Torres, por todas las horas que pasamos arreglando los láseres y la cabina de luz hasta dar lugar a un nuevo proyecto aprendiendo tanto por el camino. A Esther, parte fundamental para mí del paisaje de la oficina y apoyo en los momentos más difíciles tanto personales como profesionales. A Mariajo y Alejandro, dos de las personas más positivas y que menos se rinden ante la adversidad que he conocido, y sobre todo capaces de transmitirlo a los que les rodean. No podrían faltar Bea y Lucía, inseparables y de esas personas que sabes que jamás te dejan de lado. También a Carlos Concheso, un currante y un grandísimo profesional, capaz de arreglar un láser como de llenar dos folios de fórmulas, cada charla contigo es siempre un reto intelectual. Y por supuesto a tantos con los que he tenido la suerte de compartir oficina, laboratorio y tiempo libre, Marcos, David, Andrea, Eduardo, Erika, María, Sergios (Alonso, Nocito, Frauca, García, y estoy seguro que me dejo alguno), Amaya, Oscar, Fernando, Javier, Daniel, Lander, Guillermo, Lorena, Alfredo, Sandra, Sara, Irene, Isabel, Laura, Miguel y muchos otros que seguro que me olvido. A los exBSH por el CPS, Marta, Clara y Eloy con charlas siempre liberadoras. A mis antiguos compañeros del laboratorio de hornos Quique, Lourdes, Carlos y Joaquín.

No me puedo olvidar de mis compañeros de fatigas en atletismo. Sin ellos no sería ni la mitad de persona que soy. Fuera del trabajo ellos me han sostenido en los momentos de flaqueza y me han ayudado a olvidar cada día las dificultades de la tesis. A Roberto, mi hermano pequeño, no sabes cuánto valoro tu compañía. A Jacobo, apoyo moral y físico con sus consejos y sus manos milagrosas. Al otro ranger Saúl, a las pequeñas y ya no tan pequeñas Mar, Raquel, Marta, Pilar, Esther, Fiona, Irene, a Saúl y el "pequeño" Sebas, al señor Domingo y como no a nuestros entrenadores Ángel y Raúl.

Agradecer a BSH por ofrecerme la oportunidad de iniciar la tesis en un campo tan aplicado a la industria como son los láseres, y en especial a Fran Ester y a Andrés Escartín.

Como no agradecer a mi familia todo su apoyo, a lo largo de la tesis y de mi vida entera. A mis padres, pilar fundamental en toda mi formación y estudios, siempre animándome a que aspirara a lo máximo y ayudándome más allá de lo humanamente posible. Mi padre, capaz de transmitirme su amor por la música, la lectura y la historia. Mi madre, por su capacidad infatigable y su amor al prójimo. A mis abuelos, ellos formaron parte de mi niñez y me dieron todo lo que uno puede desear. Sobre todo mi abuelo Argimiro, si alguien encendió en mí la llama de la ciencia y las matemáticas especialmente fue él, el me enseñó a leer y a sumar, además de a intentar vivir lo más dignamente posible, que más se puede decir. A mi novia Carolina, no hay palabras para describir tu apoyo incondicional y ayuda constante con cualquier detalle, esta tesis es medio tuya. También por supuesto a mis amigos de toda la vida por estar siempre ahí y aguantar mi chapa con la tesis.

Por último agradecer al científico y divulgador Carl Sagan el que yo hoy aspire a ser doctor en Física. Aunque él ahora no lo pueda saber, tantos le debemos la pasión por la ciencia y por las estrellas.

Publicaciones y patentes

Durante el desarrollo de esta tesis se han publicado los siguientes artículos científicos:

- C. Lavieja, M. J. Clemente, L. Oriol, and J. I. Peña, "Influence of the Wavelength on Laser Marking on ABS Filled with Carbon Black," *Polym. - Plast. Technol. Eng.*, 2017.

- M. J. Clemente, C. Lavieja, J. I. Peña, and L. Oriol, "UV-laser marking of a TiO2 containing ABS material," *Polym. Eng. Sci.*, 2017.

Y las siguientes patentes:

- **Publication Number: ES 2533218 (B1)** – Componente para un aparato doméstico, y procedimiento para fabricar un componente para un aparato doméstico

- **Publication Number: ES 2603785 (B1)** – Método para fabricar un componente de aparato doméstico que comprende un elemento base.

Resumen

El uso de la tecnología láser está ampliamente extendido en sectores tan diferentes como el aeroespacial, la automoción, la industria maderera o la electrónica de precisión. Sus aplicaciones cubren un rango muy diverso de materiales, desde la soldadura o el corte de metales, al tratamiento superficial de plásticos o el curado de pinturas y tintas. Los procesos mediante radiación láser presentan ventajas tales como una alta coherencia y una elevada monocromaticidad. La alta densidad de energía y direccionalidad alcanzada con el láser permiten focalizar el tratamiento sobre el material con una resolución espacial mejor que 100 μm. Así mismo, se trata de una tecnología sin contacto por lo que permite evitar vibraciones además de que mediante el control numérico remoto se obtiene una gran flexibilidad durante el procesado. Sin embargo, presenta algunas desventajas a tener en cuenta, como el alto coste del equipo y el posible daño no deseado en el material.

Tradicionalmente, la decoración estética de los polímeros, en concreto de aquellos usados en la gama blanca de los electrodomésticos, se ha realizado empleado técnicas como la tampografía o la estampación. Estas técnicas presentan ventajas tales como la posibilidad de usar múltiples colores o la durabilidad de la impresión. Sin embargo, adolecen de flexibilidad tanto en el proceso de impresión, donde cambiar de diseño conlleva cambiar el patrón de impresión, como en el proceso productivo, ya que es necesario un tiempo de curado de la tinta. Ambos inconvenientes dificultan notablemente la integración total del proceso de decoración en la línea de montaje.

Así pues, en esta tesis se propone el estudio del marcado láser como alternativa a las técnicas tradicionales de decoración estética. En particular, se aborda un caso específico como es la decoración de las piezas plásticas estéticas de los electrodomésticos fabricados por la compañía BSH electrodomésticos. Estos

componentes se fabrican principalmente empleando el termoplástico ABS (Acrilonitrilo-Butadieno-Estireno).

Así pues, se propone como primer objetivo de esta tesis:

- **Estudiar el tratamiento laser del ABS produciendo marcas estéticas de alta calidad. Durante este estudio se realizará la caracterización física y química de las marcas con el objetivo de optimizar el proceso de marcado.**

Del mismo modo, empleando las posibilidades que ofrece el láser como herramienta en el procesado de materiales, se plantea el siguiente objetivo:

- **Producir marcas funcionales de tal modo que se afecte a la mojabilidad del material tratando de conseguir comportamientos superhidrófobos y superhidrófilos. El control de esta propiedad es interesante para futuras aplicaciones como serían por ejemplo la limpieza de superficies o favorecer la actividad biocida. Mediante la alteración controlada de la topografía superficial del material a partir de micro-estructuración láser se busca conseguir estas propiedades.**

Finalmente y como parte de un estudio preliminar, se amplía el marcado estético láser con el objetivo de conseguir marcas más allá de la escala de grises, tratando de obtener una gama amplia de colores. Para ello se emplearán tres técnicas diferentes: aditivos químicos especialmente preparados para interaccionar con el láser produciendo cambio de color, procesos interferométricos de dos haces láser y reestructuración láser de superficies que presenten resonancias plasmónicas centradas en el espectro óptico visible.

Index

1. Introduction 1

1.1. Polymeric materials 6

1.1.1. Polymer additives 9

1.1.2. Processing of polymers 10

1.1.3. Polymer in home appliances 13

1.1.3.1. Acrylonitrile-Butadiene-Styrene (ABS) 13

1.1.3.2. Polypropylene (PP) 16

1.1.3.3. Polystyrene (PS) 17

1.2. Laser technology 19

1.2.1. The laser idea 19

1.2.2. Solid state laser – Nd:YAG 23

1.2.3. Frequency conversion 26

1.2.4. Laser optics and guiding systems 27

1.2.4.1. Gaussian optics 27

1.2.4.2. Optical components of an industrial laser 29

1.2.4.3. Laser parameters 33

1.2.5. Laser interaction with matter 36

1.2.5.1. General laser interaction mechanism 37

1.2.5.2. Laser interaction with polymers 38

2. Experimental techniques 47

2.1. Lasers for material processing and polymers 47

2.1.1. Laser systems 47

2.1.1.1. PowerLine E25 laser from Rofin 49

2.1.1.2. Trumark 6230 laser from Trumpf 51

2.1.1.3. PowerLine E20 THG laser from Rofin 53

2.1.1.4. Brilliant laser from Quantel....55
2.1.1.5. FDSS 532-150 from Crystal Laser Systems....56
2.1.2. Polymeric materials....57
2.1.2.1. White ABS....57
2.1.2.2. Black ABS....58
2.1.2.3. Other polymers....60
2.2. Characterization techniques....61
2.2.1. Spectroscopic techniques....61
2.2.1.1. Colourimetry....61
2.2.1.2. UV-Vis-NIR spectroscopy....65
2.2.1.3. IR (ATR-FTIR) spectroscopy....65
2.2.1.4. XPS....66
2.2.2. Microscopic techniques....67
2.2.2.1. Stereoscopic microscope....67
2.2.2.2. Confocal microscopy....67
2.2.2.3. Environmental Scanning Electron Microscopy (ESEM)....68
2.2.3. Thermal analysis....69
2.2.3.1. Thermogravimetry (TGA)....69
2.2.3.2. Inductively coupled plasma optical emission spectrometry (ICP-OES)....70
2.2.4. Contact angle goniometer....70
3. Aesthetic laser marking on ABS....75
3.1. Polymer additives on laser marking....78
3.2. White ABS laser marking....82
3.2.1. Preliminary material characterisation....83
3.2.2. Colour changes by laser marking....87
3.2.3. Topographical changes on laser marks....98
3.2.3.1. Surface topography....98
3.2.3.2. Penetration depth of the laser changes....105

3.2.4. Chemical changes on laser marks 107
3.2.4.1. ATR-FTIR analysis 107
3.2.4.2. XPS analysis 113
3.2.5. Conclusions 122
3.3. Black ABS laser marking 124
3.3.1. Preliminary material characterisation 125
3.3.2. Colour changes by laser marking 127
3.3.3. Topographical changes on laser marks 136
3.3.3.1. Surface topography 136
3.3.3.2. Penetration depth of the laser changes 140
3.3.4. Chemical changes on laser marks 141
3.3.4.1. ATR-FTIR analysis 142
3.3.5. Influence of a commercial additive for laser marking processes 144
3.3.6. Conclusions 149
4. Control of the wettability of an ABS surface by laser micro-structuring 157
4.1. Laser treatment to control the wettability 162
4.2. Laser ablation of ABS 165
4.2.1. Laser ablation: formation of holes 166
4.2.2. Laser ablation: formation of lines 171
4.2.3. Conclusions 174
4.3. Control of the wettability by direct laser ablation patterning 176
4.3.1. Topography of the patterned laser surface 178
4.3.2. Theoretical modelling of the contact angle 183
4.3.3. Influence of the topography in the wettability 187
4.3.4. Conclusions 194
4.4. Wettability modification by laser roughness control 195
4.4.1. Topography of the affected laser surface 196
4.4.2. Influence of the topography in the wettability 201

4.4.3. Conclusions 207
4.5. Wettability modification by direct laser interferometry patterning 208
4.5.1. Topography of the patterned laser surface 210
4.5.2. Theoretical modelling of the contact angle 214
4.5.3. Influence of the topography on the wettability 216
4.5.4. Conclusions 217
5. Colour laser marking 227
5.1. Colour marking based on additives 230
5.1.1. Marking of injection moulded plastic samples containing laser additives 231
5.1.2. Laser marking of samples processed by in-mould labelling (IML) 234
5.1.3. Example of application of a real design 236
5.1.4. Conclusions 238
5.2. Colour marking based on laser reshaping of plasmonic structures 239
5.2.1. Fabrication of the plasmonic crystal and laser reshaping 240
5.2.2. Example of application 245
5.2.3. Conclusions 246
5.3. Colour marking based on iridescence colours produced by DLIP 247
5.3.1. Iridescent colours related to the microscopic structure 249
5.3.2. Example of application 253
5.3.3. Conclusions 254
6. General conclusions 261
7. Conclusiones generales 265

1. Introduction

"Laser... inter eximia naturae dona numeratum plurimis compositionibus inseritur."

"The laser is numbered among the most miraculous gifts of nature and lends itself to a variety of applications" [1.1]

Laser, or Laserpitium, in the classical antiquity, was an essence extract from a plant considered as a god gift for many diseases like snake poison, pleurisy or epidemic infection. Even it was used as an exquisite dressing to the best cuisine. It was cultivated in the Cyrenaica, in modern Libya, and it was one of the essential, valuable resources of the area and basis of their prosperity. A rare anecdote told that several thousand of Roman soldiers crossed the Cyrenaica desert conducted by Cato the Younger during the Roman civil wars only chewing laserpitium. Unfortunately, in the late antiquity, the plant disappeared from the sources, and it is believed that it was extinct during the 2nd century A.D. Figure 1.1 presents an ancient coin from the North Africa area (1st century B.C.) with the plant image and a Laconian black-figure kylix showing the extraction process of the Laser essence.

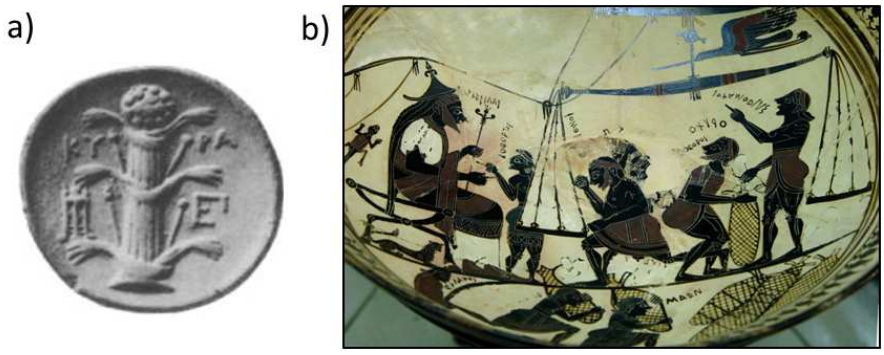

Figure 1.1. a) Cyrenaica coin showing a Laserpitium [1.2]; b) Arcesilao King of Cyrenaica supervising the Laser essence extraction from the plant [1.3].

Today, the modern idea of what is a laser is entirely different; however, this word still recalls to a critical feature used in a wide range of applications. The laser has been one of the important leading technologies developed during the 20^{th} century. The laser is associated with a powerful and monochromatic light source, able to interact with matter producing important phenomena in a controlled way. So, the laser is considered as a flexible tool whose applications are in such different fields as Material Science, Medicine, Geography or Telecommunications.

One interesting field of applications, in particular for industrial purposes, is the interaction with matter to produce permanent marks on materials. This type of processing has been historically used to identify the origin of the pieces on no visible parts. However, to make aesthetical decorations of pieces has always been a challenge because of the high quality required.

So far, this type of decoration has been made using traditional techniques like pad printing or hot stamping. The main disadvantage of these processes is the lack of flexibility: the different designs have to be previously prepared on a stamp. In addition, these techniques involve the use of inks, resulting in curing times that affect the production cycle in addition to sustainability issues and the need for a consumable material.

So, this thesis proposes to study the laser marking as a valid alternative to traditional techniques of aesthetical decoration. In particular, the focus is on a specific case: the decoration of polymeric parts that form the aesthetical components of household appliances as the fabricated by the company BSH Home Appliances. One of the most used materials to produce these parts is the thermoplastic ABS (Acrylonitrile-Butadiene-Styrene). Figure 1.2 displays an example of a BSH home appliance with ABS components decorated by a standard technique, as pad printing.

Figure 1.2. Standard pad printing decoration of a polymeric ABS frontal part in a washing machine from BSH. The zoom shows some of the decorated areas.

The principal advantage of the laser technology is the evolution from traditional decoration to digital printing techniques. Thus, the designs can be stored in a computer as digital data in such way that the laser will reproduce the models with high precision, allowing a great flexibility and customisation [1.4]. Also, the laser marking is a non-contact technique where there are no consumables needs. It will enable the decoration process to be fully integrated into the assembly line, thus improving the cycle time of the manufacturing process.

So, the first objective of this thesis can be summarised as:

- **To study the laser treatment of ABS to produce high-quality aesthetical marks. This study includes the physical and chemical characterisation of the marks in an attempt to optimise the laser marking process.**

Furthermore, using the possibility that offers the laser as a powerful tool in material processing, the following objective is also defined:

- **To produce functional marks that affect the material wettability in an attempt to obtain superhydrophobic and superhydrophilic behaviours. The control of wettability is attractive for future applications in the field of surface cleaning or biocidal activity. These functional properties can be induced by altering the surface topography by laser micro-structuring processes.**

Laser marks of these objectives are on the grey scale. Finally, as part of a very preliminary study, the possibility to expand the aesthetical marking to produce not only marks in the grey scale but also in a range of colours, using laser additives, laser interferometry or plasmonic colours will also be analysed.

According to these general objectives, this thesis can be structured as follows:

- Firstly, some basic concepts of polymeric materials are introduced in addition to their manufacturing processes. Additionally, laser technology is presented, mainly focused on the Nd:YAG laser, the type of laser used in this study. Also, the laser interaction with polymeric materials is briefly explored.

- Hereafter, the experimental techniques are presented. They are divided into two parts. Firstly, the processing techniques, the laser equipment and the polymeric materials used in this thesis; and secondly, the characterisation techniques used to define and understand the material changes produced by laser irradiation.

- Then, the aesthetical laser marking on ABS is studied. After a brief presentation of state of the art, the experimental results achieved on white and black ABS will be discussed.

- The different techniques to surface micro-structuring by the laser are subsequently discussed and how influence on the wettability. Similarly to the previous chapter, the background information is briefly commented before showing the experimental results.

- As a last experimental chapter, the possibility of colour laser marking is preliminarily explored.

- Finally, general conclusions are presented.

1.1. Polymeric materials

The use of naturally occurring polymers, derived from plants and animals, has been widely extended for many centuries, e.g. wood, rubber, cotton, wool, leather and silk. Also, other natural polymers such as proteins, enzymes, starches and cellulose are important in biological and physiological processes in plants and animals [1.5]. Bakelite (a thermosetting resin based on phenol-formaldehyde) is considered the first entirely synthetic polymer, introduced by L. H. Baekeland in 1909 [1.6]. Along the 20^{th} century, especially from the World War II, the discovery of new synthetic polymers revolutionised the field of Material Science. These synthetic materials can be produced quickly and cheaply, presenting even better characteristics than their natural counterparts, so they have replaced metal and woods parts in many applications [1.5].

From a chemical point of view, polymers are materials made of molecules of high molecular weight that are usually called macromolecules. These macromolecules derived from monomers or low molecular weight molecules that are covalently linked one to each other to form long chains having a high number of repeating units (derived from the monomers). Usually, these long chains are based on carbon-carbon single bonds. Also, carbon-oxygen and carbon-nitrogen single bonds, carbon-carbon double bonds, phenylene rings, and even silicon-oxygen single bonds can be found in different polymers [1.7]. The chemical structure of the macromolecules and the interaction between them will define the material properties. If the macromolecules can move freely relative to its neighbours, it is consider being not crosslinked. On the opposite, if the macromolecules are linked among them, they are crosslinked, usually by covalent bonds [1.8].

So, like metals and ceramics, the properties of polymers are closely related to their structures and bonds. The molecular analysis allows understanding the macroscopic behaviour related to their mechanical or thermal properties. Furthermore, the final characteristics of materials based on polymers can be modified through the use of fillers, reinforcing agents and chemical additives. Thus, it is possible to find polymeric materials in many engineering applications, such as mechanical components under stress, low-friction, heat- and chemical- resistant components, electrical parts, housing applications and many others [1.6].

From an industrial point of view, also related to the molecular structure, a division of polymeric materials into three general classes can be done: Thermoplastics, Thermosets and Elastomers. The thermoplastics are materials that solidify as they are cooled from a molten state, no longer allowing the long molecules to move freely. However, if they are heated again, they regain the ability to flow due to the molecules can slide past each other [1.9]. By contrast, thermosets are those that solidify via a chemical curing process that causes cross-linking among the macromolecules, resulting in a network of macromolecules that cannot slide past each other. Finally, the elastomers are flexible macromolecules slightly crosslinked and allowing a high deformation of the materials. However, crosslinks hinder macromolecules from sliding past each other, making even large deformations reversible. Because at room temperature crosslinked elastomers are significantly above their glass transition temperature, they are very soft and elastic solids [1.8].

The principal interest in this thesis is related to the **laser marking on Acrylonitrile-Butadiene-Styrene (ABS)**. ABS is a thermoplastic copolymer, and their properties as material are due to its macromolecular structure but also to the polymer additives and the processing techniques. A copolymer is a macromolecule composed of two or more monomeric repeating units in the same chain. There are

different types of copolymers depending on how the different monomers are arranged in the polymer chain: random, alternating, block or graft copolymers are the most common types. A scheme of their monomer arrangement can be seen in figure 1.3.

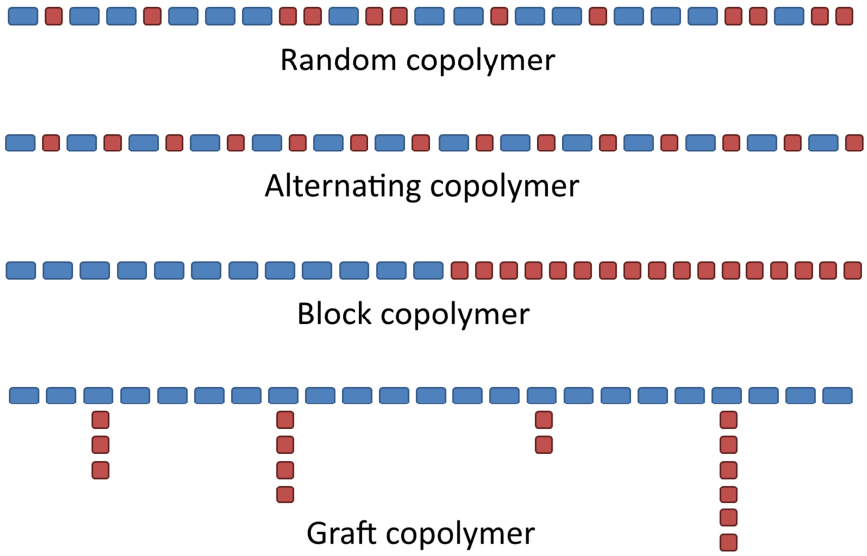

Figure 1.3. Schematic representation of different copolymers. The colour blocks represent each monomer.

A thermoplastic polymer is defined a polymeric material that becomes mouldable above a specific temperature and solidifies upon cooling, using various polymer processing techniques. The temperature above a mouldable state is reached, is the glass transition temperature, T_g, in the case of amorphous polymers or melting transition, T_m, in the case of semicrystalline polymers. A polymer is considered amorphous if, after the solidification, their molecules solidify in a random arrangement, or as a semicrystalline polymer, which presents alignment between neighbour molecules forming regions with a three-dimensional order.

The T_g divides two behaviour states of an amorphous thermoplastic material. So, under the T_g, the material behaves like a viscoelastic solid, while above the T_g it can be more easily deformed. To easily flow the material, a higher temperature should be

reached, the softening temperature (T_s), at which it behaves like a viscoelastic fluid. The typical temperature range where T_s is found in an amorphous thermoplastic is about 50 degrees above the T_g [1.8].

In the case of semi-crystalline thermoplastics, some crystalline structures are formed during the solidification like lamellar crystals. The degree of crystallinity in a typical thermoplastic will vary from grade to grade. The physical properties are dependent on the crystallinity degree, for example, the density and strength are increased as the crystallinity grows. Two temperature transitions can be found in a semicrystalline polymer, the glass transition temperature (T_g), and the melting temperature (T_m) where the material will flow completely [1.8].

1.1.1. Polymer additives

Polymer additives are mixed with a polymer to enhance or change their physical properties making them more suitable for each application. For example, there are additives to decrease Tg of the polymeric materials improving their flexibility and processability (plasticisers) or additives to prevent the growth of the microorganism (antimicrobial). Also, other additives are used to reinforce the physical properties of the material (fillers) or to enhance the electrical conductivity reducing the formation of electrical charge on the surface (antistatic agents) [1.10]. Below, some of them are briefly reviewed.

- Colourants are additives introduced in the polymers to alter their original colour, generally for aesthetical purposes. They are introduced by a dispersion process into the polymer at a fluid state [1.11]. As they change the optical appearance of the material, they play a crucial role in their optical absorption properties. They are either organic colourants or inorganic (pigments). The ABS is usually coloured using

pigments, for example, the most common whitener is the TiO_2 while the darkener is the Carbon Black (CB).

- The polymers may suffer degradation by sunlight. UV light absorption can induce photochemical reactions like crosslinking or degradation. The absorption depends on the chemical structure of the material and the incident light wavelength. The high energetic UV photons cause a significant deterioration, so there are additives designed to absorb the UV photons. UV absorbers dissipate UV radiation by a nondestructive process for the polymer. For example, ABS can be mixed with benzotriazoles that absorb the UV light preventing the formation of free radicals [1.10], which can degrade the polymer causing the ageing effect of yellowing.

- Flame retardants: The polymers are flammable materials due to their organic composition. The flammability of polymer can be determined by the parameter limiting oxygen index (LOI). This value defines the minimum volume percent of oxygen concentration, mixed with nitrogen, needed to support combustion of the polymer under standardised conditions. So, some chemical compounds can be used to reduce the possibility of either starting combustion within a polymer component or, once ignited, reduce the rate of flame spread. Usually, the compounds added contain halogens such as bromine, chlorine or phosphorous [1.8].

1.1.2. Processing of polymers

As well as the polymer molecular properties are essential for their final application, the manufacturing process to obtain the final object plays an important role in the physical properties of the final material. There are different methods to process polymeric materials; two of them are briefly explained hereafter, extrusion

and injection moulding. Others possible processes are coating, calendaring, foaming or compression moulding.

By polymer extrusion, it is possible to manufacture a high volume of molten polymeric material to be adapted to a continuous profile. It is used to produce items like pipe, deck railing, plastic films, coatings, and so on. The mechanism of extrusion works by the thermal and mechanical melting of the polymer. The material is thrown into the barrel of the extruder. Gradually, the material is melted by the effect of the heaters while the polymer and additives are mechanically mixed and homogenised. These effects are produced by a worm screw and band heaters distributed along a barrel. Then, the polymer material is forced to flow into a die, which will provide the final shape to the material once solidified. Figure 1.4 illustrates the essential components of a single screw plastic extruder.

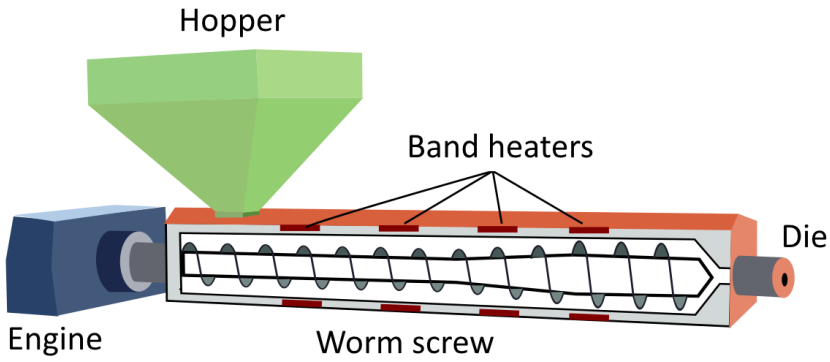

Figure 1.4. Schematic of a single screw extruder [1.12].

By injection moulding, it is possible to manufacture designed parts by injecting the material into a mould. The polymer is fed into a heated barrel, mixed, and forced into a mould cavity. Then the polymer is cooled and solidified to take shape according to the configuration of the cavity. The moulds are made of metal, usually steel or aluminium. This process is used to manufacture a wide variety of parts, from

small to big components, e.g. of the automotive or aeronautic industry. This technique is highly versatile in the preparation of objects made from polymeric materials.

The first steps of the injection process are quite similar to the extrusion. The material is thrown into a barrel with a screw, where it is melted by heat and pressure injecting the polymeric material into the mould cavity. The material begins to cool inside the moulds due to the temperature difference. Once the cavity is filled, a holding pressure is maintained to compensate for material shrinkage. Then the screw retracts to be prepared for the next shot. Once the part is sufficiently cooled, the mould opens, and the polymeric component is ejected by a mechanism used to avoid its adherence. [1.8]. A scheme of an injection machine is presented in figure 1.5.

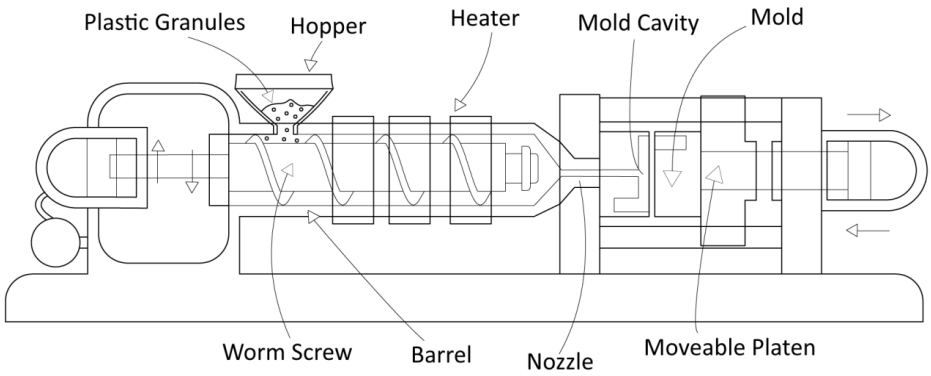

Figure 1.5. Scheme of an injection machine [1.13].

There are several variations of the conventional injection moulding processes, for instance, the in-mould labelling technology (IML), which was used in the processing of some materials studied in this thesis. This technique consists of the use of compatible polymeric thin labels during the process of injection in such way that the final product will be covered entirely or partially with the label. This technique is usually utilised to label objects directly, but it can also be used to have a polymer in bulk covered by a thin film of other compatible material providing new

characteristics, e.g. laser additives for colour marking. By this way, the sensitive and expensive pigments are concentrated in a small region instead of being dispersed throughout the whole plastic object. The film covers only some interesting areas of the polymer surface carrying the desired additives. The layer films have a width of less than 100 µm. Both polymeric materials should be compatible to assure an optimum adhesion.

1.1.3. Polymers in home appliances

The use of polymeric materials has gradually replaced metals in home appliances because of their excellent properties combined with the versatile design possibilities offered by polymeric materials. For example, all the small appliances like irons, hair dryers or coffee makers are mainly made by PP. Also, the major devices have parts of PP, generally those intended to internal components, while their aesthetical elements, which are visible to the user, are made of ABS. This material is considered a better-looking plastic with higher mechanical properties.

Considering the purpose of this thesis, focus on the aesthetical decoration of home appliances, the ABS is further explained. Also, some samples made in PP and PS were used during the colour marking study, so these materials are also described.

1.1.3.1. Acrylonitrile-Butadiene-Styrene (ABS)

Acrylonitrile-Butadiene-Styrene (ABS) is an amorphous thermoplastic copolymer with high impact resistance and toughness developed in the early years of the 1950s. It is formed by a copolymerization process based on a free-radical-initiated chain polymerization. Three monomers are responsible for the chemical structure of ABS:

acrylonitrile, butadiene and styrene. Acrylonitrile contributes to chemical resistance, heat resistance and high strength; butadiene contributes to improve toughness, impact strength and low-temperature property retention; styrene adds rigidity, surface appearance (gloss) and processability [1.6]. A scheme of the monomeric repeating units forming ABS is shown in figure 1.6.

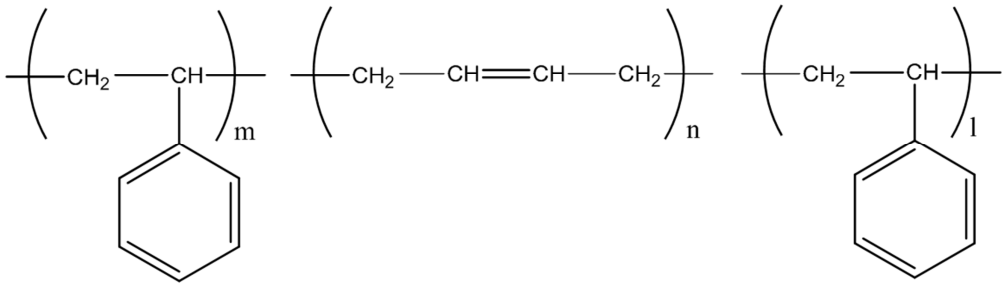

Figure 1.6. Monomeric repeating units of ABS.

Two different ways produce the ABS; by blends of styrene-acrylonitrile copolymers with butadiene-acrylonitrile rubber or by interpolymers of polybutadiene with styrene and acrylonitrile. Various types of ABS can be obtained changing not only the ratios of the monomers, but the way in which they are assembled into the final polymer can also be the subject of considerable variations [1.6].

The characteristics of the ABS are superior to other thermoplastics, commonly is described as tough, hard and rigid. Also, after the moulding process, it exhibits an excellent surface appearance. The chemical resistance is adequate for ordinary applications; it is slightly affected by water, weak acids or inorganic salts, although alcohols and hydrocarbons may affect the surface. The resistance to the UV light is inadequate, significant changes in appearance and mechanical properties can occur by UV irradiation [1.6]. The glass transition temperature is found approximately at 105°C [1.14].

ABS is used in a wide range of applications, like camera housings, telephone handsets, electrical hand tools, gears, refrigerator liners, pipe and fitting or sporting

goods. It is a critical material in the automotive sector, e.g. for the production of various components as doors handle, door trim, instrument panels, consoles, and so on. The ABS without colour pigments has a yellowing colouration. Using additives like TiO_2 or Carbon Black, it is possible to obtain white or black colour respectively.

ABS polymer is widely used in major home appliances defined as dishwashers or washing machines, in particular, in their aesthetical parts. These parts are described as the user-visible component of each device. The primary interest in this thesis is in the upper part element, the frontal panel that carries the visible decoration. This decoration usually is due to symbols that indicate the different working tasks or setups of the device; and on the other hand, brand logos or model types that help to identify the machine, see figure 1.7.

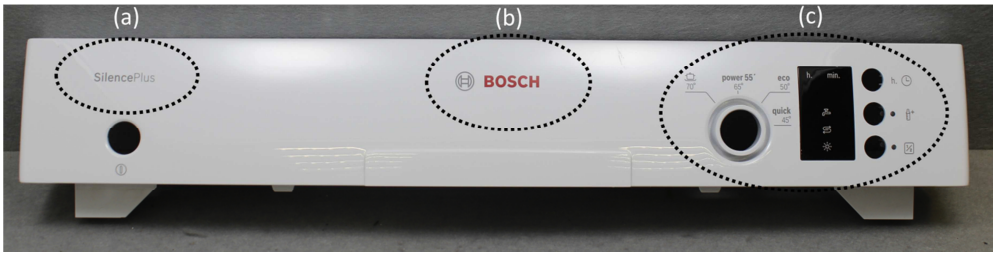

Figure 1.7. A frontal panel of a dishwasher mainly made of ABS (the black window is made of PMMA) showing the different decoration that carries: a) Model type; b) Brand logo; c) Working task options.

Usually, the decoration is done by traditional techniques, mainly by pad printing. This method, also called tampography, allows transferring an image to a substrate using a pad filled with ink. Each design is needed to be firstly prepared on a cliché enabling the pad to move the decoration to the polymer. This technique is considered as analogical because it is not possible to transfer directly digital designs to the samples; firstly they have to be prepared for the clichés, slowing down the process. Also, the use of inks has some disadvantages: they are consumable materials that generate a chemical waste and, moreover, they need some time to cure, around one or

two days depending on its composition. All this processing is not possible to be integrated into the assembly line mainly because of the curing times. This fact generates an extra problem of storage of the decorated panels. Also, the production has to be carefully planned before the assembling of the appliance to assure the stock of each model.

1.1.3.2. Polypropylene (PP)

Polypropylene (PP) is a semicrystalline thermoplastic polymer (isotactic polypropylene is the conventional PP) widely extended to a massive number of applications. This polyolefine was first produced in the last 1950s by Hercules in the United States, by Montecatini in Italy and by Farbenwerke Hoechst AG in Germany [1.8]. The commercial process of manufacturing the PP has been slurry polymerization in liquid hydrocarbons diluents, e.g. hexane or heptane. These are carried out either in stirred batches or continuous reactors [1.6]. The polymerisation temperatures usually are in the range of 45-80°C with pressures sufficient to maintain propylene in the liquid phase. A scheme of the basic monomer of the PP is shown in figure 1.8.

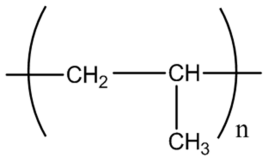

Figure 1.8. Monomeric repeating unit of PP.

Propylene can be polymerised to give not only homopolymers but also different copolymers with other monomers. PP presents low density and high melting point, so it is used for many applications, e.g. packing, furniture, bags, bottles, handles for

pots and pans, kitchenware, or even for medical equipment due it is resistant to many chemical solvents and bacterial growth.

PP is translucent to visible light (semicrystalline polymer). Additives are needed to improve the thermal and UV-light stability of PP. Also, additives to give some colouration to the material to PP materials as the same pigments previously cited for the ABS, e.g. TiO_2 and CB.

Considering the home appliances field, the PP is used both in major and small devices, e.g. washing machines, dishwashers, coffee makers, hairdryers, vacuum cleaners, floor and ceiling fans and so on. Usually, it can be found in their structural pieces, although new formulations and manufacturing processes are gradually increasing their characteristics allowing a future use in their aesthetical parts.

The PP current techniques of decoration are similar to the ABS, generally by pad printing.

1.1.3.3. Polystyrene (PS)

Polystyrene (PS) is a thermoplastic polymer made of bulk or suspension polymerisation of styrene. This polymer (atactic PS is the conventional polystyrene) is widely used due to its low cost. As main characteristics can be described its rigidity, transparency, high refractive index, no taste, smell or toxicity, excellent electrical insulation characteristics, low water absorption and ease of colouring and processing. By contrast, the material present high brittleness, that has led to the development of rubber-modified polystyrene [1.6]. The basic monomeric repeating unit forming the PS is shown in figure 1.9.

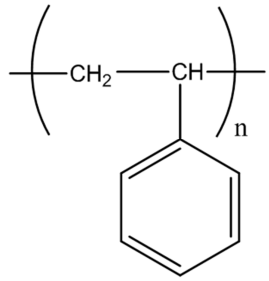

Figure 1.9. Monomeric repeating unit of PS.

In addition to its rigid shape, the PS is used in numerous products in the form of polymeric foams, which is a mixture of approximately 5 % polystyrene and 95 % air. It can be found this material in such diverse areas as packaging, toys, recreational products, housewares, electronic appliances, low-cost insulators, furniture, and building insulation uses.

The use of PS in the home appliances field is reduced. It can be mainly found in the form of extended foam as a heat insulating in the fridges. However, its excellent compatibility with the ABS allows labelling this polymer using IML technique with a thin transparent layer of PS able to carry laser additives.

1.2. Laser Technology

The word laser has been widely extended in the popular culture since its first appearance in the James Bond film "Goldfinger" (1964) where the 007 (Sean Connery) was close to being split in half by a terrible ray able to cut through metal. The laser technology had been developed a few years early. The film was a tremendous success, and the image of that ray able to produce such effects was deeply introduced in the mind of the viewers. Just a few years later, in 1967, two researchers, Arthur Sullivan of the Services Electronics Research Laboratories in Harlow and Peter Houldcroft of the Welding Institute in Abington, were able to cut through steel one-tenth of an inch in thickness using the beam from a carbon dioxide laser [1.15]. The fantasy idea showed in a film was taken into reality becoming the beginning of a new promising tool for high-quality material processing. Some years later, it was again popularised, also as a weapon tool, in the famous film "Star Wars" (1977), where the uses of the technology were diverse, from sophisticated swords to destruction rays able to destroy entire planets. Until now, we have not reached such level of destruction with a laser, but the development and applications have grown since then to be now one of the most promises and ubiquitous technology in such diverse fields as Medicine, Material Processing, Astronomy, Metrology or Spectroscopy.

1.2.1. The Laser idea

The origin of the word laser came from the acronym for Light Amplification by Stimulated Emission of Radiation [1.16]. The first working laser was developed by Theodore H. Mainman in 1960 [1.17] using a solid-state flashlamp-pumped synthetic

ruby crystal to produce laser light at 694 nm. During the 1960's, the first gas laser based on He-Ne was developed by the Iranian physicist Ali Javan, that was also the first laser able to emit a continuous wave (CW) radiation. During that decade, the diode [1.18] and the semiconductor [1.19] based laser were also developed. In addition, the techniques of modulation the output of lasers were developed like Q-switching [1.20], [1.21] and mode locking [1.22], [1.23] to obtain short pulses of high-energy, together to the fundamental phenomena of frequency conversion by harmonic generation [1.24]–[1.27]. In the 1970's, the first lasers able to operate at room temperature were manufactured [1.28], [1.29]. During the following years, an increased number of new lasers were developed trying to improve the power, the efficiency, the number of emission wavelengths and to decrease the pulse duration in the case of the non-continuous lasers, being increasingly specialised and optimised.

The idea of the laser is based on the concept of stimulated emission of energy in a medium. The light is generated by transitions between high and low states of energy in species (atoms, ions and molecules) in various media. Three main components are needed, a gain medium to generate the light, a pump source to induce the physical phenomena in the medium and an optical cavity to maintain and amplify the emission, see figure 1.10.

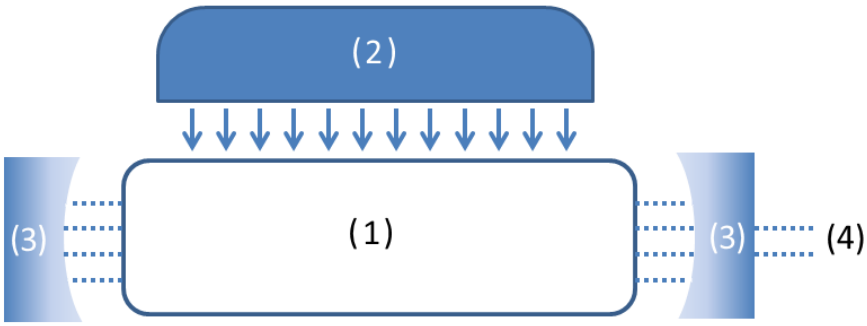

Figure 1.10. Essential components of a laser: 1) Gain Medium; 2) Pump source; 3) Optical cavity; 4) Output beam.

The main properties of the laser light that makes it so unique are a coherent and monochromatic beam of low divergence and high brightness [1.15]. Furthermore, it can be added short time duration on pulsed lasers.

- Monochromaticity: Due to the phenomena of stimulated emission, only an electromagnetic (e. m.) wave of determinant frequency (ν_0) can be amplified. Also, the energy oscillation is characterised by the cavity resonance features, resulting in a very narrow spectrum emitted light.

- Coherence: There are two different types of coherence, spatial and temporal. The spatial coherence can be defined as the distance where the e.m. wave keeps it phase correlation. In the same way, the temporal coherence can be defined changing the spatial distance for a temporal range. It is important to point out that the two concepts of temporal and spatial coherence are indeed independent one of each other.

- Low divergence: This property is a direct consequence of the fact that the active medium is placed in a resonant cavity. The laser beam presents a high directionality so only a wave propagating in a direction orthogonal to the mirrors can be sustained in the cavity.

- Brightness: The brightness is defined as the power emitted per unit of surface area per unit solid angle. A laser beam of even moderate power (e.g. a few mW) has a brightness that is several orders of magnitude higher than that of the brightest conventional sources. Thus, the focused intensity of a laser beam can reach high values, a feature which is exploited in many applications of lasers.

- Short time duration: By different pulsed techniques it is possible to produce light pulses whose length is roughly equal to the inverse of the

linewidth of the laser levels transitions. Thus, with gas lasers, whose linewidth is relatively narrow, the pulse-width may be of ~0.1-1 ns. On the other hand, the linewidth and liquid lasers can be 10^3-10^5 times larger than of a gas laser, and, in this case, much shorter pulses may be generated, down to ~10 fs.

Notice that the short time duration, which implies energy concentration in time, is the counterpart of monochromaticity, which means energy concentration in wavelength. Therefore, a laser can be extremely monochromatic; however, only lasers with a broad linewidth, i.e. solid state and liquid lasers may produce pulses of very short time duration.

Lasers can be classified according to the active medium, for example, gas lasers, excimer lasers (a particular type of gas laser although it is always considered as another group), semiconductor lasers, solid-state lasers and so on. The active medium will characterise principally the output wavelength of the laser, their monochromaticity and thus the pulse duration. Depending on the application and the operating parameters the laser should be carefully chosen. Based on the previous experience in our group, to produce a change on a polymer surface, besides, to work on an industrial level; the laser-based in a solid-state active medium seems to be a suitable solution. So, during the development of this thesis, different lasers are used, all based on a solid-state active medium.

1.2.2. Solid state laser – Nd:YAG

A solid-state laser presents an active medium with ion spaces introduced as impurities in an otherwise transparent host material (in crystalline or glass form). Thus, semiconductor lasers are not usually included in this category, the mechanisms for pumping and laser action are in fact different [1.30]. While operating as a laser, this material absorbs and emits optical radiation in a controlled thermal environment, and thus its optical spectroscopic properties are critical to its performance [1.31]. As hosting crystal are used either oxides, e.g. Al_2O_3, or fluorides, e.g. $ILiF_4$. The impurities are ions belonging to one of the series of transition elements of the Periodic Table, like rare-earth (RE) or transition metal ions. The first laser ever built, the ruby laser is made of a natural crystal of Al_2O_3 (corundum) in which some of the Al^{3+} ions are replaced by Cr^{3+} ions. These lasers were extensively used in the past for the first mass production but nowadays have been replaced by others like Nd:YAG or Yb:Er:glass lasers.

In fact, the Nd:YAG lasers are the most popular and widely used type of solid-state lasers. The name came from an acronym for Yttrium Aluminium Garnet (YAG). Usually, the crystal medium is made of $Y_3Al_5O_{12}$ in which some of the Y^{3+} ions, around 1 % weight, are replaced by Nd^{3+}. The doping of the crystal medium becomes a transparent material into a pale purple one because of the Nd^{3+} absorption bands in the red. The active medium is usually presented in the form of a rod, performing as a primary advantage its excellent thermal stability [1.15]. It is also possible to use as host media fluorides (e.g. $YLiF_4$) or vanadates (e.g. YVO_4) as well as some phosphate or silicate glasses.

A simplified energy level scheme for Nd:YAG is shown in figure 1.11. The primary pumping process is the absorption of lamp energy from the ground state $^4I_{9/2}$ into the level $^4F_{5/2}$ (~0.8 μm) followed by transfer to the upper laser level $^4F_{3/2}$. This

consist of some closely spaced levels, two of this, labelled as R_2 and R_1 are responsible for two transitions, $\lambda_2 = 1.06415$ µm and $\lambda_1 = 1.0646$ µm respectively. Both transitions are homogeneously broadened at room temperature with $\Delta\nu \sim 2 \times 10^{11}$ Hz, and therefore they are so close in frequency that they form a single asymmetric peak, where the effective overall gain of the laser is placed near 1.06415 µm. A Nd:YAG laser can work in a mode-locking regime with pulses as short as 5 ps and also due to the long lifetime of the upper laser level ($\tau \sim 230$ µs) it is possible to work in Q-switch mode [1.30].

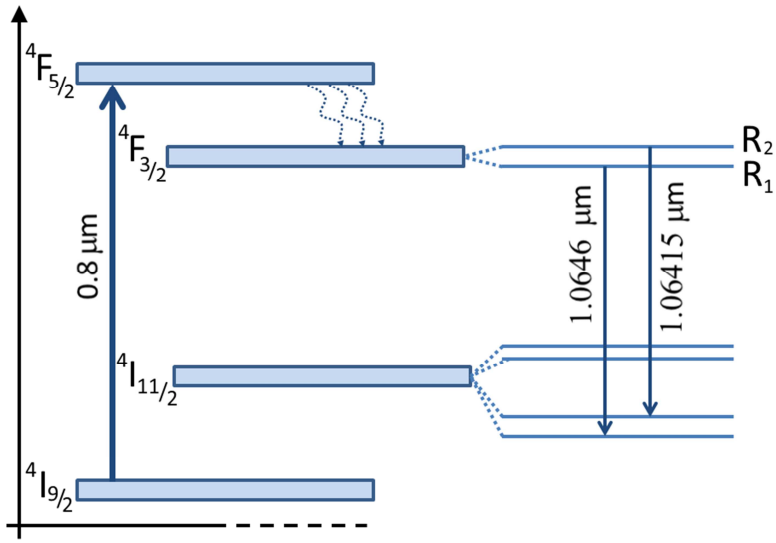

Figure 1.11. Simplified energy levels of Nd:YAG.

The lower laser level is depopulated by thermal transitions to the host by a thermal process, causing the heating of the YAG rod. So, mechanism of cooling together to a particular design of the optical cavity is needed to avoid efficiency losses [1.15]. Convective air or deionised water flows are used to cool the rod.

The pumping process can be done by either a lamp or an AlGaAs semiconductor laser. Xe lamps and high-pressure (4-6 atm) Kr lamps are used for the pulsed and CW cases, respectively. More recently the use of longitudinally diode-pumping (with

powers up to 15 W) and transversally diode-pumping (with powers above 100 W) allowed to achieve slope efficiency much higher than for lamp pumping and may exceed 10 % [1.30].

Nd:YAG lasers are widely used in a variety of applications: drilling, medical applications, laser ranging and so on. In our case, it is especially interesting their use as remote tool for surface treatment of materials, such as ablation [1.32], [1.33], marking [1.34], welding [1.35]–[1.37], material deposition [1.38], controlled oxidation [1.39], [1.40] or micro/nano-structuring [1.41], [1.42].

Similarly, it is possible to substitute the YAG by a silicate glass. The Nd:Glass present the same energy levels however the linewidths of the laser transition are much larger as a result of the inhomogeneous broadening arising from the local field inhomogeneities typical of a glass medium. The primary laser transition (1.054 µm) is much broader (by ~40 times), so by mode-locking, it is possible to achieve ultrashort pulses (~100 fs). Other crystal materials have been used as a host for the Nd^{3+} ions like the $YLiF_4$ (YLF) and the YVO_4. With them, it can be obtained higher quality beams or shorter pulses. Furthermore, other doping ions can be used with the YAG like Er:YAG, Yb:YAG or Tm:YAG, each with specific characteristics that fit better with some specific applications [1.30].

Furthermore, mechanism of frequency conversion can be used to change the output wavelength, for example, it can be halved to produce green light (532 nm) or divided by three to give ultraviolet light (355 nm).

1.2.3. Frequency conversion

A laser beam can be transformed to broaden the range of applications. If the transformation occurs when the beam is made merely to propagate through free space or a suitable optical system, we refer to this as a spatial transformation. Also, the conversion can be done when the laser beam passes through an amplifier, being then an amplitude transformation. A third case occurs when the wavelength of the beam is changed as a result of propagating through a suitable nonlinear optical material, resulting in frequency conversion. Finally, it is also possible to transform the temporal behaviour of a laser beam, and then we refer to time transformation.

By this mechanism, the fundamental wavelength of light produced by a laser can be converted by a result of frequency multiplication. The new frequency obtained is a multiple of the fundamental thus transforming one wavelength into light of another frequency. To produce this phenomenology some crystalline materials and liquids, which interact in a non-linear way to an electric field, are used. The incident light interacts with the electrons in the material producing an electromagnetic wave. The oscillation of the field inside the material can be generated twice the rate of the original wave. Phenomena called phase matching should occur, there is a privileged direction in the crystal where the velocity of the fundamental beam matches the generated e.m. wave [1.30]. Examples of selected materials used to produce the frequency conversion are KDP (KH_2PO_4), ADP ($NH_4H_2PO_4$), KTP ($KTiOPO_4$) or BBO (β-BaB_2O_4). High conversion efficiencies have been obtained, close to 100 %.

The phenomena production of double frequency is usually called second-harmonic generation (SHG). It is also possible to produce a tripled frequency, (THG, Third-Harmonic-Generation) by using two consecutive non-linear crystals. The first one creates the doubled frequency, while the fundamental frequency and the double one

are combined in the second crystal generating the third harmonic, see figure 1.12 that schemes this process.

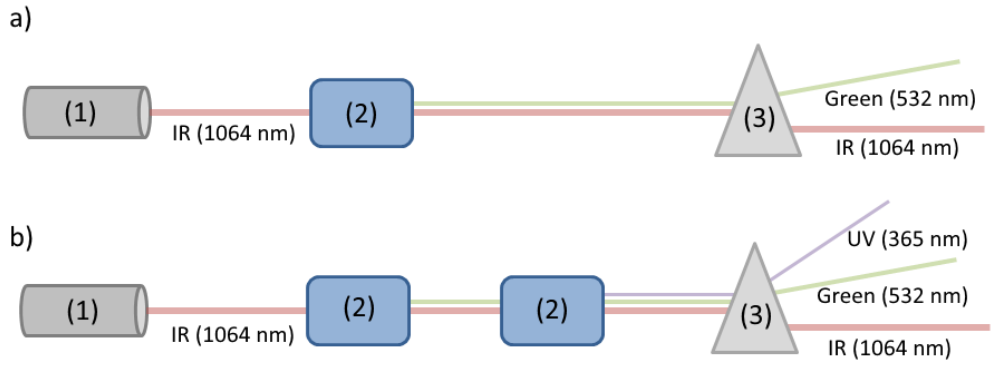

Figure 1.12. Scheme of the frequency conversion process used for a) SHG; b) THG. The devices used are 1) Laser light source; 2) non-linear crystal; 3) Prism.

This type of transformation is used in the Nd:YAG lasers to produce a green wavelength (532 nm) from the fundamental (1064 nm) or even to go further generating a laser beam in the near UV (365 nm).

1.2.4. Laser optics and guiding systems

Unlike traditional machine tools, a laser produces a beam of light with unique characteristics that make it a flexible device. The understanding of the behaviour of the laser beam is high importance to control it accurately. Thus, the primary optics characteristics and mechanisms used to control a laser beam are presented below.

1.2.4.1. Gaussian optics

The laser beam is described as electromagnetic radiation whose transverse electric field and intensity (irradiance) distributions are well approximated by Gaussian functions. Gaussian beams that go across a lens or mirrors maintain the Gaussian

form and enable the laser beam to be guided easily. The general equation that describes the intensity of a Gaussian beam along the z-axis of propagation is:

$$I(r,z) = I_0 \left(\frac{w_0}{w(z)} \right)^2 e^{2(r/w(z))^2} \tag{1.1}$$

where r is the radial distance to the axis of propagation z; w (z) is the amplitude radius of the beam; while w_0 is the amplitude radius in the focus or waist.

Also, a laser beam exhibits both spatial electromagnetic modes, longitudinal and transversal; which are independent one to each other. The longitudinal mode number is large in industrial lasers and can be ignored when characterising the beam since it has little influence on the essential beam characteristics. By contrast, the transversal electromagnetic modes (TEM) are of far greater significance. The TEM is depending on the cavity geometry, the alignment and spacing of the internal cavity optics, the gain and propagation properties of the active medium and the presence of apertures in the resonator [1.15]. Commonly, the cavity is designed to achieve only TEM_{00} oscillation that is more suitable to process materials, but other modes can be obtained varying the cavity design. Different TEM modes of a He-Ne laser in a rectangular cavity can be observed in figure 1.13.

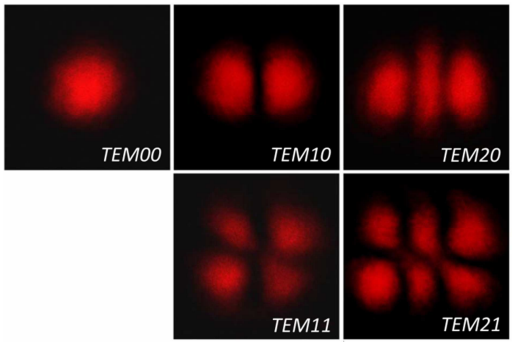

Figure 1.13. Laser modes of a He-Ne laser of a rectangular symmetry cavity (taken in our labs).

1.2.4.2. Optical components of an industrial laser

Industrial lasers present a set of common optical elements:

- **Lenses**
- **Beam expander**
- **Scanning system**

In addition, all the systems are usually integrated and controlled by computer software (CAD). The components are briefly described below.

-The laser beam is converged over the sample by a lens system. Usually, telecentric lenses are used to eliminate the parallax error characteristic of the standard lens by having a constant, non-angular field of view. At any distance from the lenses, the telecentric lenses will always have the same field of view [1.43].

The focal distance f usually characterises the lenses. Also, some parameters are defined to describe a laser beam after the lens system. Typically, the spatial parameters considered are:

- R_z: Rayleigh range
- z_0: Waist location
- θ: Beam divergence
- M^2: Quality beam factor

The Rayleigh range is defined as the distance along the longitudinal axis where the beam amplitude w(z) has been multiplied by the root of 2.

$$w(z_R) = 2\sqrt{2}w_0 \tag{1.2}$$

So, the Rayleigh range regarding the beam waist and the laser wavelength is described as:

$$Z_R = \frac{\pi w_0^2}{\lambda} \tag{1.3}$$

Therefore, the beam amplitude at any point of the propagation axis z in terms is:

$$w(z) = w_0 \sqrt{1 + \frac{(z - z_0)^2}{z_R^2}} \tag{1.4}$$

Finally, the beam divergence is:

$$\theta = \frac{2\lambda}{\pi w_0} \tag{1.5}$$

A graphical scheme of the beam shape along the propagation axis can be seen in figure 1.14.

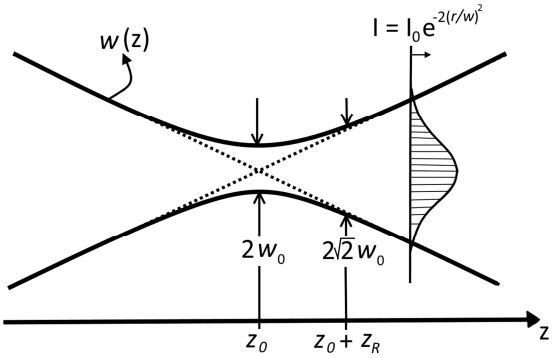

Figure 1.14. Propagation properties of the pure Gaussian, fundamental-mode beam.

The M^2 model is the preferred way of quantitatively describing a laser beam, including its propagation through free space and lenses, accurately, as ratios of parameters concerning the pure theoretical Gaussian laser beam [1.44]. An ideal laser

will present value of one for M^2. Figure 1.15 illustrates the difference between a pure and a real Gaussian beam related to the M^2 model.

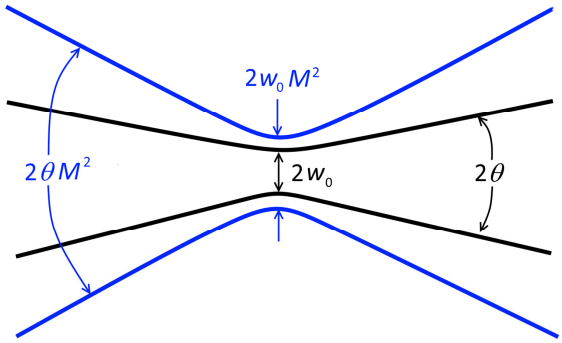

Figure 1.15. Relation between laser ideal (black) and real (blue) Gaussian beams.

So, a real beam waist, usually called the beam spot size or spot diameter (w_{0R}), can be described as:

$$w_{0R} = \frac{4M^2 f \lambda}{\pi D_0} \tag{1.6}$$

where D_0 is the beam diameter before the lens system and f the focal distance. So the minimum spot size is determined by the final lens. Furthermore, the output lens will define the maximum size area able to be treated without moving the laser, the marking field or marking area. A bigger lens allows a bigger area to be treated, but the beam waist will also be increased.

-A beam expander is an optical system that allows expanding the laser beam without losing its directionality. The design is such that the object rays, located at infinity, enter parallel to the optical axis of the internal optics and exit parallel to them [1.45]. So, this system can be placed at any point of a collimated laser beam to increase or decrease its diameter. Using this method is possible to increase the beam size before the lens achieving a smaller spot size on the sample, although the Rayleigh distance will be shorter. Figure 1.16 shows the two possible configurations

of beam expander using refracting lenses. An advantage of the Galilean configuration is that the complete system can be much shorter than as the Keplerian design.

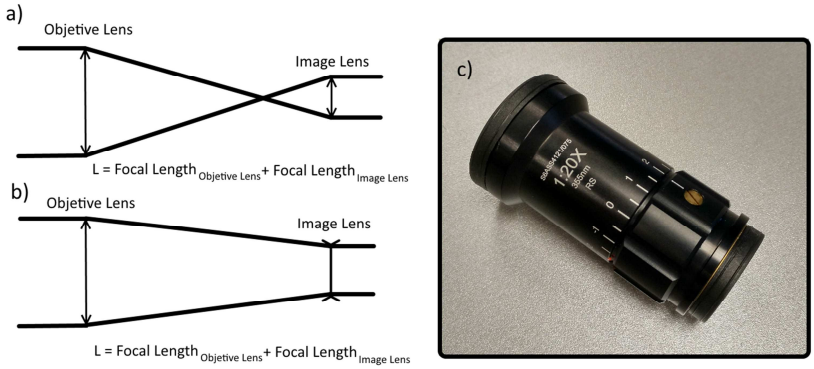

Figure 1.16. Beam expander by a) Kepler design; b) Galileo design; c) Photograph of a UV laser beam expander of 20 magnifications.

-The laser scanning is the system that allows moving the laser beam over a surface called processing area o marking area (which dimensions are related to the focal distance of the lens). There are multiple configurations of scanning system; below it is explained the typical configuration of our industrial laser machines: pre-objective scanning with galvanometric mirrors.

The scanning mechanism is placed before the lenses system in a pre-objective configuration. The distance from the scanner to the lenses depends on the entrance pupil diameter, the input beam geometry, and the angle of the scanned field. The complexity of the scanner depends on the optical correction required over a finite scanned field, that is, spot size, scan linearity, astigmatism, and depth of focus (DOF).

A galvanometer scanner consists of two mirrors whose movement is controlled using an electrical current. They are used extensively in laser scanning. The movement speed of the mirrors determines the writing velocity. They are used to have a system for two-axis scanning. Both mirrors should be placed separated. Figure

1.17 illustrates the configuration of a galvanometric scanning pre-objective system [1.44].

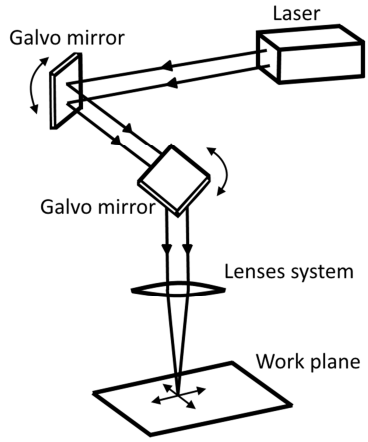

Figure 1.17. Scanning pre-objective system with two galvanometric mirrors.

-The laser systems are usually controlled by computer-aided design (CAD) software. The CAD facility for off-line programming is an essential component. It allows simulating and optimising the beam paths that are going to be constructed. The required features are drawn in the CAD system and then translated into motion control commands for execution. The motion control used was a multi-axis beam direction through arms fixed to a base that moves along Cartesian axes.

1.2.4.3. Laser parameters

We have seen how the laser beam is controlled using a laser scanning and lenses. So, the laser beam can be considered as a precise pen that distributes a series of pulses along a surface in a controlled way. Usually, the method of filling an area is to draw a range of consecutive lines separated a determined distance. Each line is made of a sequence of pulses. So, there are some parameters, controlled by software,

which is used to determine the sample processing. The primary laser parameters used were:

- **Laser scanning speed**: Processing speed of each line, usually measured in mm/s.
- **Hatch distance**: Distance between consecutive lines, usually measured in mm.
- **Pulse frequency**: Frequency of the laser pulses, usually measured in kHz.

Also, it is also possible to change the focal position to modify the incident spot width on the sample just following the eq. (1.4). Furthermore, the angle of lines or the number of repetitions can be tuned.

So, a laser marked area can be filled with consecutive spot whose distance in one axis (speed axis) is determined by the processing speed and the frequency of the pulses and in the other axis (hatch axis) directly by the hatch distance. The figure 1.18 illustrates how consecutive spots cover a square area.

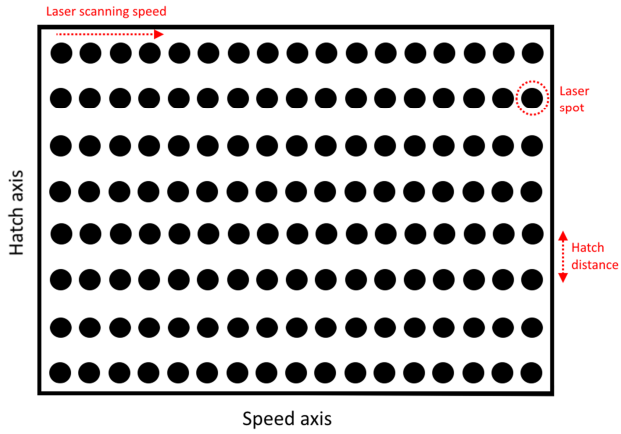

Figure 1.18. Illustration of a rectangular area filled by successive spots and both axis usually called speed and hatch axis respectively.

So, the following parameters and physical magnitudes can be defined (considering the usual units for each parameter):

- Energy per pulse (E_p):

$$E_p(\mu J) = \frac{1000 \times P_m(W)}{f(kHz)} \tag{1.7}$$

where P_m is the mean power of the laser and f the pulse frequency.

- Fluence (F) or energy deposited per unit of area:

$$F(J/cm^2) = \frac{100 \times E_p(\mu J)}{\pi\left(\frac{d_{spot}(\mu m)}{2}\right)^2} \tag{1.8}$$

where d_{spot} is the spot size over the sample

- Irradiance (I) or instant power deposited per unit of area:

$$I(GW/cm^2) = \frac{100 \times E_p(\mu J)}{t_p(ns) \times \pi\left(\frac{d_{spot}(\mu m)}{2}\right)^2} \tag{1.9}$$

where t_p is the pulse width.

- Dots per inch (DPI) that is calculated differently depending on the axis:

$$DPI_{speed\ axis} = 1000 \times \frac{f(kHz)}{v(mm/s)} \times \frac{25.4\ mm}{inch} \tag{1.10}$$

$$DPI_{hatch\ axis} = \frac{1}{hatch(mm)} \times \frac{25.4\ mm}{inch} \tag{1.11}$$

- Spots number per unit of area:

$$spots\ number/cm^2 = \frac{10^5 \times f(kHz)}{v(mm/s) \times hatch(mm)} = \frac{DPI_{speed\ axis} \times DPI_{hatch\ axis}}{6.4516} \quad (1.12)$$

- Cycle time (t_c), the time needed to process a square centimetre in terms of the selected laser parameters:

$$t_c(s/cm^2) = \frac{100}{v(mm/s) \times hatch(mm)} = \frac{DPI_{speed\ axis} \times DPI_{hatch\ axis}}{f(kHz) \times (25.4mm)^2} \quad (1.13)$$

1.2.5. Laser interaction with matter

As it was mentioned above, the laser is a powerful tool in material processing with a spatial resolution of better than 10 nm [1.46]. This resolution is possible because of the high energy density and directionality of the laser. Besides, the time of the process can be controlled considering the short laser pulses available (even under 10^{-15} s). Furthermore, it is possible to select a specific wavelength controlling the treatment depth and the interaction mechanisms. Industrially, high processing speeds can be achieved, much higher than the achieved by using mechanical tools or conventional heat sources. Also, the laser characteristics can be adequately controlled to ensure a constant process. Finally, laser processing is not limited to planar substrates but also allows working with 3D pieces [1.46].

Firstly, the general interaction mechanism between laser and matter is considered before going to the particular case of polymer processing.

1.2.5.1. General laser interaction mechanism

The laser interaction mechanism can be divided into two groups: conventional laser processing and laser chemical processing [1.46]. The principal difference between both is the presence of changes in the overall chemical composition of the processed material that happens in the second case. However, this classification is not precise, and both types of processes may occur at the same time.

-Conventional laser interaction: The interaction mechanism will be different depending on the laser parameters and the physical and chemical properties of the material. The lasers used are in the range of infrared wavelengths, which can excite free electrons within a metal or vibrations within an insulator. Considering a semiconductor material, both types of excitation are possible [1.46]. The energy is dissipated as heat, at low intensities the laser can just be considered as a heat source which induces a temperature increase on the surface. At high intensities, above a certain value I_v, the process is characterised by significant material vaporisation, a vapour plume above the substrate surface is formed. If that plume is highly ionised as a result of a higher intensity, I_p, a plasma vapour is formed. The plasma presents a high absorption and a non-linear response to the laser beam, so small changes in the laser light may cause substantial changes in the material.

-Laser chemical interaction: It is usually called laser-induced chemical processing (LCP). It can be used to patterning, coating and to induce a physicochemical modification of a solid surface by activation of real chemical reactions. These reactions can result in a material deposition, ablation/pulsed-laser deposition (PLD), etching, synthesis, surface modification (doping, alloying, oxidation, reduction, nitridation exchange of surface atoms/molecules), metallization, decomposition and polymerisation. The first step in a laser-induced reaction can be described schematically as:

$$AB + M + h\nu \rightarrow A\ (\downarrow) + B\ (\uparrow) + M$$

Where the molecule AB interacts with the laser photons dissociating in the two forming species A and B. M is the surrounding media, which can be a gas, a liquid solvent or a solid [1.46].

The reactions may be activated thermally (photothermally, pyrolytically), or photochemically (photolytically), or by a combination of both (photophysically). A reaction is considered activate thermally if the thermalisation of the laser excitation energy is fast compared to any other process, the laser should be viewed as a heat source. On the other hand, a photochemical reaction presents the first step faster than the thermalisation of the excitation energy.

1.2.5.2. Laser interaction with polymers

The unique properties of polymers characterise the laser interaction with polymers with respect to other materials: low absorption, low thermal diffusion and particularly a degradation behaviour that affects the rest of the features dynamically. Also, the plastic materials are complex materials including several components. All these constraints increase the difficulty of understanding the polymer processing in comparison to other materials processing as metals. However, a general overview of the optical and thermal properties is needed to understand what type of processes can be found in the laser effect.

The energy absorption will be defined by the polymer optical properties meanwhile the subsequent energy distribution will be characterised by the thermal properties. The thermal diffusion can be negligible due to the low thermal diffusion of the polymers considering a short laser pulse in the range of nanoseconds. So, the energy distribution should be the result of the optical penetration, generally

according to Lambert's law, and the Gaussian energy distribution in the laser spot [1.47].

So, according to the Lamberts law, the absorption (α) of each layer of equal thickness is described by:

$$\frac{dF}{dz} = -\alpha \times F \tag{1.14}$$

Thus, integrating the previous eq, it can be obtained the laser fluency regarding the penetration depth (z):

$$F_z = F_z e^{-\alpha z} \tag{1.15}$$

In that way can be defined the optical penetration depth δ_0 as the depth where the laser fluence is decreased by a factor of 1/e:

$$\delta_0 = \alpha^{-1} \tag{1.16}$$

This value will be dependent on the absorption spectrum of the material so that it will change depending on the used laser wavelength. For example, using a 1064 nm laser, the optical penetration depth for ABS is 7020 μm meanwhile the thermal penetration depth for pulses of 10 ns is around of 0.08 μm [1.47]. So, the thermal penetration can be considered negligible, the energy absorbed will produce a rise in the temperature only in volume that it is absorbed.

However, non-linear effects and inhomogeneities are not taken into account in the Lamberts law. In the case of nanosecond pulses, it should be considered the size of the additives and the degradation of the polymer as main possible non-linear effects. So, if the size of the additives is bigger than the laser wavelength, they can act as an

island with different properties than the polymer volume. By contrast, if the additives are smaller than laser wavelength, the material properties should be considered together with the polymer and the additive characteristics. Also, the degradation of the polymer by the effect of the pulses will change their optical properties usually increasing the absorption coefficient, so the penetration depth will be reduced meanwhile the heating of the surface will be increased [1.47].

Therefore, a classification of the laser effects on the polymeric material can be done considering the different phenomena that happen in the polymers under laser irradiation. These phenomena will be dependent on the material optical properties and the interaction mechanism. Also, they seldom occur isolated, the laser interactions with the polymer matrix and the additives are quite complex; consequently, this classification is only focused on overall effects in the material.

- **Ablation:** Laser ablation is considered a method to structure polymers or selective retire material by evaporation using high-intensity pulses. Two types of processes are considered: photothermal, where the energy absorbed causes directly a temperature increment in the polymer; and photochemical, where the energy is directly absorbed causing their breaking of chemical bonds. The material evaporation can happen instantly on the surface or inside the material, creating a rupture in the surface by internal gas pressure [1.48]. The ablation threshold energy is defined as the minimum energy needed to observe some material evaporation.

- **Melting:** The laser energy is absorbed by the polymer producing a temperature increase enough to melt the material but without producing direct evaporation like in the ablation process. Using polymer melting it is

possible to reshape the surface of the polymeric materials or to weld different materials.

- **Alloying/doping:** As well in the melting process, the laser energy produces a temperature increment in the material. However, in this case, the phase change is used to facilitate the diffusion of other material particles inside the polymeric material, like dyes, pigments or metallic compounds. These types of processes are usually called as LIFT or laser-induced foil transfer. They are used to create multi-colour surfaces or to create conductive tracks for example.

- **Foaming:** The foaming is produced when the energy of the laser is absorbed, thermally or chemically, causing a partial degradation of molecules below the surface giving rise to gas bubbles. They get trapped inside the material being visible due to the differences in the refractive index between the walls and the gas, generally forming white colour by light scattering.

- **Oxidation/Reduction:** Laser energy can produce a change in the electronic state of the polymeric molecules or additives. For example, the oxidation of the PP under UV exposure generates chemical groups that react with inks to get a reliable adhesion. On the opposite, by UV light is possible to change the whitener molecule TiO_2 causing reduced species that exhibit a characteristic blue-black colouration [1.47].

- **Carbonization:** The laser energy produced pyrolysis of the polymer causing a degradation of the organic forms into carbon forms. This process creates a darkening on the material

- **Bleaching:** Bleaching is defined as the loss of colour due to pigment degradation [1.47]. This process can happen without affecting the polymer matrix using short-pulses, avoiding the heating of the material. Furthermore, special additives, which can absorb the laser radiation, can be used to prevent the absorption by the polymer matrix. This additives transfer their energy to the pigment to degrade it without affecting the polymer.

References

[1.1] Plinius, *Naturalis historia book XXII.* .

[1.2] British Museum Dept of Coins and Medals, *Guide to the principal gold and silver coins of the ancients from circa BC 700 to AD 1.* British Museum Dept of Coins and Medals, 1895.

[1.3] Laconian black-figure kylix by the Arkesilas Painter, "King Arcesilaus watching over the preparation of silphium." Cabinet des médailles of the Bibliothèque Nationale de France.

[1.4] Joanna Izdebska Sabu Thomas, *Printing on polymers*, 1st ed. Elsevier, 2016.

[1.5] W. Callister and D. Rethwisch, *Materials science and engineering: an introduction*, 7th ed. New York: John Wiley & Sons, 2007.

[1.6] M. Chanda and S. L. Roy, *Industrial polymers, specialty polymers, and their applications*, 1st ed. Boca Raton: CRC Press, 2009.

[1.7] J.-L. Halary, F. Lauprêtre, and L. Monnerie, *Polymer materials - macroscopic properties and molecular interpretations*, 1st ed. Hoboken, New Jersey, 2011.

[1.8] T. A. Osswald and G. Menges, *Material science of polymers for engineers*, 3rd ed. München: Hanser, 2012.

[1.9] T. A. Osswald, *International plastics handbook: the resource for plastics engineers*, 4th ed. Cincinatti: Hanser Gardner Pubns, 2006.

[1.10] J. K. Fink, *Additives for thermoplastic polymers*, 1st ed. Salem: Wiley, 2010.

[1.11] R. M. Christie, "Pigments, dyes and fluorescent brightening agents for plastics: An overview," *Polym. Int.*, vol. 34, no. 4, pp. 351–361, Aug. 1994.

[1.12] W. Commons, "Extrusion (adapted)." [Online]. Available: https://en.wikipedia.org/wiki/Extrusion. [Accessed: 15-Sep-2017].

[1.13] W. Commons, "Injection moulding (adapted)." [Online]. Available: https://en.wikipedia.org/wiki/Injection_moulding. [Accessed: 15-Sep-2017].

[1.14] Prospector, "Prospector plastics." [Online]. Available: https://plastics.ulprospector.com/generics/1/c/t/acrylonitrile-butadiene-styrene-abs-properties-processing. [Accessed: 01-Sep-2017].

[1.15] J. C. Ion, *Laser processing of engineering materials*, 1st ed. Oxford: Elsevier, 2005.

[1.16] A. B. Gould and R. Gordon, "The LASER, light amplification by stimulated emission of radiation," in *The Ann Arbor Conference on Optical Pumping, the University of Michigan*, 1959.

[1.17] T. H. MAIMAN, "Stimulated optical radiation in ruby," *Nature*, vol. 187, no. 4736, pp. 493–494, Aug. 1960.

[1.18] R. N. Hall, G. E. Fenner, J. D. Kingsley, T. J. Soltys, and R. O. Carlson, "Coherent light emission from GaAs junctions," *Phys. Rev. Lett.*, vol. 9, no. 9, pp. 366–368, Nov. 1962.

[1.19] N. Holonyak and S. F. Bevacqua, "Coherent (visible) light emission from Ga(As1−xPx) junctions," *Appl. Phys. Lett.*, vol. 1, no. 4, pp. 82–83, Dec. 1962.

[1.20] F. J. McClung and R. W. Hellwarth, "Giant optical pulsations from ruby," *Appl. Opt.*, vol. 1, no. S1, pp. 103–105, 1962.

[1.21] W. G. Wagner and B. A. Lengyel, "Evolution of the giant pulse in a laser," *J. Appl. Phys.*, vol. 34, no. 7, pp. 2040–2046, Jul. 1963.

[1.22] L. E. Hargrove, R. L. Fork, and M. A. Pollack, "Locking of He–Ne laser modes induced by synchronous intracavity modulation," *Appl. Phys. Lett.*, vol. 5, no. 1, pp. 4–5, Jul. 1964.

[1.23] D. Kuizenga and A. Siegman, "FM and AM mode locking of the homogeneous laser - Part I: Theory," *IEEE J. Quantum Electron.*, vol. 6, no. 11, pp. 694–708, 1970.

[1.24] P. A. Franken, A. E. Hill, C. W. Peters, and G. Weinreich, "Generation of optical harmonics," *Phys. Rev. Lett.*, vol. 7, no. 4, pp. 118–119, Aug. 1961.

[1.25] J. A. Armstrong, N. Bloembergen, J. Ducuing, and P. S. Pershan, "Interactions between light waves in a nonlinear dielectric," *Phys. Rev.*, vol. 127, no. 6, pp. 1918–1939, Sep. 1962.

[1.26] J. A. Giordmaine and R. C. Miller, "Tunable coherent parametric oscillation in LiNbO3 at pptical frequencies," *Phys. Rev. Lett.*, vol. 14, no. 24, pp. 973–976, Jun. 1965.

[1.27] J. F. Ward and G. H. C. New, "Optical third harmonic generation in gases by a focused laser beam," *Phys. Rev.*, vol. 185, no. 1, pp. 57–72, Sep. 1969.

[1.28] Z. Alferov, "Double heterostructure lasers: early days and future perspectives," *IEEE J. Sel. Top. Quantum Electron.*, vol. 6, no. 6, pp. 832–840, 2000.

[1.29] I. Hayashi, "High power, fundamental transverse mode operation in double heterostructure lasers," 1973.

[1.30] O. Svelto, *Principles of lasers*, 5th ed. Milano: Springer, 2010.

[1.31] R. C. Powel, *Physics of solid-state laser materials*, 1st ed. New York: Springer, 1998.

[1.32] D. E. Martínez-Tong *et al.*, "Formation of polymer nanoparticles by UV pulsed laser ablation of poly (bisphenol A carbonate) in liquid environment," *Appl. Surf. Sci.*, vol. 418, pp. 522–529, Oct. 2017.

[1.33] O. V Mkrtychev, V. E. Privalov, A. E. Fotiadi, and V. G. Shemanin, "Laser ablation studies of nanocomposites," *St. Petersbg. Polytech. Univ. J. Phys. Math.*, vol. 1, no. 1, pp. 82–86, 2015.

[1.34] Y. M. Noor, S. C. Tam, L. E. N. Lim, and S. Jana, "A review of the Nd:YAG laser marking of plastic and ceramic IC packages," *J. Mater. Process. Technol.*, vol. 42, no. 1, pp. 95–133, 1994.

[1.35] S. Saravanan, K. Raghukandan, and N. Sivagurumanikandan, "Pulsed Nd: YAG laser welding and subsequent post-weld heat treatment on super duplex stainless steel," *J. Manuf. Process.*, vol. 25, pp. 284–289, 2017.

[1.36] G. Sivakumar, S. Saravanan, and K. Raghukandan, "Investigation of microstructure and mechanical properties of Nd:YAG laser welded lean duplex stainless steel joints," *Optik (Stuttg).*, vol. 131, pp. 1–10, 2017.

[1.37] N. Kumar, M. Mukherjee, and A. Bandyopadhyay, "Comparative study of pulsed Nd:YAG laser welding of AISI 304 and AISI 316 stainless steels," *Opt. Laser Technol.*, vol. 88, pp. 24–39, 2017.

[1.38] Y. P. Kathuria and Y. Uchida, "Pulsed Nd-YAG laser deposition of TiN and TiAlN coating," *Phys. Procedia*, vol. 12, no. PART 1, pp. 506–511, 2011.

[1.39] Q. Dong, J. Hu, Z. Guo, J. Lian, J. Chen, and B. Chen, "Surface morphology study on chromium oxide growth on Cr films by Nd-YAG laser oxidation process," *Appl. Surf. Sci.*, vol. 202, no. 1–2, pp. 114–119, 2002.

[1.40] J. J. Pérez and P. Sakanaka, "An improved three-dimensional model for growth of oxide films induced by laser heating," *Appl. Surf. Sci.*, vol. 176, pp. 703–708, 2001.

[1.41] B. Zhang and K. C. Yung, "Frequency-tripled Nd:YAG laser ablation in laser structuring process," *Opt. Lasers Eng.*, vol. 44, no. 8, pp. 815–825, 2006.

[1.42] S. Dobroiu, F. C. M. J. M. van Delft, E. van Thiel, K. L. Hanson, and D. V. Nicolau, "Laser-assisted structuring of metal-polymer bilayers for protein patterning," *Microelectron. Eng.*, vol. 87, no. 5–8, pp. 1190–1194, 2010.

[1.43] Edmund optics, "The advantages of telecentricity," *Imaging Resource Guide*, 2017. [Online]. Available: https://www.edmundoptics.com/resources/application-notes/imaging/advantages-of-telecentricity/. [Accessed: 01-Nov-2017].

[1.44] S. Edition, *Handbook of optical and laser scanning*, 2nd ed. Boca Raton: CRC Press, 2012.

[1.45] Edmund optics, "Beam expanders," *Imaging Resource Guide*, 2017. [Online]. Available: https://www.edmundoptics.com/resources/application-notes/lasers/beam-expanders/. [Accessed: 01-Nov-2017].

[1.46] D. Bäuerle, *Laser processing and chemistry*, 4th ed. Berlin: Springer, 2011.

[1.47] J. Bosman, "Processes and strategies for solid state Q-switch laser marking of polymers," Twente, 2007.

[1.48] T. Lippert, A. Yabe, and A. Wokaun, "Laser ablation of doped polymer systems," *Adv. Mater.*, vol. 9, no. 2, pp. 105–119, 1997.

2. Experimental techniques

The experimental techniques chapter is divided into two parts. Firstly, the different employed lasers, as well as the polymeric materials, are described. Secondly, the characterisation techniques to study both the unmarked material and the laser marks are detailed.

2.1. Lasers for material processing and polymers

2.1.1. Laser systems

During this thesis, different laser systems have been used. The polymer marking and micro-structuring processes were made using three different industrial laser sources. Furthermore, two more laser systems, laboratory systems, were employed to perform the holographic and plasmonic reshape.

The used industrial lasers present similar components. They are lasers prepared to work in an industrial environment, so their optical elements are inside of a closed box to be protected. This type of integration restricts the customisation of the laser. Only two optical components can be tuned: the beam expander and the output lens, which affect the spot size and the marking field. These systems have a beam scanner controlled by a CAD system. Also, the laser source is attached to a motorised arm able to move the laser in one or more axis. Furthermore, they can have a motorised table (where the samples to be marked are placed) that can be used to expand the marked area by the laser. A deionised water circuit refrigerates these lasers.

The following industrial lasers were used:

- **PowerLine E25** laser from Rofin: Nd:YAG laser of 1064 nm.
- **Trumark 6230** laser from Trumpf: Nd:YVO_4 laser of 532 nm.
- **PowerLine E20 THG** laser from Rofin: Nd:YAG laser of 355 nm.

The other two lasers employed in this work were laboratory systems. This term means that these systems are not adequately prepared to work in an industrial environment for different reasons. For example, they lack a scanning system and a motorised stage or are unstable working at long regimes. These lasers were placed on an optical table together with some lens and mirrors to guide the beam.

The following laboratory lasers were used:

- **Brilliant laser** from Quantel: Nd:YAG laser of 355 nm.
- **FDSS 532-150** from CryLas: Diode laser of 532 nm.

2.1.1.1. PowerLine E25 laser from Rofin

This laser is mounted on a motorised arm able to move the laser source along one perpendicular axis to the marking area. There are two beam expanders and two lenses available, but only one of each component was used. Their main characteristics, a photograph and the power calibration curves are shown in table 2.1, figures 2.1 and 2.2, respectively. Throughout this work, this laser is referred as **IR laser** to simplify.

Table 2.1. Main characteristics of the laser PowerLine E25 from Rofin.

IR laser	
Laser active medium	Nd:YAG
Wavelength	1064 nm
Nominal Power	18 W @ 20 kHz
Pulse frequency range	0 – 200 kHz
Pulse width	20 ns @ 20 kHz
M^2	< 1.3
Lens used	254 mm
Beam expander	x2
Working field	180 x 180 mm
Spot size on focus	90 µm

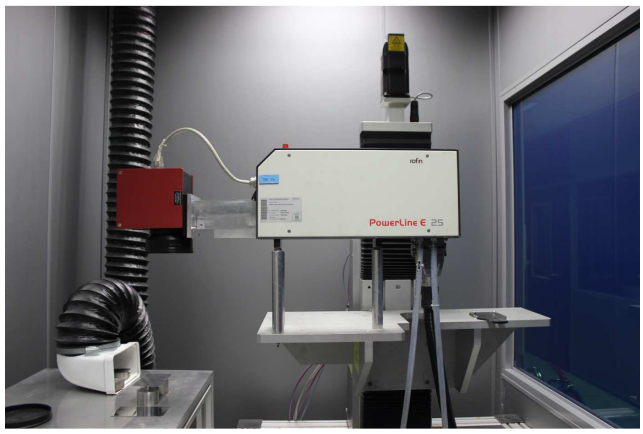

Figure 2.1. Image of the industrial PowerLine E25 from Rofin (IR laser) used in this work.

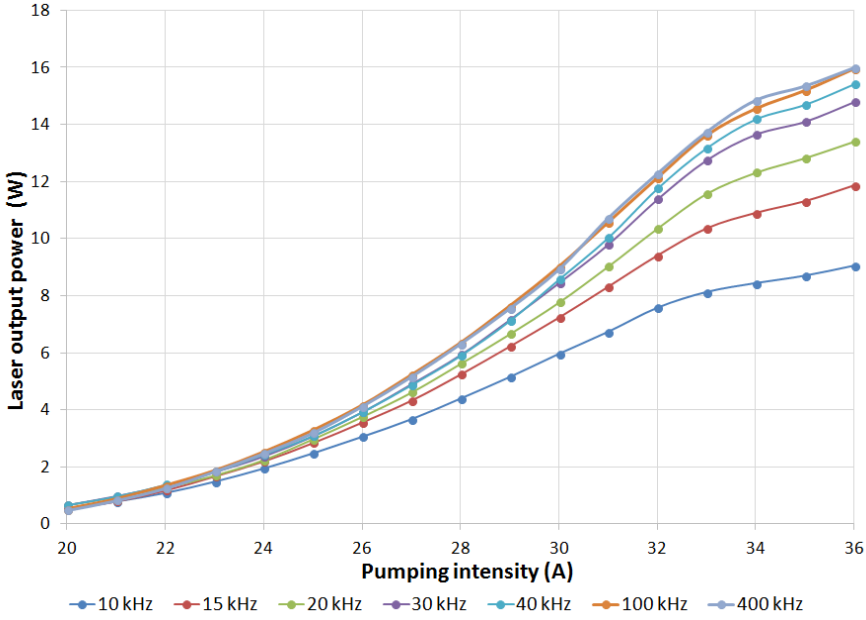

Figure 2.2. Laser calibration power in terms of the pulse frequency and the pumping intensity for the PowerLine E25 from Rofin (IR laser).

2.1.1.2. Trumark 6230 laser from Trumpf

This laser is mounted on a motorised arm able to move the laser source along two axes, one vertical and another one parallel to the marking surface. The system also has a motorised table ready to move the marking surface in the remaining axis. In this case, the laser has two different lenses and no beam expander; both lenses were used. The main characteristics, a photograph and the power calibration curves are shown in table 2.2, figures 2.3 and 2.4, respectively. Throughout this report, this laser is referred as **green laser** to simplify.

Table 2.2. Main characteristics of Trumark 6230 from Trumpf (green laser).

Green laser	
Laser active medium	Nd:YVO_4
Wavelength	532 nm
Nominal Power	8 W @ 30 kHz
Pulse frequency range	1 – 120 kHz
Pulse width	18 ns @ 30 kHz
M^2	< 1.2
Lens used	330 and 100 mm
Beam expander	None
Working field	340 x 340 and 55 x 55 mm
Spot size on focus	60 and 30 µm

Figure 2.3. Image of the industrial Trumark 6230 from Trumpf used in this work (green laser).

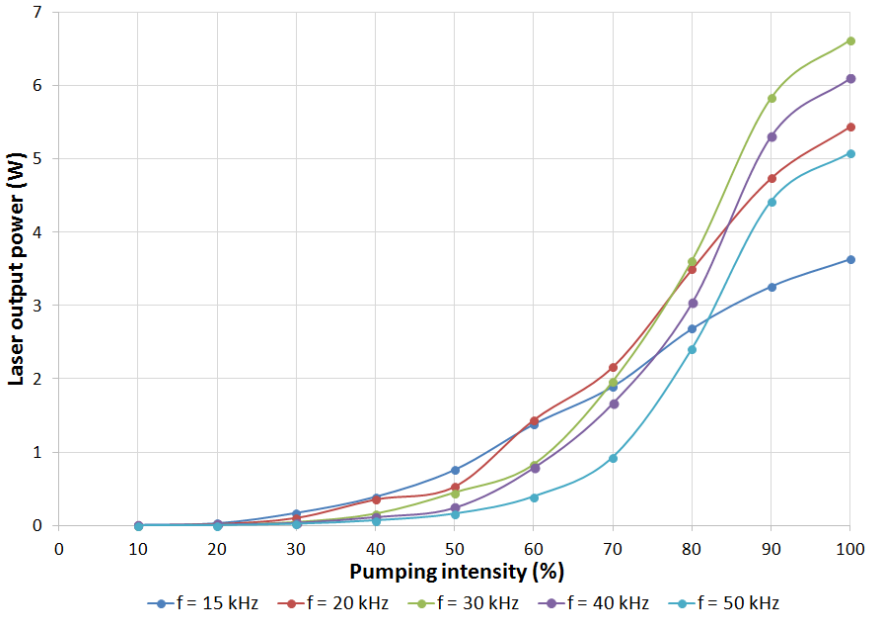

Figure 2.4. Laser calibration power in terms of the pulse frequency and the pumping intensity for the Trumark 6230 from Trumpf (green laser).

2.1.1.3. PowerLine E20 THG from Rofin

This laser is mounted on a motorised arm able to move the laser source along the three spatial axes. In this case, the laser has two different lenses and beam expanders. The used configuration was always the same pair of lens and beam expander to have two different spot sizes. The main characteristics, a photograph and the power calibration curves are shown in table 2.3, figures 2.5 and 2.6, respectively. Throughout this work, this laser is referred as **UV laser** to simplify.

Table 2.3. Main characteristics of PowerLine E20 THG from Rofin (UV laser).

UV laser	
Laser active medium	Nd:YAG
Wavelength	355 nm
Nominal Power	2 W @ 15 kHz
Pulse frequency range	15 – 100 kHz
Pulse width	10 ns @ 15 kHz
M^2	< 1.5
Lens used	511 and 100 mm
Beam expander used	x5 and x20
Working field	340 x 340 and 55 x 55 mm
Spot size on focus	104 and 7 µm

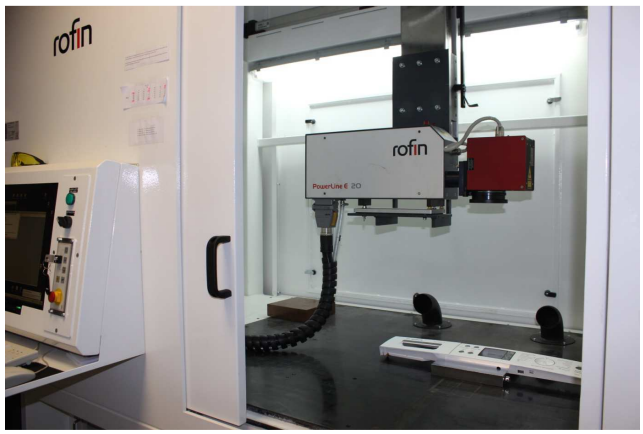

Figure 2.5. Image of the industrial PowerLine E20 THG from Rofin used in this work (UV laser).

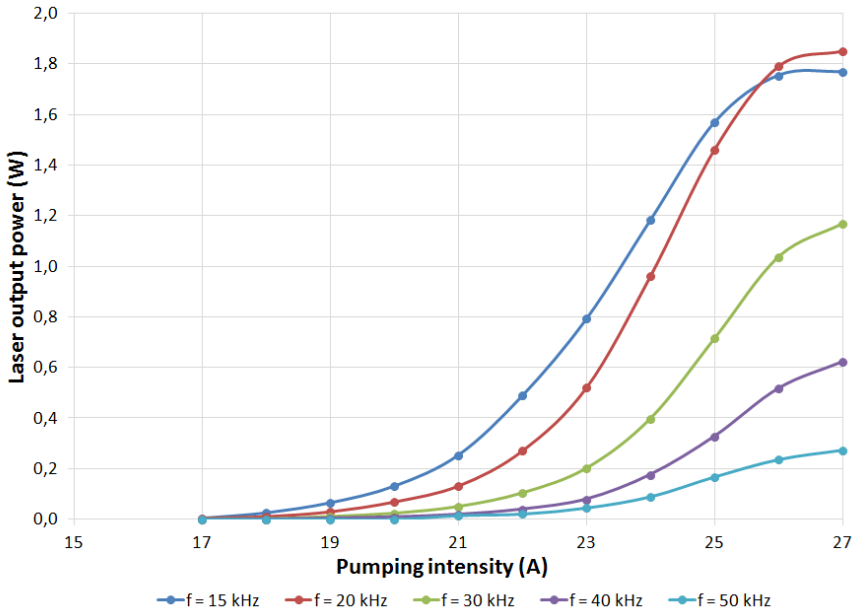

Figure 2.6. Laser calibration power in terms of the pulse frequency and the pumping intensity for the PowerLine E20 THG from Rofin (UV laser).

2.1.1.4. Brilliant laser from Quantel

This laser is modular; each module allows changing the output wavelength by successive harmonic generation. In our case, we used two modules, so our output wavelength was 355 nm. The laser has no lens in the beam exit; the beam is collimated with a divergence less than 0.5 mrad. The main characteristics and a photograph of the system are shown in table 2.4 and figure 2.7 respectively. Throughout this work, this laser is referred as **interf UV laser** to simplify.

Table 2.4. Main characteristics of Brilliant from Quantel (interferometric UV laser).

Interf UV laser	
Laser active medium	Nd:YAG
Wavelength	355 nm
Mean Energy	100 mJ @ 355 nm
Pulse frequency range	10 Hz
Pulse width	4 ns
M^2	< 1.5
Spot size on exit	500 µm

Figure 2.7. Image of the Brilliant with the harmonic modules from Quantel used in this work (interf UV laser).

2.1.1.5. FDSS 532-150 from Crystal Laser Systems

This laser is a diode-pumped passively Q-switched solid-state laser. It has no lens or scanning system; the beam is collimated with a divergence less than 5.5 mrad. The main characteristics and a photograph of the system are shown in table 2.5 and figure 2.8 respectively. Throughout this work, this laser is referred as **plasmonic green laser** to simplify.

Table 2.5. Main characteristics of FDSS 532-150 from CrysLas (plasmonic green laser).

Plasmonic green laser	
Laser active medium	Unknown
Wavelength	532 nm
Mean Energy	$>$ 100 µJ
Pulse frequency range	1 kHz
Pulse width	1.5 ns
M^2	$<$ 1.5
Spot size on exit	500 µm

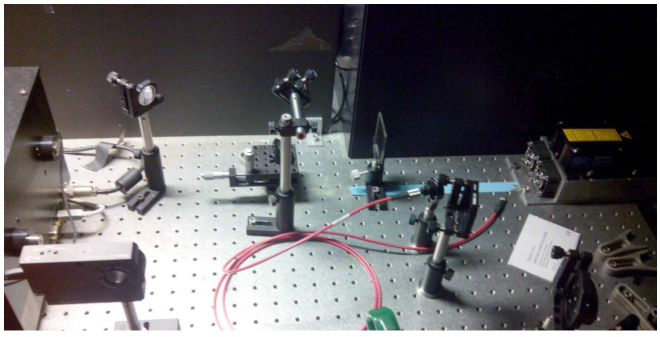

Figure 2.8. Image of the FDSS 532-150 from Crystal Laser Systems and the optical devices used to guide the beam (plasmonic green laser).

2.1.2. Polymeric materials

During this work different polymeric materials were used. The most used polymer in this work was ABS (black or white ABS depending on the corresponding additives), although PP and PS were also utilised in some specific experiments. The material was selected taking into account the materials used by BSH in their home appliances. All the polymeric materials were processed by injection moulding in two external providers of BSH, MYPA S.L. and Wirthwein A.G. The polymeric materials were processed into flat plates. Three different moulds were used, two of them for processing rectangular samples of 80x50x2 mm and 90x60x2 mm respectively, and one for circular samples of 100 mm of diameter and 2 mm of width. The material was always cleaned with isopropanol before being marked.

2.1.2.1. White ABS

The white ABS used was provided by Elix Polymers S.L.; in particular, this white ABS is used for the aesthetical parts of the BSH washing machines (P2H-AT LNS 202 11236). The same commercial polymer but without the white additive, also called ABS natural by the manufacturer (P2H-AT LNS 202) was employed for marking as a reference. Also, a third material was prepared by additivating this natural ABS with controlled concentrations of TiO_2 (2%, 4%, 5%, 6% and 8% weight) in two crystalline forms, anatase and rutile. ABS/TiO_2 compoundings were prepared by extrusion of the polymer matrix and different percentages of TiO_2 Kronos® 2500 (rutile form) [2.1] and Kronos® 1071 (anatase form) [2.2] provided by KRONOS Worldwide Inc. The Kronos® 2500 presents a minimum content of 97.5% of rutile TiO_2, and aluminium oxide and organic compounds covering the surface of its particles. The Kronos® 1071 shows a minimum content of 96% of anatase TiO_2, and

aluminium and silicon compounds covering the surface of its particles. Both particles presented an average size between 200 and 300 nm. A summary of the different materials used in this work for white ABS marking can be seen in table 2.6. Abbreviations are used along this work to simplify; they are indicated in the table.

Table 2.6. Summary of the different white ABS materials used in this work.

Base material reference name	Extra additive added	Abbreviated nomenclature
P2H-AT LNS202	-	natural-w ABS*
P2H-AT LNS202	2, 4, 5, 6 and 8% TiO_2 rutile or anatase	X% TiO_2 rutile or anatase ABS
P2H-AT LNS202 11236	-	white-c ABS

*The letter w is used to describe the natural ABS used for white ABS.

2.1.2.2. Black ABS

Black ABS was also provided by Elix Polymers S.L.; in particular, this black ABS is used for some of the aesthetical parts of the BSH washing machines (M203 BK901510). The same ABS but without the colour pigment CB is referenced by the provider as ABS natural (M203 BK901000). In this case, this natural ABS was charged with controlled concentrations of black additive, Carbon Black (0.05%, 0.1%, 0.2% and 0.5% by total weight). ABS/carbon black compoundings were prepared by extrusion of the polymer matrix and different percentages of carbon black additive to obtain pellets for moulding injection. The CB used was Printex® 90 supplied by Evonik Industries AG (now sold by Orion Engineered Carbons) [2.3]. This material is a carbon black pigment also used as UV protector, conductor or even thermal insulator. The particles presented an average size of 14 nm.

Also, the laser special additive Iriotec® 8835 from Merck [2.4] was also used and added to the black ABS. This material is used to enhance the foaming effect on a black polymer. The amount used in this work was the recommended by the manufacturer. A summary of the different material for black ABS marking used in this work can be seen in table 2.7. Abbreviations used along this work to simplify, they are indicated in the table.

Table 2.7. Summary of the different black ABS materials used in this work.

Base material reference name	Extra additive added	Abbreviated nomenclature
M203 BK901000	-	natural-b ABS*
M203 BK901000	0.05, 0.1, 0.2 and 0.5% CB	X % CB ABS
M203 BK901510	-	black-c ABS
M203 BK901000	0.05, 0.1, 0.2 and 0.5% CB + 0.4% Iriotec® 8835	X% CB ABS + Iriotec
M203 BK901510	0.4% Iriotec® 8835	black-c ABS + Iriotec

*The letter b is used to describe the natural ABS used for black ABS.

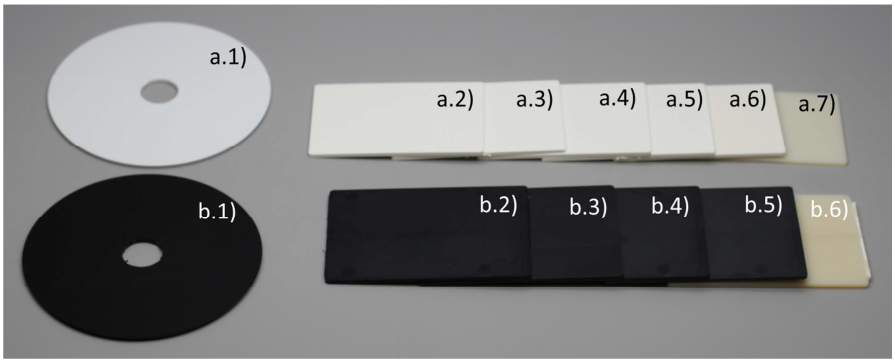

Figure 2.9. ABS samples processed from; a) P2H-AT LNS202 : 1) white-c ABS; 2) 8% TiO_2 Rutile ABS; 3) 6% TiO_2 Rutile ABS; 4) 5% TiO_2 Rutile ABS; 5) 4% TiO_2 Rutile ABS; 6) 2% TiO_2 Rutile ABS; 7) natural-w ABS; b) M203 BK901000: 1) black-c ABS; 2) 0.5% CB ABS; 3) 0.2% CB ABS; 4) 0.1% CB ABS; 5) 0.05% CB ABS; 6) natural-b ABS.

2.1.2.3. Other polymers

The PP (homopolymer) was provided by Repsol and was the same material used for aesthetical parts of some BSH small appliances like coffee makers or irons. As similar to the previous cases, two types of materials were used; the commercial PP polymer with TiO_2 additive and without the colour pigment (translucent), both based on the Repsol Isplen® PP084D2M. No extra additives were added to the materials. A summary of the different materials used in this work can be seen in table 2.8.

Table 2.8. Summary of the different PP materials used in this work.

Base material reference name	Abbreviated nomenclature
Isplen® PP084D2M white	white-c PP
Isplen® PP084D2M translucent	translucent-c PP

In the case of PS, the polymeric material was used in the form of a colloidal dispersion of spheres of PS in water. The spheres are 400 ± 9 nm of diameter, and its density is 1.05 g/cm^3. The material is provided by ThermoFisher scientific.

2.2. Characterization techniques

Different characterisation techniques were used throughout this work to study the interaction mechanism between the laser and polymeric material and to characterise the properties of the laser marks.

This section has been divided into three parts depending on the type of characterisation study. Firstly, different spectroscopic techniques are introduced. Hereafter the microscopic methods used are explained. Finally, other characterisation techniques employed are exposed.

2.2.1. Spectroscopic techniques

Through the use of different light wavelengths and their interaction with matter, it is possible to learn about the chemical structures of the polymer or their physical properties. The techniques used are described below.

2.2.1.1. Colourimetry

Colour properties are of particular interest in the characterisation of the laser marking of polymeric materials, in particular for aesthetical purposes. Colour is the aspect of any object that may be described in terms of hue, lightness, and saturation. In physics, colour is associated with electromagnetic radiation of a specific range of wavelengths visible to the human eye, the visible spectrum. Our perception of colour come from the stimulation of cone cells in the eye by electromagnetic radiation of the visible spectrum of light (generally considered from 400 to 700 nm). The colour

associated with an object is determined by the type of illumination, the physical characteristics of the material like reflectivity, and the cone eye stimulation.

It can be defined three primary attributes of colour [2.5]:

- **Brightness**: Attribute of a visual perception according to which an area appears to exhibit more or less light.
- **Hue**: Attribute of a visual perception according to which an area appears to be similar to one or proportions of two, of the perceived colours red, yellow, green and blue.
- **Colourfulness**: Attribute of a visual perception according to which an area appears to exhibit more or less of its hue.

Moreover, three relative perceptual attributes of colour that are:

- **Lightness**: The brightness of an area judged relative to the brightness of a similarly illuminated area that appears to be white or highly transmitting.
- **Chroma**: The colourfulness of an area judged in proportion to the brightness of a similarly illuminated area that appears to be white or highly transmitting.
- **Saturation**: Colourfulness of an area judged in proportion to its brightness.

Colours can be identified by numerical coordinates defining a colour space. It is possible to describe different colour spaces like RGB, associated with the human trichromacy, CMYK or CIELab. Along with this thesis, CIELab was selected. This selection was made because this colour space is useful for colours in the range of

black and white, and it is widely employed in the definition of colours for coloured polymers. The figure 2.10 shows the CIELab colour space where each colour is defined by three coordinates: L* that goes from 0 (darkest black colour) to 100 (brightness white colour); a* that goes from a range of ±100 covering from red/green opposite (red, positive, and green, negative numbers); and b* that goes from a range of ±100 covering from yellow/blue opposite (yellow, positive, and blue, negative, numbers).

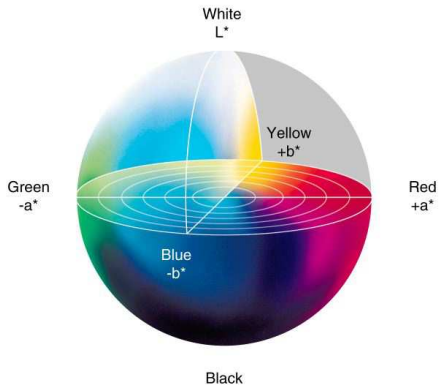

Figure 2.10. CIELab colour space.

The colour difference is defined according to the formula CIE 1976, eq. (2.1). Modifications to this formula were proposed over the years like CIE94 or the most recent, CIEDE2000. However, these formulae aimed to improve the performance of the equation (2.1), in some cases by adding some extra terms. However for our purpose, with colour changes along the L* axis together with small deviations in the other coordinates, the use of the CIE 1976 seems to be more appropriated to simplify.

$$\Delta e^* = \sqrt{(\Delta L^*)^2 + (\Delta a^*)^2 + (\Delta b^*)^2} \tag{2.1}$$

Also, it is essential to consider the light sources in colourimetry. The colour perception varies upon the illumination. There are different homologated light illuminants; in our case, we have selected the recommended Standard Illuminant D65

because it corresponds roughly to the average midday light [2.6]. The symbol represents the type of illuminant, D for daylight at different locations, and the temperature of the colour, 6504 K for normal daylight. For example, other light sources used to simulate daylight illuminations are D50 (5000 K) or D55 (5500 K).

Therefore, the colour of the samples was analysed using a spectrophotometer from Konica Minolta. This device presents a spot diameter of 6 mm. The measurement conditions used were an observer angle of 10° and standard illuminant D65. Finally, the tool allows measuring only the diffuse component or including also the specular component of the colour. However, it was experimentally observed that the changes between both measurements in our particular case, laser marks on the polymer, were negligible. So, the data reported correspond to both components together, usually called "Specular Component Included" (SCI) on colour devices. A photograph of the measurement equipment used is shown in the figure 2.11.

Figure 2.11. Image of the spectrophotometer from Konica Minolta used.

2.2.1.2. UV-Vis-NIR spectroscopy

The UV-Vis-NIR spectroscopy corresponds to the absorption or reflectance spectroscopy in a wavelength range whose correspond to the visible and adjacent regions.

In our case, this technique gave information about the polymer absorption characteristics for each laser wavelength. The optical spectra were measured using a Cary 5000 UV-VIS-NIR spectrophotometer from Agilent Technologies in a range from 325 to 1200 nm in reflectance mode.

2.2.1.3. IR (ATR-FTIR) spectroscopy

Attenuated Total Reflectance (ATR) is a technique of infrared spectroscopy used to characterise the chemical structure of a sample surface, which is directly examined without further preparation. This method allows exploring a wide range of materials, from solids to liquids.

The techniques measure the changes in an IR wavelength signal after a single or multiple internal reflections; see figure 2.12 (scheme of multiple reflections ATR accessory is displayed as an example). The ATR crystal is a dense optical crystal with a high refractive index. The reflections create an evanescence wave that extends beyond the crystal into the sample. This wave interacts with the material, and it will be absorbed or reflected according to its wavelength. This evanescence wave only extends beyond the crystal until around 5 µm, so the sample must be in direct contact with the ATR crystal. The changes in the evanescence wave are passed back to the IR beam and will be finally detected with an IR detector in a conventional IR spectrometer. The signal (similar to a transmission IR spectrum) will be characterised

by a succession of peaks corresponding to the different chemical absorptions of the material.

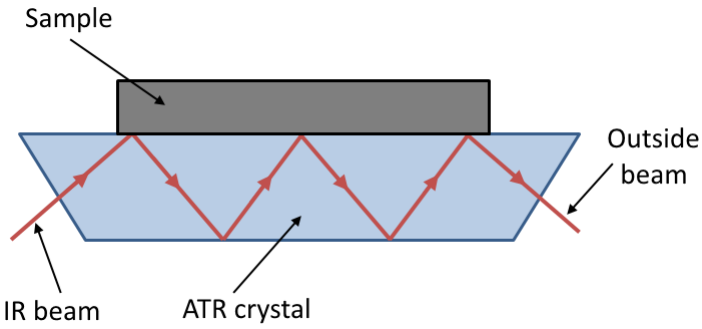

Figure 2.12. Scheme of multiple reflection ATR systems.

In our case, this technique allowed identifying an alteration of chemical groups or moieties as consequence of the laser marking process. The equipment used was a Vertex 70 Bruker FTIR with a Golden Gate Specac diamond ATR accessory (single reflection). The measurements were carried out in the 600-4000 cm^{-1} range, and resolution of 2 cm^{-1}. The spectra were then corrected for ATR, baseline corrected and normalised to the 1452 cm^{-1} peak height (scissoring mode of the CH_2 peak), which was assumed to be invariant during laser treatment.

2.2.1.4. XPS

X-ray photoelectron spectroscopy (XPS) is a quantitative spectroscopic technique that measures the elemental composition, empirical formula, chemical state and electronic state of the elements presented on a surface. A sample is impacted by X-ray photons in such way that electrons are ejected. The kinetic energy of those photoelectrons is directly related to the binding energy which in turn is dependent on the final state configuration after photoemission. This last state is characterised by full relaxation of all atomic orbitals towards the hole in the core level [2.7]. Results

obtained from this technique are expressed in atomic percentage values. The measuring depth is approximately 10 nm. Additionally, ion beam etching can be performance to measure as a function of depth.

Two different types of measurements can be done using this technique, the wide scan or survey spectrum and the high-resolution spectrum. The first one provides information about the elementary composition of the sample while the second one is useful to detect the percentages of atomic species.

Small changes were detected in the superficial irradiated area employing this technique. The equipment was a Kratos AXIS Ultra DLD (Mono Al Ka, Power: 120 W (10mA, 15kV)). The binding energies were calibrated using the C 1s signal (284.6 eV) of adventitious carbon.

2.2.2. Microscopic techniques

2.2.2.1. Stereoscopic microscope

A stereoscopic microscope was used to measure the penetration depth of the laser treatment through the observation of the cross-section of the marked samples. The device used was a Motic SMZ-168 stereo zoom, with a zoom magnification of 45×.

2.2.2.2. Confocal microscopy

A confocal microscope was used to analyse the topography. Confocal microscopy is based on removing the reflected light from out of focus planes through optical filters. Therefore, it enables a subsequent reconstruction of three-dimensional structures from sets of images obtained at different depths. It is possible to calculate

various structural parameters like roughness or area mean depth using this topography. The roughness showed the arithmetical mean deviation of the assessed profile.

The used device was a Sensofar Plu 2300 confocal microscope (see figure 2.13) with magnifications from 100x to 1000x.

Figure 2.13. Sensofar Plu 2300 confocal microscope.

2.2.2.3. Environmental Scanning Electron Microscopy (ESEM)

The ESEM has been defined as a SEM that can operate with a specimen chamber pressure from high vacuum up to at least a pressure level that can maintain thoroughly wet specimens, up to 609 Pa which is the saturation water vapour pressure at 0°C [2.8]. Thus, it is possible to observe samples that cannot be studied

with a conventional SEM, for example living cells or polymeric materials without a metallic coating, the presence of the gas acts as a charge dissipation medium instead of the conductor layer of the SEM. This technique provides information about superficial topography and microstructure.

In our case, this technique was used to observe the roughness created by micro-structuration over the polymer surface. The equipment used was QUANTA FEG 250.

2.2.3. Thermal analysis

2.2.3.1. Thermogravimetry (TGA)

The thermogravimetry (TGA) allow studying the changes in weight of a sample as a function of temperature and time. Typically, a sample in a balance is introduced into an oven and heated up to high temperature (even up to 1200°C depending on the type of thermobalance model). Weight is registered during the heating of the sample to obtain a curve of weight loss vs temperature [9]. Weight loss may be due to the presence of volatiles, low-boiling temperature components, thermal decomposition and so on. Inorganic residues can also be measured.

In our case, it was used to obtain the amount of TiO_2 of the white-c ABS and the CB from the black-c ABS once the organic material was decomposed. Thermogravimetric analysis (TGA) was performed using a TGA Q5000IR from TA Instruments at a rate of 10°C/min under air atmosphere up to 750°C. Polymer pellets were previously cut into small pieces before analysis.

2.2.3.2. Inductively coupled plasma optical emission spectrometry (ICP-OES)

The Inductively coupled plasma optical emission spectrometry (ICP-OES) uses a plasma flame to produce excited atoms and ions that emit electromagnetic radiation at wavelengths characteristic of a particular element. This technique is used to detect metal particles in other mediums.

In our case, it was used to obtain the amount of TiO_2 forming the white-c ABS. ICP-OES was performed using an IRIS ADVANTAGE of Thermo Jarrel Ash. ABS pellets were first calcinated at 500 °C for 5h before ICP-OES analysis.

2.2.4. Contact angle goniometer

The contact angle goniometer is a device that allows measuring the angle formed by a drop of water over a surface, the contact angle, which will be dependent on the interaction between the liquid and solid surfaces. Two types of measurements can be done, the static and the dynamic contact angle. Also, using different fluid drops the surface free tension can be calculated. The measurement is done using a sessile drop of water of 8 µL. A high-speed camera records the fall and stationary state of the drop over the surface, the static contact angle. Also, it is possible to tilt all the equipment measuring the dynamic contact angle.

The equipment used was a Theta Lite Optical Tensiometer from Biolin Scientific, see figure 2.14.

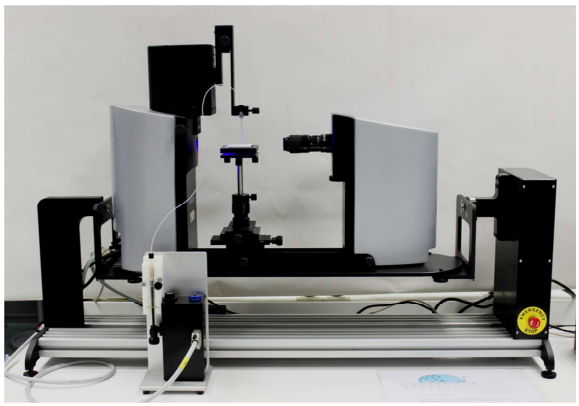

Figure 2.14. Photograph of the contact angle device used in this work.

References

[2.1] Kronos®, "Kronos® 2500," 2017. [Online]. Available: http://kronostio2.com/en/products/kronos-pigments-for-plastics/kronos-2500. [Accessed: 28-Oct-2017].

[2.2] Kronos®, "Kronos® 1071," 2017. [Online]. Available: http://kronostio2.com/en/products/kronos-special-grades/kronos-1071. [Accessed: 28-Oct-2017].

[2.3] The Cary Company, "PRINTEX® 90 Powder," 2017. [Online]. Available: http://www.thecarycompany.com/carbon-black-printex-90-pwd#specifications. [Accessed: 28-Oct-2017].

[2.4] Merck, "Iriotec® 8835," 2017. [Online]. Available: http://www.merck-performance-materials.com/en/product_finder.html?type=PM&pmView=detail&productNo=104786&productId=1365&language=en&asimoid=000000120002571200040023&owner=MDA&unit=CHEM. [Accessed: 28-Oct-2017].

[2.5] R. W. G. Hunt and M. R. Pointer, *Measuring colour*, 4th ed. Chennai, India: John Wiley & Sons, Ltd., 2011.

[2.6] Y. Lam and J. H. Xin, "Evaluation of the quality of different D65 simulators for visual assessment," *Color Res. Appl.*, vol. 27, no. 4, pp. 243–251, 2002.

[2.7] Lee H.L. and F. N.T., "X-Ray photoelectron spectroscopy," in *Handbook of Applied Solid State Spectroscopy*, 1st ed., Boston, MA: Springer, 2006.

[2.8] Danilatos G.D., "Environmental scanning electron microscopy," in *In-Situ Microscopy in Materials Research*, 1st ed., Boston: Springer, 1997.

[2.9] T. A. Osswald and G. Menges, *Material science of polymers for engineers*, 3rd ed. München: Hanser, 2012.

3. Aesthetic laser marking on ABS

The marking of polymeric materials is one of the processes integrated into the manufacturing of plastics usually made to identify the material allowing easy evaluation of their main characteristics and tracking. For instance, this procedure is essential for making a correct segregation in recycling technologies, in which a bright and legible mark is desirable to make a proper identification of the material. Traditionally, these marks have been made by including the symbol inside the mould or by embossing, melt imprinting or other legible and indelible process on the polymer surface [3.1], [3.2]. During the past decades, these processes have been gradually replaced by laser marking. Lasers are particularly useful because can be safely integrated into assembly lines, applied to products with different geometries and computer controlled, thus resulting in high reproducibility, speed, and throughput. This technology provides rapid identification in mass production. Moreover, laser marking avoids the use of inks and the pretreatment of the material surface. Applications range from product recognition and identification to the printing of alphanumeric characters and symbols [3.3].

A combination of the effects presented in the section 1.2.5.2 can lead to a permanent mark on the plastic material by laser marking. For instance, laser irradiation can give rise to different phenomena on plastic materials such as engraving, ablation, foaming, carbonisation, photo-reduction, bleaching and colour formation. The legibility characteristics of a mark, such as contrast and minimum width, are dependent on the material properties, i.e. absorptivity, as well as on the laser marking parameters like power density, focal position and processing speed. Usually, laser marking has been carried out employing IR lasers such as CO_2 or Nd:YAG [3.4], [3.5], both based on producing permanent marks involving thermal

polymer degradation. An alternative option is the use of UV wavelength excimer lasers. They have high energy photons that are capable of inducing photochemical reactions resulting in colour changes with negligible thermal side effects [3.6]. Most of the previous studies performed on polymers were carried out using excimer laser sources [3.7]–[3.15]. It has been reported that thermal effects and photochemical processes coexist during ablation [3.16], [3.17] and, on operating with laser fluences below the material ablation threshold, UV photons modify the original polymer surface [3.18], which result on photolytic modification and activation [3.19]. However, the development of high-efficient processes of harmonic generation enables the use of Nd:YAG lasers as available sources for UV wavelength. This THG (third-harmonic generation) lasers have a low cost, good stability and simplicity for industrial processes.

One step further can be the extension of the laser marking to the aesthetical decoration of plastics. This type of marking is intended to provide different functions such as marketing, brand logo or product customisation. In this case, the visibility is not the only essential characteristic, but also the quality and the durability of the marks. They should exhibit a well visible appearance to improve the appreciation of the product quality. Furthermore, the durability is critical to ensure the correct use of the functions during the life cycle of the machine.

This project is focused on achieving high-quality aesthetical marks on the surface of ABS (acrylonitrile-butadiene-styrene) objects. ABS is a material of interest to study the enhancement of aesthetical marking involving a change in colour, for instance from a white pigmented polymeric material to a grey colour. The majority of polymeric materials, including polyolefins and styrenic polymers, are not easy to be marked employing laser technology. The incorporation of some polymer additives makes the plastic receptive to laser light [3.20] and, as a consequence, high contrast and visible marks can be achieved at relatively low laser intensity in the range of IR

wavelengths [3.21]–[3.23]. However, the quality of the marks may be not sufficient for aesthetical applications. In this sense, understanding the influence of the pigments can contribute improving that quality.

3.1 Polymer additives on laser marking

As said above, some polymer additives interact with the laser energy modifying the absorption of the material. The additives can be classified into two types bearing in mind these interactions. On the one hand, those that are designed for other purposes in the life cycle of the polymer, like UV absorbers or pigments, but capable of interacting with the laser beam. On the other hand, those specially designed to absorb the laser energy producing a visible change in the polymer.

Depending on the polymer and additive absorption, the mechanism of laser interaction will vary. For example, if the absorption of the polymer matrix is higher than the absorption of the additives, the matrix dominate all the processes, and the additives only play a role in the thermal diffusion. However, if the additives have a higher absorption, the energy exchange will be the opposite. These changes in absorption can be dependent on the laser pulse width and wavelength, so an in-depth study of the influence of these variables is desirable [3.24].

Pigments like titanium dioxide or zinc oxide (white pigments), or carbon black (CB, black pigment) can act as absorber centres of the laser irradiation. Also, organic dyes dissolved in the polymer matrix may affect the material laser interaction. Finally, even the defects in the polymer like holes or air bubbles may induce local changes in the absorption. We focus on TiO_2 and CB as the most important pigments used for white and black ABS respectively.

TiO_2 is a widely used additive mainly employed as a whitening agent in polymers due to its light scattering properties and excellent thermal and chemical stability. It has been widely used as pigment [3.25]. It can be naturally found in several kinds of rock and mineral sands. This oxide presents a characteristic white colour in a pure form. The pigments are commercialised in a size range between 200 and 350 nm.

TiO_2 absorbs UV-radiation, and it has been described as a powerful photo-catalyst [3.26], the material exhibits a high photo-activity [3.25]. So, this material is also used as a potent UV absorber additive for polymer protection. Furthermore, the small particles characterised by their transparency in the visible range are used as a sun skin protector.

Two crystalline varieties of TiO_2 are usually used as whitening agents, rutile and anatase. A third one can be found in nature, brookite, but it is barely used for this purpose. The rutile form has a refractive index of 2.7 while the anatase refractive index is 2.5. The rutile has a higher opacity and is less photo-catalytically active than the anatase, so rutile is preferred for its use in polymers. Also, a surface treatment is done on the TiO_2 to reduce the degradation of the surrounding polymer by photocatalysis that can cause loss of gloss and chalking effect. The coating is made of alumina or combinations with silica, acting as a barrier. Then the TiO_2 can be used as a UV stabiliser because it can absorb the radiation and transform into heat with minor damage to the polymeric matrix. The material presents a bandgap around 3.0 eV (depending on the particle size and crystalline state, ~3.0 eV for rutile and ~3.2 eV for anatase) responsible for a higher absorption from about 415 nm to lower wavelengths [3.25].

Particular interest presents the so-called black TiO_2. The optical response of the TiO_2 can be changed by hydrogenation, thus increasing the absorption of the visible spectrum extended to infrared region [3.27]. This material is produced by introducing Ti^{3+} defect state and/or oxygen vacancies into the TiO_2 structure [3.28]. Different strategies were used from calcinations at high pressure under H_2 atmosphere [3.27], plasma treatment [3.29], electron beam treatment [3.30] or electrochemical reduction [3.31]. The black TiO_2 exhibits a colour change from white to different grades of grey, blue or black depending on the preparation methods and conditions. The change in

colouration can be associated with a progressive narrowing of the bandgap in addition to a localised band bending caused by the introduction of the hydroxyls groups [3.32]. Therefore, the optical spectrum of the black TiO_2 is profoundly altered mainly in the visible region [3.33], [3.34]. In addition to the previously described, it has been experimentally proved that under intense UV laser irradiation an observable change in colour was detected on TiO_2 [3.35]–[3.39]. It has been reported that this change can be associated with the generation of reduced species of titanium like black TiO_2 [3.35], [3.36], [3.38]. Also, the amount of TiO_2 added to a material can play an essential role in the mark quality [3.21], [3.40].

CB is used in black coloured polymers. This group of manufactured fine-particle products has a variety of different trade names and physicochemical properties, but they share a chemical composition of nearly pure elemental carbon [3.41]. The material is massively produced by the incomplete combustion of heavy petroleum products (furnace process); although other methods are used such as thermal decomposition of acetylene gas or collecting soot from fumes generated by burning oils or pine wood. Their structure is complex; it is formed by a group of particles fused together presenting on their surfaces different functional groups like hydroxyl or carboxyl. The material characteristics are determined by the particle size, the aggregation structure and the functional groups on the surface [3.42]. In addition to its use as pigments on polymers, it is also employed as UV stabiliser or as reinforcing or electrical conductive filler. Therefore, the presence of this additive alters the physical characteristics of the polymer, i.e., the thermal and electrical conductivity and the optical absorption [3.43], [3.44].

As far as the IR wavelength is concerned, the CB can absorb the energy of the laser pulses and, taking into account the interaction time (tens of ns), this energy is directly transformed into an increase in the pigment temperature. This process can

produce pyrolysis and thermal decomposition of the surrounding polymer [3.45], [3.46]. The mechanism in the case of the UV laser source can be mainly characterised by a photochemical effect [3.47]. The interaction with green lasers has been poorly studied although probably both effects may be produced.

Different companies commercialise additives specially designed for enhancing laser marking. These additives are, in general, designed to work on the near IR improving the absorption of the polymer. For example, PolyOne™ or Merck™ sell laser-marking additives designed to be injected together with the plastic material to produce permanent marks. They usually absorb the laser light and convert it into thermal energy. In this way, thermal degradation is produced in the polymer giving rise to foaming or carbonisation, thus producing a mark. These techniques have been proved not to be a suitable solution for white polymers to produce high-quality aesthetical marks. On the other hand, the aesthetical marks on black plastic materials can be produced by foaming between other effects, so an additive that enhanced this may be useful. In this case, the additive Iriotec® 8835 from Merck™ can be an alternative. The compound is an inorganic, mica-based oxide coated base substrate. This additive is designed to transform laser light into heat inducing a colour change in the polymer itself. This additive is designed to be injected together with the raw material, and it is specially appropriated for white marking on dark materials. This additive also gets darker the material acting as a black pigment.

3.2. White ABS laser marking

In the present study, it is reported the laser marking of ABS filled with titanium dioxide (TiO_2). The influence of the pigment TiO_2 is examined employing different samples corresponding to the natural-w ABS charged with various amounts of TiO_2 both rutile or anatase form, and the white-c ABS. See section 2.1.2.1 for a detailed description of these materials. The natural-w ABS samples with different amounts of TiO_2 rutile are displayed in figure 3.1.

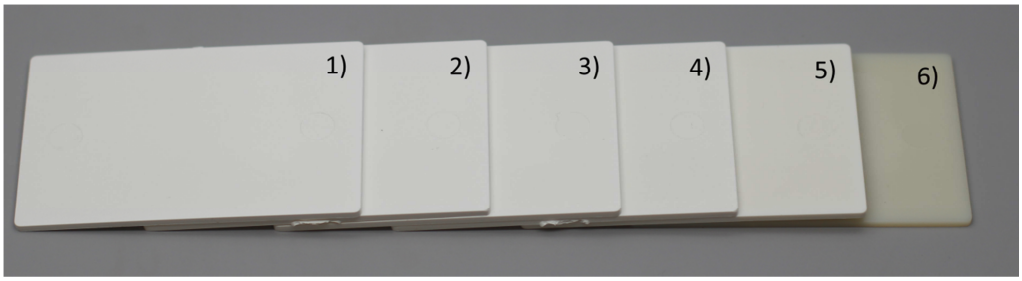

Figure 3.1. Samples of the natural-w ABS charged with different amounts of TiO_2; 1) 8% TiO_2 rutile ABS; 2) 6% TiO_2 rutile ABS; 3) 5% TiO_2 rutile ABS; 4) 4% TiO_2 rutile ABS; 5) 2% TiO_2 rutile ABS; 6) natural-w ABS.

The laser marking was done using three different laser wavelengths: 355 nm (UV), 532 (Green) and 1064 nm (IR). The lasers used were the three industrial devices introduced in the section 2.1.1, the IR laser, the green laser and the UV laser. These lasers were chosen to compare the different effects that can be induced in the selected polymeric materials. The use of UV lasers on plastics materials has been scarcely described in comparison with IR or green lasers, which may provide new possibilities on the marking of plastics.

The laser marking was done using the same fluence for the three lasers to compare the effect of the wavelength. As the limiting factor was the power of the UV laser, the selected power was 2 W. The optical configuration used for the three lasers

was those that produced a spot width close to 100 µm. The green laser did not have any optical configuration with that spot width, so it was obtained by placing the sample out of the focal position. Therefore, the fluence used was around 1.7 J/cm^2 in all the cases. Also, the laser processing was done using DPI (dots per inch, see section 1.2.4.3) from 100 to 1200 in successive steps of 100 DPI considering symmetry for both axes (speed and hatch).

This study begins analysing the optical properties of the unmarked material to continue with the characterisation of the laser marks. Different superficial analyses were carried out to describe the characteristics of the affected surface, including the microstructure, roughness and colour to characterise the quality of the mark. Furthermore, the way in which the chemical structure of the polymer is affected by the UV-laser marking was investigated. For this purpose, several spectroscopic and microscopic techniques were employed.

3.2.1. Preliminary material characterisation

The exact composition of the white-c ABS was unknown; it belongs to the manufacturer business area. Thermogravimetric analysis (TGA) was performed to determine the inorganic residues [3.35]. Thermal analyses were reproducible and the final solid residue detected was around 6.5 wt%, which can be mainly assigned to the white inorganic pigment (see figure 3.2 as an example). The titanium content was also obtained by inductively coupled plasma atomic emission spectroscopy (ICP-OES). The data indicated that the percentage of titanium dioxide was around 6%. The percentages of TiO_2 used to charge the natural-w ABS were selected according to this result and both lower and higher percentages were selected. However, the use

of a higher amount of additive did not enhance the results, so only one amount higher than 6% was selected.

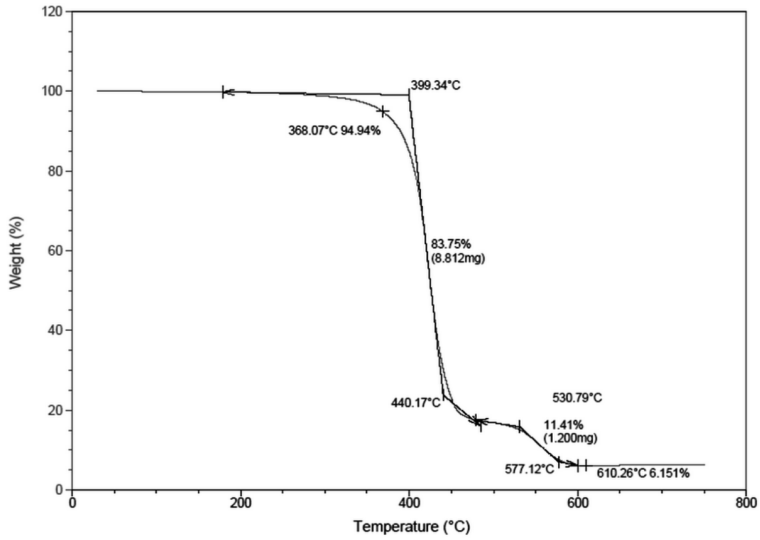

Figure 3.2. TGA of the white-c ABS unmarked.

Before the laser marking, the optical properties of the different polymeric samples were studied. Figure 3.3 shows the optical absorption from 350 to 1200 nm of the X% TiO_2 rutile ABS and natural-w ABS. The units of the vertical axis are arbitraries and normalised to 100 (the same scale it was also used for the black materials); the results should be taken as a relative for a comparative study. The vertical dashed lines represent the wavelength of the lasers used in the marking process: IR (1064 nm), green (532 nm) and UV (355 nm).

Concerning the absorption changes due to the incorporation of TiO_2, in the visible and near IR region (450-1200 nm), the presence of TiO_2 decreased the absorption when the amount of the additive increased. By contrast, in the near UV (below 400 nm) the materials exhibited a high absorption due to the UV absorber behaviour of TiO_2 [3.25], [3.26], in accordance with bibliography [3.48]. Furthermore, there were slight differences between the different amounts of the TiO_2 in the UV

(changes below 1%) while the spectrum in the visible and IR presented changes decreasing the absorption with the charge of the additive (changes higher of 25%). These changes will influence the behaviour of each laser wavelength. Finally, it is reported on the bibliography that the optical properties of the anatase crystalline form were quite similar to the rutile form although some changes were detected. The anatase absorption for the visible and IR wavelengths is higher than for the rutile form. Also, there is a displacement to lower wavelengths in the absorption increment observed at the near UV for the anatase form compared to the rutile [3.49]. This change is associated with differences in their optical absorption gaps, 3.0 EV (413 nm) for the rutile and 3.2 eV (387 nm) for the anatase [3.25], [3.50], [3.51].

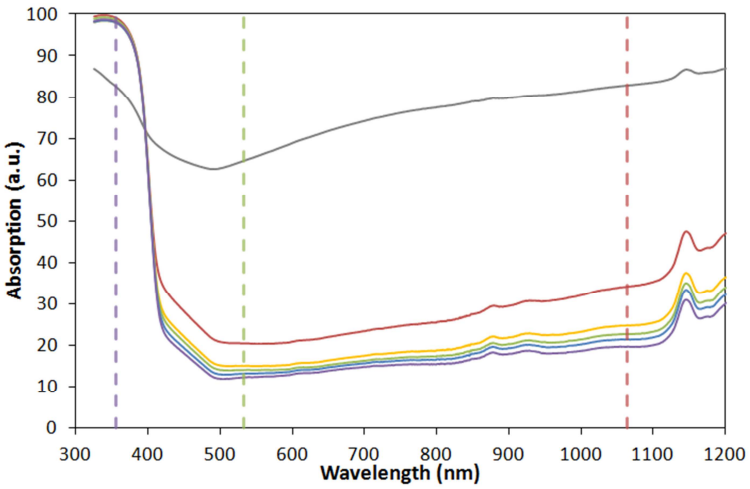

Figure 3.3. The absorption spectrum of the natural-w ABS filled with% TIO_2 rutile. Grey: natural-w ABS line; red: 2% TIO_2 rutile ABS; yellow: 4% TIO_2 rutile ABS; green: 5% TIO_2 rutile ABS; blue: 6% TIO_2 rutile ABS; purple: 8% TIO_2 rutile ABS. The vertical dashed lines represent the wavelengths corresponding to each laser (UV laser: purple line; green laser: green line; IR laser: red line).

In addition to the analysis of the optical spectrum, the CieLab colour parameters (see section 2.2.1.1.) of the samples processed from natural-w ABS samples charged with TiO_2 were measured as a reference for laser marking. Figure 3.4 displays the

evolution of the colour coordinates in terms of the additive amount for both crystalline forms of TiO_2. Only very slight differences were observed for samples containing the rutile or anatase crystalline forms. The evolution was similar for both crystalline forms; the three coordinates tended gradually to saturate. It was remarkable that, while the a* coordinate tended to 0, b* reached a value close to 5 that represent significant differences to colours in the grey scale, the material exhibited a light yellowish appearance. The white-c ABS was also measured, their CIELab coordinates were L* = 92.1 ± 1.5; a* = -1.0 ± 0.5; b* = -0.3 ± 0.5. The commercial compound presented a similar value in the L* coordinate while the a* and b* are almost zero. This difference can indicate the presence of other types of colour additives in this material than the TiO_2.

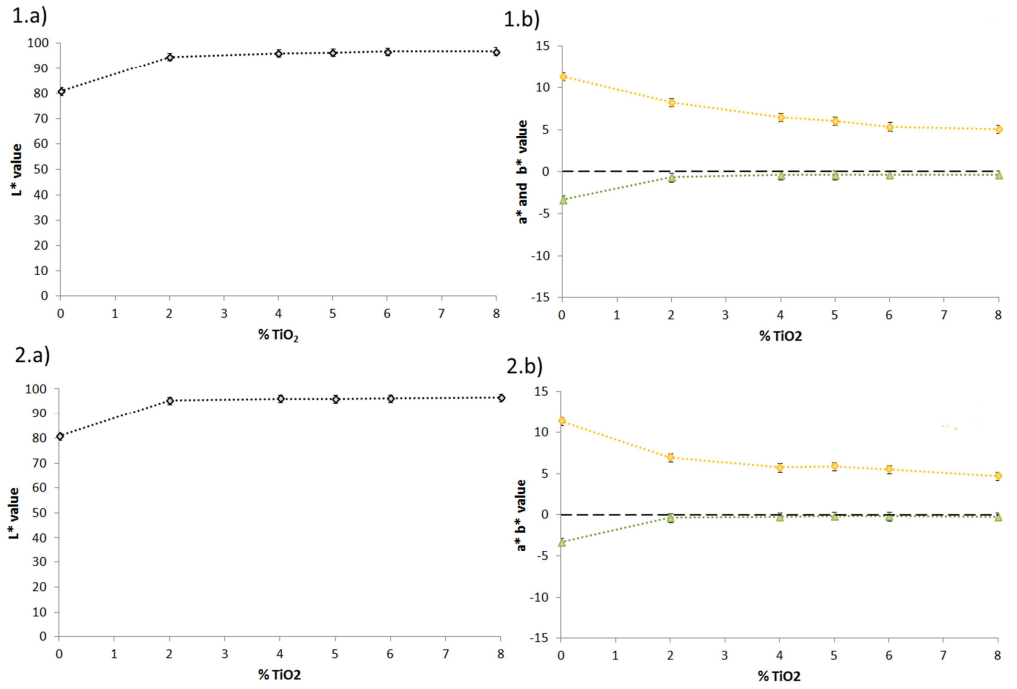

Figure 3.4. Influence of the TiO_2 percentage added to the natural-w ABS of both crystalline forms used 1) rutile and 2) anatase; on the CIELab coordinates a) L*; b) a* (green symbols) and b* (yellow symbols).

3.2.2. Colour changes by laser marking

The natural-w ABS plates with different TiO_2 contents were subsequently marked using the three different lasers irradiating at 355 nm, 532 nm and 1065 nm (UV, Green and IR lasers respectively) with the aim of achieving black marks. The experimental conditions were fixed by varying the DPI from 100 to 1200 DPI (intervals of 100 DPI) and keeping constant the fluence, as it was explained in the introductory part of this section. Laser marks done in samples of natural-w ABS and 2% TiO_2 rutile ABS, as examples of the compounding made with TiO_2, are presented in figure 3.5.

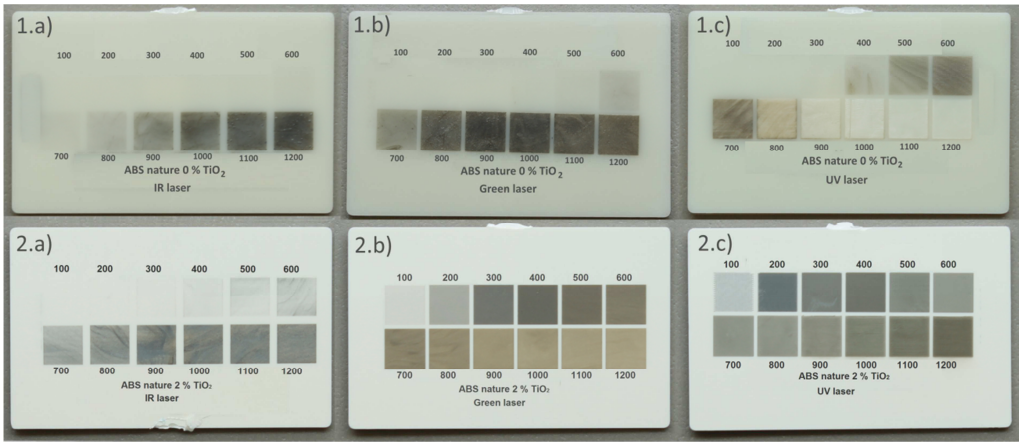

Figure 3.5. Example of some of the laser marks on white ABS plates; 1) natural-w ABS; 2) 2% TiO_2 rutile ABS; a) IR laser marks; b) green laser marks; c) UV laser marks.

The values for the luminosity L* colour coordinate and the contrast Δe*, according to eq. (2.1), were further analysed. The objective was to obtain good black marks, which is directly related to values in the L* coordinate as low as possible. It should be taken into account that the reference colour of the unmarked material was not always the same, see figure 3.4, as depends on the TiO_2 percentage.

The experimental results are presented in three different figures. Figure 3.6 displays a comparative in the L* coordinate between the different laser marks for samples of ABS with different percentage of TiO_2 (including the initial natural-w ABS). Figure 3.7 shows the difference measured in the same coordinate L* between both crystalline forms for each laser only for two compounds, 2% and 6% TiO_2 ABS. Finally, figure 3.8 displays the L* coordinate and the contrast (calculated from the eq. 2.1) considering only the DPI where the best values were achieved for each polymeric compound. However, the contrast should be carefully analysed because it also includes changes in the other two colours coordinates.

Marks made with the UV laser showed the lowest and therefore the best L* values, although the green laser marks values were similar, see figure 3.6. However, the best marks with both lasers were produced at different DPI values, which is a significant difference. The DPI values are directly correlated to the cycle time of the process (see eq. 1.13), the total number of pulses (see eq. 1.12) and therefore to the total energy deposited on the surface. Consequently, it is desirable to keep as low as possible the DPI value to reduce the processing time (a critical factor in an industrial process) and a possible affection to the material related to the increment of the deposited energy. Marks made with the IR laser presented in general higher L* values than the exhibited by marks made with the other laser, although at high DPI values they were similar to those produced by the green laser. According to the absorption curves presented in figure 3.3, the differences between the UV and the green lasers can be associated with their differences in energy absorption. However, the polymers presented a similar absorption on the IR and green wavelengths, so their differences might be associated with different internal mechanisms of interaction between the laser photons and material.

Samples from X% TiO_2 ABS exhibited a different behaviour than the initial natural-w ABS. The presence of the additive enhanced the absorption in the UV wavelength (see figure 3.3). Therefore the use of the laser UV allowed achieving a higher difference between the L* value of the unmarked material and the laser mark. The natural-w ABS marked with the UV laser reached a minimum L* value at around 400-500 DPI to increase again at higher DPI value. However, the L* of UV marks on samples derived from ABS charged with TiO_2 reached a minimum value at low DPI (around 200 DPI) before slightly increased to finally decreasing at DPI higher than 800-900 approx, associated to carbonisation of the polymer. The difference in the case of green and IR wavelength was more challenging to be explained by the absorption spectrum. The presence of TiO_2 added to the natural-w ABS decreased the absorption for both laser wavelengths. Also, the absorption decreased with the increment of the additive amount. However, while taking into account that the L* value difference with the unmarked material reached was similar in the material with pigment than in the natural-w ABS, a significant difference was found in the DPI evolution. The DPI values where the material started to be marked were lower in the natural-w ABS with TiO_2 added being this effect more evident for samples marked with the green laser.

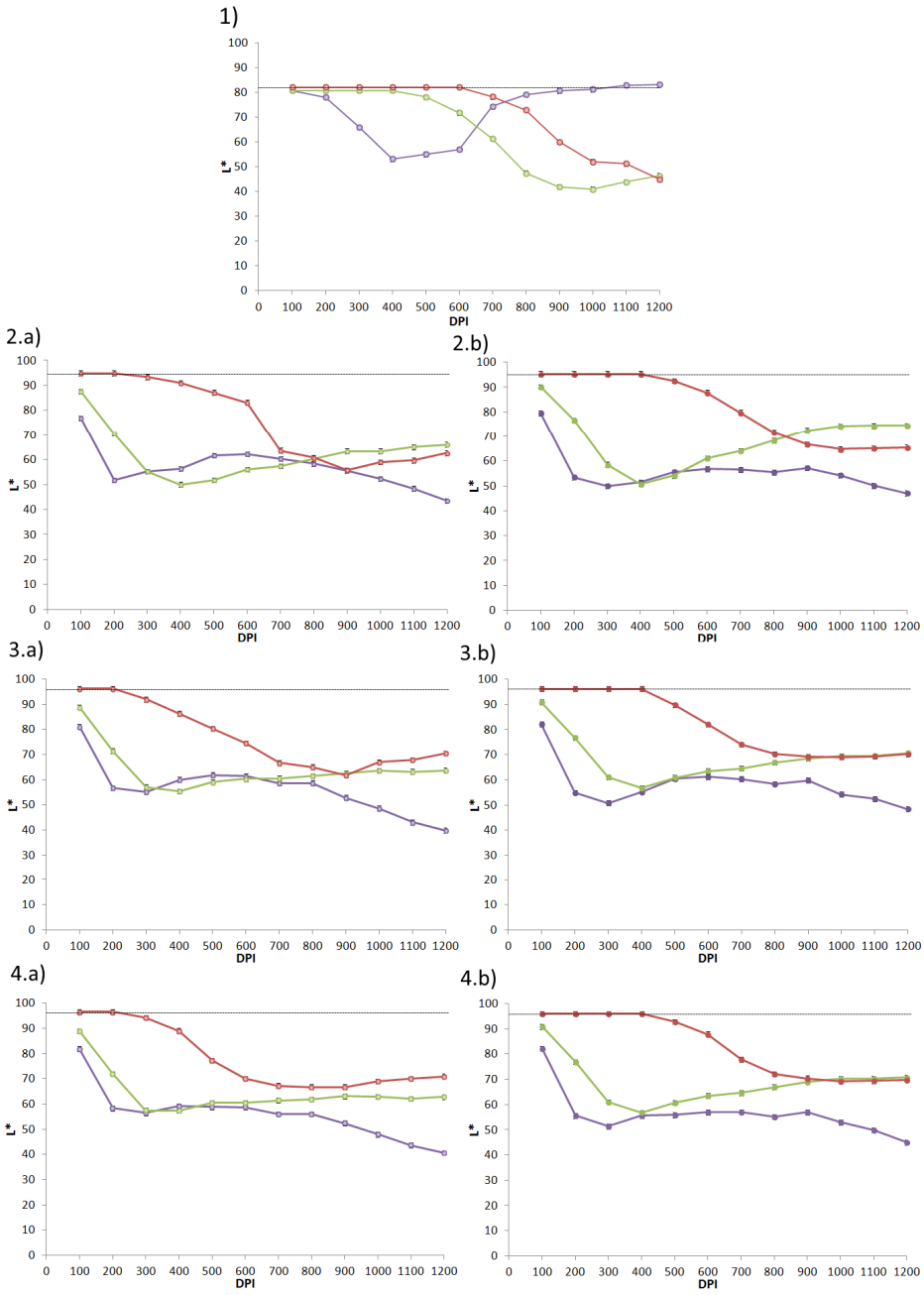

Figure 3.6. Influence of the laser wavelength and the DPI on the L* coordinate value. 1) natural-w ABS; 2) 2% TiO_2 ABS; 3) 4% TiO_2 ABS; 4) 5% TiO_2 ABS; 5) 6% TiO_2 ABS; 6) 8% TiO_2 ABS; a) rutile crystalline form; b) anatase crystalline form. Purple symbols: UV laser; green symbols: green laser; red symbols: IR laser. The black dashed line is the unmarked material L* value. *Continued on next page.*

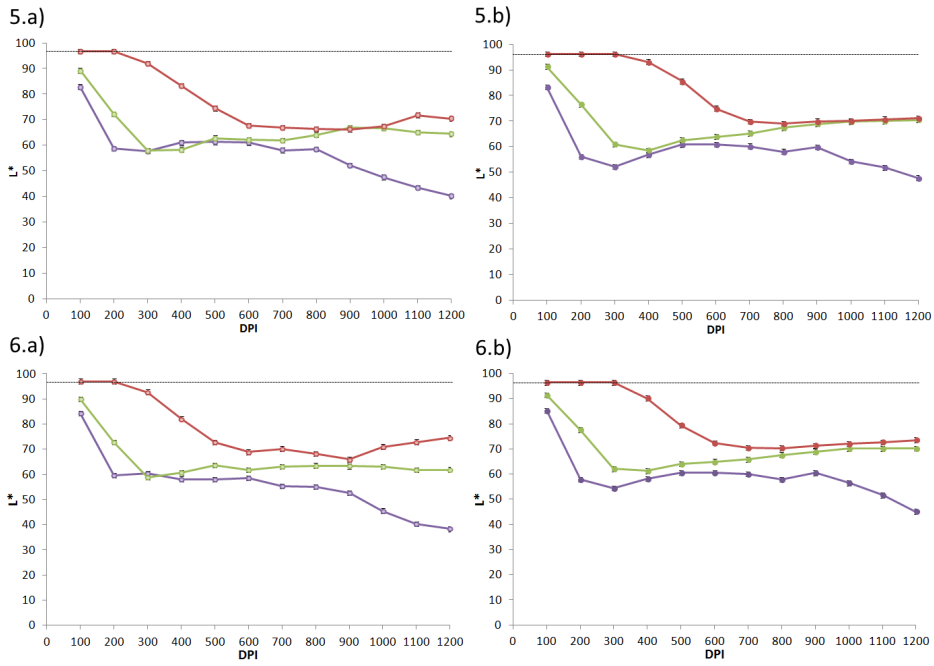

Figure 3.6. (*continuation*) Influence of the laser wavelength and the DPI on the L* coordinate value. 1) natural-w ABS; 2) 2% TiO_2 ABS; 3) 4% TiO_2 ABS; 4) 5% TiO_2 ABS; 5) 6% TiO_2 ABS; 6) 8% TiO_2 ABS; a) rutile crystalline form; b) anatase crystalline form. Purple symbols: UV laser; green symbols: green laser; red symbols: IR laser. The black dashed line is the unmarked material L* value.

The crystalline form of the TiO_2 seemed to have a low influence on the resulting mark, as can be seen in figure 3.7. The TiO_2 rutile presented a slightly better performance than the anatase form under the green laser and especially using the IR laser. By contrast, using the UV laser, the results are similar or slightly better in the anatase form.

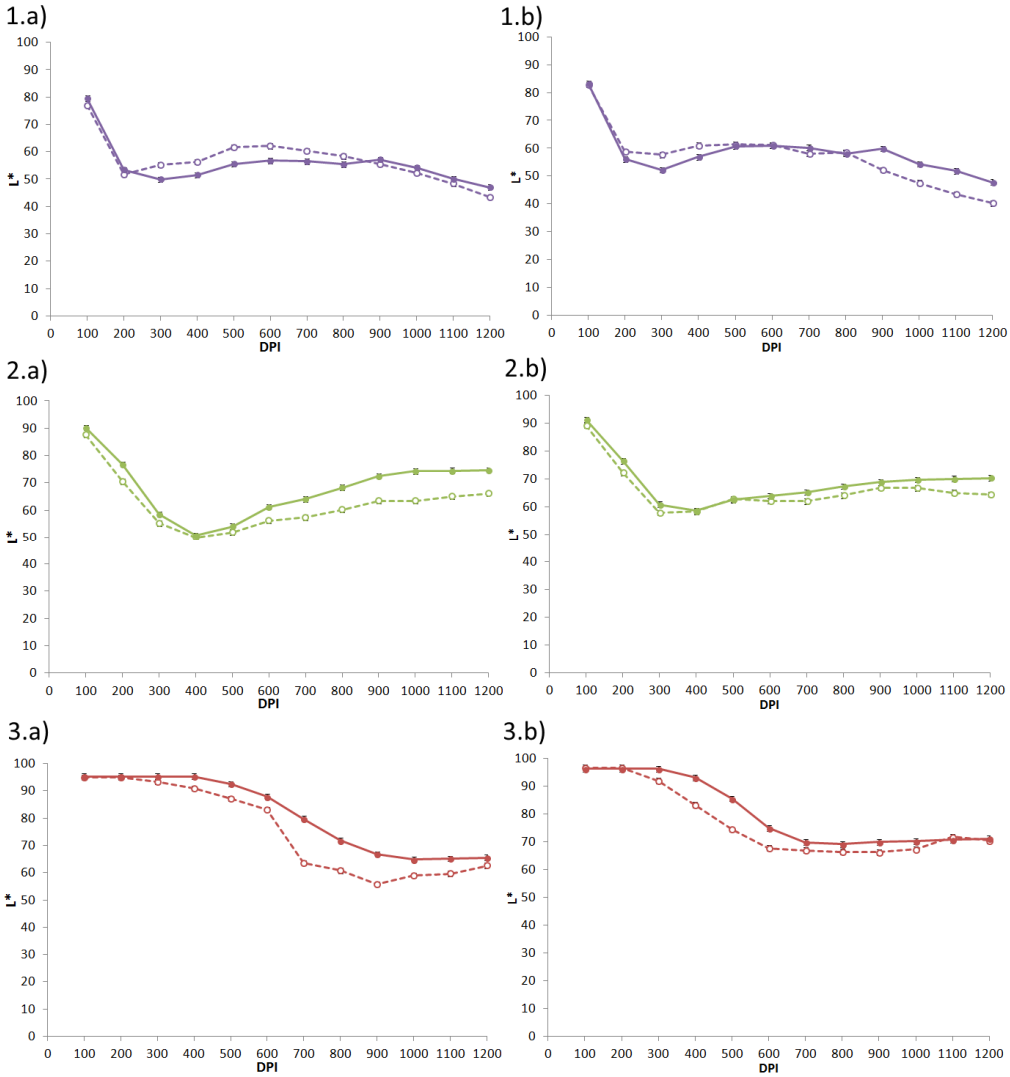

Figure 3.7. Influence of the TiO_2 percentage added to the natural-w ABS on the L* coordinate; 1) UV laser; 2) green laser; 3) IR laser; a) 2% TiO_2 ABS; b) 6% TiO_2 ABS; rutile form: dashed line; anatase form: continuous line.

The evolution of L* and contrast with respect to the amount and crystalline form of TiO_2 can be seen in figure 3.8. According to this figure, the presence of TiO_2 has a clear influence on the marking process meanwhile the percentage of the additive has a minor influence. The best contrast was obtained at samples with 2% TiO_2 for all the laser wavelengths. If the amount of pigment was increased, the reached contrast

slightly decreased. It could be associated with the overall whitening effect of the TiO_2 additive. The UV and green laser have similar contrast for rutile but for anatase form the UV laser seems to have, in general, a better performance. In all the cases, the IR laser achieves less contrast being more significant this effect in the anatase form.

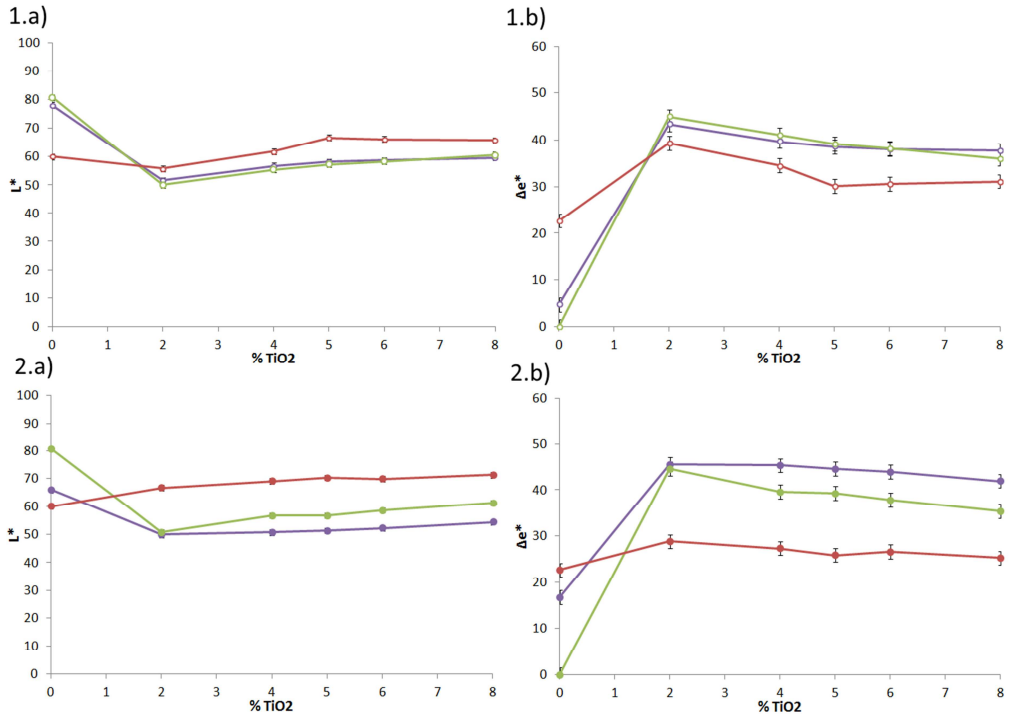

Figure 3.8. Influence of the TiO_2 percentage added to the natural-w ABS (0% means the natural-w ABS) considering only one DPI value (those where the maximum contrast was found in each case) on the colour coordinates. 1) rutile form (UV laser: purple symbol, 200 DPI; green laser: green symbol, 400 DPI; IR laser: red symbol, 900 DPI) 2) anatase form (UV laser: purple symbol, 300 DPI; green laser: green symbol, 400 DPI; IR laser: red symbol, 900 DPI); a) L* colour coordinate; b) contrast Δe*.

According to these results, the colour of the marks depends on the laser wavelength, having better results using the UV laser, and also on the additive amount added and slightly on its crystalline form. So, it can be concluded that the TiO_2 acted as a UV absorber although under the green wavelength its presence also

affected clearly to the results obtained. By contrast, the IR laser seemed not to interact directly with the pigment, and probably the differences observed were related to changes in the thermal properties of TiO_2 containing ABS.

From an application point of view, the results showed that the best L* value was obtained with the UV and green laser on samples processed from 2% TiO_2 rutile or anatase ABS (the values were very similar). However, till now the other two colour coordinates that represent deviations from the grey scale had not been considered. Figure 3.9 presented the values of the colour coordinates a* and b* in the case of the 2% and 6% TiO_2 rutile ABS (the other percentages were similar to those that are shown). The values of a* were in all the cases almost zero, although a significant deviation was produced with the green laser. The evolution of the b* coordinate was different. The unmarked material presented a deviation from the grey scale, especially when the TiO_2 amount is low. The IR tended to produce marks whose values were lower than the unmarked material (dashed line as reference). The UV and green laser marks also exhibited values below the reference at low DPI, in particular in the case of the UV laser. However, at DPI higher than around 400 the green laser-induced yellowing of the material (to a minor extent the UV laser marks also exhibited this behaviour at very high DPI).

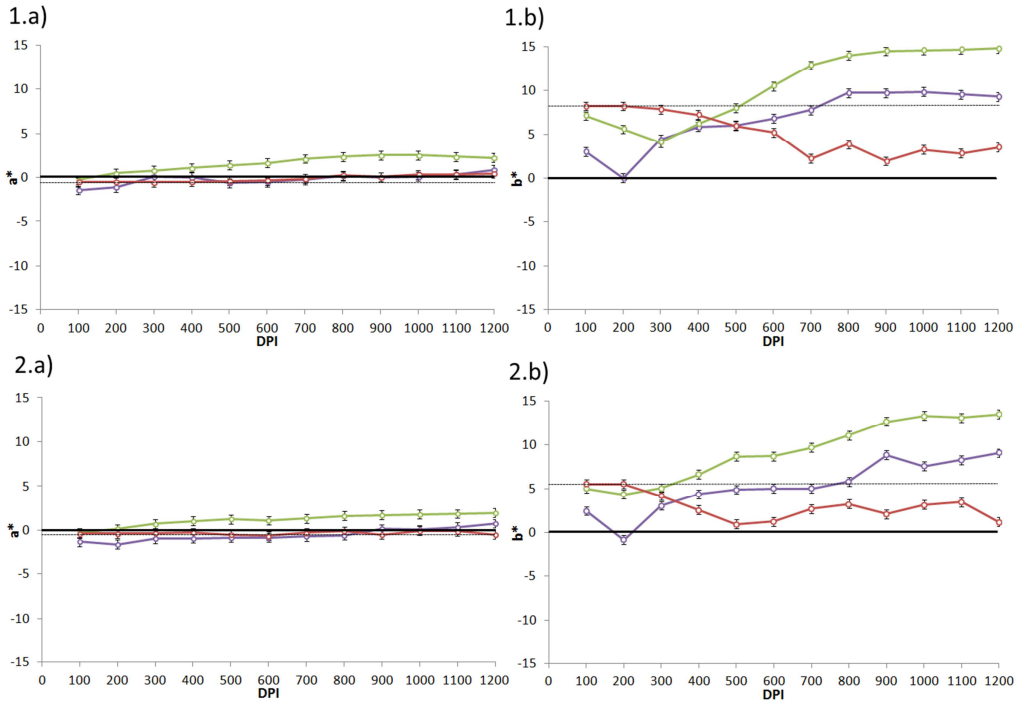

Figure 3.9. Influence of the TiO2 percentage added to the natural-w ABS on the a* and b* colour coordinates. 1) 2% TiO_2 rutile ABS; 2) 6% TiO_2 rutile ABS; a) a* coordinate; b) b* coordinate. Purple symbols: UV laser; green symbols: green laser; red symbols: IR laser. The black dashed line is the unmarked material a* or b* values.

Furthermore, the marking process using the three lasers was done on the white-c ABS, see figure 3.10. The experimental conditions were the same used in the previous experiment, 100 to 1200 DPI keeping the fluence constant between the different lasers.

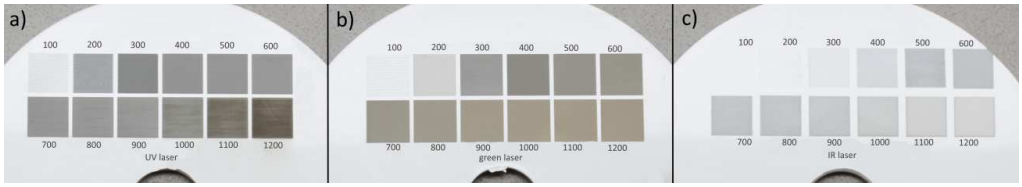

Figure 3.10. White-c ABS marked with the three lasers: a) UV laser; b) green laser; c) IR laser.

Figure 3.11 present the evolution of L* coordinate and the calculated Δe* (eq 4.1) corresponding to the marks shown in figure 3.10 on the white-c ABS. In this case, the UV laser marks exhibited lower L* values and higher contrast than the green and IR laser marks in almost all the cases. The L* value decreased to around 300 DPI, where a minimum was reached, and it remained almost constant at higher DPI values although it decreased slightly from 600 DPI to 1200 DPI. The L* values of marks obtained with the green laser were similar at DPI around 300-500. Finally, the IR laser produced marks with the worst contrast.

Therefore, to select the best aesthetical mark, low DPI values are preferred to minimise surface damage, the UV at 300 DPI or even the green at 400 DPI can be a suitable option for an industrialisation process of this material.

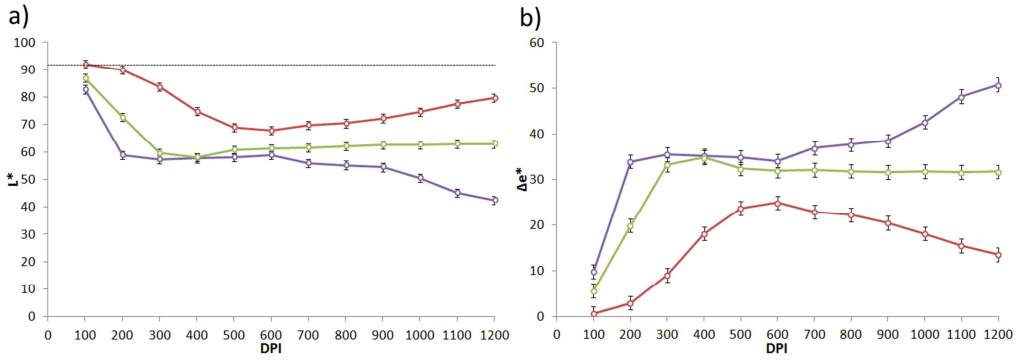

Figure 3.11. Colour coordinates of the laser marks made on white-c ABS. a) L* coordinate; b) contrast Δe*. Purple symbols: UV laser; green symbols: green laser; red symbols: IR laser. The black dashed line is the unmarked material L* value.

Finally, the values of the a* and b* coordinates are showed in figure 3.12. The same effect observed for the X% TiO_2 ABS samples can be seen on the marks made with the white-c ABS, the a* coordinate values were close to zero while the b* coordinate values were significantly different from zero, especially those marks made with the green laser. For example, although the green laser at 400 DPI exhibited L* value close to the UV laser at 300 DPI (both were the best values obtained), the b*

value was higher for the first case than for the second one causing a visible brownish effect in the mark, see figure 3.10.

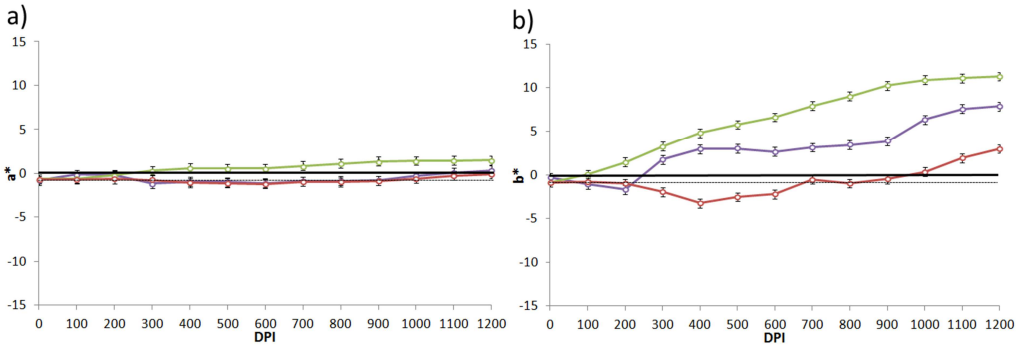

Figure 3.12. Colour coordinates of the laser marks made on white-c ABS. a) a* coordinate; b) b* coordinate. The black dashed line is the unmarked material a* or b* values.

So, considering all the results obtained, the white-c ABS marks were similar to those obtained on the 6% TiO_2 ABS. These results were according to the pigment amount measured using the TGA and the ICP-OES as it was described above in this section.

In addition, reducing the amount of TiO_2 seems to increase the obtained contrast (see figure 3.8), so probably a modification in the white-c ABS might be done in that direction. However, the pigment amount affects to the final colour of the material, so a balance between both factors should be taken into account. Furthermore, the use of the crystalline rutile form is desirable for this application.

3.2.3. Topographical changes on laser marks

This part is divided in the analysis of the surface of the marks and the penetration depth of the laser treatment. The analysis was performed on samples processed form ABS additivated with rutile (the results were similar for both crystalline forms).

3.2.3.1. Surface topography

The surface topography of the marks was studied using confocal microscopy and ESEM, see section 2.2.2. The confocal microscopy was used to obtain the height of the mark compared to the unmarked material, and the mean roughness R_a. The height of the mark provides information about a possible engraving effect (in the case that the mark height is below zero, defined as the surface level before marking), or a foaming effect (the mark height is above zero). Also, the mean roughness (R_a) can be used to check how the surface is affected. On the other hand, the ESEM allows observing the surface topography in detail for the most interesting cases.

Figure 3.13 shows the mark height and mean roughness measured on the natural-w ABS additivated with different amounts of TiO_2 rutile. Figure 3.14 displays the same values in a comparative, as in the colour analysis, illustrating only the DPI values where the highest contrast was achieved for each polymeric compound and laser.

The differences observed in the natural-w ABS behaviour compared to the material charged with TiO_2 in the colour measurements (see the previous section) can also be observed in the topography. The three lasers produced a foaming effect on the surface of the natural-w ABS. The mean roughness measured on the UV laser marks was higher than the observed for the rest of the marks.

As it can be expected from the colour changes described above, the laser wavelength had a high influence in the final topography of the samples processed from ABS additivated with rutile. The IR laser marks were characterised by overall foaming of the surface, an effect that seemed to saturate at high DPI values. The mean roughness measured presented the same behaviour, in all the cases is below 3 µm. The green laser produced an engraving of the material, more and more evident when the DPI value increased. The mean roughness in this case grown until an approximate value between 3 and 6 µm, and is lower when the percentage of TiO_2 increases. Finally, the UV laser marks exhibited similar characteristics to green laser marks, although the samples that had a content of $TiO_2 \leq 5\%$ showed a more complex behaviour since at low DPI (approx. around 300 DPI) a positive mark height was detected meanwhile an engraving effect was observed at higher DPI. The mean roughness was similar to the exhibited by marks made by grees laser or slightly higher. The measurements tended to a value, close to 6 µm where they stabilised.

The changes between the different $\%TiO_2$ samples denote that, although the colour measurements were similar for all samples, the amount of additive influence the material energy absorption giving rise to a higher material removal by engraving for the green and UV wavelengths. On the other hand, no changes were clearly detected on the IR marks made on samples with different amounts of TiO_2.

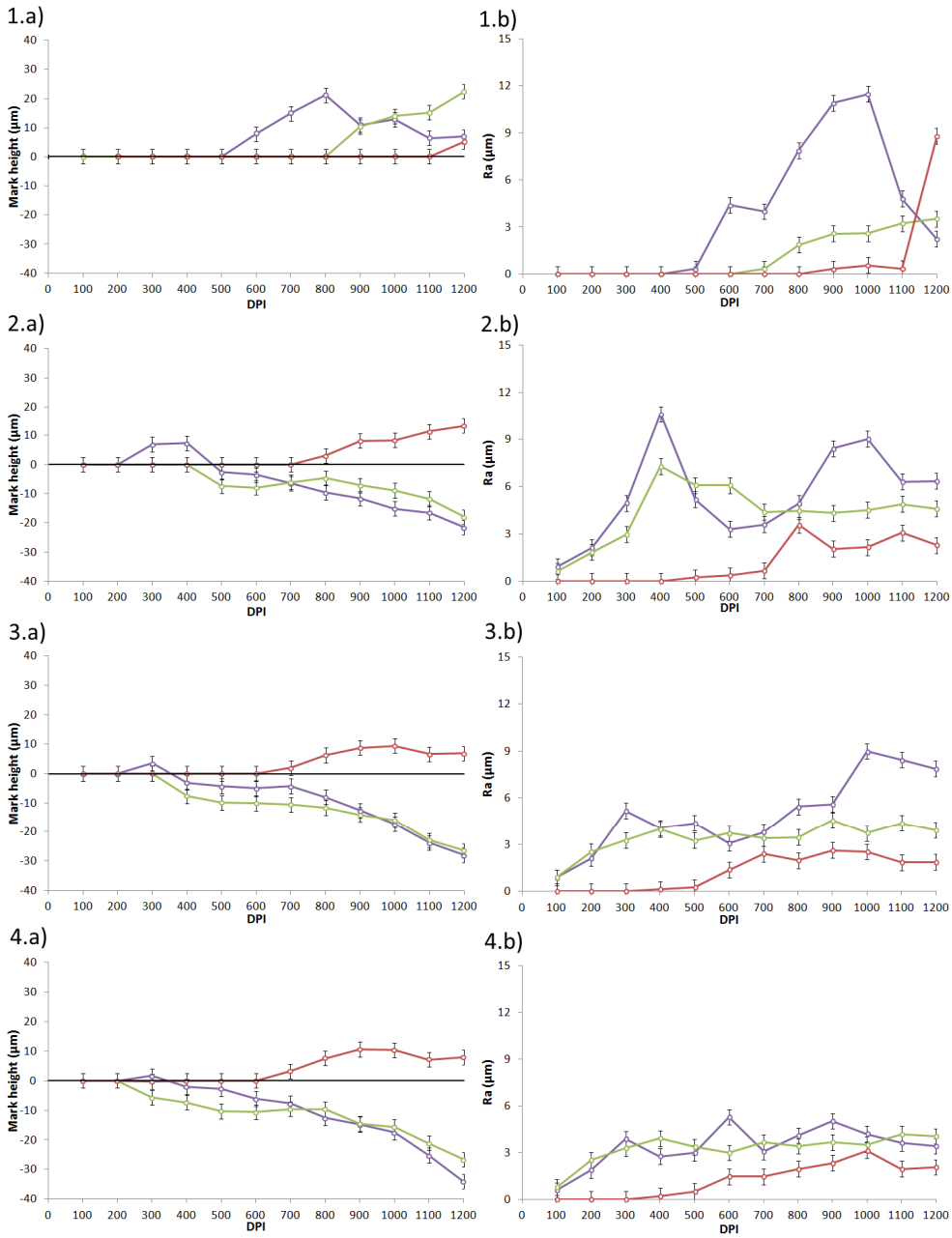

Figure 3.13. Influence of the laser wavelength and the DPI on the surface topography. 1) natural-w ABS; 2) 2% TiO_2 rutile ABS; 3) 4% TiO_2 rutile ABS; 4) 5% TiO_2 rutile ABS; 5) 6% TiO_2 rutile ABS; 6) 8% TiO_2 rutile ABS; a) mark height; b) Ra. Purple symbols: UV laser; green symbols: green laser; red symbols: IR laser. *Continued on next page.*

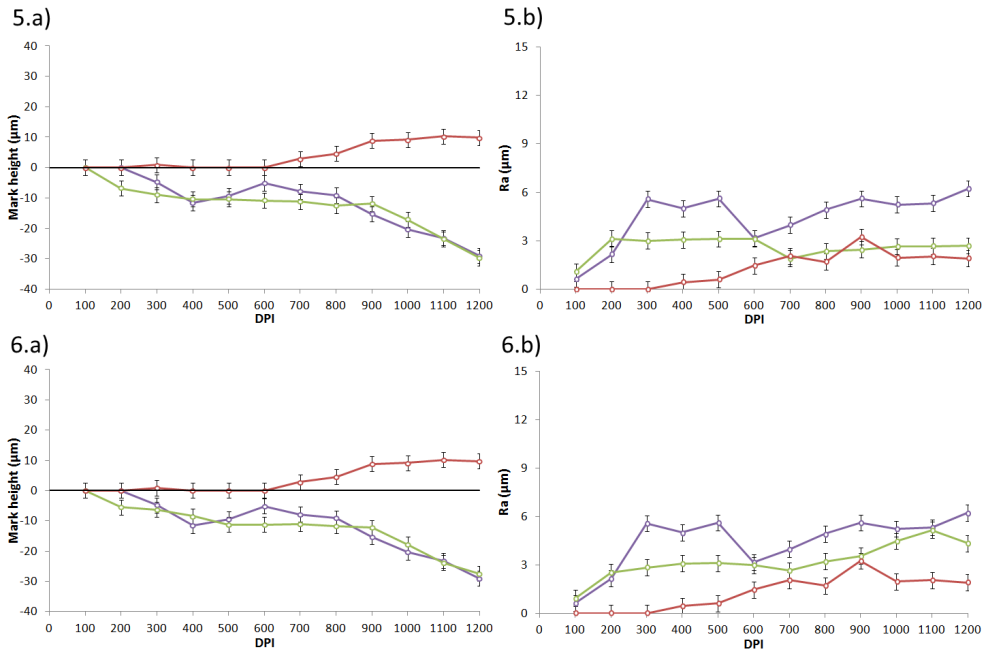

Figure 3.13. (*Continuation*) Influence of the laser wavelength and the DPI on the surface topography. 1) natural-w ABS; 2) 2% TiO_2 rutile ABS; 3) 4% TiO_2 rutile ABS; 4) 5% TiO_2 rutile ABS; 5) 6% TiO_2 rutile ABS; 6) 8% TiO_2 rutile ABS; a) mark height; b) Ra. Purple symbols: UV laser; green symbols: green laser; red symbols: IR laser.

Finally, considering only the best colour marks measured in terms of the L* coordinate for each compound in figure 3.14, the differences for each laser were clear. As it was mentioned before, the IR laser marks were characterised by foaming of the material while the green laser marks presented an engraving of the polymer, an effect that grew when the additive amount was increased. The UV laser marks did not exhibit an appreciable height profile change (considering sample with the best contrast). Also, the mean roughness values were in the same direction.

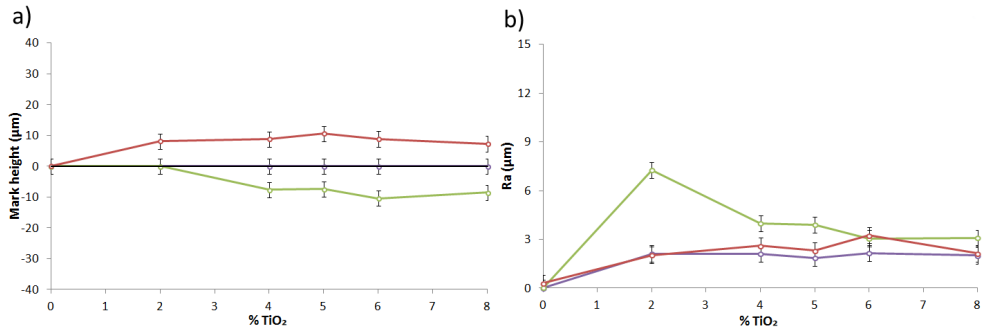

Figure 3.14. Influence of the TiO_2 rutile percentage added to the natural-w ABS considering only one DPI value (those where the maximum contrast is found in each case) on the surface topography. Purple symbols: UV laser, 200 DPI; green symbols: green laser, 400 DPI; red symbols: IR laser, 900 DPI; a) Mark height; b) Ra.

Additionally, the topography of the white-c ABS marked with the three lasers was studied, see figure 3.15. The evolution of the depth for each laser was different; the IR produced a foaming effect, the UV engraving meanwhile the green seemed not to modify the surface until high DPI values. By contrast, the roughness was higher when the green laser was used.

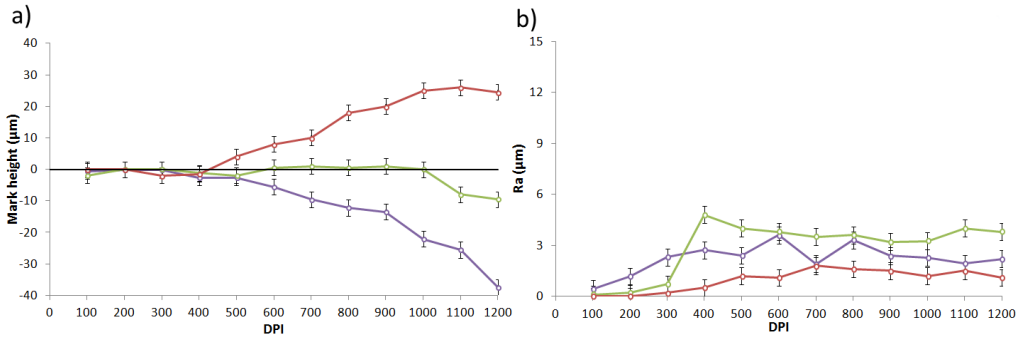

Figure 3.15. Surface topography of the laser marks made on white-c ABS. Mark height; b) Ra. Purple symbols: UV laser; green symbols: green laser; red symbols: IR laser.

Figure 3.16 presented a three-dimensional image of the topographical profile for two different DPI values in the UV laser marks. As can be observed, the engraving effect was visible when DPI increased, and the marked area exhibited a roughness in accordance with the R_a values measured.

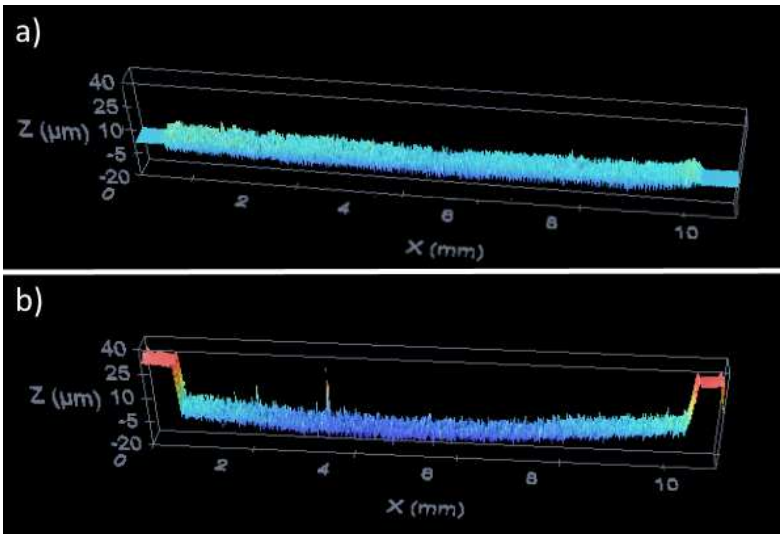

Figure 3.16. Three-dimensional profile confocal images of the marked zone by the UV laser on white-c ABS. a) 400 DPI; b) 1200 DPI. The area under the laser effect is in the middle of each figure, while both edges are the unmarked area.

Finally, using the ESEM, it was possible to observe the marked surface with high detail. Figure 3.17 presents two of the marks made on the white-c ABS by the UV laser. The mark of 400 DPI was selected because had the lowest L* value measured together with low total energy deposited on the surface. By comparison, the energy deposited was the highest in the 1200 DPI mark. Also, the ESEM allowed measuring the chemical composition by EDX in the studied samples.

The 400 DPI mark exhibited a surface with a fibrous structure. By contrast, the 1200 DPI also showed a rough surface but apparently with clusters of polymeric material. The difference in the laser processing of both surfaces was the DPI value that it is directly correlated to the processing speed and hatch distance (eq. 3.10 and

eq. 3.11). Therefore, it seemed that at low DPI the surface suffered a temperature increment that might cause the material to melt and solidify again forming a fibrous structure, but the total material ablated was not high. By contrast, if the DPI number was high, the material suffered an important surface ablation (see figure 3.16.b).

The images with high magnification (see figure 3.17.b images) allowed distinguishing several white dots that were specially detected in the 1200 DPI mark. EDX analysis revealed that these points mainly correspond to TiO_2 particles; the intensity of the signal corresponding to the Ti element was three times higher than in the rest of the material.

Finally, the images with the highest magnification used (see figure 3.17.c) exhibited a similar structure in both marks, a small dotted structure appeared.

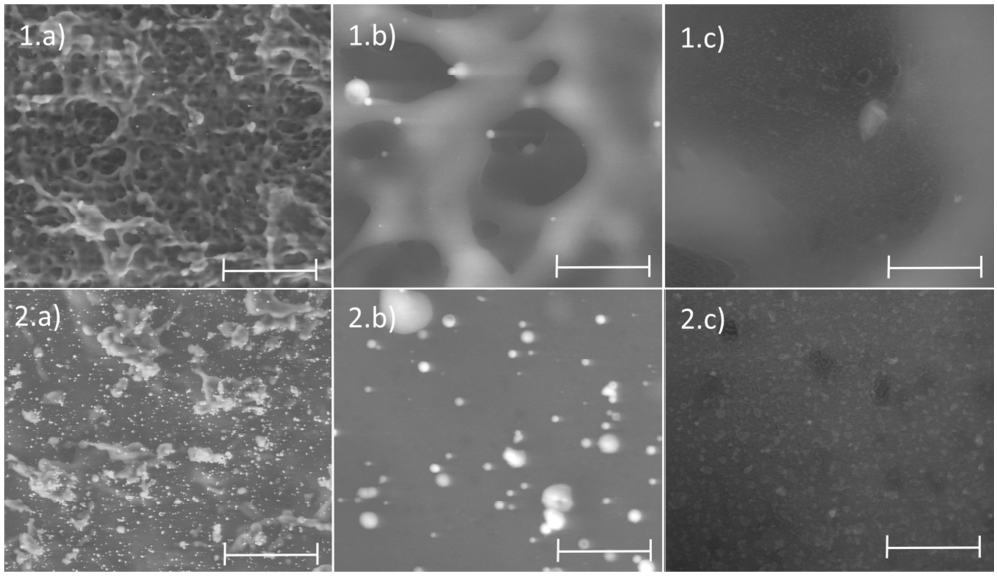

Figure 3.17. ESEM images of the surface of a marked white-c ABS with the UV laser: 1) 400 DPI; 2) 1200 DPI. a) 2800x, scale bar 30 µm; b) 24000x, scale bar 3 µm; c) 80000x, scale bar 1 µm.

3.2.3.2. Penetration depth of the laser changes

The transversal view of the marks give information about how deep is the penetration of the laser changes inside the material and also if there are differences under the surface depending on the laser wavelength like bubbles trapped. The marks were observed transversally by a stereoscopic microscope. Samples, once laser marked, were immersed in liquid nitrogen and then fractured.

Figure 3.18 presents the evolution of the penetration depth of the laser changes, studied using a stereoscopic microscope, on samples marked with the different lasers (UV, green and IR). Samples of the initial ABS (before mixing with TiO_2) exhibited visible changes at deeper regions than the pigmented material; TiO_2 seems to decrease the penetration of lasers or smooth the changes. However, there were no significant changes in samples with different percentage of the additive. The penetration of the green and UV lasers was quite similar, around 30 µm in all the cases, while for the IR laser marks the changes were detected until approximately 60 µm.

The difference in the penetration depth for the IR wavelength can be associated to the absorption spectrum (see figure 3.3). However, the green and UV laser exhibited approximately the same values while the material absorption for those wavelengths was different. Again, it seemed that the green laser interacts with the additive and the energy was absorbed faster than with the IR wavelength.

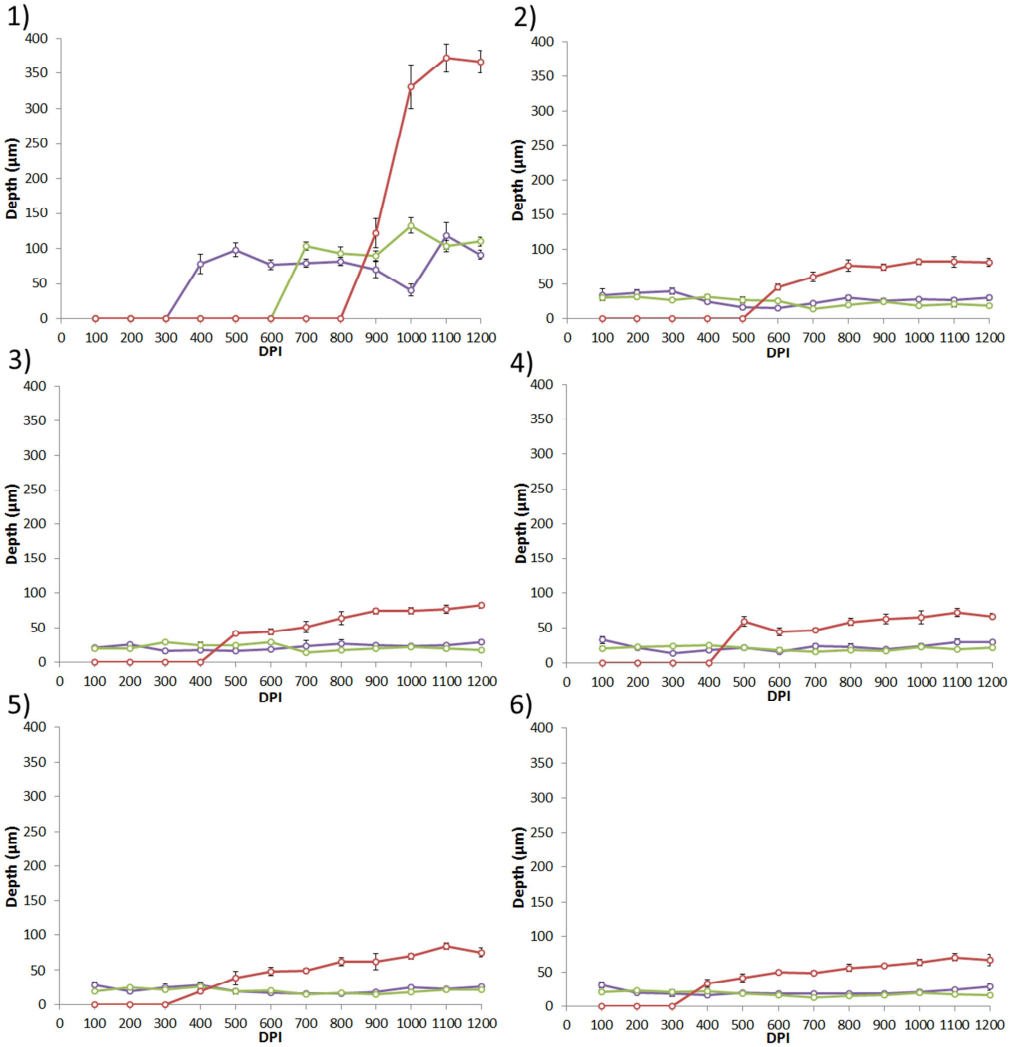

Figure 3.18. Transversal depth obtained from the cross-section observed by stereoscopic microscope for the laser marks on natural-w ABS filled with TiO_2 rutile. 1) natural-w ABS; 2) 2% TiO_2; 3) 4% TiO_2; 4) 5% TiO_2; 5) 6% TiO_2; 6) 8% TiO_2. Purple symbols: UV laser; green symbols: green laser; red symbols: IR laser.

3.2.4. Chemical changes on laser marks

The characterisation of chemical changes produced during the marking process was carried out by ATR-FTIR and XPS, see section 2.2.1.

3.2.4.1. ATR-FTIR analysis

By ATR-FTIR spectroscopy, it is possible to detect changes in the functional groups of the polymer due to the laser marking the process, as the IR spectra of the surface material are measured (see section 2.2.1.3). Spectra of marked samples of the different ABS were registered from 4000 to 600 cm^{-1}. Similarly, the samples were analysed before and after being processed by laser.

The spectrum of natural-w ABS before the laser treatment was compared with ABS spectrum found in the bibliography. Main peaks (cm^{-1}) are: 3028, 2921, 2858, 2244, 1602, 1496, 1454, 966, 910, 759, 698. The signal at 2244 cm^{-1} corresponds to CN stretching vibration from nitrile group (acrylonitrile). Peaks at 1602 cm^{-1} and 1496 cm^{-1} corresponds to stretching vibrations while 759 cm^{-1} and 698 cm^{-1} are associated with deformation, both of the styrenic rings. The peak at 1454 cm^{-1} corresponds to the scissoring mode of the CH_2. Finally, the unsaturated groups from the polybutadiene phase of ABS correspond to peaks of trans-1,4 (966 cm^{-1}) and vinyl-1,2 (910 cm^{-1}) isomers [3.52]. Experimentally it was found that the peak found at 1454 cm^{-1} remained relatively stable under irradiation, and it was taken as reference.

Figure 3.19 shows the spectrum of the natural-w ABS filled with different amounts of TiO_2 before being irradiated. Peaks corresponding to ABS (i.e. signals corresponding to styrene, acrylonitrile and butadiene monomeric moieties) were detected in all the compounds, as can be expected. There were slight changes in the intensity of peaks and the shoulder detected in the region at 800-600 cm^{-1} (due to the titanium dioxide), in this case, the variation was clearly detected. Figure 3.20 shows

a zoom of this area. The intensity of these peaks slightly decreased with the increment of %TiO_2. By contrast, the shoulder close to 600 cm^{-1} exhibited a different behaviour; its intensity grows when the amount of the additive was increased. These changes may be associated with the presence of an additive, and this region can provide information about alterations in the additive structure due to laser irradiation.

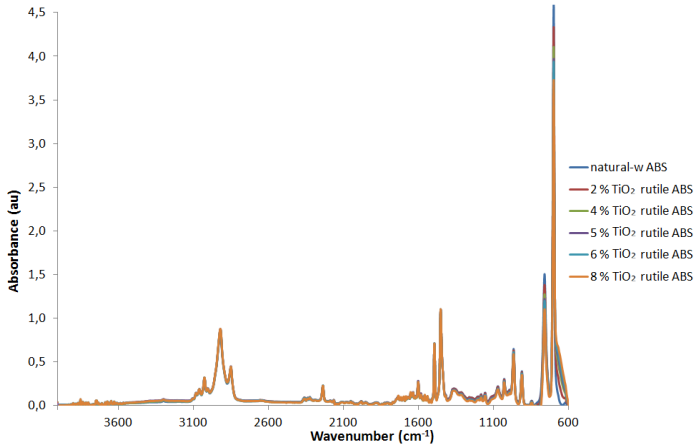

Figure 3.19. ATR-FTIR spectrum of the samples of natural-w ABS filled with different %TiO_2 before laser marking.

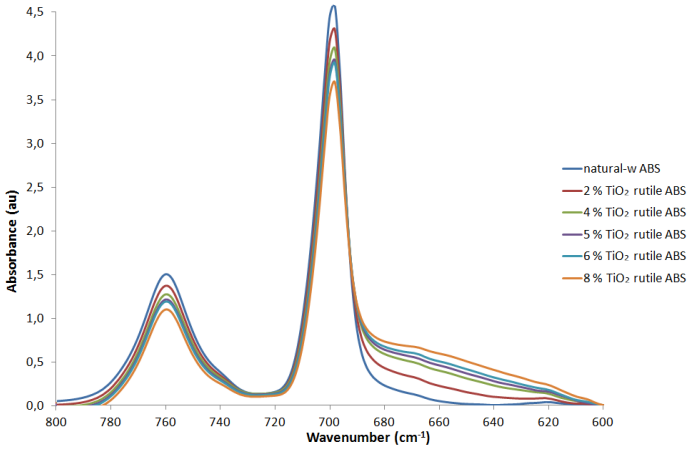

Figure 3.20. Zoom on the area corresponding to 800 to 600 cm^{-1} of the ATR-FTIR spectra of the natural-w ABS filled with different %TiO_2 rutile before laser marking.

The ATR-FTIR spectra of different laser marks were measured and compared with the unmarked material. The peaks obtained were the same, although there were minor changes in the intensities of some peaks. Again, a zoom was done in the area between 800 and 600 cm^{-1}, see figure 3.21. The spectra were almost identical, and only the peak of 698 cm^{-1} was slightly affected in the case of the UV laser, while the spectrum of the green and IR laser marks remained unaltered.

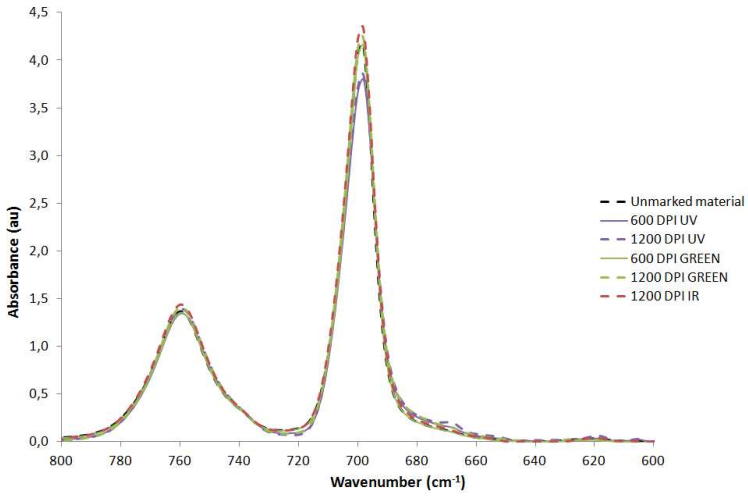

Figure 3.21. Zoom on the area corresponding to 800 to 600 cm^{-1} on the ATR-FTIR spectrum of the marks done with the different lasers on the natural-w ABS compared to the unmarked material (the mark done with the IR laser at 600 DPI is not displayed because the material was visible unaffected by the laser at those parameters).

As an example of the spectra of the laser marks on ABS additivated with TiO_2, figure 3.22 shows the ATR-FTIR spectra of the marks done on samples of 5% TiO_2 rutile ABS. As can be seen, the spectra correspond to ABS, and there were no significant changes with respect to the spectrum of the unmarked area. Figure 3.23 displays a zoom of the region from 800 to 600 cm^{-1}. Although both peaks remain, they exhibited changes in their intensities depending on the laser wavelength, being more accused this effect with the UV wavelength. Furthermore, the part of the

spectrum corresponding to the shoulder was affected by the green and UV wavelength while the IR laser marks seemed not to be altered. The most significant modification observed correspond to the mark done at 600 DPI with the UV. These effects were observed on all the ABS samples charged with TiO_2.

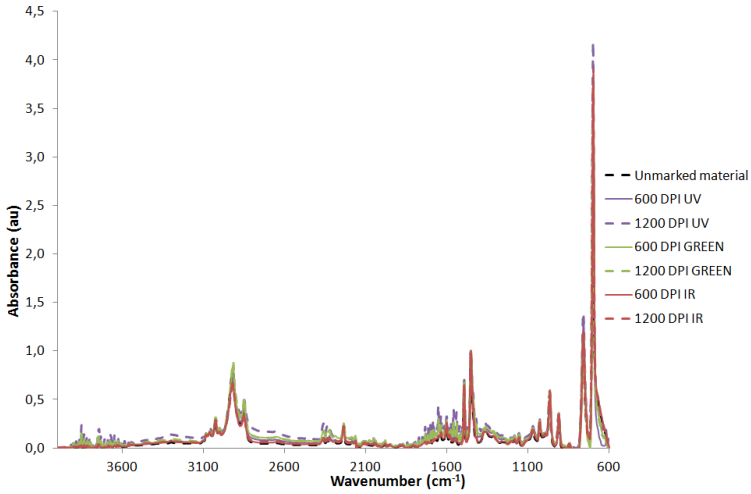

Figure 3.22. ATR-FTIR spectrum of the marks made with the different lasers on samples of 5% TiO_2 rutile ABS compared to the unmarked material.

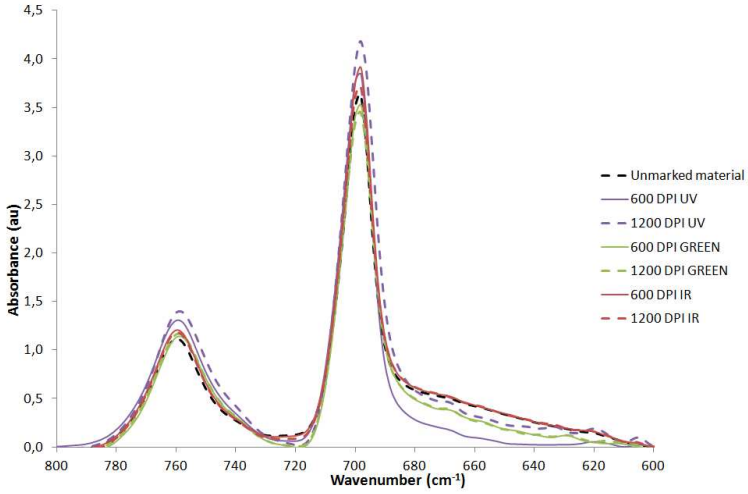

Figure 3.23. Zoom on the area corresponding to 800 to 600 cm^{-1} on the ATR-FTIR spectrum of the marks done with the different lasers on the 5% TiO_2 rutile ABS compared to the unmarked material.

Figure 3.24 shows a comparison between some UV laser marks at 600 DPI on natural-w ABS filled with different amounts of TiO_2. The behaviour of the signal intensity of both peaks seemed to grow with the marking process, although no clear tendencies were detected. On the other hand, the shoulder corresponding to the TiO_2 is affected by the laser irradiation. The intensity detected on the laser marked samples was between the 2% TiO_2 rutile ABS and the natural-w ABS curves.

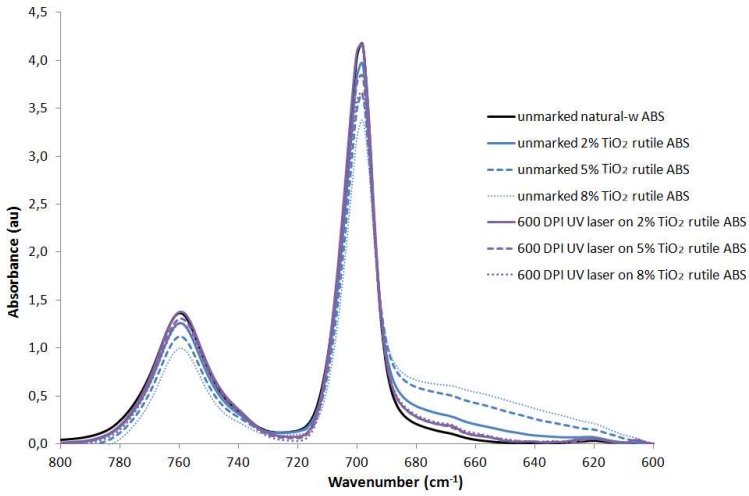

Figure 3.24. Zoom on the area corresponding to 800 to 600 cm^{-1} on the ATR-FTIR spectrum of the marks made with the UV lasers on natural-w ABS filled with different %TiO_2 rutile compared to the unmarked material.

Therefore, the ATR-FTIR techniques showed that there were no significant modifications in the functional groups. However, changes were observed in the shoulder of the region around 660 nm that can be correlated to the TiO_2 added the natural-w ABS. Furthermore, it was observed that the UV laser affected the intensity of this area while these changes happened to a lesser extent for the green laser marks and were not detected on IR laser marks.

In addition, this analysis was extended to the white-c ABS. No significant differences were observed in the signal of the unmarked commercial material in

comparison with the rest of the ABS used. There were only changes in the intensity of the area between the peaks probably associated with the presence of some additives in the commercial material. Also, it was detected the appearance of the final tail near to 600 cm^{-1}, which previously it had been associated with the TiO_2 molecule.

Finally, the affection of the material after the laser processing was examined. As in the previous cases, there were no modifications in the peak distribution after the laser treatment, only the intensity had changed in some cases. Figure 3.25 displays the spectra of the marks presenting the best contrast for each laser together with the unmarked material in the area corresponding to 800 to 600 cm^{-1}. The effects observed were similar than those detected in the ABS charged with TiO_2, the UV and the green lasers decreased the signal in the zone of the shoulder. This modification was more significant for the UV wavelength. On the other hand, the IR laser even increased the shoulder signal, although it can be related to the increment observed in the peaks signal.

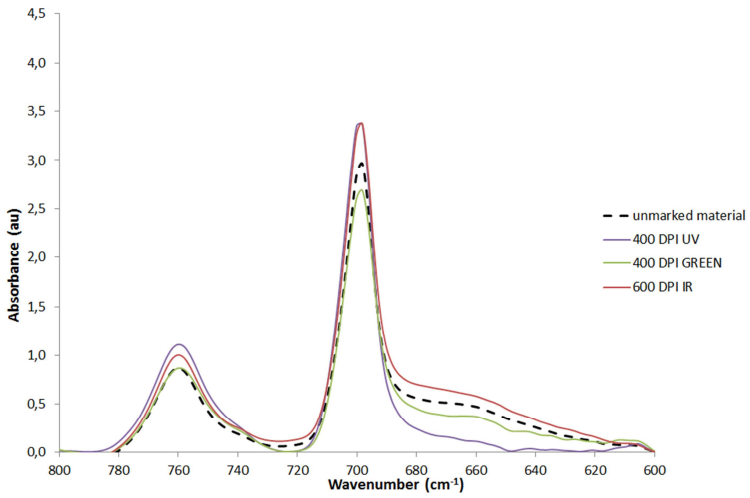

Figure 3.25. Zoom on the area corresponding to 800 to 600 cm^{-1} on the ATR-FTIR spectrum of some representative marks made with the lasers on the white-c ABS compared to the unmarked material.

Therefore, the ATR-FTIR allowed to examine the influence of the TiO_2 additive in the ABS and to observe its modification after the laser treatment. It has seen that the pigment altered the signal meaningfully in the final part of the spectrum, especially those corresponding to the shoulder of the 698 cm^{-1} peak. Also, the signal of this area was modified depending on the laser wavelength. The highest changes were detected in those laser marks made by UV laser. The green laser seemed to modify that signal too, although to a lesser extent. Finally, the IR wavelength was not able to modify this part of the spectrum.

3.2.4.2. XPS analysis

X-ray photoelectron spectroscopy (XPS) provides information about the elemental composition and electronic state of the elements presented in the material surface (see section 2.2.1.4). This technique allows detecting changes in the irradiated surface and, in particular, in the TiO_2 additive as they were observed using the ATR-FTIR. The sample containing the highest amount of pigment was selected to ease that molecule changes observation on the polymer under the laser. The calibration was done in all the cases using the C-C at 284.9 eV. The selection of the peaks energies was made according to references provided by the equipment manufacturer [3.53], [3.54].

The survey spectrum of the 8% TiO_2 is shown in figure 3.26. The signal corresponding to the Ti^{4+} was detected around 455 eV, although it was very weak. As could be expected, the peak corresponding to C atoms was the highest.

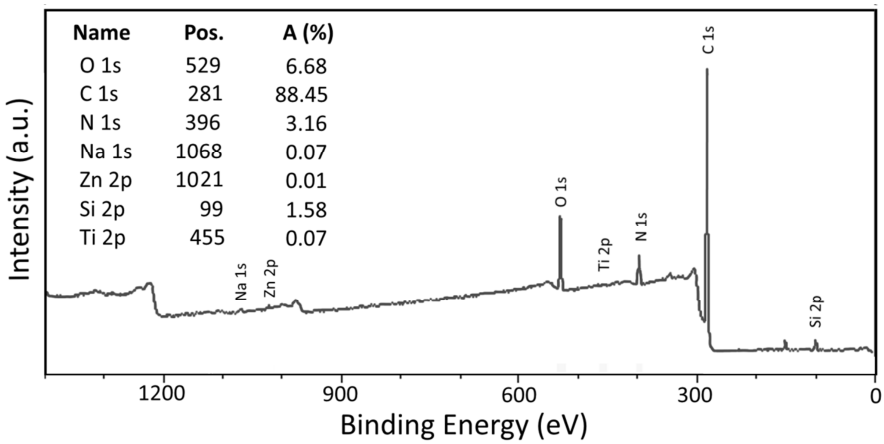

Figure 3.26. XPS spectrum of the unmarked 8% TiO_2 rutile.

High-resolution spectrum was done on the sample surface; however, it was not possible to observe a clear peak corresponding to the Ti. Nevertheless, the samples had been cut to be introduced in the system, so also a measurement was made on the edge where it was possible to detect the titanium signal. Probably, the Ti molecules disappear from the immediate surface of the polymer during the injection process hampering its observation. The measurement made on the sample edge is exhibited in figure 3.27. A peak is identified at 459 eV corresponding to Ti^{4+} $2p^{3/2}$. The peak associated to the Ti^{4+} $2p^{1/2}$ is barely observed at 464 eV. No more oxidation states were detected.

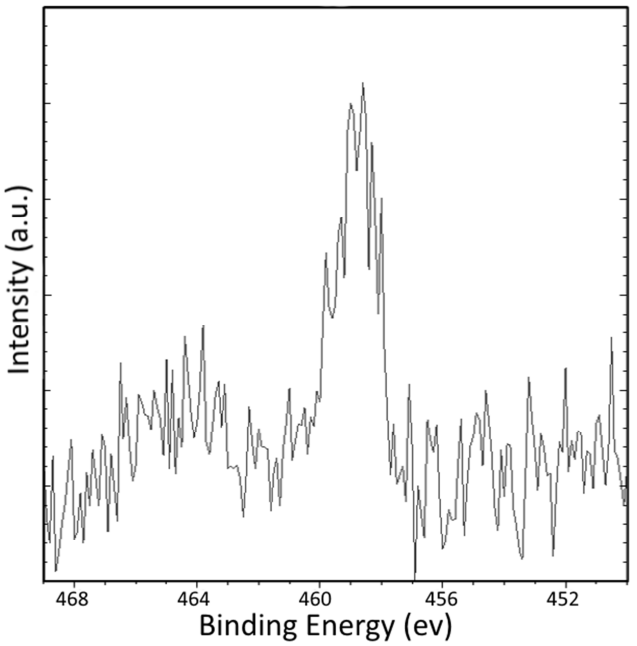

Figure 3.27. High-resolution spectrum of the unmarked 8% TiO_2 rutile.

Therefore, in order to improve the signal of the Ti peak, measurements were done on the TiO_2 powder in rutile form used to additivate the samples, see section 2.1.2.1. The powder was compressed using a manual press to obtain plane plaques. These plaques were subsequently marked using the three lasers, see figure 3.28. Successive laser repetitions at 1200 DPI were done until a visible change was observed on the powder. The surface was affected differently by the UV laser than using the other two laser wavelengths. On the one hand, the square pattern used to mark was only visible in the plaque affected by the UV laser (figure 3.28.d). That square was visible after employing only one laser repetition. Successive repetitions increased the visible contrast until the grey colour observed in the figure. On the other hand, the plaques marked using the IR and green lasers (figure 3.28.a and b) exhibited an inhomogeneous black dot. The dot grew progressively with the number of laser repetitions.

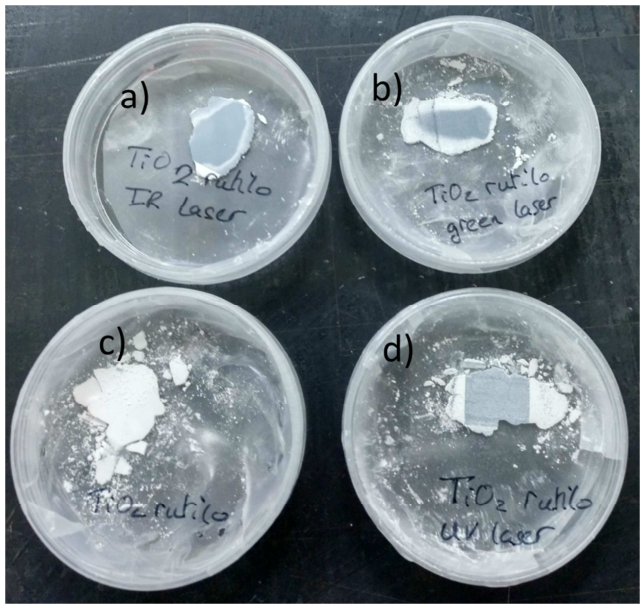

Figure 3.28. TiO_2 rutile powder after being pressed: a) marked with the IR laser; b) marked with the green laser; c) unmarked; d) marked with the UV laser.

High-resolution experiments were carried out on the TiO_2 powder plaques to understand how laser irradiation influences the pigment. Figure 3.29 illustrates the region corresponding to Ti 2p for the three marked samples and the reference. Additionally, a deconvolution of the peaks was done trying to observe the contributions of the different titanium oxidation states. In the original unmarked ABS sample (figure 3.29.4), peaks for Ti^{4+} $2p^{3/2}$ and $2p^{1/2}$ were detected at 458.5 eV and 464.2 eV, respectively, and these correspond to titanium dioxide. The peak deconvolution also showed a small contribution of Ti^{3+} of around 1.5% of the total area. On the marked samples two changes were detected, the peaks for Ti^{4+} $2p^{3/2}$ and $2p^{1/2}$ were slightly displaced to 458.7 eV and 464.4 eV and the presence of Ti^{3+} growth until around 5% of the total area. The highest amount of this oxidised state was found in the green laser sample.

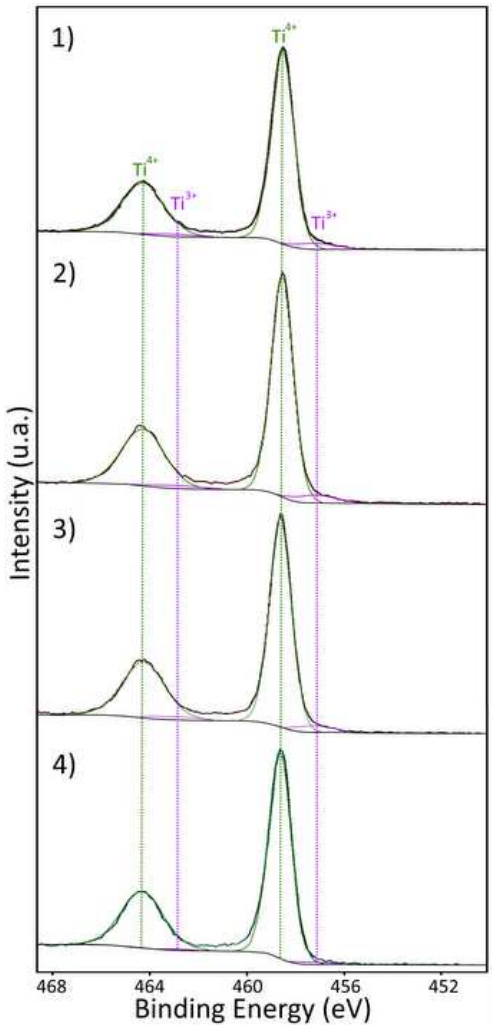

Figure 3.29. High-resolution spectrum of the TiO_2 powder samples after being marked by: 1) UV laser; 2) green laser; 3) IR laser; 4) unmarked reference sample.

The measurements on the laser marked 8% TiO_2 rutile were done on three different DPI conditions for each laser (the highest contrast mark, 600 and 1200 DPI). The spectra and detected atomic composition were reproducible within the same area, and the elements observed in the surface of the unmarked sample were the same to those identified in marked ABS samples. No significant evidence of modification was found in the total percentages of the atomic species observed. Nevertheless, in all the laser marks the signal corresponding to the Ti peak was

increased around five times. High-resolution experiments were performed on the marked samples. Figure 3.30 showed the region of binding energies corresponds to Ti 2p for the best contrast marks achieved with each laser as an example. The main difference exhibited was the presence of another peak at lower energies. This peak was found for all the samples marked using the UV and green lasers analysed, and it was barely visible in the IR marked samples.

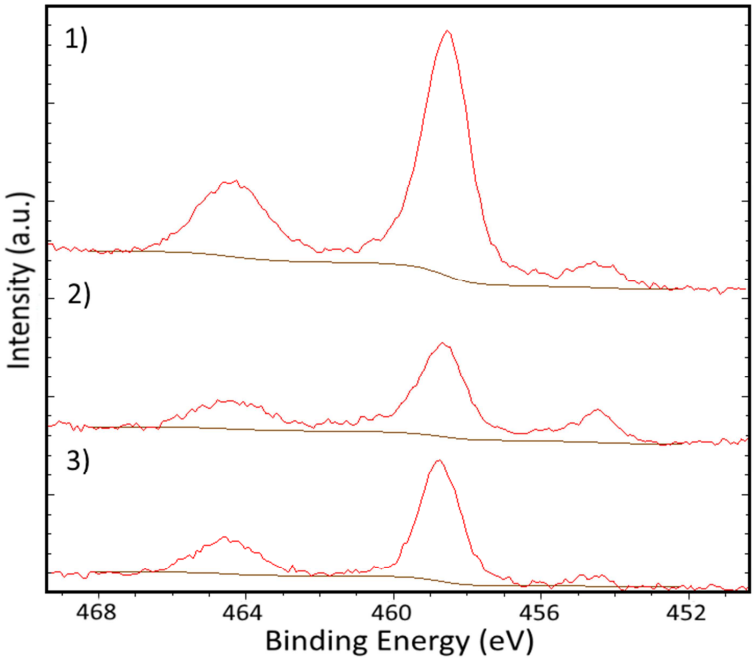

Figure 3.30. High-resolution spectrum of the 8% TiO_2 rutile after being marked by: 1) 200 DPI, UV laser; 2) 400 DPI, green laser; 3) 900 DPI, IR laser.

As before, a deconvolution process was done on the marked samples. Figure 3.31 displays the spectrum of the 8% TiO_2 rutile marked at 600 and 1200 DPI with the three lasers. In the marked samples it was possible to observe the peaks associated with Ti^{4+} $2p^{3/2}$ and $2p^{1/2}$ at 458.7 ± 0.2 eV and 464.4 ± 0.2 eV, with Ti^{3+} $2p^{3/2}$ and $2p^{1/2}$ at 457.3 ± 0.2 eV and 463.0 ± 0.2 eV, Ti^{2+} $2p^{3/2}$ and $2p^{1/2}$ at 455.5 ± 0.2 eV and 461.2 ± 0.2 eV. Also, another two peaks (denoted in the figure as X^+ and X^-)

were needed to justify the apparition of the peak at low energy at 454.5 ± 0.2 eV and 460.4 ± 0.2 eV. These peaks have been ascribed in literature to an oxidation state of the Ti forming TiC [3.55], [3.56].

The area percentage of the different peaks depends on the marked sample. The percentage of the total area associated to the peaks of Ti^{3+} in all the samples was low, below 5%. The peak associated to the reduced state Ti^{2+} was detected in the samples marked with the UV and green lasers in a percentage of around 10% while the area percentage in the case of the IR laser marks was below 5%. Finally, the most significant differences between the lasers were detected in the peaks corresponding to the TiC. In the IR laser marked samples, the area of this peaks was also below 5%. By contrast, this area was around 15% of the total area in the green laser samples while the DPI number influenced in the UV laser marks ranged the total from 5% to 20% as the DPI number was increased. Consequently, the peak associated to Ti^{4+} was reduced, from 85% to 65%. During the ATR-FTIR studies, it was detected that the biggest modification of the area associated with the pigment was for the 600 DPI. This difference may be associated with the penetration depth of each technique, lower in the case of the XPS. Therefore, the superficial composition is not exactly the same that in the first microns, probably the highest DPI value caused the highest carbonisation of the polymer masking some of the pigment reduction. A high-resolution spectrum was also done in the region of C; however, no significant influences under the laser were detected in any case.

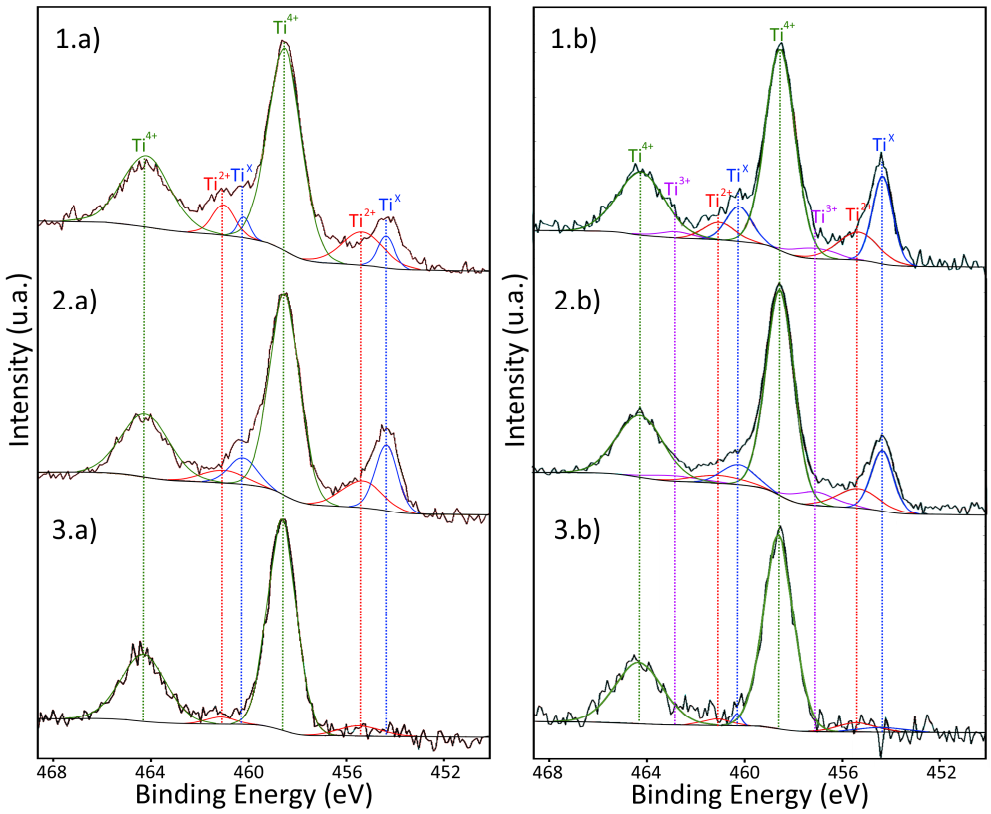

Figure 3.31. High-resolution spectrum of the 8% TiO_2 rutile after being marked by: 1) UV laser; 2) green laser; 3) IR laser; a) 600 DPI; b) 1200 DPI.

These experiments were also performed in the white-c ABS marked with the UV laser using two DPI values, 400 and 1200 DPI. The high-resolution spectrum of the Ti region can be observed in figure 3.32. As before, the signal of the unmarked sample was small; it was only possible to be detected measuring in the cut region. Additionally, the signal of the marked samples exhibited the same peak, which after the deconvolution process was also mainly associated with the TiC. The evolution of areas was similar than in the 8% TiO_2 rutile ABS, from 10% to 20% in the analysed samples.

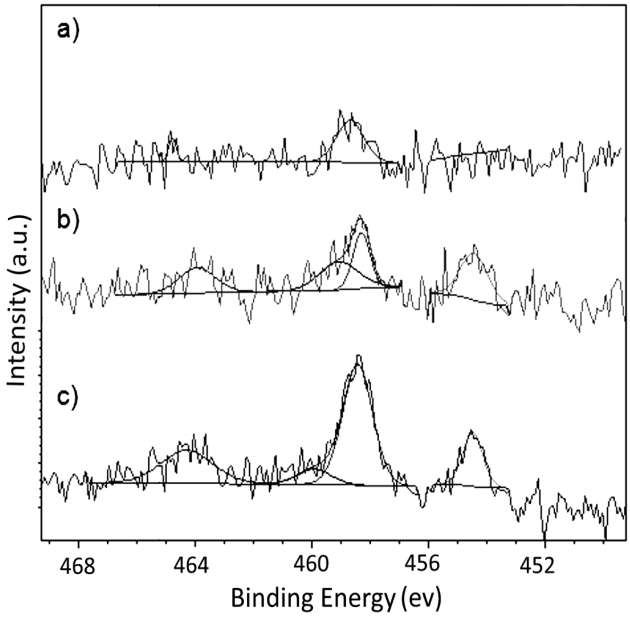

Figure 3.32. High-resolution XPS spectrum of the white-c ABS: a) unmarked material; b) 1200 DPI, UV laser; c) 400 DPI, UV laser.

Therefore, different oxidation states of Ti were observed with the XPS. On the pigment powder, the presence of black TiO_2 (Ti^{3+}) was enhanced by the effect of the three lasers. The creation of this reduced species probably caused the darkening of the pigment. However, the behaviour of the TiO_2 mixed with the ABS was different. The formation of the reduced species Ti^{3+} was significantly lower than the apparition of Ti^{2+} and especially of TiC under the green and UV wavelengths. This fact seems to be related to photoinduced processes that occur during the laser marking, which affect the pigment included in the ABS. These changes lead to an overall darkening of the resulting mark.

3.2.5. Conclusions

The laser marking on samples of ABS with different percentages of TiO_2 has been carried out using three lasers irradiating at 355 nm, 532 nm and 1064 nm. For that purpose, two crystalline forms of TiO_2 were used, anatase and rutile. Additionally, a commercial material was also studied.

It was shown that the presence of the additive modified the energy absorption of the ABS; in the UV region of the spectrum the absorption increased, and below 400 nm the absorption decreased. Therefore, the presence of the additive affected the visual appearance of the material, according to its use as a whitening agent.

The laser marking was influenced by the laser used, the pigment amount and, to a minor extent, its crystalline form. The best results were obtained using either the UV laser on the 2% TiO_2 anatase or the green laser on the 2% TiO_2 of both crystalline forms. The IR laser marks exhibited in almost all the cases a worse contrast. However, the green laser marks had high values in the a* coordinate that implies a brownish colouration of the marks. Therefore, the best aesthetical marks were obtained using the UV laser where the a* value was close to zero. The highest amount of additive did not improve the quality of the marks.

The topographical analysis showed that the increment of total energy deposited (DPI number) caused ablation of the material for UV and green lasers while foaming of the material characterised the effect on the IR laser marks. The surface morphology depended on the energy deposited as it can be observed using ESEM. Finally, the transversal depth of the changes induced by the laser varied from the lasers; the most significant values were obtained with the IR laser, probably because of the high thermal effect associated with this wavelength.

ATR-FTIR and XPS detected changes on the TiO_2 additive after the laser marking process. These changes were negligible employing the IR laser, while the green and to a greater extent the UV laser wavelength marks seem to have a higher influence on the additive. By ATR-FTIR it was possible to observe the decrease of the 660 cm^{-1} shoulder associated to TiO_2 for the both previously mentioned wavelengths depending on the laser parameters. Also, the XPS study showed a progressive reduction of Ti, also for the UV and green lasers. This reduction led mainly to the formation of TiC.

Therefore, the laser wavelength used to mark the ABS exhibited a high influence on the final results. The black colour of the IR laser marks can be attributed to carbonisation of the polymeric matrix because the minor modification of the pigment molecule detected. By contrast, the green laser and especially the UV laser marks exhibited a reduction effect on the titanium. This progressive reduction of the pigments leads to a darkening of the polymer surface, although if the laser energy is high enough, a carbonisation of the ABS was observed. Lower energies were needed to produce the best contrast using the UV laser, so the use of this laser is preferable.

3.3. Black ABS laser marking

In this section, the laser marking of ABS filled with carbon black (CB) as black pigment will be discussed. The influence of the pigment CB was examined employing five different ABS materials: natural-b ABS charged with various amounts of CB, and the black-c ABS. See section 2.1.2.2 for a detailed description of these materials. The natural-b ABS samples with different amounts of CB are displayed in figure 3.33.

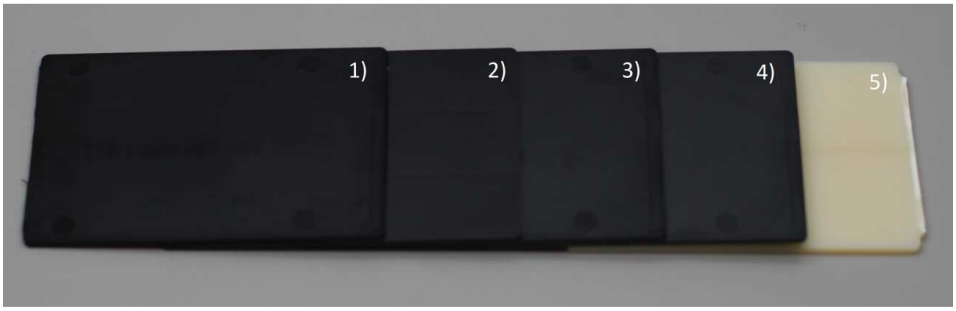

Figure 3.33. Samples of the natural-b ABS charged with different amounts of CB; 1) 0.5% CB ABS; 2) 0.2% CB ABS; 3) 0.1% CB ABS; 4) 0.05% CB ABS; 5) natural-b ABS.

The laser marking was done in the same way that with white ABS samples, using the three industrial lasers introduced in the section 2.1.1, the IR laser, the green laser and the UV laser. The laser parameters selected were also the same, from 100 to 1200 DPI employing a 100 µm spot. Also, the analysis techniques used were the same employed in the previous section.

Finally, the use of a laser marking special additive specially designed to produce white marks on a black polymer was aimed. This analysis was performed using the Iriotec® 8835 provided by the company Merck. The objective of this additive is to enhance the laser marking process improving the final colour contrast of the marks.

3.3.1. Preliminary material characterisation

As the exact composition of the black-c ABS belongs to the manufacturer business area, a TGA analysis was performed to determine the inorganic residue. This study was requested to Netzsch in the framework of a European Project. Samples were analysed twice according to the following parameters: under Nitrogen (flow rate: 20mL/min) from 25 to 700°C at 10 °C/min; from 700 to 250°C at 20 °C /min, an isotherm at 250°C for 10 min, switch to synthetic air (20mL/min) from 250 to 1000 °C at 5 °C/min. The amount of residuum, which may be assigned to CB, was between 1.1 and 1.2%. In the samples of natural-b ABS charged with CB, the amount of additive was progressively increased till 0.5% CB. The results obtained for samples with higher contents did not improve the quality of the marks.

Before the laser marking, the optical properties of the different polymeric samples were studied. The optical absorption of these materials from 350 to 1200 nm in terms of the amount of the CB additive is shown in figure 3.34. The vertical axis used was the same as the white ABS study. The vertical dashed lines represent the wavelength of the lasers used in the marking process: IR (1064 nm), green (532 nm) and UV (355 nm).

Once filled with CB, the absorption spectrum was flat, and there were small differences in the absorption of the three laser wavelengths, 355nm, 532 nm and 1064 nm [3.20], [3.57]. As it could be expected, the presence of the additive increased the absorption of the polymer for the entire measured spectrum, and there were small changes in the absorption depending on the additive amount.

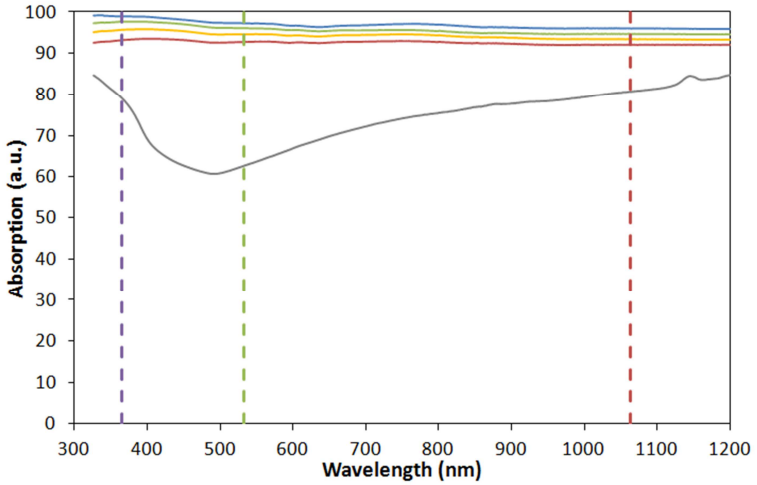

Figure 3.34. The absorption spectrum of the natural-b ABS filled with% CB. Each line represents grey: natural-b ABS line; red: 0.05% CB ABS; yellow: 0.1% CB ABS; green: 0.2% CB ABS; blue: 0.5% CB ABS. The vertical dashed lines represent the wavelengths corresponding to each laser (UV laser: purple line; green laser: green line; IR laser: red line).

The CieLab colour parameters (see section 2.2.1.1.) of plates processed from natural-b ABS samples charged with CB were measured as a reference for laser marking. Figure 3.35 shows the evolution of the colour coordinates in terms of the additive amount. The three coordinates tended to saturate to a maximum value. L* coordinate, which is related to the grey scale, exhibited a saturation effect at a value close to 25, while a* and b* coordinates were close to 0. So, the samples were almost on the grey scale of colours, see figure 3.33. The black-c ABS were also measured, their CIELab coordinates were L* = 26.6 ± 1.5; a* = -0.1 ± 0.5; b* = -1.0 ± 0.5. Samples of the black-c ABS had a lower value in the L* coordinate while the a* and b* were also almost zero.

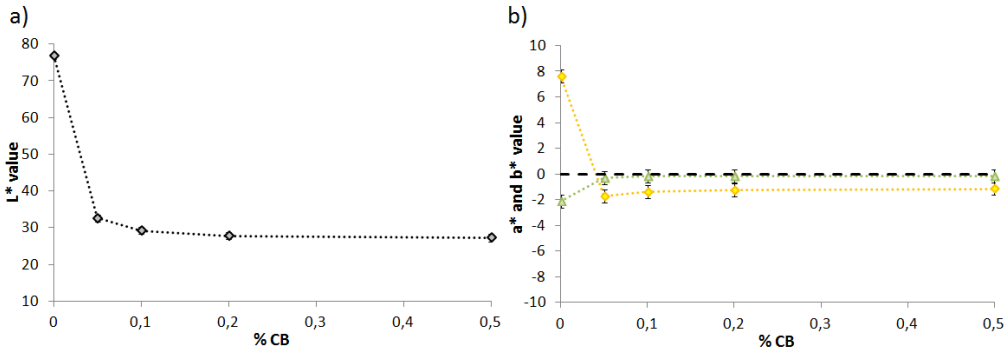

Figure 3.35. Influence of the CB percentage added to the natural-b ABS of CB on the CIELab coordinates a) L*; b) a* (green symbols) and b* (yellow symbols).

3.3.2. Colour changes by laser marking

The natural-b ABS plates with different CB contents were subsequently marked using the three different lasers irradiating at 355 nm, 532 nm and 1065 nm with the aim of achieving white marks, which are expected to be associated with a foaming effect in the plastic material. Foaming is usually caused by the laser-induced formation of gas bubbles under the surface of the material. The gas inside the bubbles has a different refractive index compared to the surrounding walls and gives rise to the white appearance due to light scattering [3.58], [3.59].

The experimental setup was the same used for the white ABS study and explained in the introductory part of this chapter. Examples of the laser marks made in the different polymers used are shown in figure 3.36. It can be observed that generally, the marks were whiter when the CB percentage was lower. Furthermore, IR laser marks tended to exhibit a higher contrast than those produced by the UV laser while the green laser marks presented a brownish effect.

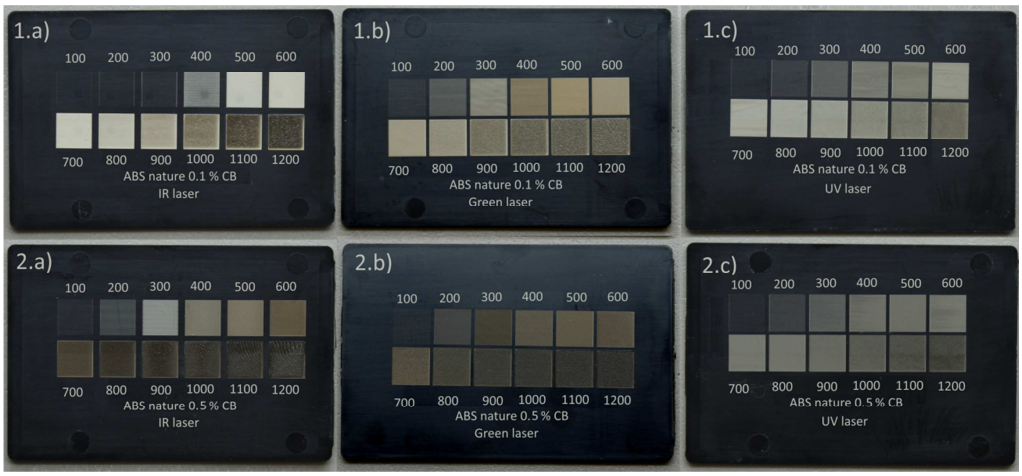

Figure 3.36. Example of some of the laser marks on black ABS plates; 1) 0.1% CB ABS; 2) 0.5% CB ABS; a) IR laser marks; b) green laser marks; c) UV laser marks.

The values for the luminosity L* colour coordinate and contrast Δe* (according to eq. 2.1) of the marked regions are collected in the figure 3.37. The objective was to obtain marks as white as possible, so a high value in the L* coordinate was desirable in addition to low values of the a* and b* coordinates. The Δe* value provides information about the best mark in terms of the colour but should be considered that it is also associated with changes in the a* and b* coordinates. Dependence with the laser and the additive percentage was found in the colour of the marks. The behaviour under the lasers of natural-b ABS was the same as the natural-w ABS; black foamed marks were produced. Thus, the comparison with the material without the additive has no sense in this case.

The highest values of L*, for different % of CB, were obtained in all cases on marks made using the IR laser, except for the lowest amount of CB studied 0.05%, where the highest L* value was obtained with the green laser. The differences between the lasers decreased when the amount of the additive was increased. The DPI dependence was similar for the three lasers: the contrast increased until a maximum was achieved, and then decreased.

The additive amount influenced on the laser L* value; in all the cases, the measured values decreased when the percentage of CB in the material was increased. IR and green lasers exhibited more significant changes than those detected on the marks created by the UV laser. The best results were obtained for the lowest amount of additive in the case of green and UV lasers, while the IR presented better result for the case of 0.1% CB.

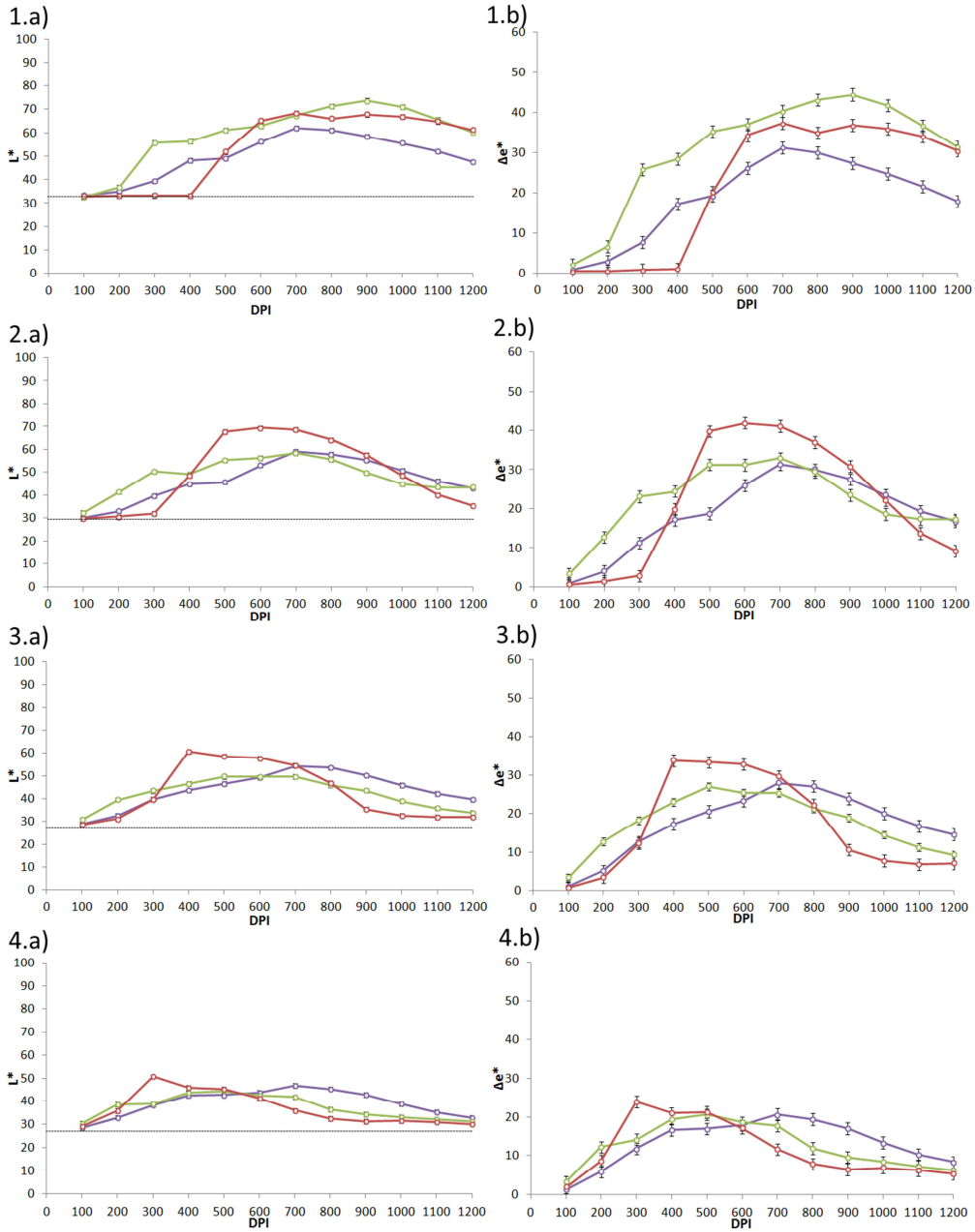

Figure 3.37. Influence of the laser wavelength and the DPI on a) L* coordinate values; b) Δe* calculated values: 1) 0.05% CB ABS; 2) 0.1% CB ABS; 3) 0.2% CB ABS; 4) 0.5% CB ABS;. Purple symbols: UV laser; green symbols: green laser; red symbols: IR laser. The black dashed line is the unmarked material L* value.

The DPI value where the maximum contrast was achieved with each composition varies in the case of the green and IR lasers, while for the UV laser it remained constant. Figure 3.38 shows the evolution of this DPI value for the three lasers. The DPI value is directly correlated to the cycle time of the process (see eq. 1.13), the total number of pulses (see eq. 1.12) and therefore to the total energy deposited on the surface. In the case of samples marked with the IR and green lasers, the maximum contrast value was achieved at lower DPI as the CB content increased. However the case of the UV laser marked samples was different, the DPI at which the highest L* was found was the same. This fact indicated a difference in the marking mechanism between the three wavelengths. In the case of the IR and green lasers, the CB apparently interacted with the light by transferring the thermal energy to the polymer matrix and, as a consequence, a high amount of this additive led to higher absorbed energy and a lower DPI value was required for better contrast. However, no changes were observed for the UV laser in that DPI value, so the concentration of CB seemed to have a minor influence in the energy absorption at this wavelength.

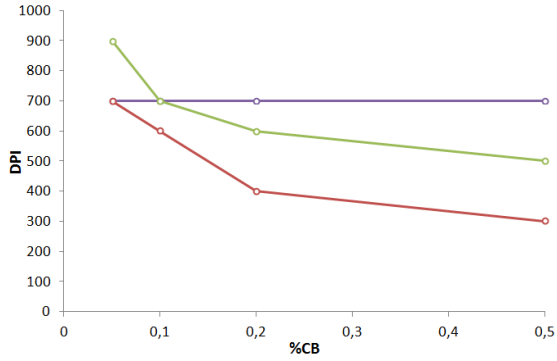

Figure 3.38. Influence of the CB percentage added to the natural-b ABS on the DPI value where the maximum contrast was found for each laser. Purple symbols: UV laser; green symbols: green laser; red symbols: IR laser.

The highest contrast calculated was obtained for the case of the green mark and 0.05% CB. However, the CIELab coordinates a* and b* should also be taken into account. Figure 3.39 displays the values of these coordinates for each laser mark and percentage of CB additive. The values obtained for a* were close to zero in all the cases. However, higher values were obtained in the b* coordinate, especially on those marks made with the green laser. These values were associated with a brownish look. The UV laser marks presented the lowest values in all the cases. The increment in the CB amount decreased the b* values of the marks although they still were not close enough to zero causing the brownish effect observed in the marks. Nevertheless, the best experimental conditions were achieved for the 0.1% CB ABS and the IR laser.

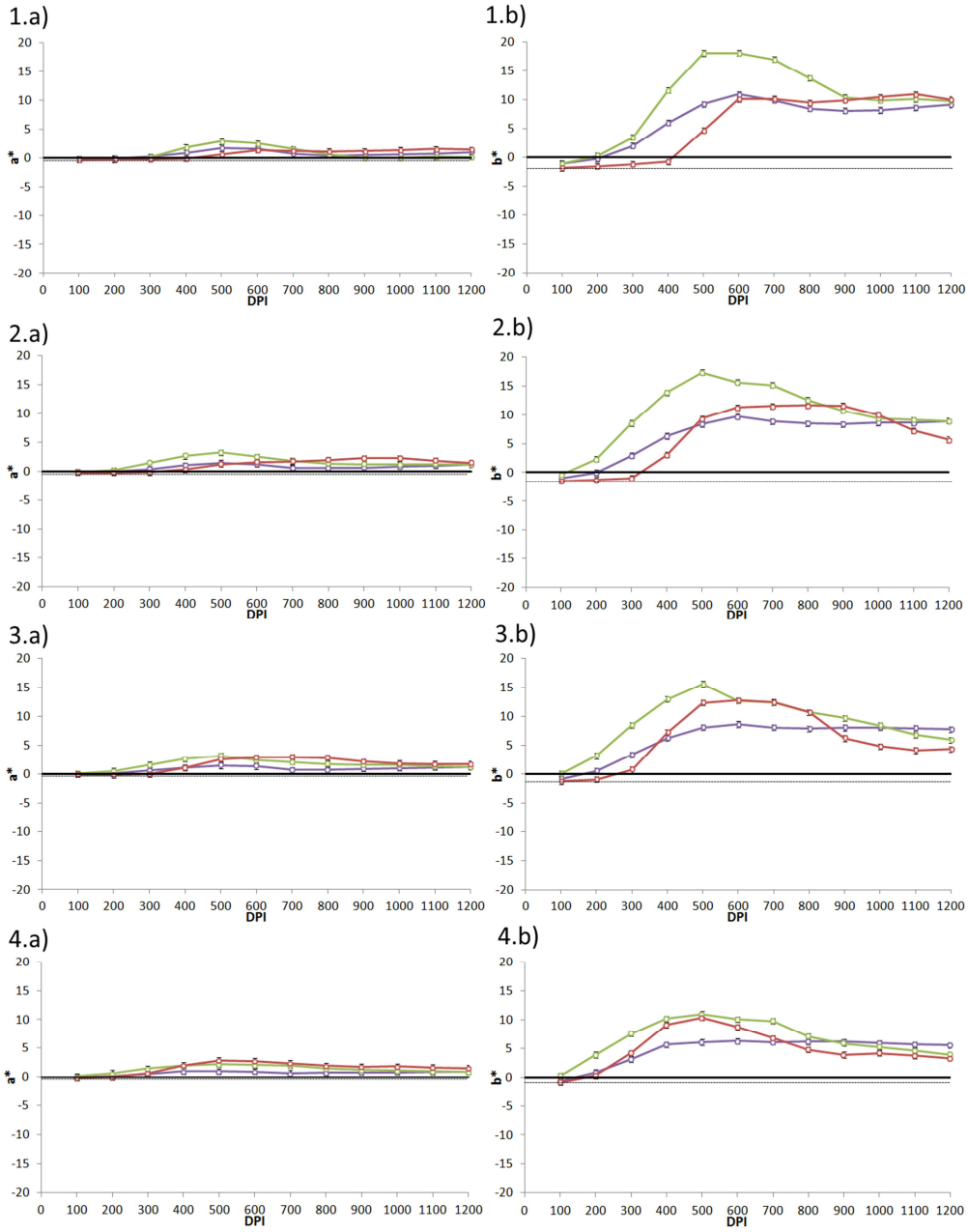

Figure 3.39. Influence of the laser wavelength and the DPI on a) a* coordinate values; b* coordinate values. 1) 0.05% CB ABS; 2) 0.1% CB ABS; 3) 0.2% CB ABS; 4) 0.5% CB ABS. Purple symbols: UV laser; green symbols: green laser; red symbols: IR laser. The black dashed line is the unmarked material a* or b* value.

In addition, the analysis of the laser marking process was done on the commercial material, the black-c ABS. The marks made with the three lasers on this material can be seen in figure 3.40. The experimental conditions were the same used in the previous experiment, 100 to 1200 DPI keeping the fluence constant between the different lasers.

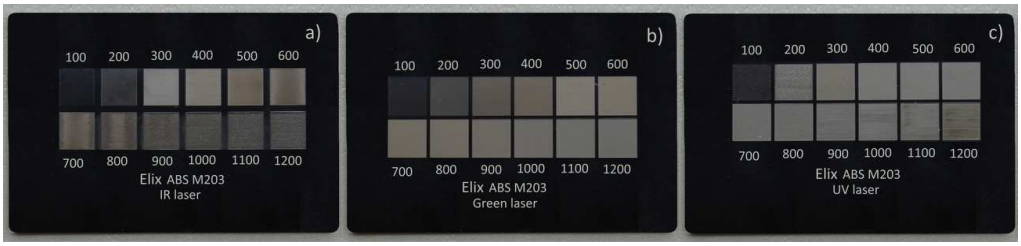

Figure 3.40. Black-c ABS marked with the three lasers: a) UV laser; b) green laser; c) IR laser.

Figure 3.41 shows the evolution of the L* coordinate and the calculated Δe^* (eq 2.1) corresponding to the marks presented in figure 3.40. As can be observed, IR laser marks at 300 and 400 DPI had higher L* value than the other two laser marks, although the differences were small. Thus, the best L* value was achieved at 300 DPI using the IR laser; higher DPI values with this laser did not improve the contrast, it worsened probably because of carbonisation of the polymer matrix. For the other lasers, the best results were obtained at 500 DPI and 700 DPI for the green and UV wavelengths respectively.

The contrast measured exhibited the same evolution than the L* coordinate. This shift indicated that the other two coordinates influence was low. The results obtained in a* and b* coordinates are showed in the figure 3.42. The a* values were close to zero while the b* values were slightly different, which indicated a brownish effect in some marks as can be seen in figure 3.40.

In addition, L* value and contrast measured were worse than those obtained in the CB compounds while a* and b* were lower. This evolution of the colour coordinates could be related to the measures obtained in the case of the material with different percentages of CB if we considered that the commercial material had a higher amount of CB than 0.5%. As it was presented in the first part of this study, it was obtained that the commercial material carries around of 1.1% in weight of additive by TGA technique. Therefore, all the results were related to the amount of CB that seemed to be critical for the final colour of the marks in the laser process.

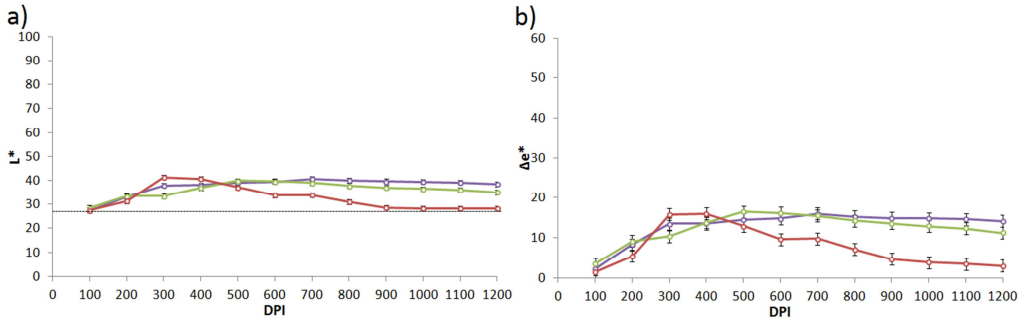

Figure 3.41. Colour coordinates of the laser marks made on black-c ABS. a) L* coordinate; b) contrast Δe*. Purple symbols: UV laser; green symbols: green laser; red symbols: IR laser. The black dashed line is the unmarked material L* value.

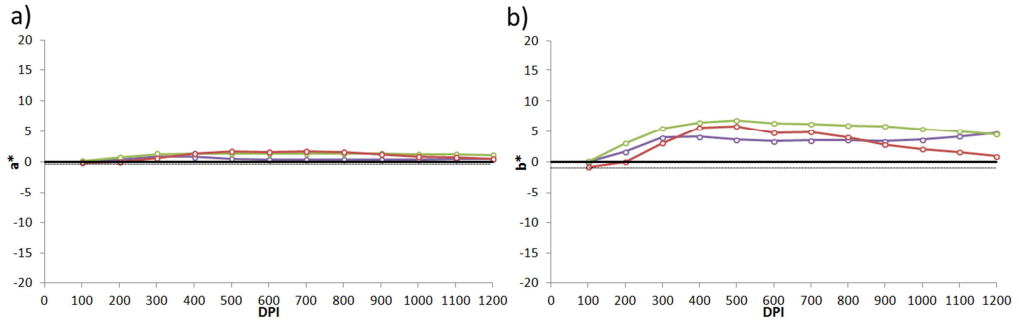

Figure 3.42. Colour coordinates of the laser marks made on black-c ABS. a) a* coordinate; b) b* coordinate. The black dashed line is the unmarked material a* or b* values.

So, it can be concluded that the amount of CB is critical for the marking process and the best results were obtained for the samples with a lower quantity of the pigment. As the CB amount determines the initial colour of the objects processed from the compounding of ABS and the pigment, a balance between the initial colour properties and the requirements to obtain laser marks of interest should be taken into account trying to reduce the pigment amount in the black-c ABS.

3.3.3. Topographical changes on laser marks

This part is divided in the analysis of the surface of the marks and the penetration depth of the laser treatment. The characterisation of the laser marks carried out with samples of the polymer mixed with CB is presented below.

3.3.3.1. Surface topography

Confocal microscopy analysed the topography of laser marks on the ABS. As in the case of white ABS, the analysis allowed obtaining the height of the mark compared to the unmarked material, and the mean roughness R_a, see section 2.2.2.2. Usually, it is expected that marks with the highest thickness of the foaming region have the best contrast. Furthermore, it is expected that the foaming is associated with a rising of the marked regions in comparison to the unmarked regions. However, some ablation can cause the reduction of the rising effect observed from the surface topography. Therefore, the association between the rising of the marks and foaming is not always clear.

The changes in the height of the marked area with respect to the unmarked zone and the mean roughness are represented in figure 3.43. The topography of the marks was dependent on the laser used in the marking process. The IR and green lasers

gave rise to a foaming effect on the material while the UV laser hardly produced any changes in the topography and only a slight engraving effect was detected at high DPI. In the case of the samples marked with the IR and green lasers, foaming was detected above a certain DPI threshold.

The evolution of the topography with the percentage of CB was similar to the colour coordinates showed before. The foaming effect decreased with the increment of the pigment, which was in accordance with the loss of contrast. The DPI threshold, where the foaming appeared, decreased with the increment of CB for the IR laser while for the green laser seemed to be constant around 300 DPI. That behaviour may indicate a different interaction for both lasers. The IR laser interacts with the CB, so higher amount of the pigment enhances the absorption producing marks at lower DPI values. By contrast, the DPI value where the foaming began did not change in the case of the green laser marks, so it indicates less interaction with the pigment than in the IR laser. However, the increment of the pigment amount altered this foaming, so this pigment probably affected to the formation of bubbles in the interior of the material by increasing the thermal conductivity. Therefore, the highest concentration of pigment studied, 0.5%, provoked that at high DPI the green laser engraved the material. Finally, the UV laser only presented engraving in marks corresponding to the highest DPI values, and this engraving is higher when increases the pigment amount. Again, it assumed that the UV laser directly interacted with the polymer matrix achieving the less foaming effect and the CB amount only influenced changing the thermal properties of the material.

The roughness values measured were different for each laser; the green laser marks exhibited the highest values while the lowest was obtained with the IR laser. The three lasers showed a similar behaviour in terms of the DPI value and no significant differences between the different amounts of CB were observed. No

tendencies related to the colour measured were detected on the roughness on any mark.

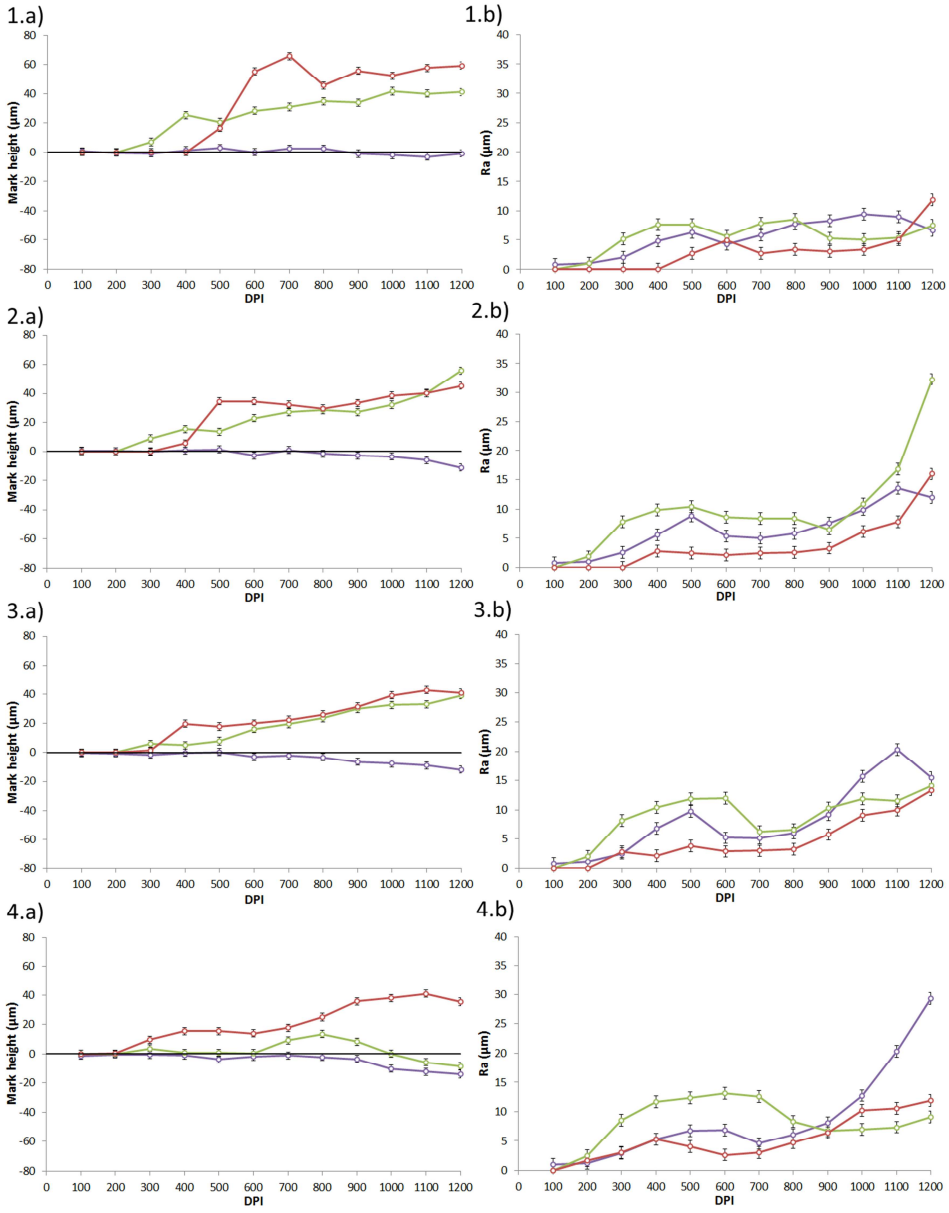

Figure 3.43. Influence of the CB percentage added to the natural-b ABS on the surface topography. 1) 0.05% CB; 2) 0.1% CB; 3) 0.2% CB; 4) 0.5% CB; a) mark height; b) Ra. Purple symbols: UV laser; green symbols: green laser; red symbols: IR laser.

Furthermore, the topography of the black-c ABS marked with the three lasers was studied and the results are shown in figure 3.44. In this case, only the IR laser was able to produce a foaming effect in the material, while the green and UV laser engraved the material. However, the IR laser engraved the material for the highest DPI values. Also, the green laser produced a high ablation effect in the material compared to the previously studied materials, where only a small ablation was detected in the ABS filled with 0.5% CB. The CB higher amount of the commercial sample provokes a change in the laser interaction causing worse results that in the samples of X% CB ABS.

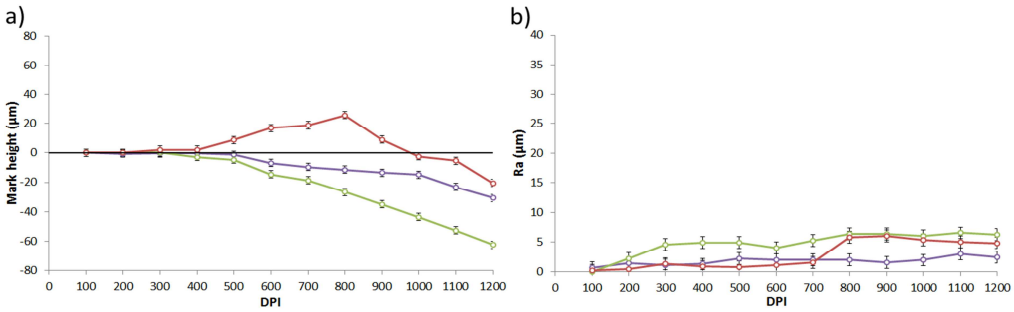

Figure 3.44. Surface topography of the laser marks made on black-c ABS. Mark height; b) Ra. Purple symbols: UV laser; green symbols: green laser; red symbols: IR laser.

3.3.3.2. Penetration depth of the laser changes

Observation of the cross-sections of the different marks allowed a rough evaluation of the changes induced by the laser across the sample thickness. These changes were seen as a white area under the stereoscopic microscope. The depth dependence on the laser wavelength and CB amount is showed in figure 3.45 in terms of the DPI value.

The depth of the area visually affected by the laser seems to follow a similar behaviour to the previously displayed; the IR and green laser marks exhibited higher depth values that tended to decrease with the increment of the CB concentration in the polymer. The most significant observed depth approximately corresponds to the highest contrast measured for the marks made with the IR laser, although this correlation cannot be done for the other laser wavelengths. Again, the colour formation observed for each case should be different. The UV laser marks exhibited a white colour that indeed cannot be associated to foaming; maybe there were other phenomena like black pigment removal. For example, the green laser marks corresponding to the sample 0.05% CB ABS (where the maximum contrast was measured) could not be only caused by the foaming effect because the foam measured was higher in the case of the IR laser marks. Maybe there was a combination of bubbles trapped under the surface with CB removal. Finally, as said before, the IR laser marks may be associated with the foam height as we observe from the direct relationship between that measured and the contrast previously showed.

In addition, the changes observed related to the concentration of CB in the polymer were the same observed in the previous sections. The height measured decreased with the increment of the pigment amount for all the lasers, although this change was more accused of the IR and green laser marks than for the UV laser marks.

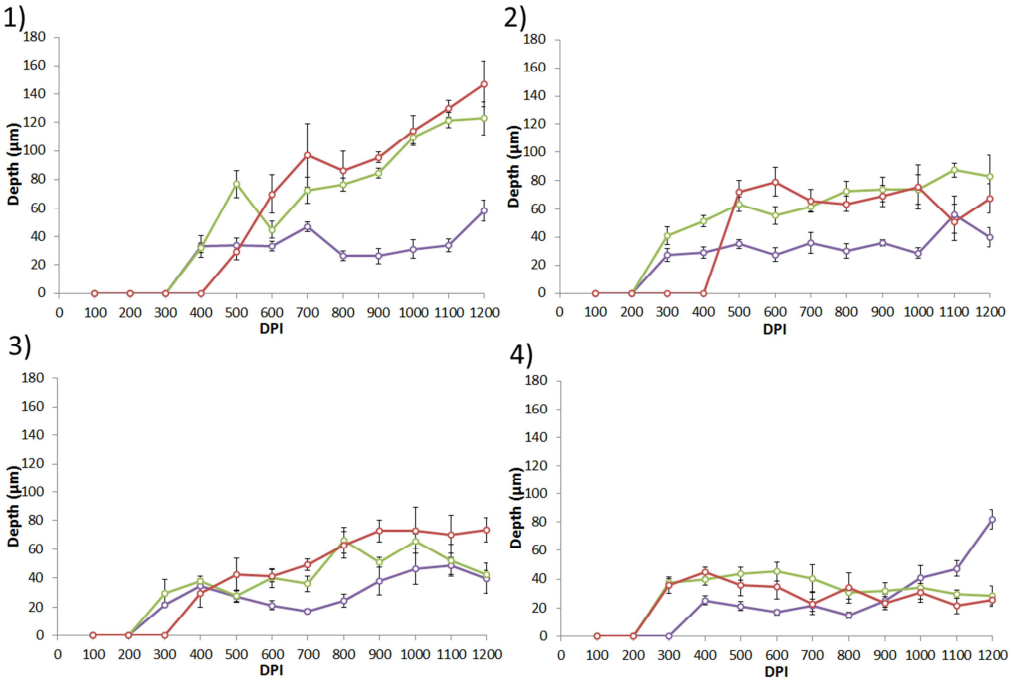

Figure 3.45. Transversal depth obtained from the cross-section observed by the stereoscopic microscope for the laser marks on natural-b ABS filled with CB. 1) 0.05% CB; 2) 0.1% CB; 3) 0.2% CB; 4) 0.5% CB. Purple symbols: UV laser; green symbols: green laser; red symbols: IR laser.

3.3.4. Chemical changes on laser marks

The characterisation of chemical changes induced by laser irradiation was carried out by ATR-FTIR, as previously described in section 2.2.1.3. XPS was also used in an attempt to observe chemical modifications, although no significant differences between were detected on spectra corresponding to laser marks and initial polymeric samples.

3.3.4.1. ATR-FTIR analysis

The results obtained for the samples derived from 0.5% CB ABS have been selected as an example (having the highest content of pigment), although the rest of materials showed similar behaviour.

As expected, the unmarked material displays the peaks corresponding to an ABS copolymer. Marks made with both lasers at 300 DPI (the highest contrast for the IR laser marks), and 1200 DPI (maximum deposited energy) were selected to compare with the unmarked material. In all cases, the spectra mainly corresponded to ABS. Changes were detected in the 1200 DPI marks in the relative area of the peak at 966 cm^{-1}, due to polybutadiene, with respect to the peak at 1494 cm^{-1}, corresponding to the aromatic ring, taken as a reference (figure 3.46). Modifications in the spectra were not observed in the UV or green laser marks selected. Both lasers seemed not to have a significant influence on the chemical structure of the plastic material.

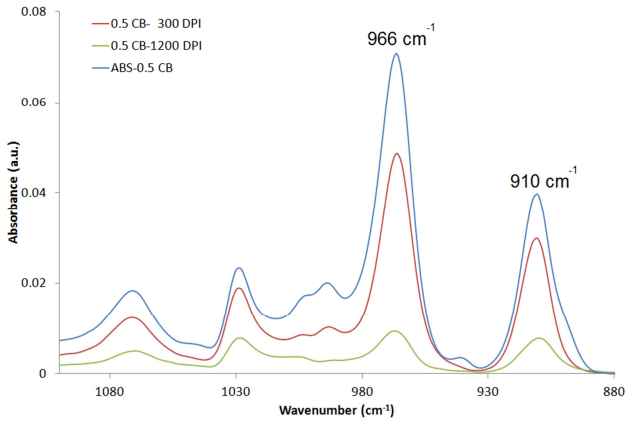

Figure 3.46. ATR-FTIR spectra of samples marked at 300 DPI, 1200 DPI with the IR laser and unmarked sample (from 880 cm^{-1} to 1100 cm^{-1}) prepared with 0.5% of CB.

The relative ratios of the different repeating units (derived from acrylonitrile, styrene and butadiene) were studied to explore the effect that the IR laser had on the

material. For this purpose, the areas corresponding to signals at 2237 cm^{-1}, 966 cm^{-1}, and 910 cm^{-1} were compared with respect to the area corresponding to the signal at 1494 cm^{-1} (aromatic ring). The area ratios of the different peaks for acrylonitrile and butadiene in comparison with the area of styrene as a function of DPI are represented in figure 3.47. As can be observed, the ratio of acrylonitrile/styrene groups seemed to be stable and, consequently, these were not markedly affected by laser irradiation. However, the ratio corresponding to monomeric units derived from butadiene decreased as the DPI increased and it was more evident for DPI ≥ 700, and even more so for samples that had a higher CB content.

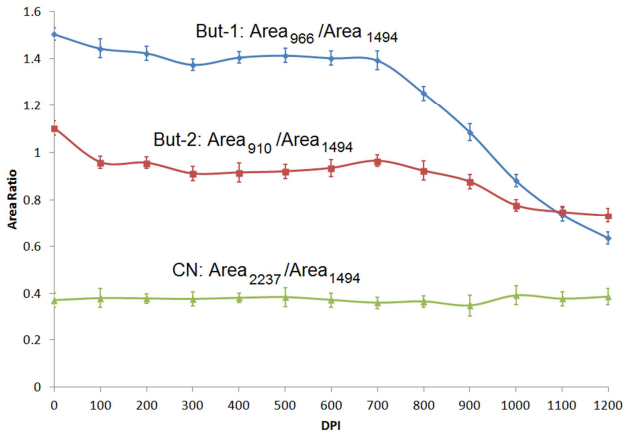

Figure 3.47. Area ratio vs DPI for a sample with 0.5% of CB marked with the IR laser. Green symbols: Area 2237 cm^{-1}/Area 1494 cm^{-1}; red symbols: Area 910 cm^{-1}/Area 1494 cm^{-1}; blue symbols: Area 966 cm^{-1}/Area 1494 cm^{-1}.

3.3.5. Influence of a commercial additive for laser marking processes

The analysis of laser marking was extended to samples containing the additive Iriotec® 8835 (Merck KGaA) for laser marking. This additive is specially designed to produce a colour change on black polymers by the laser. Therefore, a study to understand the effect of this additive was done to find an alternative solution to enhance the laser marking process.

The additive was tested on the different materials employed in this study, the natural-b ABS charged with% CB and the black-c ABS. The amount selected was the optimum recommended by the provider (0.4%). This additive is specifically designed to transform IR laser light into heat to induce a colour change in the plastic material. However, it should be remarked that the behaviour of this additive under green and UV laser light was not previously reported. The presence of this additive also made the material slightly darker which was especially evident in samples with a low CB content. These samples exhibited L* value around two units lower than samples without the laser additive. The rest of the compounds showed changes lower than one unit in the L* coordinate.

A comparison of the marks made in plates prepared from 0.05% CB ABS with and without the laser additive is displayed in figure 3.48 as an example. In samples marked with UV laser, the additive seemed not to have a significant influence on the colour properties of the marks. However, this additive seems to have an influence when the green and IR laser were used. The marks made with the green laser on the sample with the additive exhibited worse contrast than those done on the material without the additive. By contrast, the IR laser presented better results on the

material with the additive; additionally, the best results were achieved at lower DPI values compared to the samples of ABS without the Iriotec additive.

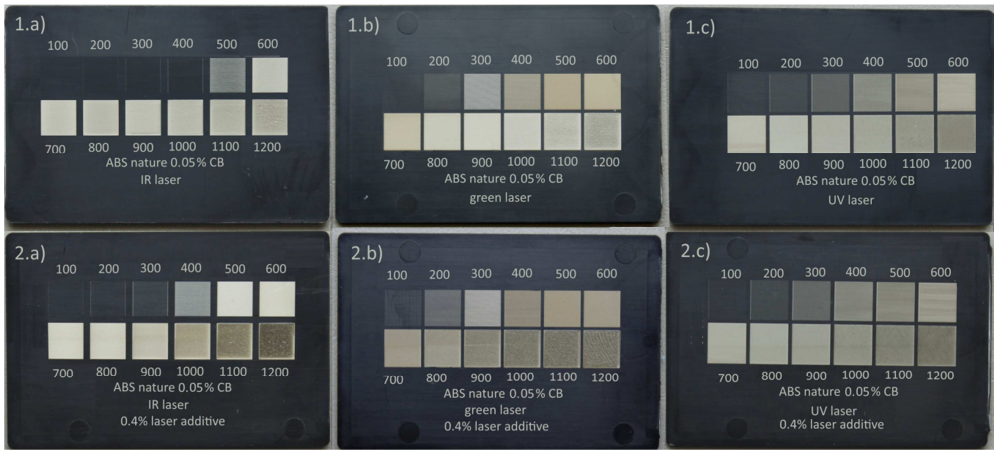

Figure 3.48. Comparison between some of the laser marks made on the natural-b ABS charged with 0.05% CB and the laser additive Iriotec. 1) 0.05% CB ABS (as reference); 2) 0.05% CB + Iriotec; a) IR laser marks; b) green laser marks; c) UV laser marks.

The comparison of the contrast values obtained using the three lasers on the samples depending on the presence of the laser additive for two of the materials, 0.05% and 0.5% CB ABS, is displayed in figure 3.49. Values of the rest of ABS materials (with 0.1% and 0.2% CB ABS) were intermediate between those results. The samples marked with the UV laser exhibited similar contrast values or slightly higher in samples without the laser additive. The effect of the additive under the green laser depended on the CB amount. The material with the lowest concentration of pigment exhibited worse contrast if the laser additive was presented while that difference almost disappeared in the case of the highest concentration. Finally, the IR laser also exhibited differences depending on the CB amount. In this case, the better contrast was achieved with the laser additive and employing a lower DPI value on the 0.05% CB ABS while the increment of the CB amount led to similar results as in

the green laser marks. Consequently, the beneficial effect of the laser additive is related to the lowest content of CB.

Therefore, this can indicate that the additive did not interact with the UV wavelength and its presence slightly darkens the final material giving a poorer final result. The presence of the additive was even worse for the green laser interaction. Probably the additive disturbed the interaction of the laser with the polymer giving an undesired final result. Finally, it can be envisaged that the additive acts as an absorber of the IR radiation. The additive improved the heat transfer to the polymer matrix, the foaming effect and consequently the final contrast.

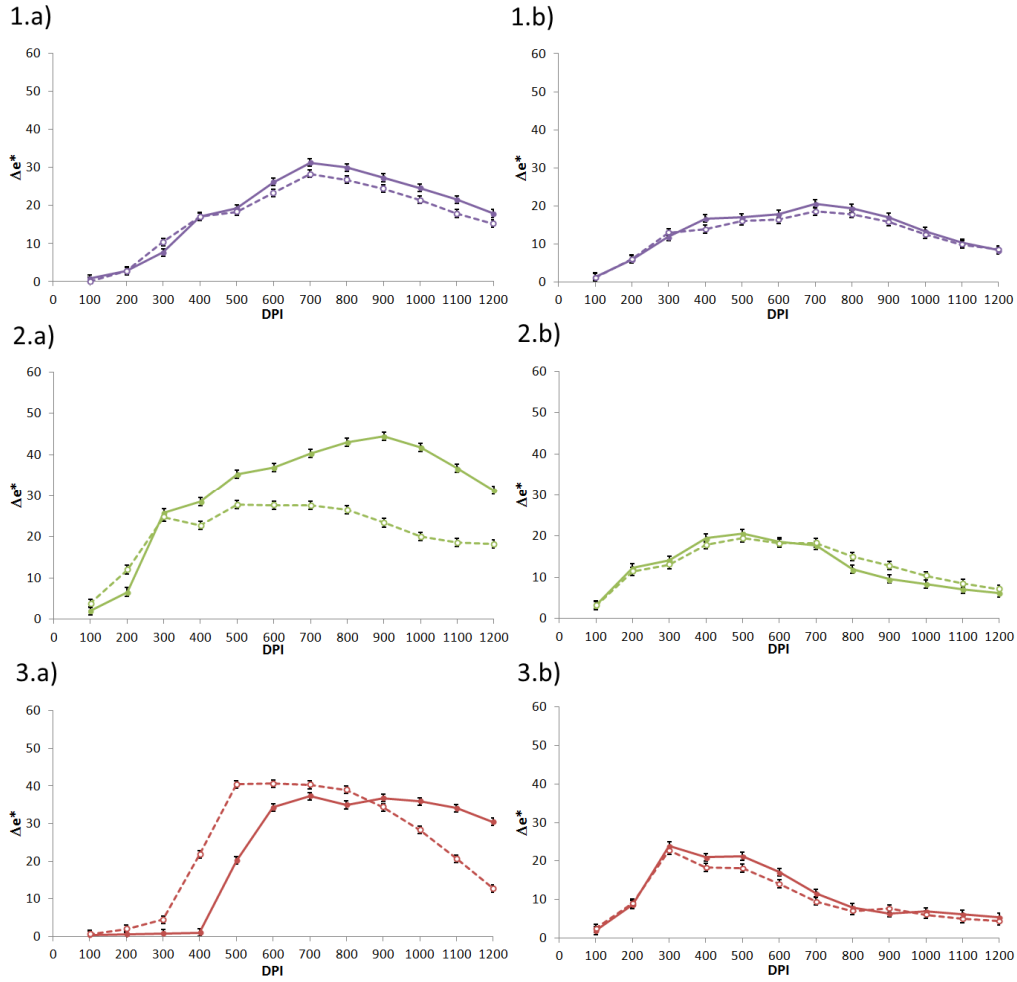

Figure 3.49. Influence of the Iriotec additive added to X% CB ABS on the contrast. 1) UV laser; 2) green laser; 3) IR laser; a) 0.05% CB ABS; b) 0.5% CB ABS. Material with Iriotec: dashed line; Material without Iriotec: continuous line.

Finally, figure 3.50 displays the contrast for the black-c ABS charged with the laser additive. In all the cases the presence of the additive worsened the results, which was in accordance with the previous results due to the CB quantity detected on the commercial material. The black pigment seems to disturb or mask the beneficial effect of the additive if its presence was higher than approx. 0.05%.

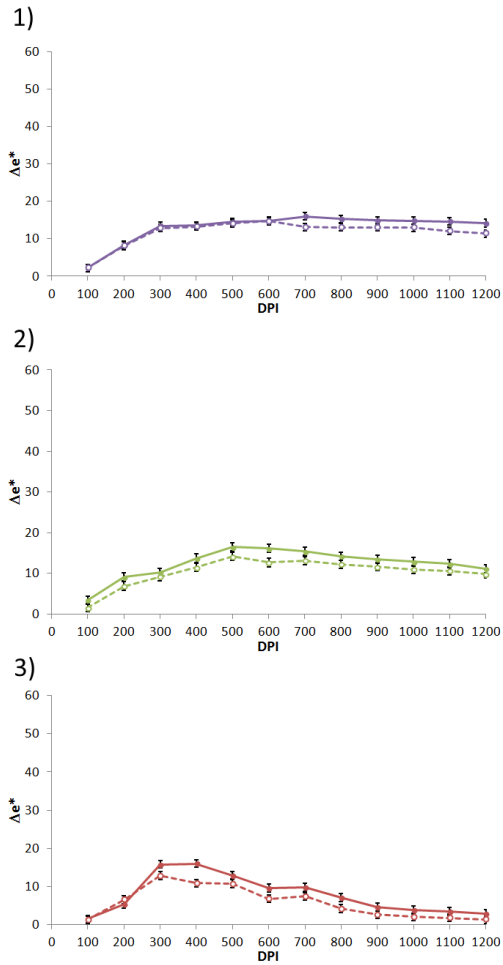

Figure 3.50. Influence of the Iriotec additive added to the black-c ABS on the contrast. 1) UV laser; 2) green laser; 3) IR laser. Material with Iriotec: dashed line; Material without Iriotec: continuous line.

Thus, it can be concluded that the use of the additive does not seem to have a beneficial effect on this marking, except for samples with a very low of CB if an IR laser is used.

3.3.6. Conclusions

The laser marking on samples derived from ABS mixed with different amounts of CB has been carried out using three lasers irradiating at 355 nm, 532 nm and 1064 nm. A commercial material was also studied. Finally, the effect of a laser additive, specially designed for IR laser marking, was also examined.

It was shown that the additive presence changed the optical spectrum of the ABS. The energy absorption on the wavelengths studied (from 325 to 1200 nm) was enhanced.

The laser marking mechanisms seem to be different for the lasers. IR laser and, to a lesser extent, the green laser irradiation led to thermally induce foaming depending on the DPI fixed in the experimental irradiation conditions. The best contrast was obtained on the 0.05% CB ABS using the green laser, although on the other compounds the best results were obtained using the IR laser. However, the marking mechanism seemed to be produced together with the foaming, a carbonisation of the polymer as can be seen in the values detected on the b* colour coordinate associated to a brownish colouration of the marks. This effect was reduced employing the IR laser that seemed to produce a better foaming effect on the material. Finally, the UV laser produced marks by a photochemical effect that was no dependent on the CB charge. That may be related to the laser produce a temperature increment that led to polymer carbonisation and pigment degradation. However, neither the topography nor the ATR-FTIR studies showed high ablation or polymer degradation, so it can be concluded that this effect should be only superficial.

Finally, the additive designed explicitly for laser marking led to slight blackening of the natural ABS. The only improvement detected in the marking process was for

the lowest quantity of black pigment analysed and under IR laser radiation. In the other cases, lower contrasts were obtained.

References

[3.1] UNE-EN ISO 11469:2001, "Plásticos. Identificación genérica y marcado de productos plásticos," Madrid, España. AENOR.

[3.2] ISO 1043-1:2011(en), "Plastics — Symbols and abbreviated terms — Part 1: Basic polymers and their special characteristics."

[3.3] F. T. L. Santo and J. P. Davim, "Laser applications in the field of plastics," vol. 9, Elsevier Sc, London, 2014, pp. 243–260.

[3.4] T. W. Ng and S. C. Yeo, "Aesthetic laser marking assessment using luminance ratios," *Opt. Lasers Eng.*, vol. 35, no. 3, pp. 177–186, 2001.

[3.5] Y. M. Noor, S. C. Tam, L. E. N. Lim, and S. Jana, "A review of the Nd:YAG laser marking of plastic and ceramic IC packages," *J. Mater. Process. Technol.*, vol. 42, no. 1, pp. 95–133, 1994.

[3.6] G. Ricciardi, M. Cantello, and G. S. Aira, "Marking of computer keyboards by means of excimer lasers," *CIRP Ann. - Manuf. Technol.*, vol. 45, no. 1, pp. 191–196, 1996.

[3.7] J. J. Pireaux *et al.*, "Excimer laser (h = 193 nm) versus Al K, X-ray damages on polymer surfaces: an XPS (core and valence levels) analysis of polytetrafluoroethylene, polypropylene and polyethylene," *Nucl. Instruments Methods Phys. Res. B*, vol. 105, pp. 186–191, 1995.

[3.8] T. Lippert, T. Nakamura, H. Niino, and A. Yabe, "Laser induced chemical and physical modifications of polymer films: dependence on the irradiation wavelength," *Appl. Surf. Sci.*, vol. 109–110, pp. 227–231, 1997.

[3.9] T. Lippert, F. Raimondi, J. Wambach, J. Wei, and A. Wokaun, "Surface modification and structuring of electrical conducting and isolating polyaniline films," *Appl. Phys. A*, vol. 69, no. 1, pp. S291--S293, 1999.

[3.10] P. Laurens, B. Sadras, F. Decobert, F. Arefi, and J. Amouroux, "Modifications of polyether-etherketone surface after 193 nm and 248 nm excimer laser radiation," *Appl. Surf. Sci.*, vol. 138–139, pp. 93–96, 1999.

[3.11] T.-C. Chang and P. A. Molian, "Excimer pulsed laser ablation of polymers in air and liquids for micromachining applications," *J. Manuf. Syst.*, vol. 18, no. 2, pp. 1–17, 1999.

[3.12] L. D. Laude, D. Martinez, C. Dicara, F. Hanus, and K. Kolev, "The ablation of polymers under excimer laser irradiation: the physics of the process and the polymer structure," *Nucl. Instruments Methods Phys. Res. Sect. B Beam Interact. with Mater. Atoms*, vol. 185, no. 1, pp. 147–155, 2001.

[3.13] J. Yip, K. Chan, K. M. Sin, and K. S. Lau, "Study on the surface chemical properties of UV excimer laser irradiated polyamide by XPS, TOF-SIMs and CFM," *Appl. Surf. Sci.*, vol. 205, no. 1–4, pp. 151–159, 2003.

[3.14] J. Yip, K. Chan, K. M. Sin, and K. S. Lau, "Comprehensive study of polymer fiber surface modifications Part 1: high-fluence UV-excimer-laser-induced structures," *Polym. Int.*, vol. 53, no. 6, pp. 627–633, 2004.

[3.15] P. Rytlewski and M. Żenkiewicz, "Laser-induced surface modification of polystyrene," *Appl. Surf. Sci.*, vol. 256, no. 3, pp. 857–861, 2009.

[3.16] Y. Feng, Z. Q. Liu, and X.-S. Yi, "Co-occurrence of photochemical and thermal effects during laser polymer ablation via a 248-nm excimer laser," *Appl. Surf. Sci.*, vol. 156, no. 1–4, pp. 177–182, 2000.

[3.17] L. Urech, T. Lippert, C. R. Phipps, and A. Wokaun, "Polymer ablation: From fundamentals of polymer design to laser plasma thruster," *Appl. Surf. Sci.*, vol. 253, no. 15, pp. 6409–6415, 2007.

[3.18] P. Laurens, M. O. Bouali, F. Meducin, and B. Sadras, "Characterization of modifications of polymer surfaces after excimer laser treatments below the ablation threshold," *Appl. Surf. Sci.*, vol. 154–155, pp. 211–216, 2000.

[3.19] J. Breuer, S. Metev, and G. Sepold, "Photolytic surface modification of polymers with UV-laser radiation," *J. Adhes. Sci. Technol.*, vol. 9, no. 3, pp. 351–363, 1995.

[3.20] M. Aden, V. Mamuschkin, and A. Olowinsky, "Influence of carbon black and indium tin oxide absorber particles on laser transmission welding," *Opt. Laser Technol.*, vol. 69, pp. 87–91, 2015.

[3.21] H. Y. Zheng, D. Rosseinsky, and G. C. Lim, "Laser-evoked coloration in polymers," *Appl. Surf. Sci.*, vol. 245, no. 1–4, pp. 191–195, 2005.

[3.22] Z. Cao *et al.*, "Laser-induced blackening on surfaces of thermoplastic polyurethane/BiOCl composites," *Polym. Degrad. Stab.*, vol. 141, pp. 33–40, 2017.

[3.23] W. Zhong *et al.*, "Laser-marking mechanism of thermoplastic Polyurethane/Bi2O3 composites," *ACS Appl. Mater. Interfaces*, vol. 7, no. 43, pp. 24142–24149, 2015.

[3.24] J. Bosman, "Processes and strategies for solid state Q-switch laser marking of polymers," Twente, 2007.

[3.25] K. Hashimoto, H. Irie, and A. Fujishima, "TiO2 photocatalysis: a historical overview and future prospects," *Jpn. J. Appl. Phys.*, vol. 44, no. 12R, p. 8269, 2005.

[3.26] J. Schneider *et al.*, "Understanding TiO2 photocatalysis: mechanisms and materials," *Chem. Rev.*, vol. 114, no. 19, pp. 9919–9986, 2014.

[3.27] X. Chen, L. Liu, Y. Y. Peter, and S. S. Mao, "Increasing solar absorption for photocatalysis with black hydrogenated titanium dioxide nanocrystals," *Science (80-.).*, vol. 331, no. 6018, pp. 746–750, 2011.

[3.28] T. Jedsukontorn, T. Ueno, N. Saito, and M. Hunsom, "Facile preparation of defective black TiO2 through the solution plasma process: effect of parametric changes for plasma discharge on its structural and optical properties," *J. Alloys Compd.*, vol. 726, pp. 567–577, 2017.

[3.29] Z. Wang *et al.*, "H-doped black titania with very high solar absorption and excellent photocatalysis enhanced by localized surface plasmon resonance," *Adv. Funct. Mater.*, vol. 23, no. 43, pp. 5444–5450, 2013.

[3.30] M. M. Khan, S. A. Ansari, D. Pradhan, M. O. Ansari, J. Lee, and M. H. Cho, "Band gap engineered TiO 2 nanoparticles for visible light induced photoelectrochemical and photocatalytic studies," *J. Mater. Chem. A*, vol. 2, no. 3, pp. 637–644, 2014.

[3.31] H. Li *et al.*, "Electrochemical doping of anatase TiO 2 in organic electrolytes for high-performance supercapacitors and photocatalysts," *J. Mater. Chem. A*, vol. 2, no. 1, pp. 229–236, 2014.

[3.32] B. Wang, S. Shen, and S. S. Mao, "Black TiO 2 for solar hydrogen conversion," *J. Mater.*, 2017.

[3.33] X. Chen, L. Liu, and F. Huang, "Black titanium dioxide (TiO2) nanomaterials," *Chem. Soc. Rev.*, vol. 44, no. 7, pp. 1861–1885, 2015.

[3.34] Y. Liu, L. Tian, X. Tan, X. Li, and X. Chen, "Synthesis, properties, and applications of black titanium dioxide nanomaterials," *Sci. Bull.*, vol. 62, no. 6, pp. 431–441, 2017.

[3.35] S.-K. Lee, P. K. J. Robertson, A. Mills, D. McStay, N. Elliott, and D. McPhail, "The alteration of the structural properties and photocatalytic activity of TiO2 following exposure to non-linear irradiation sources," *Appl. Catal. B Environ.*, vol. 44, no. 2, pp. 173–184, 2003.

[3.36] T. Le Mercier, M. Quarton, M. -F. Fontaine, C. F. Hague, and J. -M. Mariot, "Near surface defects created by 355 nm laser irradiation of rutile," *J. Appl. Phys.*, vol. 76, no. 6, pp. 3341–3346, 1994.

[3.37] H. Y. Zheng, H. X. Qian, and W. Zhou, "Analyses of surface coloration on TiO2 film irradiated with excimer laser," *Appl. Surf. Sci.*, vol. 254, no. 7, pp. 2174–2178, 2008.

[3.38] X. Chen *et al.*, "Laser-modified black titanium oxide nanospheres and their photocatalytic activities under visible light," *ACS Appl. Mater. Interfaces*, vol. 7, no. 29, pp. 16070–16077, 2015.

[3.39] H. Zheng and G. C. Lim, "Laser-effected darkening in TPEs with TiO 2 additives," *Opt. Lasers Eng.*, vol. 41, no. 5, pp. 791–800, 2004.

[3.40] L. D. Laude, N. Boutarek, and K. Kolev, "Excimer lasers for surface engineering of polymer-based composites," *Nucl. Instruments Methods Phys. Res. Sect. B Beam Interact. with Mater. Atoms*, vol. 105, no. 1, pp. 254–257, 1995.

[3.41] C. M. Long, M. A. Nascarella, and P. A. Valberg, "Carbon black vs. black carbon and other airborne materials containing elemental carbon: Physical and chemical distinctions," *Environ. Pollut.*, vol. 181, pp. 271–286, 2013.

[3.42] Mitsubishi Chemical, "What is carbon black," *About Carbon Black*, 2017. [Online]. Available: http://www.carbonblack.jp/en/cb/index.html. [Accessed: 27-Oct-2017].

[3.43] N. Hauptman, A. Vesel, V. Ivanovski, and M. K. Gunde, "Electrical conductivity of carbon black pigments," *Dye. Pigment.*, vol. 95, no. 1, pp. 1–7, 2012.

[3.44] B. Acherjee, A. S. Kuar, S. Mitra, and D. Misra, "Effect of carbon black on temperature field and weld profile during laser transmission welding of polymers: A FEM study," *Opt. Laser Technol.*, vol. 44, no. 3, pp. 514–521, 2012.

[3.45] S. E. Zelensky *et al.*, "Kinetics of light scattering in an epoxy resin suspension of carbon microparticles," *J. Appl. Spectrosc.*, vol. 78, no. 3, p. 371, 2011.

[3.46] K. S. Zelenska, S. E. Zelensky, L. V Poperenko, K. Kanev, V. Mizeikis, and V. A. Gnatyuk, "Thermal mechanisms of laser marking in transparent polymers with light-absorbing microparticles," *Opt. Laser Technol.*, vol. 76, pp. 96–100, 2016.

[3.47] N. Pagano, A. Ascari, E. Liverani, L. Donati, G. Campana, and A. Fortunato, "Laser interaction with carbon fibre reinforced polymers," *Procedia CIRP*, vol. 33, pp. 423–427, 2015.

[3.48] M. I. Khan, K. A. Bhatti, R. Qindeel, H. S. Althobaiti, and N. Alonizan, "Structural, electrical and optical properties of multilayer TiO2 thin films deposited by sol–gel spin coating," *Results Phys.*, vol. 7, pp. 1437–1439, 2017.

[3.49] E. Sennik, N. Kilinc, and Z. Z. Ozturk, "Electrical and VOC sensing properties of anatase and rutile TiO2 nanotubes," *J. Alloys Compd.*, vol. 616, pp. 89–96, 2014.

[3.50] H. Tang, K. Prasad, R. Sanjines, P. E. Schmid, and F. Levy, "Electrical and optical properties of TiO2 anatase thin films," *J. Appl. Phys.*, vol. 75, no. 4, pp. 2042–2047, 1994.

[3.51] X. Chen and A. Selloni, "Introduction: titanium dioxide (TiO2) nanomaterials." ACS Publications, 2014.

[3.52] J. G. Bokria and S. Schlick, "Spatial effects in the photodegradation of poly (acrylonitrile–butadiene–styrene): a study by ATR-FTIR," *Polymer (Guildf).*, vol. 43, no. 11, pp. 3239–3246, 2002.

[3.53] Thermo Scientific, "XPS simplified," *Titanium - Transition Metal*, 2017. [Online]. Available: https://xpssimplified.com/elements/titanium.php. [Accessed: 15-Jan-2018].

[3.54] M. Biesinger, "X-ray Photoelectron spectroscopy (XPS) reference pages," *Titanium*, 2015. [Online]. Available: http://www.xpsfitting.com/search/label/Titanium. [Accessed: 15-Jan-2018].

[3.55] M. Biesinger, "X-ray Photoelectron spectroscopy (XPS) reference pages," *Titanium*, 2015. [Online]. Available: http://www.xpsfitting.com/search/label/Titanium.

[3.56] H. Do, T.-C. Yen, C.-S. Tian, Y.-H. Wu, and L. Chang, "Epitaxial growth of titanium oxycarbide on MgO (001) substrates by pulsed laser deposition," *Appl. Surf. Sci.*, vol. 257, no. 7, pp. 2990–2994, 2011.

[3.57] D. Han, Z. Meng, D. Wu, C. Zhang, and H. Zhu, "Thermal properties of carbon black aqueous nanofluids for solar absorption," *Nanoscale Res. Lett.*, vol. 6, no. 1, p. 457, 2011.

[3.58] J. C. Ion, *Laser processing of engineering materials*, 1st ed. Oxford: Elsevier, 2005.

[3.59] D. Bäuerle, *Laser processing and chemistry*, 4th ed. Berlin: Springer, 2011.

4. Control of the wettability of an ABS surface by laser micro-structuring

The wettability of solid surfaces has a particular interest due to the wide range of applications derived from the control of this property, which is directly related to the surface structure or roughness and the chemical interactions with a liquid. Nature gives us some examples of structures that affect the wettability properties such as self-cleaning superhydrophobic surfaces on the Lotus leaf [4.1], hierarchical structures on plants [4.2], butterflies that exhibit directional wettability properties [4.3] or the Gecko toe adhesion property [4.4].

The surface interaction of a water drop deposited on a surface is characterised by a "contact angle" (CA). This angle θ is measured between the solid/liquid and liquid/air interfaces as is described in figure 4.1. The contact angle at the equilibrium (static angle) takes the name of Young's angle derived from the eq. (4.1) [4.5].

$$\gamma_{SG} = \gamma_{SL} + \gamma_{LG} \cos\theta \tag{4.1}$$

where γ is the interfacial tension and the subscript refer to solid, liquid and gas phases.

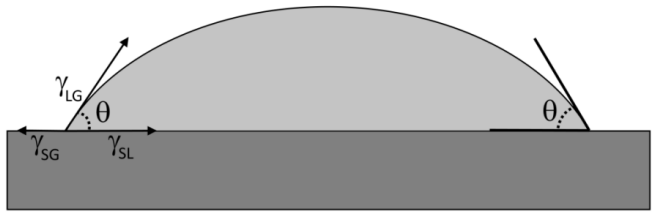

Figure 4.1. Cross section of a drop on a flat surface with the contact angle θ.

A surface is considered hydrophilic if its static CA is below 90°, and superhydrophilic if this CA is lower than 10°. By contrast, surfaces with a static CA higher than 90° are hydrophobic, and if CA is higher than 150°, it can be considered as superhydrophobic surfaces [4.6].

Additionally, a non-equilibrium situation is measured defined by the advancing (θ_A) and receding angle (θ_R) of a drop sliding on a vertical surface. However, a non-equilibrium situation is usually more useful, see figure 4.2. The contact angle hysteresis (CAH) measures the difference between both angles, eq. (4.2). A low CAH is exhibited by a surface where the drop easily descends. On the opposite, a surface with a relatively high CAH is due to a strong interaction with the surface (the drop tends to adhere to the surface) [4.7], [4.8].

$$CAH = \theta_A - \theta_R \tag{4.2}$$

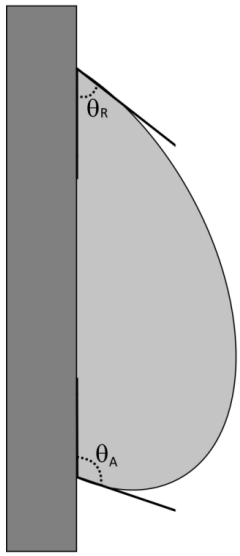

Figure 4.2. A drop sliding slowly on a vertical surface with advancing angle (θ_A) at the front and receding angle at the back (θ_R).

The roughness of the surface affects to the wettability following either the Wenzel model [4.9] when the liquid fills all the space or the Cassie-Baxter when some air bubbles are trapped between the drop and the surface [4.10], see figures 4.3.a and b respectively. In Wenzel state, the droplets pin the surface in a wet-contact mode thus high CAH is observed. In Cassie-Baxter the water droplets adopt a non-wet-contact mode on the surface and can quickly roll presenting a low CAH [4.6].

-According to Wenzel's model, the contact angle θ^w can be expressed as:

$$\cos\theta^W = W\cos\theta \tag{4.3}$$

where θ is the CA at the equilibrium determined on a flat surface, and W is the ratio of the rough area to the flat projected area, always bigger than 1.

-Meanwhile, the contact angle θ^c according to the Cassie-Baxter (C-B) model is:

$$\cos\theta^C = C\cos\theta - (1-C) \tag{4.4}$$

where θ is the CA at the equilibrium determined on a flat surface and C is the area fraction of liquid-solid contact.

Furthermore, three more states can be defined, see figure 4.3. The "lotus effect" is a special case of the Cassie-Baxter where the CAH is especially low resulting from the coexistence of a micro- and nano-structure (hierarchical structures). Also, a transitional state between Cassie-Baxter and Wenzel is defined by considering that the water droplets penetrate slightly into the roughness without being in contact with the entire surface as occurs in the Wenzel state. Thus the equilibrium CA will be placed in between those predicted by Wenzel and Cassie-Baxter. Finally, the "Gecko" state has a high CA together with a high adhesion effect. This difference with the Cassie-Baxter model is associated with the air trapped between the water and the surface. The trapped air pockets are connected to the atmosphere in C-B state while

this connection does not exist in the Gecko. The trapped air produces a negative pressure enhancing the adhesion of the water to the surface [4.6].

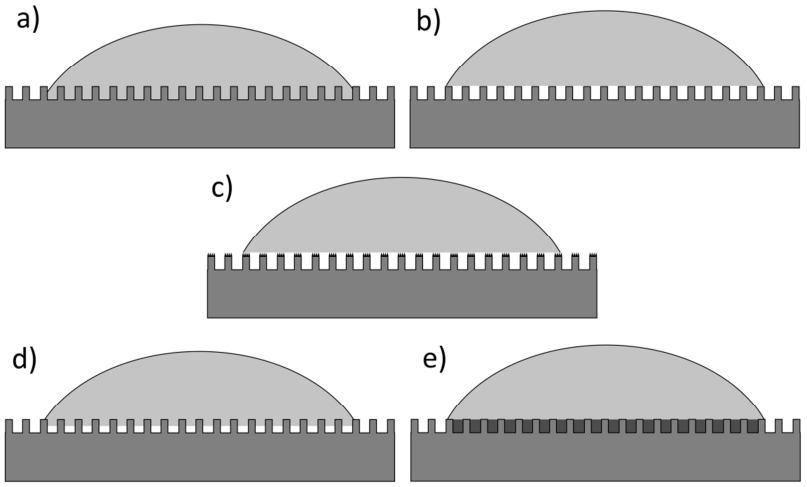

Figure 4.3. Water drop wetting scheme (the angle is only an idealisation) of a rough surface. a) Wenzel model; b) Cassie-Baxter; c) "Lotus-effect" d) transitional state between Wenzel and Cassie-Baxter; e) "Gecko" state. The shadow area represents trapped air zones.

Surface chemistry plays a key role in determining the wettability of a surface. The presence of high surface energy chemical groups such as $-OH$, $-NH_2$, $-COOH$, $-OSO_3H$, $-NH_3^+$, $-COO^-$, $-OSO_3^-$, promotes hydrophilicity, whereas materials such as hydrocarbon, fluorocarbon or silicone based polymers have low surface energy and exhibit hydrophobicity [4.11].

The control of the wettability properties of different materials is extensively studied and applied to numerous fields [4.12]. For example, special interest is on surfaces having self-cleaning properties [4.13], anti-frosting and ice resistance behaviour [4.14], [4.15], anti-fouling [4.16], [4.17], anti-corrosion [4.18], [4.19] or transparent and anti-reflective properties [4.20], [4.21]. Different chemical coatings or physical patterning processes have been used to mimic surfaces with these properties. Usually, the methods proposed work properly at laboratory scale, but are challenging

to be implemented for mass production. However, during this last two decades, an increasing number of techniques have demonstrated the potential for scale-up material processing to control surface properties [4.22]. One interesting industrial strategy to change the surface topography is the use of a laser beam as a micromachining tool [4.23].

4.1. Laser treatment to control the wettability

The use of lasers to tune the wettability properties of materials like steel [4.24]–[4.26], titanium [4.27], [4.28], silicon [4.29], [4.30] or different polymer materials [4.31]–[4.33] is widespread. Various approaches have been addressed to change the polymer wetting behaviour by lasers such as chemical activation of the surface [4.34], controlled isomerisation [4.35] or nano- and micro-patterning [4.36]–[4.39].

Different strategies can be studied to modify in a controlled way the material surface using a patterning approach [4.40]. For example, ultra-short lasers are used to produce very precise ablation reducing the thermal impact enabling high defined patterns [4.41], [4.42] or the creation of ripples [4.43], [4.44]. However, the use of these lasers is not extended in the manufacturing industry because of their expensive cost. Other proposed techniques involve processes like beam shaping control [4.45] or micro-machining of the injection mould [4.46].

Another approach creating the structures by the laser is the use of interference patterns (direct laser interference patterning, DLIP). This method is based on dividing the laser beam, usually in two different paths to eventually produce an interference pattern on the material surface. Periodical arrays can be created at micro- or nano-scale using high energy lasers. This technique can be used to generate regular structures by direct ablation [4.47] or in combination with ripples formation to create more complex topographies [4.48].

However, the use of nanosecond pulse-width lasers to modify the wettability of polymers, especially the ABS, has not been widely reported. During this chapter, the possibilities that exhibit this type of lasers to modify the wettability of ABS are

explored. These lasers have the advantage of their low cost compared to the ultra-shorts lasers. Furthermore, the thermal impact on the polymer can be reduced by using lasers in green and UV wavelengths. Three different strategies were used to modify the wettability of the ABS polymeric material: direct laser ablation to create patterns, control of the surface roughness with laser and DLIP. Before studying these different strategies, a brief preliminary study of polymer ablation was done using the same ABS samples.

The material selected was the commercial ABS employed by BSH and provided by Elix as it was introduced in the section 2.1.2, the white-c ABS. The material behaviour under the different laser wavelengths was intensely studied in chapter 3.

Different preliminary tests were performed on the white-c ABS to create the ablation patterns before this study. As it was expected, the results with the IR wavelength were not satisfactory because of its high thermal impact; the holes formed were bigger than 100 µm. Therefore, only lasers of two different wavelengths were used to perform this study, green (532 nm) and UV (355 nm). Three different laser systems were used: UV laser, green laser and interf UV laser, see section 2.1.1. The first two lasers were configured to use an optical setup in such a way that allowed the lowest spot widths possible, 7 µm and 30 µm for the UV and green lasers respectively. The interferometry was performed using a laboratory laser that provided the proper flexibility for this technique. The Brilliant laser was the most suitable option for this purpose.

The analysis of the structures created was done using a confocal microscope, see section 2.2.2.2. This device allows obtaining a 3D image of the structures formed as well as to measure their physical dimensions. In some cases, the ESEM, see section 2.2.2.3, was employed to give additional information about the topography. The wettability was measured using a contact angle goniometer, see section 2.2.4. It was

also measured the time evolution of this characteristic. The samples were placed under environmental conditions in our lab during six months. Those conditions were relatively stable: temperature ~22°C and relative humidity ~40%. UV light was avoided, and no special protection to dust was taken.

4.2. Laser ablation of ABS

The laser ablation is a widely recognised methodology of material processing since the first studies performed in the 80's [4.49], [4.50]. The primary objective of this technique is usually to create different structures or to retire material in a controlled way. There is a vast bibliography related to the ablation of polymers [4.51], being extensively studied, both theoretically [4.52], [4.53] and experimentally [4.54], [4.55]. Concerning to the origin of the ablation process, different effects have been proposed: photo-chemical [4.56], [4.57], photo-thermal [4.58]–[4.60], photo-physical [4.61] or a combination of them [4.62]–[4.64].

The temperature is a critical factor in the ablation mechanism [4.65]. During the laser ablation regime, a shorter interaction time, less than one μs, can induce drastic superheating of the polymer [4.66]. Another critical factor is the ablation threshold, the minimum energy associated with the occurrence of the ablation phenomena. This parameter is highly dependent on the polymer chemical chains [4.67], [4.68] and the laser wavelength.

Nanosecond pulse-width lasers [4.69] has been the most commonly used for this application, recently replaced by ultra-short pulsed laser [4.70]–[4.74] (pulse-width in the range of pico or femtoseconds) because the possibility of reducing the heat affected zone and the ablation threshold [4.46].

In the case of laser ablation of ABS, some studies have been done previously performing a comparison between different laser wavelengths and pulse widths [4.75] regarding the ablation depth. It was found that the ablation threshold of the ABS and SAN is 0.3 J/cm^2 in the range of ns [4.76] pulse width or 20 mJ/cm^2 for pulses in the range of 10 ps [4.77].

The objective of this section is not to make an in-depth study of the ablation mechanisms in the material. The focus is to change the wettability of ABS samples by tuning the topographical characteristics of the samples using different laser irradiation approaches. The final purpose is to know how it can be created structures on the material surface to affect the wettability of the material predictably. For this use, it is desirable to minimise undesirable effects like heat affected area or zone (HAZ).

The study is done performing two different types of textures, holes and lines. The holes were made by successive repetitions of pulses while the lines were created by grouping the pulses in a controlled distance. This type of study has been previously reported in the bibliography [4.78]. Different laser parameters were explored as power, wavelength, repetitions or scanning speed.

4.2.1. Laser ablation: formation of holes

The work methodology to create holes was not the same for both lasers. The UV laser ablation was done working on the focal position and studying the influence of different pulse numbers. The first results proved that working out of focus with the UV laser had no sense because the HAZ grew fast while the hole depth was profoundly reduced. In the case of the green laser, it was examined how the holes were created along different positions going out the focal plane. The evolution of the affected area and hole width exhibited an interesting region that proved to be useful to further microstructuring. Successive pulses on focus with the green laser caused a big increment on the HAZ, so it was not a valid solution for our purpose. The powers used for the UV and green lasers were 1.8 W and 3.6 W (maximum powers on both cases), and the spot widths were 7 µm and 30 µm corresponding to work fluences of

312 J/cm^2 and 34 J/cm^2 respectively (on focus), far beyond the ablation threshold. The pulse frequency in both lasers was 15 kHz.

Some examples of confocal topographical images of the holes created with both lasers can be seen in figure 4.4. On the one hand, figure 4.4.1 shows the topography of the hole created by the UV laser on focus after one pulse (1.a) and five consecutive pulses (1.b). It can be seen that one pulse only made a material rising over the unaffected area. By contrast, after five pulses the material was engraved in the centre of the area with a ring of elevated material around the centre. On the other hand, the results on the material ablated by the green laser are shown in figure 4.4.2, after one pulse on focus (2.a) and the same pulse 0.8 mm out of focus (2.b) The green pulse on focus was able to engrave the material. Also, a ring of elevated material around the hole was visible. This hole dimension was bigger than the observed for the UV laser, as could also be expected from their spot width differences, 7 µm and 30 µm respectively. Finally, the hole created out of focus by the green laser exhibited a different appearance than the previously analysed holes. In this case, it showed a big area affected; the region in the middle was not homogeneous and appeared some peaks and rest of material along the region created. This effect was caused probably by material melted and not directly evaporated. The peaks or pillars were less than 10 µm in size.

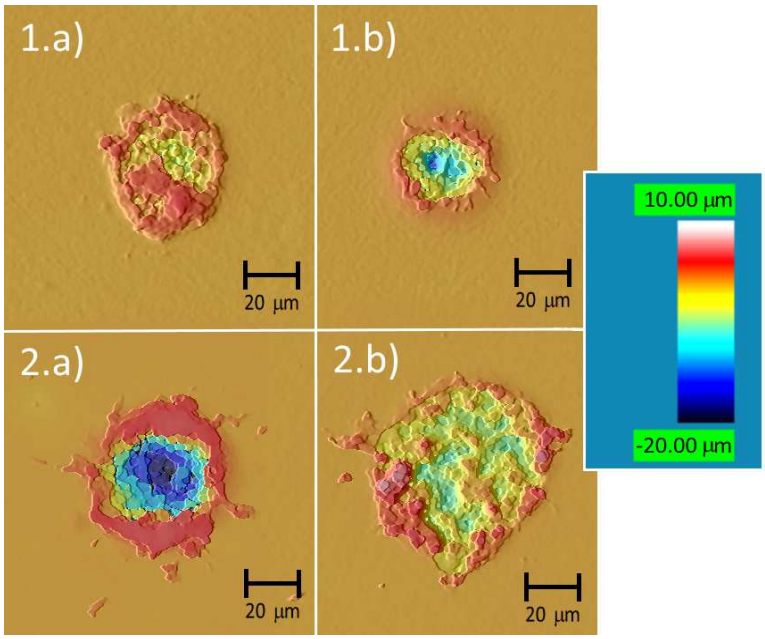

Figure 4.4. Confocal microscope image of the holes created by the lasers on the white-c ABS. 1.a) 1 pulse, UV laser; 1.b) 5 pulses, UV laser; 2.a) 1 pulse, green laser; 2.b) 1 pulse 0.8 mm out of focus, green laser.

Hereafter the measurements of the holes obtained are showed. These measurements were done according to the scheme presented in figure 4.5. The average depth of the hole was measured in the central region of the hole. The hole width was measured taking as reference the level of the unmarked region. The affected region width was measured considering the region where there was a visible change in the topographical dimension of the surface. Finally, the edge width represented the difference between the affected region width and the hole width. Some of the holes were not perfectly circular; the measurements were the average of both axis.

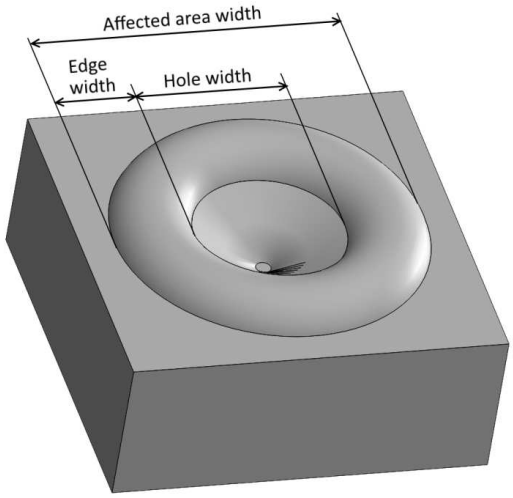

Figure 4.5. 3D model of the ablation hole created.

Firstly, the results obtained with the UV laser after successive pulses are examined. Figure 4.6 shows the evolution of the hole dimensions. The most significant changes happened for the first pulses. It can be seen that until approx. 20 pulses the depth grown quickly, then the penetration increased slowly. The different widths exhibited a remarkable initial modification, and then they tended to saturate gradually.

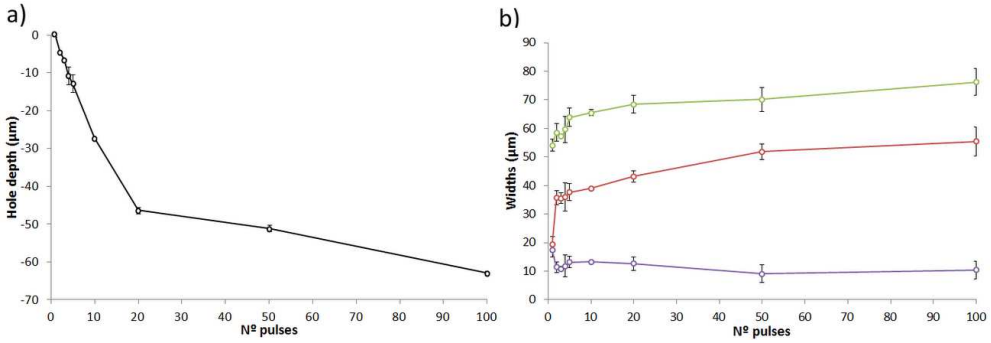

Figure 4.6. Hole dimensions created by the UV laser on the white-c ABS in terms of the number of pulses. a) Measured depth; b) Different widths measured: hole width (red line), affected area width (green line) and edges width (purple line).

Secondly, the green laser ablation results are showed. Figure 4.7 illustrates the influence of the focal position in the same hole dimensions shown for the UV laser

case. Also, it is given the theoretical spot width in terms of the focal position. As it could be expected, the maximum depth was obtained in the focal position while out of focus, the depth tended gradually to be reduced. Also, the hole and affected widths grew going out of the focus until a maximum was reached where they began to decrease. This type of behaviour is typical of studies of ablation out of focal position on materials [4.79]. The HAZ grows when the sample is moved away from the focal point until the fluence drop caused a high decrease in the material ablated. The evolution of the edges width exhibited a peculiar interest; there was a region, from 0.5 mm to 1.5 mm out of focus in both directions, where the edge width showed a minimum. Furthermore, that region matched approximately with a local minimum or plateau area observed in the depth measurement. As it will be described later, this region showed an especial interest for its wetting properties.

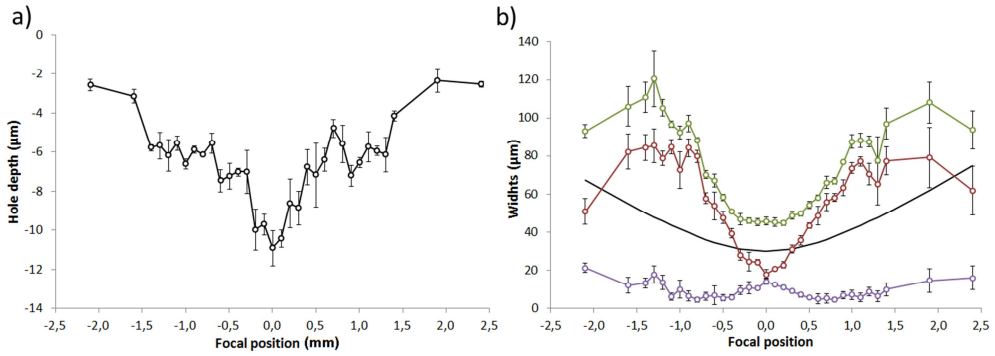

Figure 4.7. Hole dimensions created by the green laser on the white-c ABS in terms of the focal position. a) Measured depth; b) Different widths measured: hole width (red line), affected area width (green line) and edges width (purple line). The continuous black line represented the calculated spot width.

4.2.2. Laser ablation: formation of lines

In addition to the study of holes, the creation of lines is essential to create patterns with the laser. These lines were produced grouping together pulses, so the overlap between the laser spots was a critical factor. This study was only made with the UV laser because of the high thermal impact of the green laser observed on the white-c ABS when some pulses were grouped: a substantially affected area was produced in comparison to the UV wavelength. So, bearing in mind that the final purpose of this ablation study was to understand the feasibility of the creation of regular structures as smaller as possible, significantly affected areas should be avoided.

The physical dimensions of the lines determined how close the linear structures can be created. Figure 4.8 illustrates how the laser spots were grouped to form a line. The picture shows how the overlap between laser pulses was directly related to the spot distance and the spot width. The study was done varying the spot distance between laser pulses to create a row and the number of repetitions of this process to eventually give rise to the final line. Also, two laser powers were tested, 1.8 W and 1.2 W, the maximum power available and an intermediate value respectively, trying to observe if the use of a lower power reduced the HAZ.

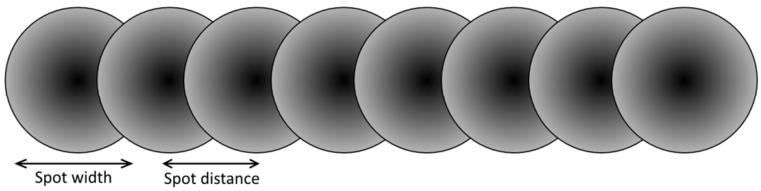

Figure 4.8. Spot configuration used to create a line. The spot distance and the hole affected area determined the overlap between the successive pulses.

The confocal images of some of the lines created with the UV laser on white-c ABS are shown in figure 4.9 displaying four examples of lines with different

characteristics depending on the variables analysed. For example, using a low spot distance (10 µm) compared to the hole width measured before, it was possible to create well-defined lines with small HAZ (figure 4.9.a). Also, reducing the power and increasing the number of repetitions, a deep line with long borders was obtained (figure 4.9.b). Increasing the distance between pulses to 45 µm showed that the holes were not enough overlapped to create a distinct line (figure 4.9.c) even for a high number of repetitions (figure 4.9.d).

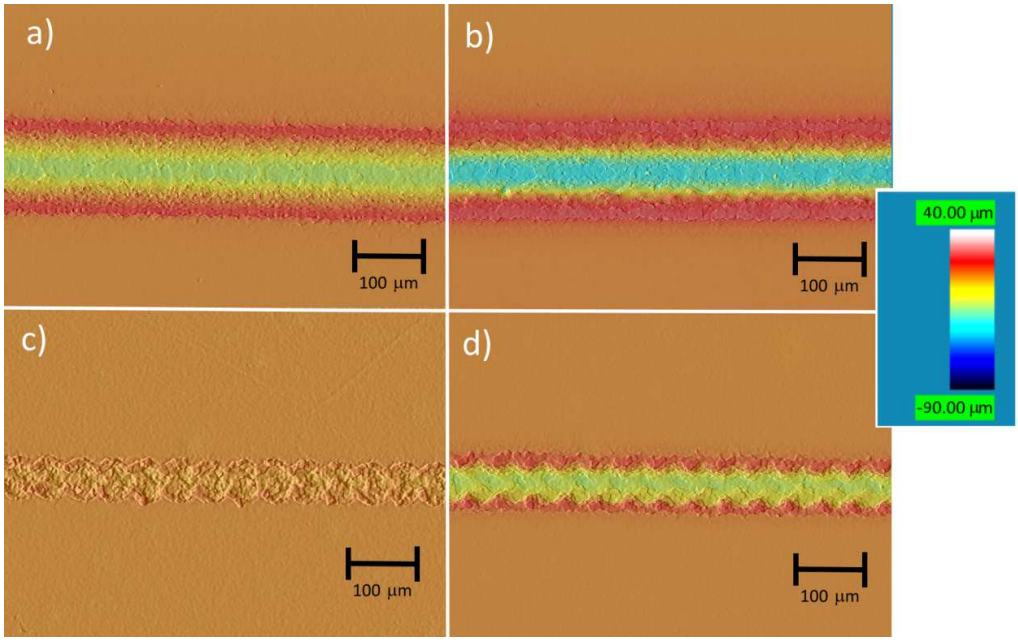

Figure 4.9. Image of the lines produced by the UV laser. a) Spot distance 10 µm, one repetition, 1.8 W; b) Spot distance 10 µm, three repetitions, 1.2 W; c) Spot distance 45 µm, one repetition, 1.8 W; d) Spot distance 45 µm, five repetitions, 1.8 W.

The figures 4.10 and 4.11 show the evolution of the line physical dimensions with reference to the spot distance and the number of repetitions for the two studied powers, 1.8 W and 1.2 W respectively. The measured parameters were the area affected (measured similarly to the case of the hole creation), the channel width (the same as the hole width), the edges height (the difference between the two previous

parameters) and the valley depth (corresponding to the mean depth of the central area).

As it could be expected, the number of repetitions increased all the measured variables. Similarly, all the parameters tended to asymptotic values when the spot distance was increased. Making a comparison between the two laser powers, both presented the same evolution in their values. The HAZ was highly reduced using the lowest power although the rest of the dimensions were also lower than using the highest power.

Experimentally it was proved that it was possible to cover almost all the experimental results obtained only using two spot distances (10 µm and 45 µm) and both laser powers. Consequently, they were used to create the patterns to modify the wettability.

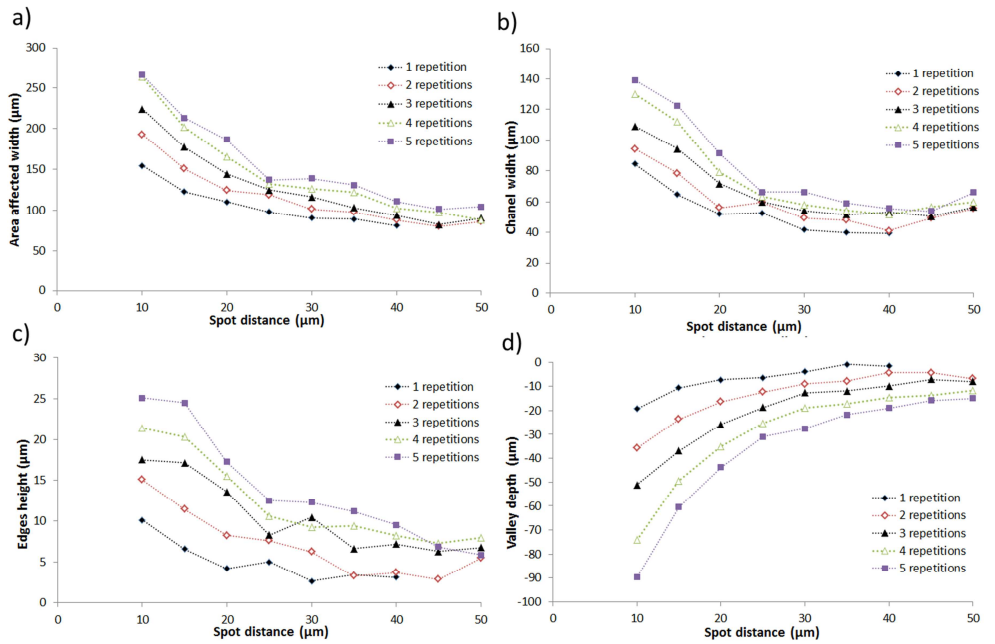

Figure 4.10. Line dimensions created with the UV laser at 1.8 W in terms of the spot distance and the number of repetitions. a) Area affected width; b) Chanel width; c) Edges height; d) Valley depth.

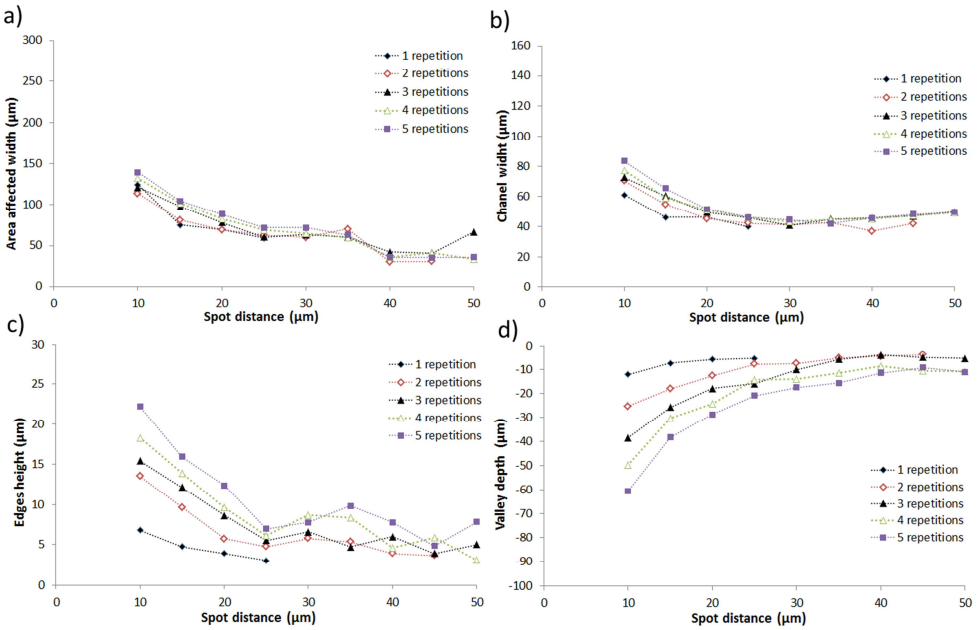

Figure 4.11. Line dimensions created with the UV laser at 1.2 W in terms of the spot distance and the number of repetitions. a) Area affected width; b) Chanel width; c) Edges height; d) Valley depth.

4.2.3. Conclusion

According to this preliminary study, the use of two different nanosecond lasers (green and UV wavelengths) proved to be a suitable solution to ablate the material and to create structures. The lasers analysed exhibited differences associated with the ablation phenomena. The green laser causes a well-known thermal impact on the polymer; the formed holes showed a crater structure with the accumulated material in the edges. Furthermore, it was possible to work outside of the focus, although the resulting holes were inhomogeneous and presented some irregular peaks on the sides. This fact may be associated with an incomplete thermal ablation of the polymer that left some remaining material. By contrast, the UV laser was not able to create a clear crater with one single pulse even considering that the fluence was higher than the

green laser (the spot width was minor). It was needed to accumulate consecutive pulses to create an ablation crater. Even that, the affected area did not grow too much, allowing the development of lines.

This study was used to select the lasers for each type of surface modification. For patterning using direct laser ablation, the UV laser is the selected alternative because of its lower thermal affection. The laser surface roughness can be controlled with the green laser because of the possibility of finely tune the shape of the holes. Finally, the direct laser interference patterning (DLIP) should be made with the interf UV laser since this laser is the only one that provides the required flexibility for this technique. Although this laser was able to work with three wavelengths, 355, 532 and 1064 nm, the use of the UV seems the most suitable to create the best-defined structures with the lowest HAZ.

4.3. Control of the wettability by direct laser ablation patterning

The first technique proposed to affect the wettability of the white-c ABS was direct laser ablation to pattern the surface of the material. According to the results of the previous section, it is possible to make either an arrangement of holes or an array of parallel and perpendicular lines [4.80], [4.81] producing different structures that can modify the wettability of the polymer surface. According to the ablation results, the UV laser was selected.

The different combination of holes and lines used to modify the wettability are shown in figure 4.12. In the case of a distribution of parallel and perpendicular lines two variables were taken into account: the distance between the lines (hatch distance), always considering symmetry between both axes, and the laser parameters used to form the lines as they were introduced in the previous section. In the case of the hole distributions, the laser setup allows performing a sequence of holes either always from left to right (unidirectional mode) or alternating direction (bidirectional mode). Further information about the laser mechanism to mark areas can be found in section 1.2.4. Using these methods, it is possible either to create a square arrangement (unidirectional mode, figure 4.12.b) or to produce a displacement of half spot distance between consecutive lines creating a triangular arrangement (bidirectional mode, figure 4.12.c). In both cases, the distance between two sequences of holes was the same than the spot distance or distance between two consecutive holes in the same sequence as it is schematically represented in figures 4.12.b and c. The laser parameters used to form the holes were introduced in the previous section.

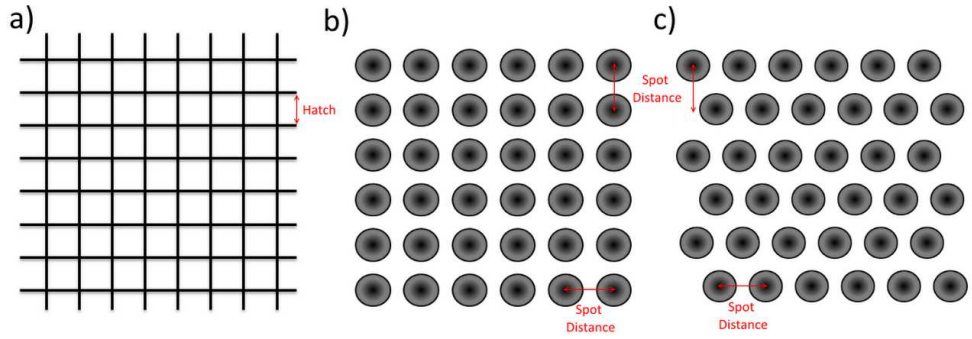

Figure 4.12. Scheme of the three different patterns used to create structures on the polymer surface. a) Symmetric distribution of parallel and perpendicular lines; b) square arrangement of holes made in a unidirectional mode; c) triangular arrangement of holes made in a bidirectional mode

Apparently, it would also be possible to make other designs by combining the lines at different angles, breaking the symmetry in each direction or distributing the holes in other arrangements. However, the patterns used were selected because of their simplicity, and the employment of alternatives was not explored in this study that it is mainly focused on understanding the influence of the topographical characteristics in the final wettability.

This section is structured in three parts. Firstly, the different structures created by the laser patterns selected will be observed by confocal microscopy. Secondly, using the theories of Cassie-Baxter and Wenzel, theoretical models of the wettability properties of the previous topographies will be calculated. Finally, their wettability behaviour will be examined and compared to the results predicted by the models.

4.3.1. Topography of the patterned laser surface

The laser parameters to form the patterns were selected according to the results described in section 4.2 of the creation of holes and lines with the UV laser. Firstly, the structure of parallel and perpendicular lines was created by choosing two different spot distances, 10 µm and 45 µm. As it was shown, the use of both distances facilitated to cover almost all the combinations of topographical dimensions like line width or depth. Furthermore, working with a spot distance of 10 µm allowed creating structures with very defined and deep lines. By contrast, the lines formed by a spot distance of 45 µm presented a worse deep and definition but showed smaller HAZ. Furthermore, different distances between the lines and two laser powers, 1.2 W and 1.8 W were explored. Therefore, using both powers (1.2 W and 1.8 W) and the ablation results obtained previously, the following parameters were selected: for the lines created at 10 µm of spot distance, the hatch between adjacent lines ranged from 70 µm to 230 µm in successive increment of 10 µm; meanwhile, for the lines created at 45 µm of spot distance, the hatch distance used ranged from 50 µm to 200 µm, (10 µm increment). The number of repetitions to create each line was also varied for both cases, from 1 to 5.

All of these variables introduced a high number of combinations. The study was done in successive steps taking into account our previous experience. For example, it could be seen that increasing the number of pulses allowed producing higher cones, or employing 45 µm of spot distance instead of 10 µm made possible to reduce the distance between the lines. Therefore, this permitted rejecting some of the combinations of parameters and selecting suitable laser parameters to perform the experiments.

Figure 4.13 showed the confocal 2D and 3D images of some representative examples of the achieved structures. Approximately, all the laser parameters under

study form the same topography, a set of elevated truncated cones in the areas non-irradiated, while in the intersection of the lines a hole was created. This hole can be simulated as an inverted truncated cone, which experimentally shows approximately the same dimensions that the elevated cone. Therefore, the structure was presented as a distribution of truncated cones in both directions, up and down, with respect to the surface (see next section for the theoretical modelling). Different degrees of resolution of this structure were observed depending on the experimental irradiation conditions. For example, figure 4.13.1 represents the "standard structure". The laser parameters were 1.8 W, line distance 80 µm, spot distance 10 µm and one repetition. Figure 4.13.2 exhibits a "high-defined structure". The laser parameters were 1.2 W, line distance 100 µm, spot distance 10 µm and three repetitions. In this case, the structure was also made by truncated cones, but they were higher and deeper than in the previous case. Finally, figure 4.13.3 represents a "poorly-defined structure". The laser parameters were 1.8 W, line distance 60 µm, spot distance 45 µm and five repetitions. This surface also showed the structure of cones although they were unequal and in some cases, the line was not created entirely appearing a bridge between the elevated areas. Thus, the rest of the laser parameters exhibited topographies according to these three examples. However, the use of lines closer than 60 µm was not possible because the resultant structure was undefined. The lines were so close that the creation of each line destroyed the line previously built. Also, height distance between the top and down cones higher than 50 µm was rarely found, and it was usually inhomogeneously distributed. Probably more upper cones may be done increasing the number of repetitions, but taking into account that implied a more distance between lines.

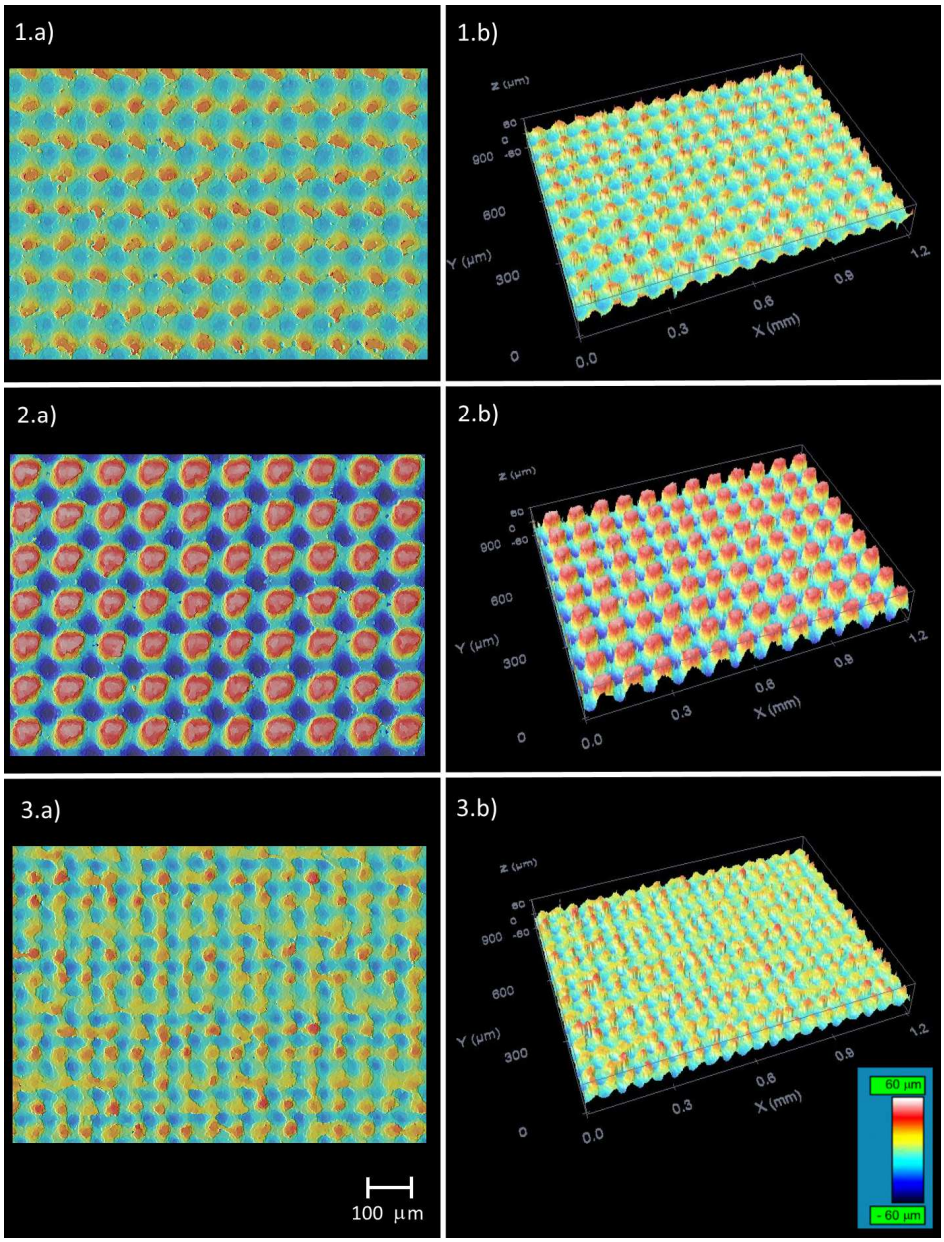

Figure 4.13. Topographical images of representative structures created by UV laser considering a distribution of parallel and perpendicular lines. Laser parameters: 1) Spot distance = 10 µm, one repetition, hatch = 80 µm, P = 1.8 W; 2) Spot distance = 10 µm, three repetitions, hatch = 100 µm, P = 1.2 W; 3) Spot distance = 45 µm, five repetitions, hatch = 60 µm, P = 1.8 W; a) 2D image; b) 3D image. The scale presented on the bottom is the same for all the figures.

Secondly, in the case of structures based on holes, the experimental conditions were selected according to the results shown in section 4.2. The holes were created using 5 to 20 consecutive pulses in successive steps of five pulses each time. The chosen spot distance was from 60 µm to 90 µm from ten to ten. Finally, the power used was 1.8 W. The selection of parameters was the same for both operation modes, bidirectional and unidirectional.

The number of hole structures created was lower than in the case of line structures. Also, the relation complexity between the different variables was also reduced.

Figure 4.14 shows the confocal 2D and 3D images of two hole structures. Figure 4.14.1 presents a structure made using the bidirectional approach. The holes were distributed in a triangular arrangement; each line was displaced half spot distance with respect to the previous one. The parameters used to create that structure were 20 pulses and 60 µm of spot distance. The holes created were well-defined; they seemed to have a shape closer to a cylinder than to an inverted cone. The ring of matter that can be seen in the ablation study was not appreciated here. However, the samples made with a spot distance higher than 80 µm showed that ring. Thus, in the case of the figure, the holes were so close that their rings were overlapped. Figure 4.14.2 presents the pattern of holes created using the unidirectional approach. The holes here exhibited a square arrangement. The parameters used to create that structure were 20 pulses and 70 µm of spot distance. The same comments done to the bidirectional mode holes can be made here.

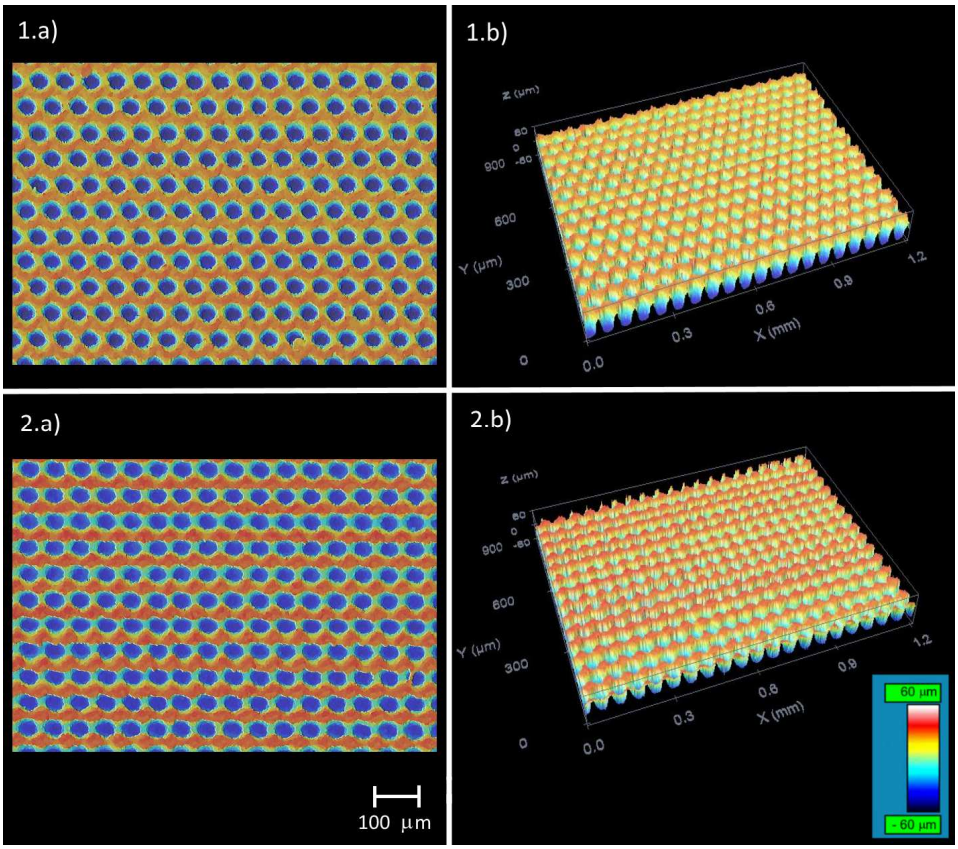

Figure 4.14. Topographical images of some of the structures created by UV laser considering a square or triangular arrangement of holes. Laser parameters: 1) Bidirectional mode, spot distance = 60 µm, 20 pulses, P = 1.8 W; 2) Unidirectional mode, spot distance = 60 µm, 20 pulse, P = 1.8 W; a) 2D image; b) 3D image. The scale presented on the bottom is the same for all the figures.

4.3.2. Theoretical modelling of the contact angle

The models of Wenzel and Cassie-Baxter can be used to make a prediction of the CA that may be expected, according to the equations (4.3) and (4.4). These results will be used later to compare the wettability measurements of the patterned laser structures to the corresponding models. The use of these models allowed understanding how each structure behaves and how they could be improved. Wettability can be theoretically predicted before laser marking but due to the wide range of surface topologies (considering the broad range of variables), this methodology is not an effective approach to the problem. The chosen approach was to make first the structures with the laser and then to analyse the limits of the different topographical parameters in order to establish a relationship with their wetting properties.

Therefore, the constants W and C can be calculated for the patterns of the previous section. These constants were calculated taking into account different topographical variables associated with each situation. Only two separate cases were considered, the first was related to the structure of lines while the second can be used for both types of holes distribution used. Both models are an approximation to the real topography, the results obtained should be assessed carefully.

1. The pattern of parallel and perpendicular lines created a distribution of truncated cones in both directions, up and down, with respect to the surface as it was introduced in the previous section. The dimensions of the cones were considered to be the same regardless of their orientation up or down, in accordance with the experimental results. Additionally, the distance between the cones was the same as the hatch distance defined in the laser parameters. Figure 4.15 showed the 3D model of the structure created where the following topographical variables were defined:

h = distance between consecutive cones

r_1 = radius of the cone bases

r_2 = radius of the cone truncated bases

d = height or depth of the cones

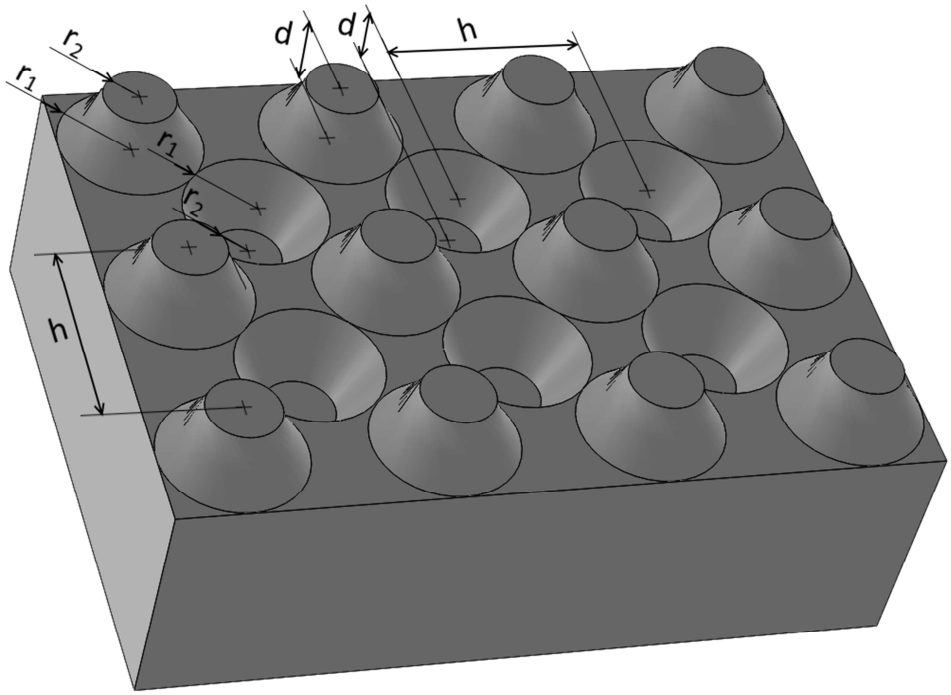

Figure 4.15. 3D model of the structure created by the pattern of parallel and perpendicular lines.

It was considered that the base of the cones up and down was in contact with the edges, so the following relationship should be satisfied:

$$h^2 + h^2 = (4r_1)^2 \rightarrow h = 2\sqrt{2}r_1 \tag{4.5}$$

In addition, it can be defined the area of the exterior wall of the truncated cones F as:

$$F = \pi(r_1 + r_2)\sqrt{(r_1 - r_2)^2 + d^2} \tag{4.6}$$

- The Cassie-Baxter constant can be calculated as:

$$C = \frac{\pi r_2^2}{h^2} = \frac{\pi r_2^2}{8 r_1^2} \tag{4.7}$$

- Meanwhile, the Wenzel constant was:

$$W = \frac{h^2 - 2\pi r_1^2 + 2\pi (r_1 + r_2)\sqrt{d^2 + (r_1 - r_2)^2}}{h^2} = \\ = \frac{(4 - \pi) r_1^2 + \pi (r_1 + r_2)\sqrt{d^2 + (r_1 - r_2)^2}}{4 r_1^2} \tag{4.8}$$

2. The structure of distributed spots produced a topography of equidistant holes. The holes can be considered as cylinders in accordance with the experimental results. The three-dimensional scheme of the structures created in both unidirectional and bidirectional modes are presented in figures 4.16 and 4.17 respectively. Mathematically, the constants C and W obtained can be applied to both arrangements. The following dimensions were defined:

r = hole radius

p = hole depth

d = distance between parallel lines

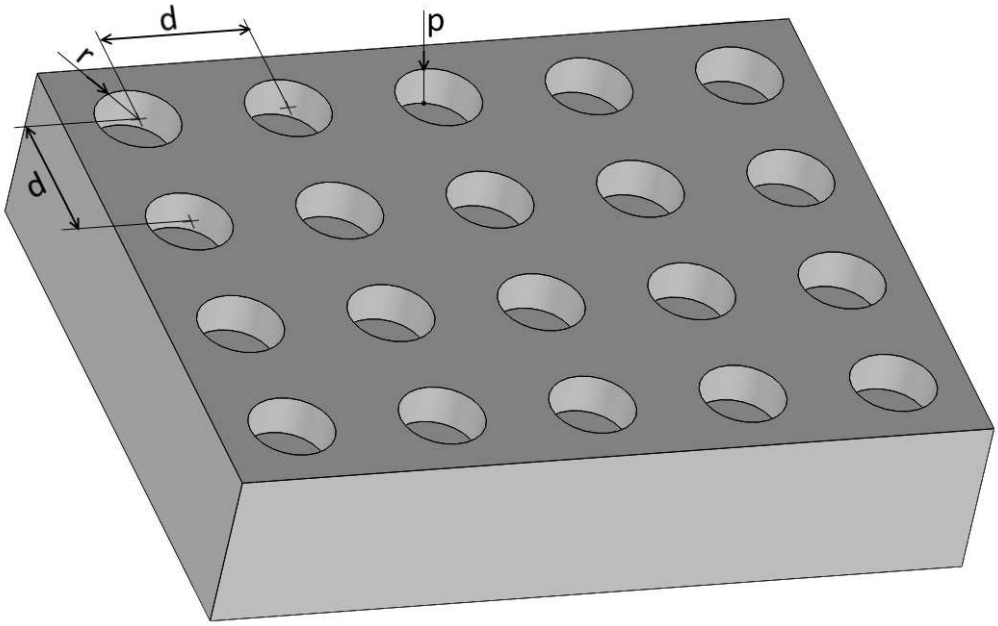

Figure 4.16. 3D model of the structure created by the pattern of symmetric holes in a square arrangement.

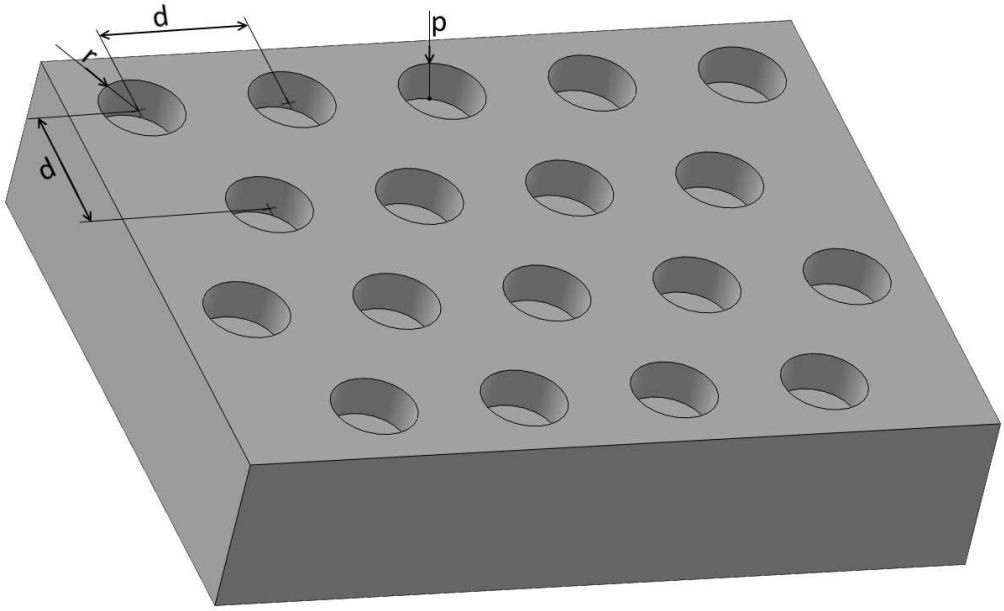

Figure 4.17. 3D image of the structure created by the pattern of symmetric holes in a triangular arrangement.

- The Cassie-Baxter constant can be calculated as:

$$C = \frac{d^2 - \pi r^2}{d^2} = 1 - \frac{\pi r^2}{d^2} \tag{4.9}$$

- Meanwhile, the Wenzel constant was:

$$W = \frac{d^2 + 2\pi rp}{d^2} = 1 + 2\pi \frac{rp}{d^2} \tag{4.10}$$

4.3.3. Influence of the topography in the wettability

The wettability of the different surfaces was studied. According to the Wenzel and Cassie-Baxter models, their topography should exhibit a high impact in their CA. Using the experimental measurements of the topographical parameters above described for the models, the constants W and C from the equations (4.3) and (4.4) can be calculated to estimate the theoretical Wenzel or Cassie-Baxter CA of each created structure. First of all, the CA of the reference white-c ABS material before laser patterning was measured. The material had a CA of 62.8 ± 1.7° (previously cleaned with isopropanol). After one month of ageing in the environmental conditions previously described, the CA increased to 74 ± 6°, probably due to some particles or dust adhered to the surface since the material was measured without being cleaned again to simulate real conditions of use.

The CA of the different patterns was also studied. A summary of the topography dimensions and the predicted and measured CA of the most significant structures patterned with the UV laser are shown in Table 4.1 and Table **4.2**. In each table are displayed the laser parameters used to create the different patterns and the physical dimension of the structures measured by the confocal microscope, the theoretical CA obtained from the material sizes using either the Wenzel or Cassie-Baxter models and

the CA measured with a contact angle goniometer just after marking, one day after and one month after. The samples were left in the ambient conditions described in section 4.1 to observe the temporal evolution of their CA.

Table 4.1 collects the most representative results of the structures based on parallel and perpendicular lines. The predictions according to Wenzel and Cassie-Baxter exhibited completely different values as could be expected. On the one hand, the CA predicted by the Wenzel model was in all the cases lower than the angle measured on the unmarked ABS as correspond to the increment in the surface area by the patterning. On the other hand, the CA should be increased in accordance with the Cassie-Baxter model as the top surface of the material was decreased by the patterning. It can be observed that neither superhydrophobic nor superhydrophilic behaviour was predicted.

The marked samples exhibit a temporal evolution of their CA depending on the initial value. Thus, it tended to grow if the initial angle was below 90° and to maintain its initial value when it was higher than 90°. Evolution one week and one month after marking are only included in the table. Additional measurements were registered, three and six months later, but no further evolution was detected. This behaviour may be related to a chemical modification of the patterned laser surface that evolves with time. According to previous studies, the time evolution of the CA can be assigned to the well-known photocatalytic effect of the TiO_2 produced under UV light and its progressive disappearance without being irradiated again [4.82].

Nevertheless, depending on the cones dimensions, the results were closer to either Wenzel or Cassie-Baxter models, although they were generally in between both models, thus associated with a transitional state. Neither the “Lotus-effect” nor the “Gecko” states were observed in these structures.

Table 4.1. Topography and CA predicted and measured of some of the structures created by an array of parallel and perpendicular lines.

Laser parameters			**Topographical measurements**				**CA predictions**		**CA measured**		
Power (W)	Spot dist (µm)	Nº rep	h (µm)*	r_1 (µm)*	r_2 (± 1.5 µm)	d (± 1.5 µm)	Wenzel	Cassie-Baxter	after marking	one day later	one month later
1.8†	10	1	80	28.3	21.6	23.2	49°	132°	< 10°	< 10°	50 ± 8°
1.8	10	1	90	31.8	16.8	26.1	51°	147°	< 10°	43 ± 9°	52 ± 3°
1.8	10	1	100	35.4	15.5	25.3	55°	153°	< 10°	50 ± 8°	61 ± 3°
1.8	10	1	110	38.9	13.9	27.8	55°	158°	< 10°	43 ± 3°	69 ± 7°
1.8	10	2	120	42.4	20.1	35.2	51°	151°	93 ± 6°	92 ± 10°	96 ± 2°
1.8	10	5	180	63.6	41.7	85.8	20°	139°	112 ± 3°	120 ± 8°	120 ± 3°
1.8†	45	5	60	21.2	13.0	25.4	33°	142°	103 ± 11°	108 ± 5°	107 ± 2°
1.8	45	5	70	24.7	11.7	27.4	41°	151°	68 ± 7°	96 ± 8°	93 ± 7°
1.8	45	5	80	28.3	12.4	28.4	45°	153°	94 ± 9°	102 ± 4°	94 ± 9°
1.8	45	5	90	31.8	20.4	29.0	47°	140°	83 ± 9°	98 ± 9°	106 ± 3°
1.2	10	1	70	24.7	14.2	20.0	51°	144°	27 ± 3°	108 ± 10°	90 ± 8°
1.2	10	1	80	28.3	9.9	21.8	53°	158°	44 ± 2°	78 ± 4°	89 ± 9°
1.2	10	1	90	31.8	12.9	28.0	50°	155°	< 10°	94 ± 13°	86 ± 6°
1.2†	10	3	100	35.4	20.4	50.6	17°	144°	116 ± 8°	122 ± 1°	126 ± 3°

*h and r_1 have no error associated due its values have been considered directly related to the laser parameters.

†Marks showed in figure 4.13.

To help with the understanding of the relationship between the different variables and the CA predicted and measured, the following variable denoted as %M is calculated:

$$\%M = \frac{CA_{measured} - CA_{Wenzel}}{CA_{Cassie-Baxter} - CA_{Wenzel}} \times 100 \tag{4.11}$$

This variable represents how close the structures were to follow one or another C-B or W models. If the %M value is 0, it indicates that the structure followed the Wenzel model while if the value is 100, the CA of the structure can be predicted by the Cassie-Baxter model. Figure 4.18 illustrates the evolution of this variable for the structure dimensions r_1/d (a), r_2/d (b) and r_1/r_2 (c). Only in the case of the ratio r_1/d, a dependence can be established. The value of %M decreased when the ratio value increased. Thus, this indicated that cones whose base width was bigger than their depth were closer to follow the Wenzel model. On the contrary, if the depth is higher than the cone base the angle can be predicted by Cassie-Baxter model. Probably, this effect can be associated with narrow and deep cones that do not allow penetrating the water inside the structure; it was almost held on the top of the structure. From the results, it seems that it is possible to roughly associate each structure to a model taking into account the physical dimensions of the cones created.

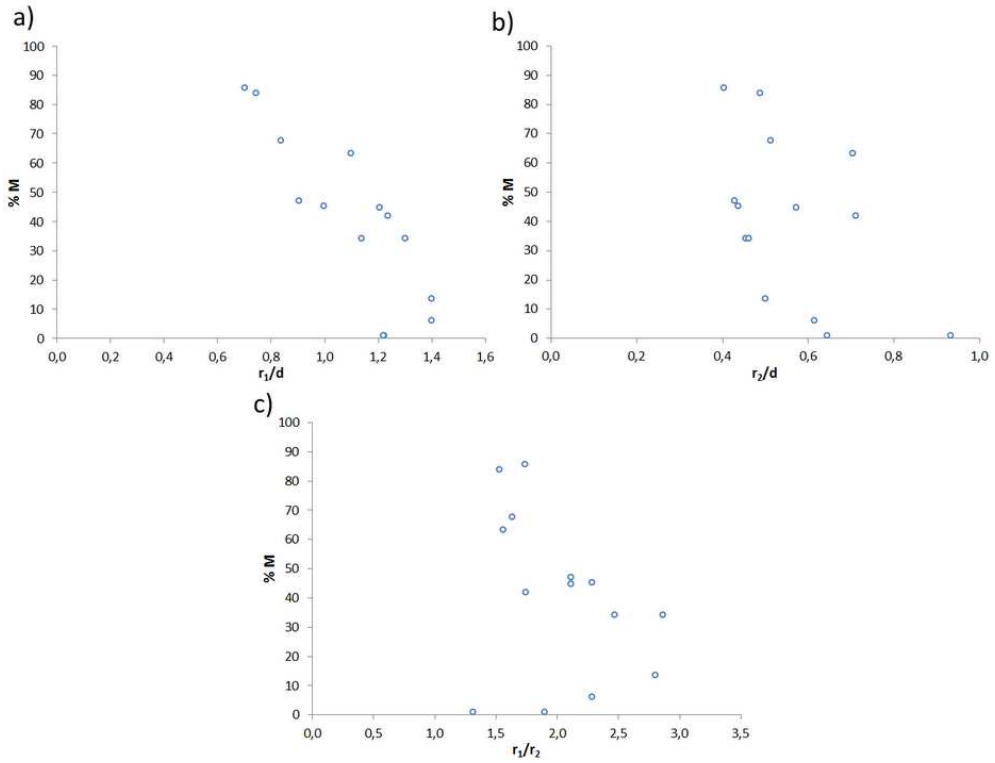

Figure 4.18. Relation between the topography and the variable % M (0 = the topography follows the Wenzel model, 100 = the topography follows the Cassie-Baxter). a) r_1/d; b) r_2/d; c) r_1/r_2.

Table 4.2 gathers the most representative results of the structures formed by a regular arrangement of holes. The table presents the laser parameters used to create the structures, the topographical measurements, the CA predictions and the evolution with time of the CA once marked the surface.

The structures created according to the Wenzel model should exhibit a low CA, in some cases a superhydrophilic behaviour. By contrast, the contact angles predicted by the Cassie-Baxter model were slightly hydrophobic, between 90° and 100°.

A temporal evolution in the measurements was again detected. As previously it tended to grow if the initial angle was below 90° and to maintain or slightly to be

reduced if it was higher than 90°. Also, there was no detected further evolution beyond one month.

Therefore, in this case, it was observed that the CA of all the surfaces measured was predicted by the model of Cassie-Baxter. Also, the detected angle was even higher than the predicted in some cases. This difference could be associated with the fact that our model had not taken into account some possible edge effects that appeared in the holes because of the accumulated material that is forming a ring decreasing the contact surface. So, these holes created seemed not to allow penetrating the water inside them. However, the observed angles were far from a superhydrophobic behaviour.

Table 4.2. Topography and CA predicted and measured of some of the structures created by a distribution of spots.

Laser parameters		**Topographical measurements**			**CA predictions**		**CA measured**		
Power (W)	Spot arrangement	d (µm)*	r (± 2 µm)	p (± 2 µm)	Wenzel	Cassie-Baxter	after marking	one day later	one month later
1.8	Triangular	60	20.0	20	37°	93°	80 ± 6°	93 ± 3°	95 ± 9°
1.8	Triangular	60	20.5	37	< 10°	94°	98 ± 3°	105 ± 10°	110 ± 7°
1.8†	Triangular	60	20.5	45	< 10°	95°	114 ± 4°	110 ± 8°	100 ± 11°
1.8	Triangular	70	25.0	15	42°	97°	68 ± 3°	92 ± 10°	95 ± 5°
1.8	Triangular	70	22.0	35	23°	89°	89 ± 10°	97 ± 2°	90 ± 5°
1.8	Triangular	70	22.5	52	< 10°	89°	94 ± 6°	100 ± 8°	88 ± 4°
1.8†	Square	60	22.0	36	< 10°	99°	114 ± 8°	99 ± 3°	105 ± 3°
1.8	Square	70	24.5	41	< 10°	96°	96 ± 6°	98 ± 6°	86 ± 7°

*d has no error associated due its values have been considered directly related to the laser parameters.

†Marks showed in figure 4.14

4.3.4. Conclusions

It has been proved that the laser irradiation is a suitable tool for structuring the white-c ABS. Two types of surfaces were created, one based on truncated cones and the other on a regular arrangement of holes. The lowest period of the created structures for both cases was around 60 µm. Predictions of the wettability behaviour were made according to Wenzel and Cassie-Baxter models. The structure based on truncated cones was adjusted to one of the models depending on their dimensions. Surfaces with deep and closely arranged cones (low r_1/d) do not allow penetrating the water. Thus, they presented a CA close to the predicted by Cassie-Baxter model. The highest achieved CA was 120°, not enough to consider a superhydrophobic behaviour. However, surfaces with having a high r_1/d exhibited low CA values, in some cases with a superhydrophilic behaviour, although a growing in their CA was observed after some time. The structure based on holes followed in all the cases the Cassie-Baxter model achieving a maximum CA of 110°.

4.4. Wettability modification by laser roughness control

The second technique studied to modify and control the wettability of the white-c ABS was the modification of the topography by laser irradiation in such a way that the final surface has a controlled roughness but in a chaotic form instead of a pattern. This phenomenon is possible because the laser can mark the surface in such a way that the final roughness can be modulated using controlled heating determined by the laser parameters. The reached surface temperature during the laser processing will be dependent on the laser parameters, like beam fluence, processing speed, and the overlap between the pulses among others. To performance the marking process the green laser was selected since this laser produces a high located thermal effect on the material. Some preliminary tests were made using other wavelengths. However, on the one hand, the use of an IR laser produced a stronger thermal impact difficult to be controlled. On the other hand, the UV laser produced low thermal changes, and the final roughness changes were not significant enough to induce substantial changes in the final wettability. Consequently, the selection of the green laser to control the final roughness seemed to be the most suitable choice according to its thermal impact.

Furthermore, as said above, the temperature of the material can be controlled by changing the laser parameters like the overlap between the pulses, the number of spots per area (DPI) or the laser fluence over the material. This study was carried out keeping constant the DPI (and consequently the total energy deposited on the surface) and controlling the fluence of the laser. However, the overlap between pulses will vary, and it should be taken into account. The fluence of the laser can be controlled by changing the laser beam size placing the sample out of the focal

position a controlled distance. This parameter also can be changed varying the laser pump power, but the green laser used in our lab did not have a stable response to variations in the pumping power (especially at low pumping values), and consequently, it was not a suitable solution to control the fluence.

The lens used was the shorter one available, 100 mm, which produced a spot size on the focus of 30 µm. In this case, the laser parameters used were always the same, 1200 DPI and working at 15 kHz using the maximum power of 3.6 W. The fluence was changed varying the focal position of the laser over the sample, scanning 2 mm up and down out of focus in successive steps of 0.1 mm. Thus, the fluence ranged from 5 to 35 J/cm^2.

In this case, it was not possible to develop a theoretical model of wettability behaviour because of the chaotic character of the created surface roughness.

4.4.1. Topography of the affected laser surface

After the laser treatment on the white-c ABS, two types of different surfaces depending on the position of the sample along the focal axis were observed. The material treated on focus exhibited a low roughness surface while defocusing around one mm the surface had a high roughness. This phenomenon happened in the two directions along the focal axis. No clear transition between both cases was detected (around 0.6 mm out of focus), the topography was inhomogeneous. Two different techniques were used to characterise the roughness: confocal microscopy and ESEM.

Figure 4.19 shows the analysis by confocal microscopy shows the two types of generated surfaces, on focus and 0.8 mm out of the focal position (the results were similar in both directions) in addition to the unmarked material. The surface before

being marked was completely flat (figure 4.19.1). After the green laser treatment on focus (figure 4.19.2) the topography detected was characterised to be almost flat, although a small ripple can be observed as colour changes from green to pale blue in the figure. Also, it was identified the presence of some small holes. Thus, the total surface area was increased in comparison to the unmarked material. By contrast, the ABS treated 0.8 mm out of the focal position (figure 4.19.3) exhibit a rugged topography characterised by the presence of peaks and valleys in the studied area. In this case, the area increment was higher than in the previous situation. These changes were detected in the two directions along the focal axis.

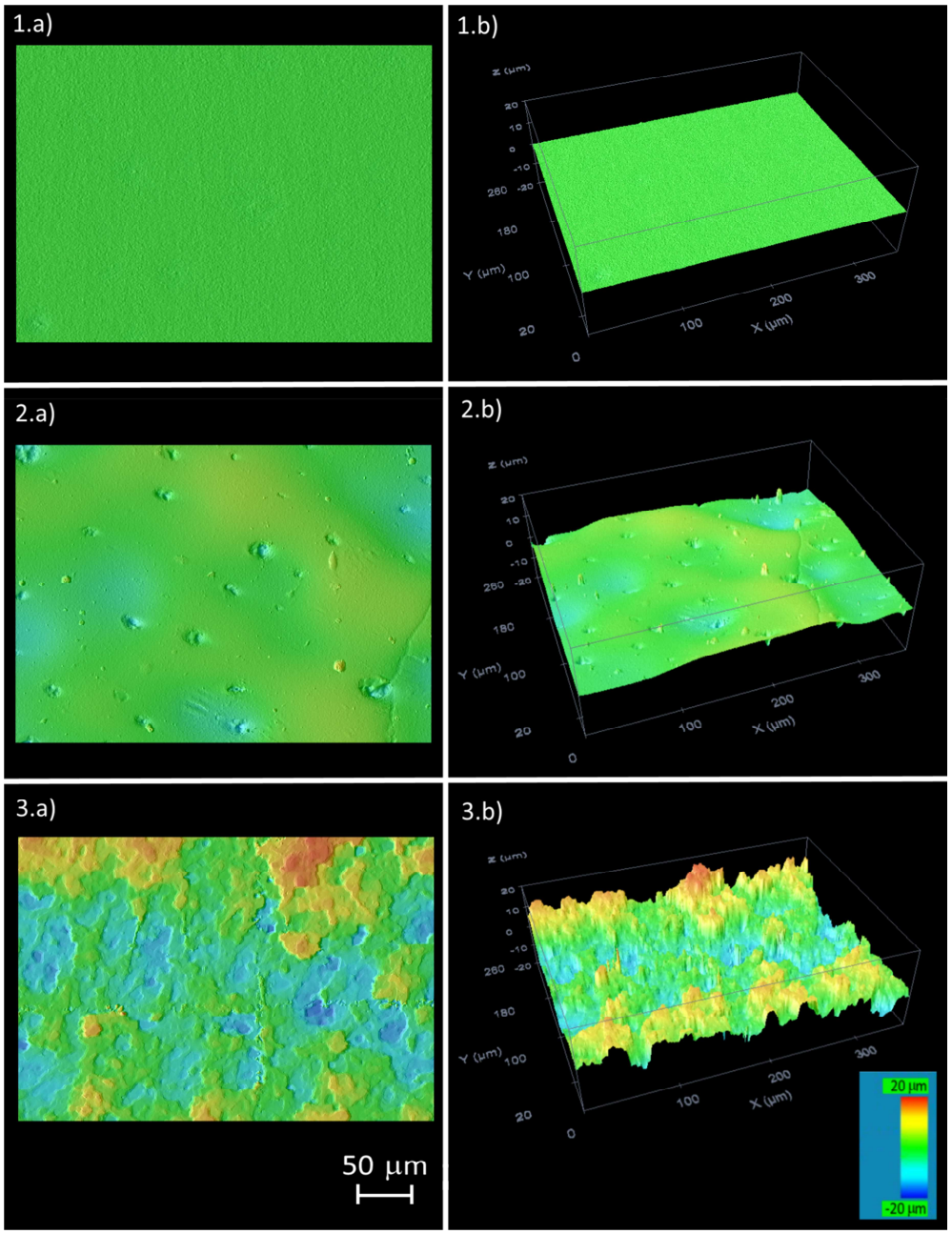

Figure 4.19. Topographical images of the white-c ABS surface roughness. 1) Before laser irradiation; 2) after green laser irradiation, 1200 DPI, on focus; 3) after green laser irradiation, 1200 DPI, 0.8 mm out of focus; a) 2D image; b) 3D image. The scale presented on the bottom is the same for all the figures.

A more in-depth detail was obtained using an ESEM microscope. The images taken by this technique of the unmarked material surface and the two surfaces made marked on focus and 0.8 mm out of focus respectively are presented in figure 4.20. The images were taken at three different magnifications, 2800x, 24000x and 80000x.

Again, clear differences between the analysed surfaces were observed. The unmarked material (figure 4.20.1 images) exhibited a smooth surface. White dots were visible in the image taken at 24000x magnification. The same points were seen on the samples marked on chapter 3. The analysis presented in the section 3.2.3.1 showed that they correspond to TiO_2 particles. The surface seen at the highest magnification exhibited a wavy area probably related to the material injection process.

The white-c ABS marked on focus (figure 4.20.2 images) also showed a smooth surface. However, as it was seen on the confocal microscope, the surface had some holes distributed along the area. In addition, the apparition of a sub-micron dotted structure was detected using the highest magnification. The diameter of those points was less than 100 nm. Also, the presence of the white dots corresponding to TiO_2 particles was detected.

Finally, the surface of the material marked at 0.8 mm out of focus (figure 4.20.3 images) exhibited a rugged topography. The surface was characterised by the presence of peaks in all the directions. Minimally tilting the samples enabled to observe that the surface was chaotic and some of the areas were forming holes and channels. They may be associated with material filaments that were melted during the laser treatment and then rapidly solidified. The sub-micron structure of points was also visible in this sample. Finally, the presence of white points associated with the TiO_2 particles was also observed, although they were difficult to observe because of the high roughness of the surface.

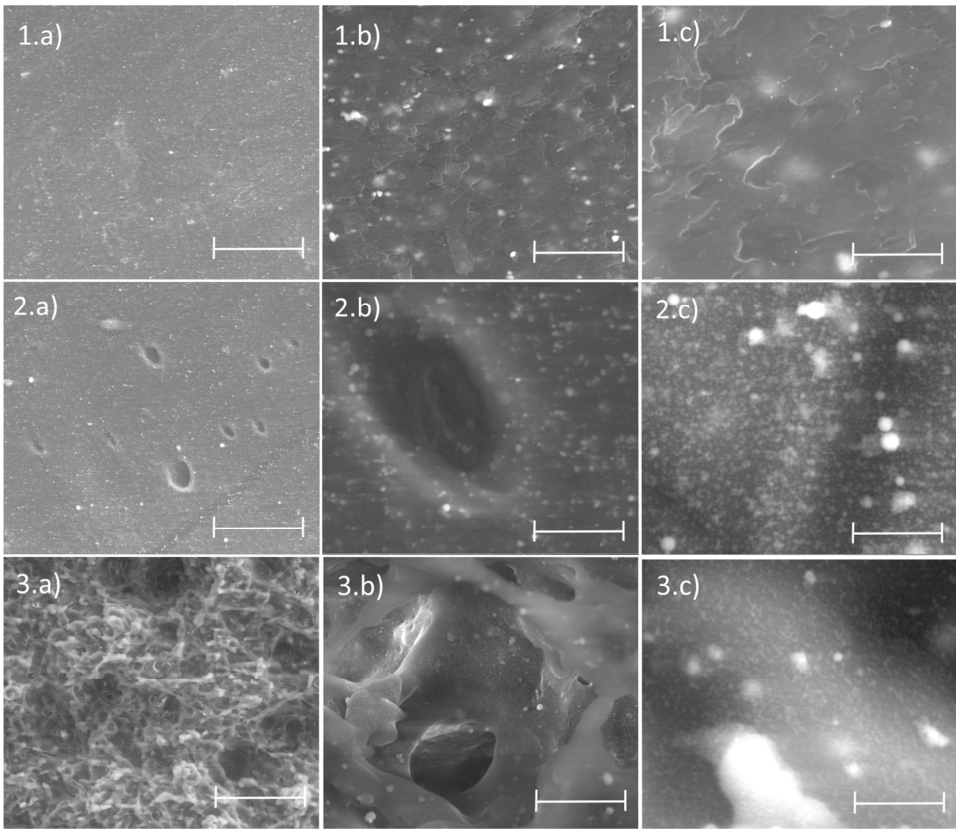

Figure 4.20. ESEM images of the white-c ABS surface roughness. 1) Before laser irradiation; 2) after green laser irradiation, 1200 DPI, on focus; 3) after green laser irradiation, 1200 DPI, 0.8 mm out of focus; a) 2800x magnification, scale bar 30 µm; b) 24000x magnification, scale bar 3 µm; c) 80000x magnification, scale bar 1 µm.

These changes related to the sample position along the focal axis can be explained by the fluence differences on the surface. The highest fluence used, on focus, caused a drastically heating on the material leading to a quasi-pure ablation effect. The surface was heated up very fast, began to flow and cooled down again very quickly making to be trapped some bubbles of air producing the apparition of small holes. By contrast, positioning the sample out of focus, the temperature reached in the surface decreases at one point that the material had not enough temperature to flow before getting cold again. Also, the laser generates an additional pressure causing bubbles and material ejections. The surface cooling provoked the freezing of

this rugged structure. Thus, the apparition of the peaks and filaments observed may be associated with an incomplete process of melting.

4.4.2. Influence of the topography in the wettability

Similarly to the previous section, the wettability of the rough structures was studied. However, in this case, predictions of their behaviour according to the Wenzel and Cassie-Baxter models cannot be done because of the chaotic topography of the structures created. Due to the high CA detected in some cases, the CAH was also measured. For this purpose, the plane containing the droplet was tilted, and the contact angles (θ_A and θ_R) were measured when the droplet started to slide down [4.8]. Finally, the temporal evolution of the angles was also studied. Nevertheless, no changes were detected during the six months of study.

The most significant results obtained in terms of the position along the focal axis are shown in Table 4.3. The experimental results can be grouped into three different regions, although only two differentiated structures were observed previously. The samples marked out of the focal position more than 1.2 mm had a high CA value, close to a superhydrophobic behaviour [4.83]. However, the drop was pinned to the surface and did not slide down when tilting even at the vertical position. By contrast, when the material was treated closer to the focus (0.8 mm or 0.9 mm), the CA value increased to values higher than 150° so it can be considered to have a superhydrophobic behaviour. Also, the measured CAH was lower than 10°; the drop exhibited no adherence to the surface and tended to slide when the plane was slightly tilted. Finally, the samples marked close to the focus (less than 0.5 mm of distance from the focal position) presented a drastic change in the wetting properties. The water drop wet the entire surface and, consequently, the CA was considered lower

than 10° having a superhydrophilic behaviour [4.83]. As it was commented before, the temporal evolution was also tested, and negligible changes were detected even after six months for all the samples.

Table 4.3. CA and CAH measured on some of the structures created with the green laser.

Power (W)	DPI	Post. respect to focus (mm)	Fluence (J/cm^2)	Overlap between pulses	Topography observed	CA	CAH
3.6	1200	0	34.4	29.4	flat	$< 10°$	-
3.6	1200	± 0.4	30.1	34.1	flat	$< 10°$	-
3.6	1200	± 0.6	26.0	38.7	inhomogeneous	unstable	-
3.6	1200	± 0.8	21.8	43.9	rugged	168 ± 3°	$< 10°$
3.6	1200	± 0.9	19.9	46.4	rugged	170 ± 3°	$< 10°$
3.6	1200	± 1.2	14.9	53.5	rugged	153 ± 5°	pinned
3.6	1200	± 1.3	13.6	55.7	rugged	143 ± 5°	pinned

Figure 4.21 shows the images of water drops on the previous surfaces taken by the contact angle goniometer camera. The water drop on the untreated material is presented in the figure 4.21.a as a reference. As it was described in the previous part, the CA, in this case, was 62.8 ± 1.7° after being cleaned the surface with isopropanol. The figure 4.21.b corresponds to the surface treated with the green laser 0.9 mm out of focus showing a superhydrophobic behaviour. The sequence of images presented in the figure 4.21.c displays the water drop on the surface marked 1.3 mm out of focus. The images were taken at different tilting angles, 0°, 45° and 90°. The drop exhibited a high adhesion to the surface as can be seen remarked on the 90° tilting angle where there were high difference between the receding and advancing contact angles. Finally, the figure 4.21.d shows the time-lapse images of a drop on the surface

marked by laser on focus. The water was dispersed on the surface in less than one second revealing a superhydrophilic behaviour.

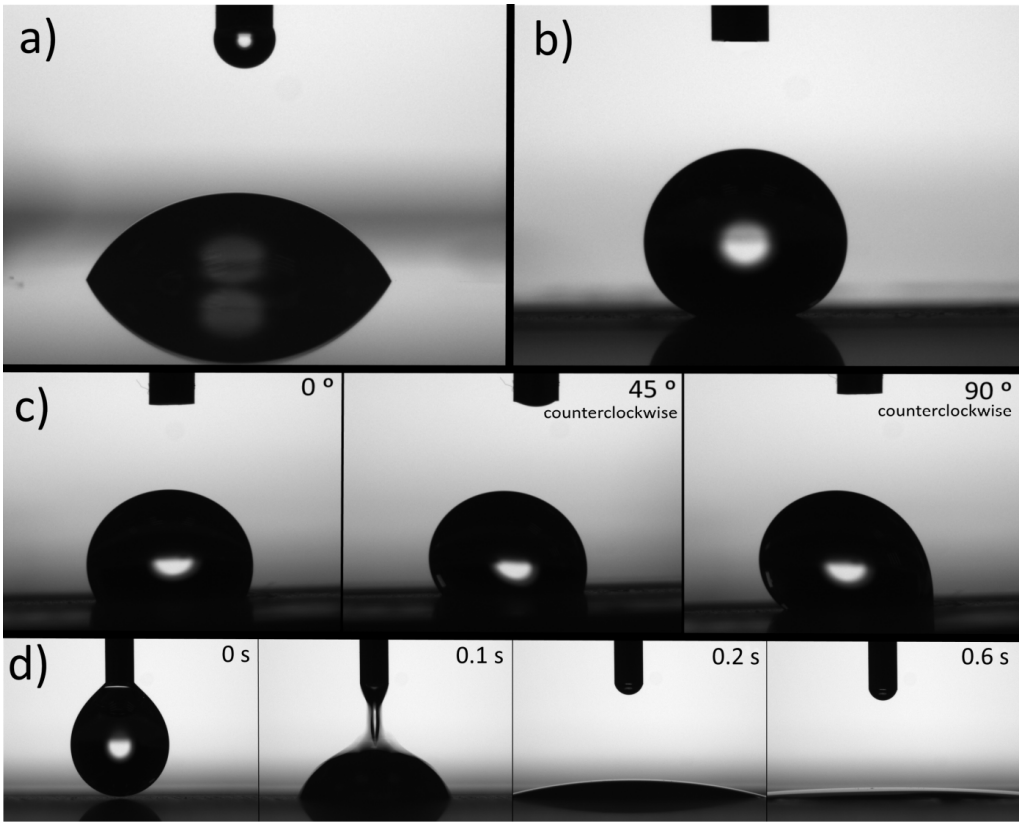

Figure 4.21. Images of water drop on ABS. a) untreated surface; b) surface irradiated by laser at 0.9 mm out of focus; c) surface irradiated by laser at 1.3 mm out of focus and taken at different tilting angles (the camera also rotates simultaneously with the surface); d) Time-lapse images of a drop on the surface treated by laser on focus.

Consequently, the wettability of the ABS can be changed employing a green laser exhibiting three different regions of wetting behaviours depending on the irradiation conditions: a region of superhydrophilic behaviour and two regions characterised by high CAs, one associated to low CAH and the other one exhibiting a high CAH. Figure 4.22 illustrates these different behaviours depending on the focal position and the corresponding fluence of the green laser. In this case, the ablation study presented

in section 4.2 is helpful to understand the results obtained. Thus, in the figure, the parameters associated to the hole ablation using the green laser are also shown.

The superhydrophilic region was associated with the focal position. The topography observed (figure 4.19.2) was characterised to be almost flat. During the ablation study, it can be seen that in this region the deepest and smallest holes were produced. This region is characterised by the highest fluence values, above 25 J/cm^2.

The surfaces treated in the transition zone to the adjacent region presented an unstable behaviour: initially, the surface seems to be hydrophobic, but under a small perturbation or after some seconds the drop began to wet the surface presenting a superhydrophilic behaviour, probably associated to the inhomogeneous topography observed.

The adjacent region exhibited a high CA together with a low CAH. In this case, the topography observed (figure 4.19.3) was rugged, characterised by filaments and holes. From the ablation study, the superhydrophobic region can barely correspond to the holes that had a minimum in the edges width (purple line). Also, the fluence associated to this region was less than in the case of the superhydrophilic region. Therefore, laser fluences approximately between 15 J/cm^2 and 25 J/cm^2 seemed to produce this behaviour.

The transition samples to the next region displayed a heterogeneous behaviour presenting both adhered and not adhered drops on the same marked surface.

Finally, the last region presented a hydrophobic behaviour and a high CAH. The topography of this region observed on confocal showed no clear differences with those corresponding to the superhydrophobic behaviour, only an apparently lower peak density. This region was associated with the holes having the highest width and

affected areas comparing to the ablation results. The less fluence studied produced this behaviour, values below 15 J/cm^2.

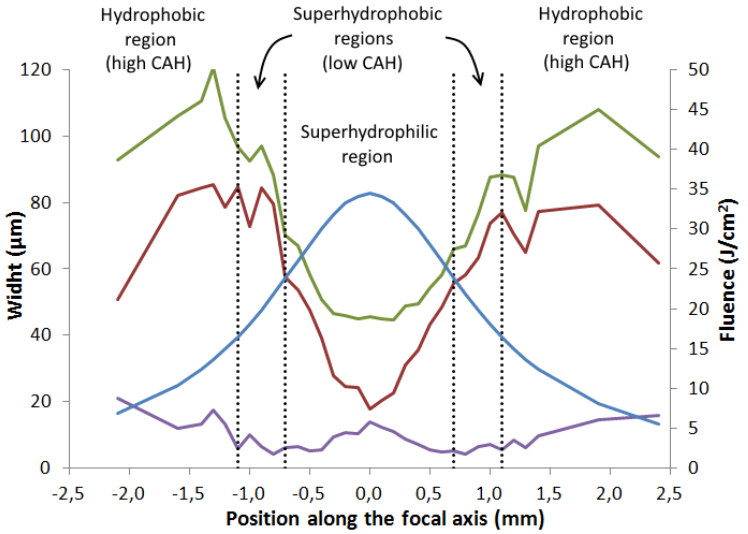

Figure 4.22. Graph of the different regions of wetting behaviour depending on the focal position on green laser irradiation compared with the ablation study. Fluence (blue line, units on the right axis), hole width (red line, units on the left axis), affected area (green line, units on the left axis), and edges width (purple line, units on the left axis).

Therefore, it is possible to correlate the topography of the surfaces analysed before with their wetting properties. The superhydrophobic surface (figure 4.20.3) exhibited a rugged topography with many peaks and holes that caused a reduction in the top material surface area. Thus, following the Cassie-Baxter model, this reduction leads to the increment of the CA and the observed superhydrophobic behaviour. Furthermore, the water did not get adhered to the material and slice easily. By contrast, the material that also presented a high CA but with a high hysteresis behaviour exhibited a rough surface too, although apparently with a lower peak density. Probably the water was able to penetrate slightly in the topography, increasing highly the adhesion to the surface. Finally, the superhydrophilic surface (figure 4.20.2) showed a structure characterised by smooth hills that increased the

ratio of the area surface compared to the unmarked material. So according to Wenzel model, the CA should be less than on the untreated surface. An approximation was made trying to model this surface. In this case, it was considered a distribution of hills and valleys. According to this, the CA should be around 30°, which denotes the influence of the topography created on the wetting properties.

Finally, figure 4.23 shows the time-lapse images of a drop falling on the superhydrophobic surface (0.8 mm out of focus). As can be seen, the drop hit the surface and did not get pinned to the surface, bounced and slid until reached the unmarked area in which it finally adhered.

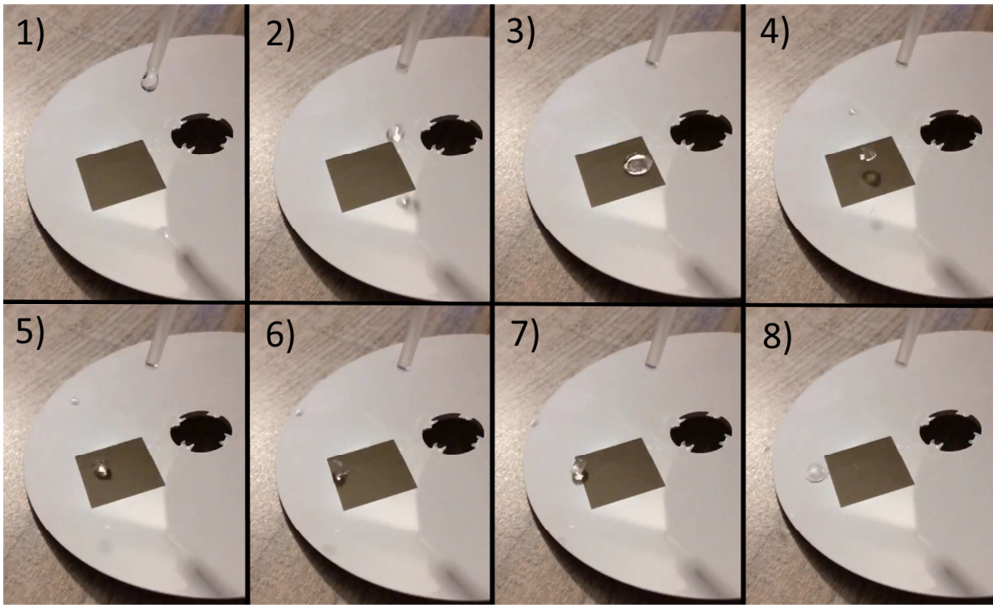

Figure 4.23. Time-lapse images (total time approx. 2 s) of a water drop on the superhydrophobic surface created by laser irradiation 0.8 mm out of focus by the green laser.

4.4.3. Conclusions

The green laser marking was an effective method to control the final wettability of the white-c ABS achieving both superhydrophilic and superhydrophobic behaviours. These wetting properties were reliant on the surface topography created that was directly related to the laser parameters like spot width and fluence. Three types of topographies were created: one smooth that presents a superhydrophilic behaviour and two with a rugged topography presenting a superhydrophobic behaviour but one with a low CAH and the other with high CAH. All the structures were temporally stable.

4.5. Wettability modification by direct laser interferometry patterning

The last technique proposed to modify the wettability of the white-c ABS sample was the direct laser interference patterning (DLIP). This technique is based on the use of an interferometry technique to create a patterning on the material surface using a distribution of energy maximum and minimum. This technique can be applied to such different materials like metals [4.84], semiconductors [4.85] or photopolymers [4.86]. In our case, the use of a UV laser is proposed to produce the interference pattern on the white-c ABS. The interaction of this wavelength with the polymer has been widely studied in chapter 3 in addition to its ablation seen in section 4.1.

The interferential phenomena caused by the interference of light after being through two slits is a well-known experiment of classical physics and even it was one of the breakthrough experiment to prove in the early 20's the double nature of the electron as wave and particle [4.87]. Similarly, it is possible to create an interference with a laser beam on a surface making a patterning on it. Optically, a laser beam can be split in two using a beam splitter. Then, it is possible to guide the beams using mirrors producing interference onto the material surface. It should be carefully calculated the way of the beams to keep matched both optical paths. The laser source should have enough coherent length to ensure a good interference pattern [4.88].

So, a pattern of parallel lines can be created using two beam interferences on the polymer surface. Considering two beams of the same intensity and linearly polarised, the period (Δ) between the lines it is determined by:

$$\Delta = \frac{2\lambda}{tg\,\theta} \tag{4.12}$$

where λ is the laser wavelength and 2θ is the angle that forms both laser beams over the sample.

The figure 4.24 shows the scheme of the optical devices used to create the interference pattern on the sample. The sample was mounted on a motorised stage to be able to create a surface covered by the laser beam. Also, it was used a zircon mask to select a part of the laser beam where the best interference pattern was produced. The mask was prepared by IR laser cutting producing a small window of 1.5 mm^2 that allowed passing the laser beam. It will be the minimum area of marking or pixel. This basic unit allowed creating extended surfaces, figures or logos by area overlapping. It should be remarked that the pulsed laser holographic technique allows moving the sample dynamically because the marking time is short enough compared to the speed of the stage movement [4.89]. In our case, the angle between the two laser beams was around 12° that according to (4.12) should produce a grating with a period of around 7 μm. The final structure will exhibit a periodical distribution only in one direction, perpendicular to the stage movement direction. Thus, to create a two-dimensional pattern, two successive marking steps were done. Firstly, the interference pattern was created in one direction. Lately, the sample was turned 90°, and the process was repeated.

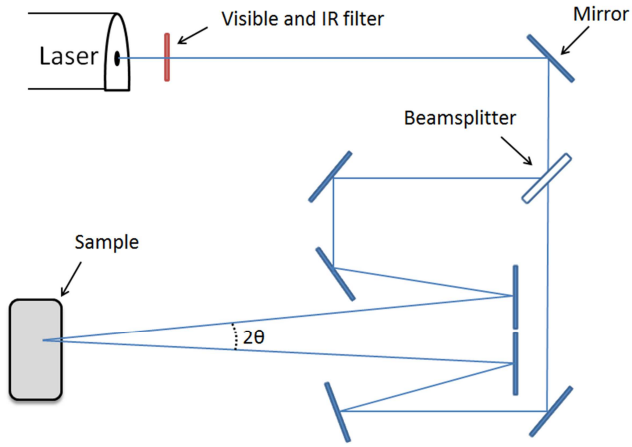

Figure 4.24. Scheme of the optical display used to make an interference pattern over the sample.

4.5.1. Topography of the patterned laser surface

Therefore, the DLIP technique was used to modify the topography of the white-c ABS. Considering that the laser worked on a frequency of 10 Hz and knowing our window mask dimension, it was possible to calculate that the speed of the motorised stage should be around 1.5 cm/s. However, after the optimisation process, the results showed that the better results were obtained if the marks were a bit overlapped. Consequently, the speed was reduced to 1.3 cm/s. A slower speed was also considered, 0.7 cm/s, to observe the effect of a high overlap between the marked areas. Figure 4.25 shows a front view of both marked areas. It can be seen that the mark made with the lower speed presented a darker visible colour associated with the higher overlap between the pulses.

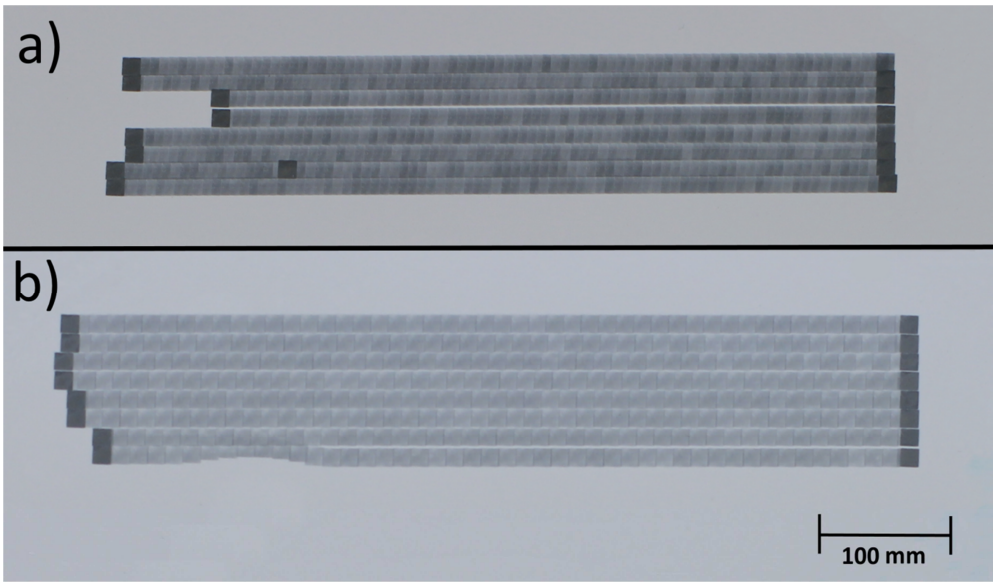

Figure 4.25. Front view of the gratings created on the ABS sample. a) Marks created at 0.7 cm/s; b) marks made at 1.3 cm/s.

The study of the topography of the sample was made by confocal microscopy. Figure 4.26 shows an optical view of the marks made at 1.3 cm/s. The gratings were homogeneously distributed along the surface and the experimental period matched to the theoretical, around 7 µm. Inhomogeneities were detected in the marked areas (as some darker or whiter points). They may be associated to inhomogeneities during the laser interaction process with the material. The marks made at 0.7 cm/s showed the same structure under the microscope. The high overlap did not improve the marking mechanism. So, to do the marking process as short as possible, the fast speed was selected.

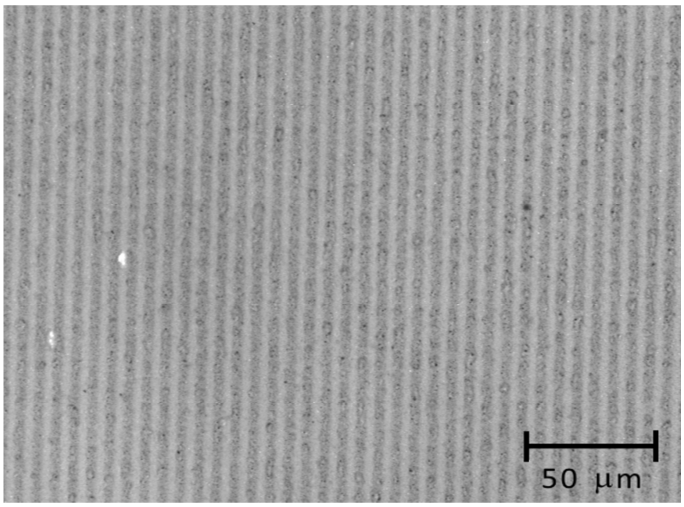

Figure 4.26. Confocal optical image of the area treated at 1.3 cm/s.

Figure 4.27 presents the topographical images of the marked material. The inhomogeneity said above was visible as irregular peaks. The laser seemed to produce a growth of the materials instead of producing an engraving at the intensity maximum. This result can be associated with the shape of a hole created by one UV laser pulse shown at the beginning of this chapter where the material was rising instead of being produced a hole (section 4.2). So, if the energy was not high enough, the material tended to grow rather than producing a hole. In this case, the resulting structure was an array of elevated lines separated by trenches along the area affected by the laser.

The period measured was 6.7 ± 0.1 µm, which implied that the angle between both laser beams was 12.2°, in accordance with our experimental setup. Furthermore, the mean height of the peaks was around 0.5 µm. However, as it was mentioned before, the height and distribution were inhomogeneous; some peaks reached heights bigger than 1 µm.

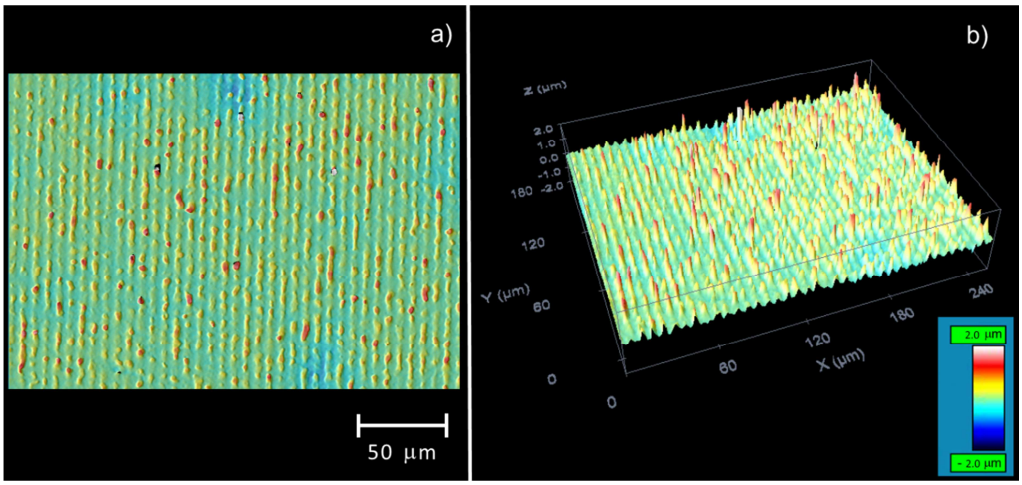

Figure 4.27. 3D topographical image of the sample taken by the confocal microscope

The marking process was done twice turning the sample 90° in the second step. Figure 4.28 shows the appearance of a lattice prepared by the perpendicular intersection of gratings. So, it was possible to create a network structure from a perpendicular intersection of two gratings. The topography of this surface also presented the inhomogeneities detected for the case of one grating; there were areas where the network structure was not formed entirely. Even so, the structure was apparently visible, and the intersection regions that had been marked twice did not exhibit any particular singularity.

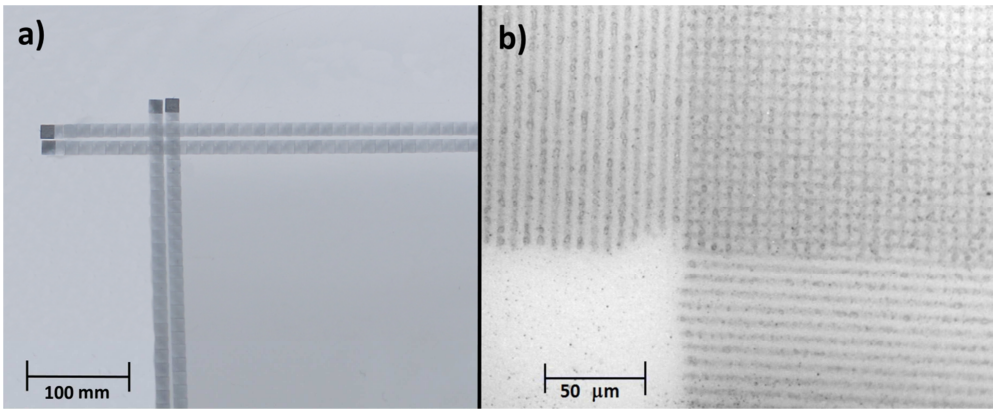

Figure 4.28. Images of the area generated by the crossing of two marked perpendicular areas.

4.5.2. Theoretical modelling of the contact angle

In the same way that the first technique used, the theoretical constant W and C can be calculated. The pattern resulting from the intersection of gratings was characterised by the interference period (T). The modelling was done considering that the grating was homogeneous, see figure 4.29. So the following topographical variables were defined:

T = Interference period

p = Network depth

a = Width of the grating

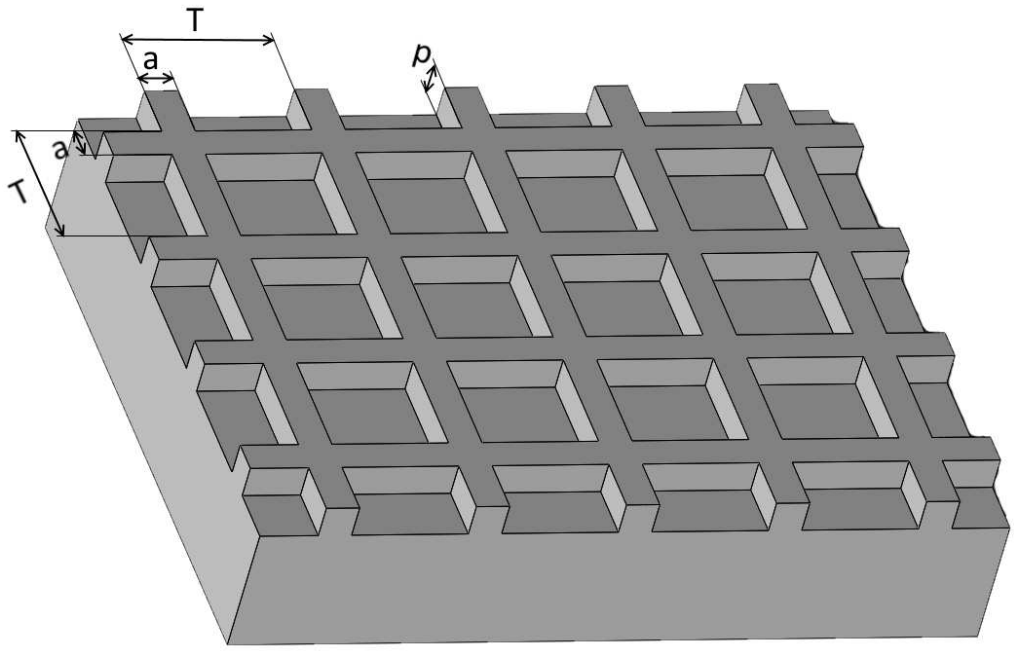

Figure 4.29. 3D model of the structure created by interferometric patterning.

- The Cassie-Baxter constant can be calculated as:

$$C = \frac{2aT - a^2}{T^2} \tag{4.13}$$

- Meanwhile, the Wenzel constant can be calculated as:

$$W = \frac{T^2 + 4p(T - a)}{T^2} \tag{4.14}$$

4.5.3. Influence of the topography on the wettability

Like the previous cases, theoretical models were used to predict changes in the wetting properties according to the topography created. So, using the constant W and C for the eq. (4.3) and (4.4), which were obtained in the previous section, the theoretical CA can be calculated. The unmarked material was used as a reference; its CA was 62.8 ± 1.7° after being cleaned with isopropanol.

Table 4.4 presents the topography parameters together with the CA predicted and measured. The samples were left in ambient conditions (previously described) to observe the temporal evolution of their CA and negligible changes were observed in this case. The dimensions of the network indicated in the table were measured using confocal microscopy. The height of the network was very inhomogeneous; as the material had some peaks, a high error is associated with the p value. It was more stable the width of the network that is characterised by the interferometric energy maxima.

The laser treatment increased the CA of the sample. The experimental result obtained fits the Cassie-Baxter model. This relationship indicated that the network structure did not allow penetrating the water inside. Although the height of the network created was low compared to the patterns made in section 4.3, the water was not able to get in. In this case, the period between lines was significantly reduced under 10 µm. So, this distance proved to be critical to design a structure that can be predicted according to Cassie-Baxter model.

Thus, according to the C-B model, the CA can be risen either increased the period of the network or decreased the width of the grating. However, if the period is too big, the water may be able to penetrate into the structure thus decreasing the CA. This effect also could happen if the walls width is decreased. So, according to the

results of section 4.3, a suitable solution should be the increment the height of the walls.

Table 4.4. Topography and CA predicted and measured of the structure created by the interference pattern.

T (µm)	p (µm)	a (µm)	CA predicted by Wenzel	CA predicted by Cassie-Baxter	CA
6.7 ± 0.1	0.5 ± 0.2	2.3 ± 0.2	56°	99°	99 ± 3°

4.5.4. Conclusions

Direct laser interference patterning (DLIP) has been used to create a patterned surface on the white-c ABS in order to modify its wettability. The network structure created exhibited a period of 6.7 µm, one order of magnitude below than the obtained by direct laser ablation patterning. The homogeneity of these structures was not optimum, and irregularities were observed in the marked samples. These processes are quite sensitive to any inhomogeneity of the laser beam or the material. The CA obtained was 99°, in accordance with the predicted by the Cassie-Baxter model.

References

[4.1] W. Barthlott and C. Neinhuis, "Purity of the sacred lotus, or escape from contamination in biological surfaces," *Planta*, vol. 202, no. 1, pp. 1–8, 1997.

[4.2] K. Koch, H. F. Bohn, and W. Barthlott, "Hierarchically sculptured plant surfaces and superhydrophobicity," *Langmuir*, vol. 25, no. 24, pp. 14116–14120, 2009.

[4.3] Y. Zheng, X. Gao, and L. Jiang, "Directional adhesion of superhydrophobic butterfly wings," *Soft Matter*, vol. 3, no. 2, pp. 178–182, 2007.

[4.4] W. R. Hansen and K. Autumn, "Evidence for self-cleaning in gecko setae," *Proc. Natl. Acad. Sci. U. S. A.*, vol. 102, no. 2, pp. 385–389, 2005.

[4.5] T. Young, "III. An essay on the cohesion of fluids," *Philos. Trans. R. Soc. London* , vol. 95, pp. 65–87, Jan. 1805.

[4.6] S. Wang and L. Jiang, "Definition of superhydrophobic states," *Adv. Mater.*, vol. 19, no. 21, pp. 3423–3424, Nov. 2007.

[4.7] L. Gao and T. J. McCarthy, "Contact angle hysteresis explained," *Langmuir*, vol. 22, no. 14, pp. 6234–6237, 2006.

[4.8] H. B. Eral, D. J. C. M. 't Mannetje, and J. M. Oh, "Contact angle hysteresis: a review of fundamentals and applications," *Colloid Polym. Sci.*, vol. 291, no. 2, pp. 247–260, Feb. 2013.

[4.9] R. N. Wenzel, "Resistance of solid surfaces to wetting by water," *Ind. Eng. Chem.*, vol. 28, no. 8, pp. 988–994, 1936.

[4.10] A. B. D. Cassie and S. Baxter, "Wettability of porous surfaces," *Trans. Faraday Soc.*, vol. 40, pp. 546–551, 1944.

[4.11] S. Sarbada and Y. C. Shin, "Superhydrophobic contoured surfaces created on metal and polymer using a femtosecond laser," *Appl. Surf. Sci.*, vol. 405, pp. 465–475, 2017.

[4.12] B. Bhushan and Y. C. Jung, "Natural and biomimetic artificial surfaces for superhydrophobicity, self-cleaning, low adhesion, and drag reduction," *Prog. Mater. Sci.*, vol. 56, no. 1, pp. 1–108, 2011.

[4.13] M. Nosonovsky and B. Bhushan, *Multiscale dissipative mechanisms and hierarchical surfaces: friction, superhydrophobicity, and biomimetics*, 1st ed. Berlin: Springer Science & Business Media, 2008.

[4.14] P. Zhang and F. Y. Lv, "A review of the recent advances in superhydrophobic surfaces and the emerging energy-related applications," *Energy*, vol. 82, pp. 1068–1087, 2015.

[4.15] D. K. Sarkar and M. Farzaneh, "Superhydrophobic coatings with reduced ice adhesion," *J. Adhes. Sci. Technol.*, vol. 23, no. 9, pp. 1215–1237, 2009.

[4.16] A. Marmur, "Super-hydrophobicity fundamentals: implications to biofouling prevention," *Biofouling*, vol. 22, no. 2, pp. 107–115, 2006.

[4.17] J. A. Callow and M. E. Callow, "Trends in the development of environmentally friendly fouling-resistant marine coatings," *Nat. Commun.*, vol. 2, p. 244, 2011.

[4.18] W. Xu, J. Song, J. Sun, Y. Lu, and Z. Yu, "Rapid fabrication of large-area, corrosion-resistant superhydrophobic Mg alloy surfaces," *ACS Appl. Mater. Interfaces*, vol. 3, no. 11, pp. 4404–4414, 2011.

[4.19] P. M. Barkhudarov, P. B. Shah, E. B. Watkins, D. A. Doshi, C. J. Brinker, and J. Majewski, "Corrosion inhibition using superhydrophobic films," *Corros. Sci.*, vol. 50, no. 3, pp. 897–902, 2008.

[4.20] X. Deng *et al.*, "Transparent, thermally stable and mechanically robust superhydrophobic surfaces made from porous silica capsules," *Adv. Mater.*, vol. 23, no. 26, pp. 2962–2965, 2011.

[4.21] J. Bravo, L. Zhai, Z. Wu, R. E. Cohen, and M. F. Rubner, "Transparent superhydrophobic films based on silica nanoparticles," *Langmuir*, vol. 23, no. 13, pp. 7293–7298, 2007.

[4.22] W. A. Daoud, *Self-cleaning materials and surfaces: a nanotechnology approach*, 1st ed. New Delhi: John Wiley & Sons, 2013.

[4.23] S. Mishra and V. Yadava, "Laser beam micromachining (LBMM)–a review," *Opt. Lasers Eng.*, vol. 73, pp. 89–122, 2015.

[4.24] P. Bizi-Bandoki, S. Benayoun, S. Valette, B. Beaugiraud, and E. Audouard, "Modifications of roughness and wettability properties of metals induced by femtosecond laser treatment," *Appl. Surf. Sci.*, vol. 257, no. 12, pp. 5213–5218, 2011.

[4.25] B. H. Luo, P. W. Shum, Z. F. Zhou, and K. Y. Li, "Preparation of hydrophobic surface on steel by patterning using laser ablation process," *Surf. Coatings Technol.*, vol. 204, no. 8, pp. 1180–1185, 2010.

[4.26] B. Wu, M. Zhou, J. Li, X. Ye, G. Li, and L. Cai, "Superhydrophobic surfaces fabricated by microstructuring of stainless steel using a femtosecond laser," *Appl. Surf. Sci.*, vol. 256, no. 1, pp. 61–66, 2009.

[4.27] A. Cunha, A. P. Serro, V. Oliveira, A. Almeida, R. Vilar, and M.-C. Durrieu, "Wetting behaviour of femtosecond laser textured Ti–6Al–4V surfaces," *Appl. Surf. Sci.*, vol. 265, pp. 688–696, 2013.

[4.28] A. Y. Vorobyev and C. Guo, "Multifunctional surfaces produced by femtosecond laser pulses," *J. Appl. Phys.*, vol. 117, no. 3, p. 33103, 2015.

[4.29] E. Skantzakis, V. Zorba, D. G. Papazoglou, I. Zergioti, and C. Fotakis, "Ultraviolet laser microstructuring of silicon and the effect of laser pulse duration on the surface morphology," *Appl. Surf. Sci.*, vol. 252, no. 13, pp. 4462–4466, 2006.

[4.30] V. Zorba *et al.*, "Making silicon hydrophobic: wettability control by two-lengthscale simultaneous patterning with femtosecond laser irradiation," *Nanotechnology*, vol. 17, no. 13, p. 3234, 2006.

[4.31] M. R. Cardoso, V. Tribuzi, D. T. Balogh, L. Misoguti, and C. R. Mendonça, "Laser microstructuring for fabricating superhydrophobic polymeric surfaces," *Appl. Surf. Sci.*, vol. 257, no. 8, pp. 3281–3284, 2011.

[4.32] M. Malinauskas, M. Farsari, A. Piskarskas, and S. Juodkazis, "Ultrafast laser nanostructuring of photopolymers: A decade of advances," *Phys. Rep.*, vol. 533, no. 1, pp. 1–31, 2013.

[4.33] G. A. Primo, C. I. A. Igarzabal, G. A. Pino, J. C. Ferrero, and M. Rossa, "Surface morphological modification of crosslinked hydrophilic co-polymers by nanosecond pulsed laser irradiation," *Appl. Surf. Sci.*, vol. 369, pp. 422–429, 2016.

[4.34] K. Gotoh and S. Kikuchi, "Improvement of wettability and detergency of polymeric materials by excimer UV treatment," *Colloid Polym. Sci.*, vol. 283, no. 12, pp. 1356–1360, 2005.

[4.35] A. Athanassiou *et al.*, "Photocontrolled variations in the wetting capability of photochromic polymers enhanced by surface nanostructuring," *Langmuir*, vol. 22, no. 5, pp. 2329–2333, Feb. 2006.

[4.36] S. van Pelt, A. Frijns, R. Mandamparambil, and J. den Toonder, "Local wettability tuning with laser ablation redeposits on PDMS," *Appl. Surf. Sci.*, vol. 303, pp. 456–464, 2014.

[4.37] D. G. Waugh, J. Lawrence, C. D. Walton, and R. B. Zakaria, "On the effects of using CO 2 and F 2 lasers to modify the wettability of a polymeric biomaterial," *Opt. Laser Technol.*, vol. 42, no. 2, pp. 347–356, 2010.

[4.38] M. H. and D. M., "Influence of laser surface modifying of polyethylene terephthalate on fibroblast cell adhesion," *Radiat. Phys. Chem.*, vol. 67, no. 3–4, pp. 381–385, Jun. 2003.

[4.39] A. Riveiro *et al.*, "Texturing of polypropylene (PP) with nanosecond lasers," *Appl. Surf. Sci.*, vol. 374, pp. 379–386, Jun. 2016.

[4.40] L. Li *et al.*, "Laser nano-manufacturing–state of the art and challenges," *CIRP Ann. Technol.*, vol. 60, no. 2, pp. 735–755, 2011.

[4.41] R. McCann, K. Bagga, R. Groarke, A. Stalcup, M. Vázquez, and D. Brabazon, "Microchannel fabrication on cyclic olefin polymer substrates via 1064nm Nd: YAG laser ablation," *Appl. Surf. Sci.*, vol. 387, pp. 603–608, 2016.

[4.42] R. Suriano *et al.*, "Femtosecond laser ablation of polymeric substrates for the fabrication of microfluidic channels," *Appl. Surf. Sci.*, vol. 257, no. 14, pp. 6243–6250, 2011.

[4.43] M. Berta *et al.*, "Nanosecond laser-induced periodic surface structuring of cross-linked azo-polymer films," *Appl. Surf. Sci.*, vol. 282, pp. 880–886, 2013.

[4.44] E. Rebollar, M. Castillejo, and T. A. Ezquerra, "Laser induced periodic surface structures on polymer films: From fundamentals to applications," *Eur. Polym. J.*, vol. 73, pp. 162–174, 2015.

[4.45] N. Sanner, N. Huot, E. Audouard, C. Larat, and J.-P. Huignard, "Direct ultrafast laser micro-structuring of materials using programmable beam shaping," *Opt. Lasers Eng.*, vol. 45, no. 6, pp. 737–741, 2007.

[4.46] D. Conrad and L. Richter, "Ultra-short pulse laser structuring of molding tools," *Phys. Procedia*, vol. 56, pp. 1041–1046, 2014.

[4.47] A. F. Lasagni, J. L. Hendricks, C. M. Shaw, D. Yuan, D. C. Martin, and S. Das, "Direct laser interference patterning of poly (3, 4-ethylene dioxythiophene)-poly (styrene sulfonate)(PEDOT-PSS) thin films," *Appl. Surf. Sci.*, vol. 255, no. 22, pp. 9186–9192, 2009.

[4.48] A. F. Lasagni, P. Shao, J. L. Hendricks, C. M. Shaw, D. C. Martin, and S. Das, "Direct fabrication of periodic patterns with hierarchical sub-wavelength structures on poly (3, 4-ethylene dioxythiophene)–poly (styrene sulfonate) thin films using femtosecond laser interference patterning," *Appl. Surf. Sci.*, vol. 256, no. 6, pp. 1708–1713, 2010.

[4.49] R. Srinivasan and V. Mayne-Banton, "Self-developing photoetching of poly (ethylene terephthalate) films by far-ultraviolet excimer laser radiation," *Appl. Phys. Lett.*, vol. 41, no. 6, pp. 576–578, 1982.

[4.50] Y. Kawamura, K. Toyoda, and S. Namba, "Effective deep ultraviolet photoetching of polymethyl methacrylate by an excimer laser," *Appl. Phys. Lett.*, vol. 40, no. 5, pp. 374–375, 1982.

[4.51] T. Lippert, "Laser application of polymers," in *Polymers and Light*, Springer, 2004, pp. 51–246.

[4.52] L. D. Laude, D. Martinez, C. Dicara, F. Hanus, and K. Kolev, "The ablation of polymers under excimer laser irradiation: the physics of the process and the polymer structure," *Nucl. Instruments Methods Phys. Res. Sect. B Beam Interact. with Mater. Atoms*, vol. 185, no. 1, pp. 147–155, 2001.

[4.53] S. I. Anisimov and B. S. Luk'yanchuk, "Selected problems of laser ablation theory," *Physics-Uspekhi*, vol. 45, no. 3, p. 293, 2002.

[4.54] S. Baudach, J. Bonse, and W. Kautek, "Ablation experiments on polyimide with femtosecond laser pulses," *Appl. Phys. A Mater. Sci. Process.*, vol. 69, no. 7, pp. S395–S398, 1999.

[4.55] H. Tsuruta, O. Dondelewski, Y. Katagiri, B. Wang, and A. Sasoh, "Ablation spot area and impulse characteristics of polymers induced by burst irradiation of 1μm laser pulses," *Acta Astronaut.*, vol. 136, pp. 46–54, 2017.

[4.56] M. C. Castex and N. Bityurin, "Is the VUV laser ablation of polymers a pure photochemical process?," *Appl. Surf. Sci.*, vol. 197, pp. 805–807, 2002.

[4.57] M. C. Castex, N. Bityurin, C. Olivero, S. Muraviov, N. Bronnikova, and D. Riedel, "VUV laser ablation of polymers: Photochemical aspect," *Appl. Surf. Sci.*, vol. 168, no. 1, pp. 175–177, 2000.

[4.58] N. Bityurin, N. Arnold, B. Luk'Yanchuk, and D. Bäuerle, "Bulk model of laser ablation of polymers," *Appl. Surf. Sci.*, vol. 127, pp. 164–170, 1998.

[4.59] N. Arnold, N. Bityurin, and D. Bäuerle, "Laser-induced thermal degradation and ablation of polymers: bulk model," *Appl. Surf. Sci.*, vol. 138, pp. 212–217, 1999.

[4.60] D. P. Brunco, J. A. Kittl, C. E. Otis, P. M. Goodwin, M. O. Thompson, and M. J. Aziz, "Time-resolved temperature measurements during pulsed laser irradiation using thin film metal thermometers," *Rev. Sci. Instrum.*, vol. 64, no. 9, pp. 2615–2623, 1993.

[4.61] B. Luk'yanchuk, N. Bityurin, S. Anisimov, A. Malyshev, N. Arnold, and D. Bäuerle, "Photophysical ablation of organic polymers: the influence of stresses," *Appl. Surf. Sci.*, vol. 106, pp. 120–125, 1996.

[4.62] L. Urech and T. Lippert, "Photoablation of polymer materials," *Photochem. Photophysics Polym. Mater.*, pp. 541–568, 2010.

[4.63] N. Bityurin, B. S. Luk'yanchuk, M. H. Hong, and T. C. Chong, "Models for laser ablation of polymers," *Chem. Rev.*, vol. 103, no. 2, pp. 519–552, 2003.

[4.64] R. S. Kappes *et al.*, "A study of photothermal laser ablation of various polymers on microsecond time scales," *Springerplus*, vol. 3, no. 1, p. 489, 2014.

[4.65] R. Fardel, M. Nagel, T. Lippert, F. Nüesch, A. Wokaun, and B. S. Luk'Yanchuk, "Influence of thermal diffusion on the laser ablation of thin polymer films," *Appl. Phys. A*, vol. 90, no. 4, pp. 661–667, 2008.

[4.66] S. L. Johnson, D. M. Bubb, and R. F. Haglund, "Phase explosion and recoil-induced ejection in resonant-infrared laser ablation of polystyrene," *Appl. Phys. A Mater. Sci. Process.*, vol. 96, no. 3, pp. 627–635, 2009.

[4.67] T. Lippert, M. Hauer, C. R. Phipps, and A. Wokaun, "Fundamentals and applications of polymers designed for laser ablation," *Appl. Phys. A*, vol. 77, no. 2, pp. 259–264, 2003.

[4.68] T. Lippert *et al.*, "Polymers designed for laser ablation-influence of photochemical properties," *Appl. Surf. Sci.*, vol. 197, pp. 746–756, 2002.

[4.69] S. Zehnder, P. Schwaller, U. Von Arx, G. Bucher, and B. Neuenschwander, "Micro structuring of transparent materials with NIR ns-laser pulses," *Phys. Procedia*, vol. 12, pp. 195–200, 2011.

[4.70] I.-A. Paun, A. Selimis, G. Bounos, G. Kecskeméti, and S. Georgiou, "Nanosecond and femtosecond UV laser ablation of polymers: Influence of molecular weight," *Appl. Surf. Sci.*, vol. 255, no. 24, pp. 9856–9860, 2009.

[4.71] A. A. Serafetinides, C. D. Skordoulis, M. I. Makropoulou, and A. K. Kar, "Picosecond and subpicosecond visible laser ablation of optically transparent polymers," *Appl. Surf. Sci.*, vol. 135, no. 1, pp. 276–284, 1998.

[4.72] E. G. Gamaly, "The physics of ultra-short laser interaction with solids at non-relativistic intensities," *Phys. Rep.*, vol. 508, no. 4, pp. 91–243, 2011.

[4.73] C. Florian, F. Caballero-Lucas, J. M. Fernández-Pradas, J. L. Morenza, and P. Serra, "Surface ablation of transparent polymers with femtosecond laser pulses," *Appl. Surf. Sci.*, vol. 302, pp. 226–230, 2014.

[4.74] J. Cheng *et al.*, "A review of ultrafast laser materials micromachining," *Opt. Laser Technol.*, vol. 46, pp. 88–102, 2013.

[4.75] T. L. See, Z. Liu, L. Li, and X. L. Zhong, "A comparison of the characteristics of excimer and femtosecond laser ablation of acrylonitrile butadiene styrene (ABS)," *Appl. Surf. Sci.*, vol. 364, pp. 467–476, 2016.

[4.76] E. W. Kreutz, H. Frerichs, J. Stricker, and D. A. Wesner, "Processing of polymer surfaces by laser radiation," *Nucl. Instruments Methods Phys. Res. Sect. B Beam Interact. with Mater. Atoms*, vol. 105, no. 1–4, pp. 245–249, 1995.

[4.77] S. Ruotsalainen, P. Laakso, R. Penttilä, and H. Pantsar, "Picosecond laser processing–material removal rates of plastics," in *Proceedings of the 11th NOLAMP Conference Nordic Laser Materials Processing Conference*, 2007.

[4.78] B. Zhang and K. C. Yung, "Frequency-tripled Nd:YAG laser ablation in laser structuring process," *Opt. Lasers Eng.*, vol. 44, no. 8, pp. 815–825, 2006.

[4.79] D. Sola, A. Escartin, R. Cases, and J. I. Pena, "Laser ablation of advanced ceramics and glass-ceramic materials: Reference position dependence," *Appl. Surf. Sci.*, vol. 257, no. 12, pp. 5413–5419, 2011.

[4.80] R. Ortiz, S. Moreno-Flores, I. Quintana, M. Vivanco, J. R. Sarasua, and J. L. Toca-Herrera, "Ultra-fast laser microprocessing of medical polymers for cell engineering applications," *Mater. Sci. Eng. C*, vol. 37, pp. 241–250, 2014.

[4.81] G. Römer *et al.*, "Picosecond laser machining of metallic and polymer substrates for fluidic driven self-alignment," *Phys. Procedia*, vol. 39, pp. 628–635, 2012.

[4.82] K. Liu, M. Cao, A. Fujishima, and L. Jiang, "Bio-inspired titanium dioxide materials with special wettability and their applications," *Chem. Rev.*, vol. 114, no. 19, pp. 10044–10094, 2014.

[4.83] Y. Xiu, L. Zhu, D. W. Hess, and C. P. Wong, "Hierarchical silicon etched structures for controlled hydrophobicity/superhydrophobicity," *Nano Lett.*, vol. 7, no. 11, pp. 3388–3393, 2007.

[4.84] N. Pérez, T. Tavera, A. Rodríguez, M. Ellman, I. Ayerdi, and S. M. Olaizola, "Fabrication of sub-micrometric metallic hollow-core structures by laser interference lithography," *Appl. Surf. Sci.*, vol. 258, no. 23, pp. 9370–9373, 2012.

[4.85] D. Wang, Z. Wang, Z. Zhang, Y. Yue, D. Li, and C. Maple, "Direct modification of silicon surface by nanosecond laser interference lithography," *Appl. Surf. Sci.*, vol. 282, pp. 67–72, 2013.

[4.86] F. J. Rodríguez *et al.*, "Surface relief gratings induced by a nanosecond pulse in a liquid-crystalline azo-polymethacrylate," *Appl. Phys. Lett.*, vol. 87, no. 20, p. 201914, 2005.

[4.87] R. P. Crease, "The most beautiful experiment," *Phys. World*, vol. 15, no. 9, p. 19, 2002.

[4.88] C. Daniel, F. Mücklich, and Z. Liu, "Periodical micro-nano-structuring of metallic surfaces by interfering laser beams," *Appl. Surf. Sci.*, vol. 208, pp. 317–321, 2003.

[4.89] O. T. Picot *et al.*, "Manufacturing of surface relief structures in moving substrates using photoembossing and pulsed-interference holography," *Macromol. Mater. Eng.*, vol. 298, no. 1, pp. 33–37, 2013.

5. Colour laser marking

Chapter 3 described the laser marking of a polymeric sample to produce aesthetical and permanent marks on ABS samples. However, the range of colours achieved was in the grey scale. In this section, some preliminary approaches to colour laser marking beyond the grey scale of polymeric samples will be shown. Colour laser marking can be controlled either using pigments or dyes (chemical control) [5.1] or by material surface structuring (structural colouration) [5.2].

Pigments or dyes induce a colouration when they are added to polymeric materials. There are some commercial additives specially designed to be activated under an intense laser beam to produce an effective colour change in the polymers focused on obtaining a visible contrast. Thus, they are usually employed to produce marks on materials that were difficult to be marked, not to obtain a range of colours [5.3]. Only one study reported the creation of a visible colouration using photo-sensitive pigments by laser-induced photo-chemical processes [5.4]. The colours were obtained employing UV radiation on a transparent polymer although they were not stable in time. These types of processes open new possibilities for laser colour marking on polymers.

Structural colours are usually defined in contraposition to pigmentary colours. Thus, they were defined as those colours whose origin is an optical phenomenon such as thin-layer interference, diffraction grating, light scattering, surface plasmon resonances and so on [5.2]. These types of colours are widely found in nature, i.e. the colour of the butterfly wings or the shell of some insects [5.5], [5.6]. Using a laser is possible to create structures by heating or micro-structuring that alters the colour perception. For example, this technique allows the creation of controlled oxidation changes that affect the incident light on metal. Varying the laser parameters is

possible to create a wide range of visible colours [5.7]–[5.9]. However, this type of process is restricted to metals, and it is not possible to reproduce it on a polymeric material. An approach combining metals and dielectric materials to change the colour appearance on a polymer surface is the use of Surface Plasmon Resonance (SPR) [5.10]. SPR can produce a range of vivid aesthetical colours that are directly dependent on the nanostructured surface [5.11]. This technique has several advantages with respect to the traditional technologies like the sub-wavelength resolution, the bright and non-fading colours and the reduced pixel area. Nevertheless, it is needed to pre-design the patterns and print them for example by e-beam lithography (EBL) or focused ion beam (FIB), both expensive and slow processes. However, new studies have proved the possibility of reshaping the nanostructure using a laser to change the final colour appearance [5.12].

Finally, using interferometric techniques, it is possible to create iridescent colours on any surface. This technique was introduced in chapter 4^{th,} and it is based on producing an interference pattern on the material surface able to create a microstructuration on it. This created structure was significantly smaller than those obtained by direct laser ablation patterning, being possible to have their dimensions in the order of visible light diffraction. Thus, these patterned surfaces can show different vivid colours depending on the angle of view [5.13]–[5.15].

In this chapter, some possible alternatives to induce a colour change in polymers by laser irradiation, beyond the grey scale, are proposed. Firstly, the use of chemical additives able to change their colour under laser irradiation in a controlled way is studied. Secondly, laser irradiation is employed to induce reshaping of a metallic layer deposited on a polymer affecting the SPR, therefore, altering its visible colour. Finally, using interferometric techniques, a holographic structure was created

producing iridescent colours. It should be remarked that, in this chapter, a preliminary study of these techniques to check their feasibility is presented.

5.1. Colour marking based on additives

Pigments reactive to laser has been widely employed to produce permanent marks [5.3]. For example, a commercial additive from Merck® was studied in the section 3.3.5 producing white marks on a black ABS. Usually, they are developed for being reactive under IR wavelengths. These additives operate converting laser energy into heat, which causes localised charring/burning in the plastics surface layer to give dark brown or grey contrasting marks. However, as it was introduced before, they are not designed to produce colour change beyond the grey scale.

The goal of this section was to produce laser marking using additives on a colour scale without damaging the polymeric surface. These additives should exhibit a visible contrast change in addition to the colour formation. Within the framework of the UV-marking EU project, it was possible to test the use of alternative additives (under development) to produce this colour laser marking as a partner of the consortium. Two types of organic pigments were used during the project, diacetylene and leucodye, although the specific chemical structure of these additives was not provided. In the case of diacetylenes, topochemical polymerisation can be induced by UV irradiation leading to a coloured polymer (or oligomer). Thus, these compounds may be transformed from a colourless to a coloured form that may exhibit a wide variety of colours like blue, magenta, red, orange or yellow. By contrast, the leucodyes can switch between two chemical forms under UV light and temperature; being one of them colourless. Therefore, both types of molecules can be activated by a UV laser after polymer processing as extrusion and injection moulding. Consequently, they should be stable to high temperatures that are reached during the manufacturing and also to environmental light.

In a first approach, the additives were first dispersed in the polymeric matrix and injected to obtain the samples to be marked. However, in order to reduce the amount of additive needed to mark the sample and solve some problems related with the presence of the polymer whitener (see below) the IML technique (see section 1.1.2) was used. All these processes of compounding, injection and IML were done by Wirthwein A.G (partner of the UV marking project) and the samples to be marked were directly supplied to our labs. The additives used are not commercially available yet; they are in a predevelopment phase and their chemical structures were not provided.

The study of marking was performed with the UV laser. Changes both on the DPI and the power were analysed, so a matrix of columns and lines was done. Each column of the horizontal axis corresponds to power changes, from 0.2 to 1.8 W in successive steps of 0.2 W. The vertical axis represents the DPI values from 200 to 1200 DPI in successive steps of 200 DPI. The polymeric materials employed were introduced in the section 2.1.2. As polymer matrix, the natural-w ABS, the white-c ABS and the translucent-c PP were used to prepare samples with the corresponding laser marking additives.

5.1.1. Marking of injection moulded plastic samples containing laser additives

In a first approach, samples processed by injection moulding and derived from ABS containing laser marking additives were processed. However, additives based on leucodyes did not withstand the temperatures needed during the ABS processing. For this reason, PP was used in the case of leucodyes as its processing temperature (around 200°C) was lower than the required by ABS. Natural-w ABS and

translucent-c PP were first mixed with the marking laser additives in a molten state. Then, the plastic compoundings were processed by injection moulding to yield flat plates. After processing, the leucodyes and diacetylenes additives can be activated by UV laser. It should be first remarked that the preliminary tests showed that the additives did not work when the samples contained TiO_2 that acts as a UV absorber as it was seen in chapter 3.

The diacetylene additives were injected together with the natural-w ABS to avoid the problem with the TiO_2. The best laser marking results obtained are shown in figure 5.1. The colour obtained ranged from a dark blue to a pale reddish-white depending on the laser parameters. Also, some marks exhibited brownish colours probably associated with a material carbonisation. The first column (low powers) showed a range of bluish colour that increases its saturation when DPI value increased. This effect was also detected in the first row (low DPI value). By contrast, the highest powers and DPI values (bottom right corner) caused white foaming at the material observed by a pale reddish-white colour. This whiter colour was also presented at high DPI values in the natural ABS without the pigment, see figure 3.5 in section 3.2.2. Therefore, the pigment seemed to absorb the laser and get activated even when the energy deposited was not high, while the foaming produced by the ABS absorption masking the effect of the additive.

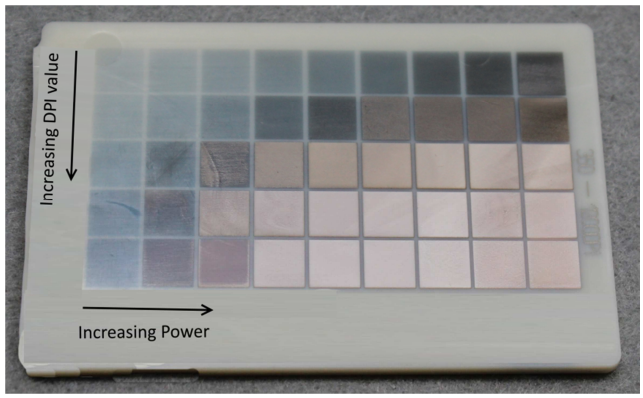

Figure 5.1. Natural-w ABS with the first generation of diacetylene additive marked with the UV laser.

In the case of the leucodyes, they were injected together with translucent-c PP and later marked with the UV laser. The resulting samples were translucent plaques that exhibited a colour change by the effect of the laser. The best results achieved are displayed in figure 5.2. Two types of colour ranges were obtained, reddish and bluish-greenish colours using different leucodyes. Depending on the laser parameters, yellowish or brownish colours were also obtained. As a difference in the diacetylene case, no whiter colouration was observed for the highest powers and DPI parameters.

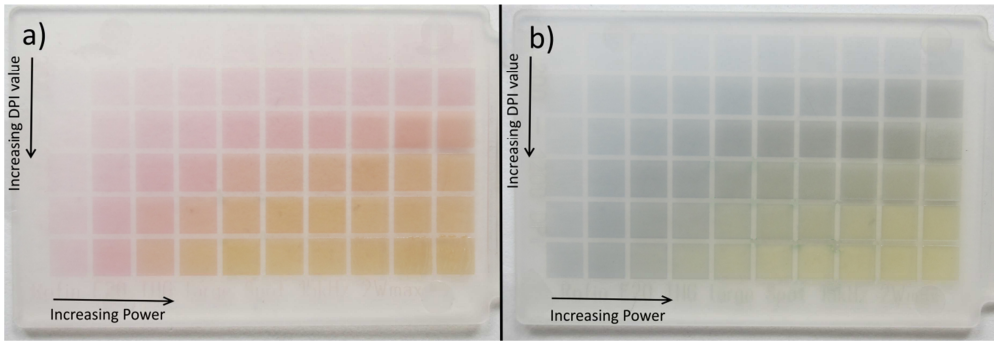

Figure 5.2. Translucent-c PP with two first generation compounds of leucodyes marked with the ns laser to obtain a) reddish colours; b) bluish-greenish colours.

Unfortunately, both additives, diacetylene and leucodyes, exhibited changes upon exposure to sunlight (UV wavelengths), so after some weeks all the samples exhibited

a pale colouration (even in regions that were not irradiated). This effect was unacceptable for a future application as colour decoration.

5.1.2. Laser marking of samples processed by in-mould labelling (IML)

The use of pigments for laser marking, as diacetylenes or leucodyes, in bulk increases the final cost of the material. Furthermore, as said above, the sunlight stability of the additives was not acceptable, and eventually, the material changed its colour. On the other hand, the laser colour additives cannot be used with white polymeric materials. Due to these reasons, in-mould labelling technique was used in subsequent experiments. Furthermore, pigments with a high thermal and UV stability were used to improve the tolerance to processing conditions.

The IML technique was introduced in the section 1.1.2. This technique involves depositing a thin film on the polymer surface during the injection moulding to label the resulting object. If this film contains the pigment, the laser marking additive can be deposited only in surface areas designated to be marked. This process is economically beneficial due to the high-cost of the additives but also improves the processability as the high temperature reached during the first steps of the injection process is avoided (the layer was placed inside the mould). Furthermore, it is possible to employ the white ABS containing TiO_2 pigment with this technique as the thin layer, with the additive, was transparent and deposited over the white polymer. The IML technique requires that the layer and the polymer were compatible to ensure a correct adhesion. Additionally, the samples were covered with a light protector spray after the laser treatment to increase its long-term stability under environmental conditions.

The carrier labels were made of PS and PP for these new leucodye and diacetylene additives respectively. The transparent PS was used because it is a compatible material with the ABS. However, the new diacetylene pigment cannot be injected with the PS because during the injection process the molecule degraded due to the processing temperature. Thus, a PP layer was used as replacement deposited onto a PP sample (PP films exhibits a poor adhesion onto ABS). The marks were produced with the same laser, the UV laser.

The best results obtained are presented in figure 5.3. The intensity of the reddish and bluish colours achieved was higher than in the previous case. Also, the IML technique proved to be a suitable solution to obtain colours on white-pigmented polymers. In the case of the leucodye (figure 5.3.a), the most intense reddish colours were obtained at high power and DPI values (bottom right corner). Furthermore, some of the marks done at intermediate parameters exhibited brownish colours, probably caused by carbonisation. It seemed that if the laser intensity was not enough to produce the colour change of the molecule, this spare energy went to the polymer matrix producing a degradation. By comparison, in the case of diacetylene additive (figure 5.3.b), the marks exhibited a light colouration at low DPI and power values (top left corner). The higher power and DPI values, the higher the colour intensity. In this case, tuning the laser parameters, it was possible to observe a range of bluish colours. However, a noticeable degradation was visible working at the maximum values (bottom right corner).

Therefore, the diacetylene additives had the colour changes at lower power and DPI values than the leucodyes. This difference may be related to the diacetylene molecules exhibited higher UV photo-activity than the leucodyes, which is preferable in a laser industrial process to reduce the cycle time.

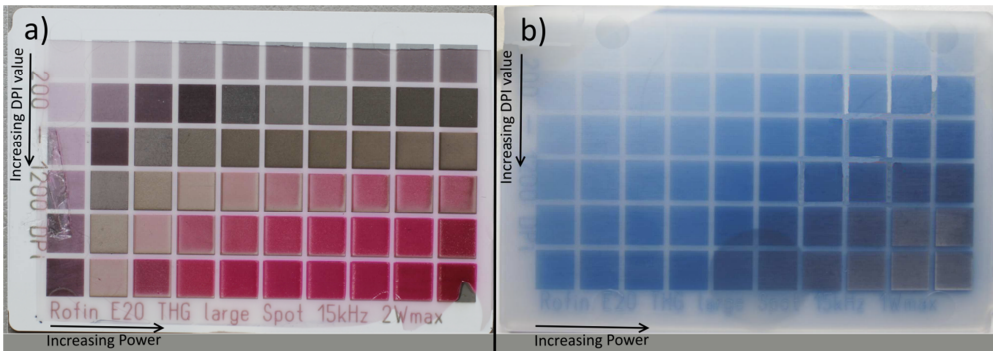

Figure 5.3. Plaques obtained with the second generation of pigments marked with the UV laser on a) PS film with leucodyes injected with white ABS; b) PP film with diacetylene injected with transparent PP.

.

5.1.3. Example of application of a real design

Finally, the same combination of additives and polymeric materials, film and base material presented before was used to inject frontal panels used in a domestic dishwasher. Two areas were covered by the films designed to be marked. One of the areas was employed to mark a real design while a decorative pattern was marked in the other one. The results after the laser processing can be seen in figure 5.4, the best parameters obtained before were selected for the laser marking process. It was possible to distinguish easily the area covered by the layer in the object shown in figure 5.4.b with a thin layer containing the diacetylene additive and due to the pale bluish colouration observed. This change was probably caused by the higher photoactivity of this molecule to ambient light.

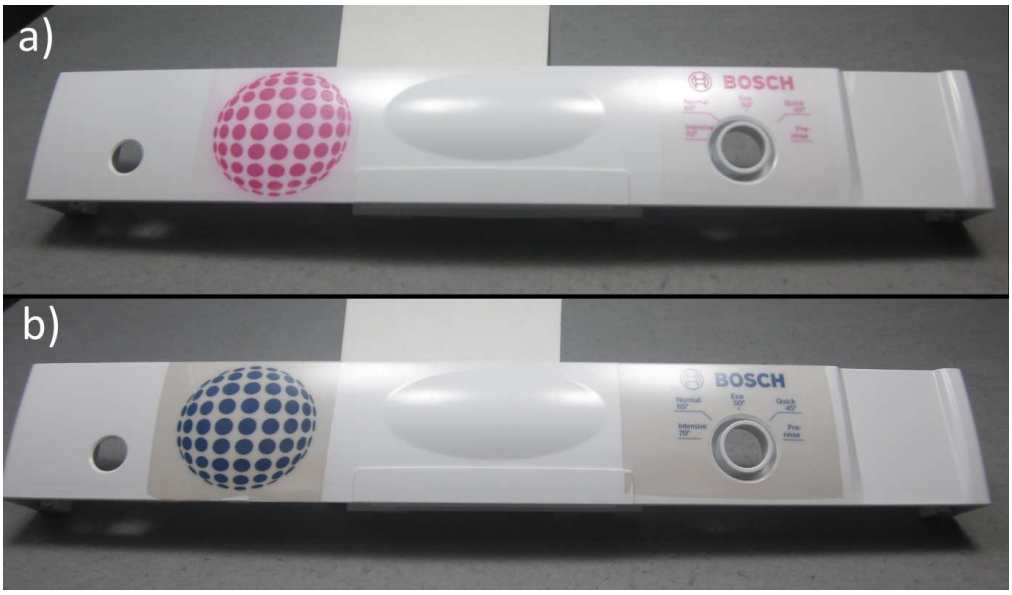

Figure 5.4. Images of the frontal panel of a dishwasher with two areas covered by a film carrying the colour additives after laser marking process. a) PS film with leucodyes injected overt white ABS; b) PP film with diacetylene injected over white PP.

In addition, figure 5.5 presents an example of possible aesthetical decoration with thin lines (less than 1 mm) created by laser on a PS film with leucodyes. There were no colour intensity losses using thin lines. It is possible to appreciate the colour change from grey scale to reddish colours caused by the additive on the left side where the film ends.

Figure 5.5. Example of possible aesthetical thin lines decoration on a frontal panel made of white ABS with a film of PS with a leucodyes additive.

5.1.4. Conclusions

This preliminary work showed that leucodyes and diacetylenes can be used as additives for colour laser marking. The best results were achieved with the IML technology. The colours obtained were a pale red and an intense blue colour. However, compatibility problems and processing temperatures limited their application. Furthermore, each colour was obtained using a different molecule, so at this point, it was not possible to make a multi-colour laser marking. Nevertheless, this technology has proved to be a solution for colour laser marking although the UV long time stability should be improved.

5.2. Colour marking based on laser reshaping of plasmonic structures

Surface plasmon polaritons (SPs) are electromagnetic excitations propagating at the interface between a dielectric and a conductor, evanescently confined in the perpendicular direction. These electromagnetic surface waves arise via the coupling of the electromagnetic fields to oscillations of the conductor's electron plasma [5.10]. Thus, the optical energy is concentrated at the nanoscale due to this SPs. Silver or gold are good plasmonic metals because they have small losses (Im $\varepsilon_m \ll$ -Re ε_m), so they are widely used to concentrate the electromagnetic wave [5.16]. Furthermore, new studies proved the suitability of aluminium as metal for plasmonic structures [5.17]. The size of the nanoscale determines the optical frequencies confined associated to the resonant oscillation of the conduction electrons, the surface plasmon resonance (SPR).

The use of structures that exhibit effects of surface plasmon resonance (SPR) has been widely explored since the last decades of the past century [5.18]–[5.20]. Nowadays, they have shown their potential for miniaturised photonic devices [5.21], sensoring [5.22]–[5.24] and colour printing considering different approaches [5.25]–[5.29]. Even it is possible to achieve structures near the optical diffraction limit [5.30] or to develop structures whose characteristics exhibit polarisation dependence [5.17], [5.31], [5.32].

However, the pre-design of the pattern and its printing by top-down nanolithography techniques [5.33]–[5.35] make difficult the scale-up of these structures. Some strategies have been proposed to achieve some tunability of the observed colours [5.36], [5.37]. It has also described a method to combine nanoimprinted plasmonic metasurface with the use of a pulsed laser to induce

transient local heat generation [5.38], [5.39] leading to melting and reshaping of the imprinted nanostructures (digital resonant laser printing – DRLP) [5.12], [5.40], [5.41]. The use of lasers enables the thermal and chemical treatments to be strongly localised both spatially and temporally, thereby leaving the surrounding material otherwise unaffected [5.42]. Furthermore, the use of a computer allows controlling the beam motion and the opportunity to digitalise the process [5.43].

This technique has been checked to create periodic sub-micron structures spanning at the centimetre-scale by colloidal self-assembling [5.44], [5.45] and a subsequent laser modification. This fast approach allows examining quickly and flexibly the modification and the further performance of different plasmonic nanostructures. The plasmonic crystals were obtained employing PS colloidal spheres covered with a thin layer either of silver or aluminium by sputtering. This work was performed during a PhD stay in the DTU nanotech (Denmark).

5.2.1. Fabrication of the plasmonic crystal and laser reshaping

The plasmonic crystal was formed by PS spheres of 400 ± 9 nm diameter (see section 2.1.1.3) prepared by a self-assembly process. The colloidal suspension was confined to two parallel glass slides under capillary forces. This technique is based on the macroscopical control of the drying front shape of the suspension, without the need of any supporting patterned substrate. In this case, it was used a rectangular wedge-shaped cell with three open sides, so the contact drying front formed by the colloidal suspension created a convex curve. Therefore, the PS spheres were arranged along the drying front because of the attractive capillary force between adjacent particles. At the initial stage, the particles followed this curved line being assembled

like a beaded chain. As the solvent was evaporated, the resulting convective flow grouped more particles together to the drying front. Consequently, a non-uniform lattice was created, and small crystalline domains were induced [5.44]. A layer of PS spheres, deposited onto a glass, of approximately 1 cm^2 was obtained by this technique. Either aluminium or silver was sputtered over the area of the colloidal crystal to fabricate the plasmonic crystal. A thin metal layer of 30 nm was deposited over the spheres in both cases. Figure 5.6 shows an SEM image of the PS particles covered with Al. Similar distribution was observed after sputtering with Ag. The particles were not entirely uniform distributed as it was predicted. Also, some gaps with missing spheres were detected. It was possible to observe some clusters of particles or domains as the bright areas that surrounding some particles, associated with an electron energy accumulation under SEM.

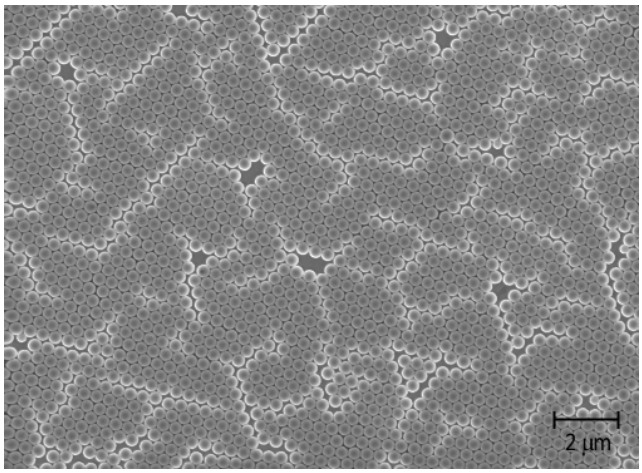

Figure 5.6. SEM image of the distribution of PS particles created by self-assembling covered with Al.

The created plasmonic structure was altered using a laser-processing technique known as digital resonant laser printing (DRLP). Here, the metallic layer was reshaped by briefly heating above its melting temperature using a nanosecond-pulsed laser. By using a laser with a wavelength close to the Localised Surface Plasmon

(LSP) resonance, we can spatially localise the heating process due to the strong electric field confinement of the LSPs.

Therefore, the spheres covered with both metals were irradiated with a green laser (plasmonic green laser, see section 2.1.1.5). The energy of the laser was tuned using a programmable beam polariser taken advantage of the fact that the laser was linearly polarised. The range of energies used was between 0-30 nJ; energies above produce ablation of the spheres. The samples were placed in the focal plane of a 10x objective (spot size ~20 μm in diameter); consequently the total fluence over the samples was lower than 0.1 $nJ/\mu m^2$. A motorised stage allowed scanning the surface of the material making different designs. Only a small central region can reach enough energy to reshape the spheres considering a Gaussian distribution of the laser energy.

DRLP melts the edges of the metal cap, which reduces their size while leaving the polystyrene spheres unchanged. The laser pulse energy tunes the magnitude of the reshaping; squares of 1 mm^2 were done at different energies, see figures 5.7 and 5.8. The visible reflected colour, illuminated under non-polarised white light, went from an original purple to different degrees of yellowish colours till dark green on the PS spheres covered by Ag. The colour of the spheres covered by Al was restricted to different grades of yellow from the original pale red. Experimentally it was observed that the minimum width of the lines created by laser was around 4 μm.

Microscopically, the laser energy was absorbed by the metal layer deposited over the particles producing a melting of the edges reducing their size. The metal layer on top was displaced to the centre of masses of the domains probably due to electromagnetic attraction; it was possible to appreciate the shadow of the spheres in the edges of the domains that remain in their original position, see figure 5.7.b. where some of the metal layers were in contact. Therefore, the distance between the clusters

was increased. Additionally, this process caused a rise in the number of domains as can be observed in the SEM images of figure 5.8 (a, b and c). Probably, the movement of the top layer caused the division of the domains in several. The magnitude of this change is related to the laser energy deposited and thus with the final colour appearance. These phenomena were observed both on Ag and Al metal layers.

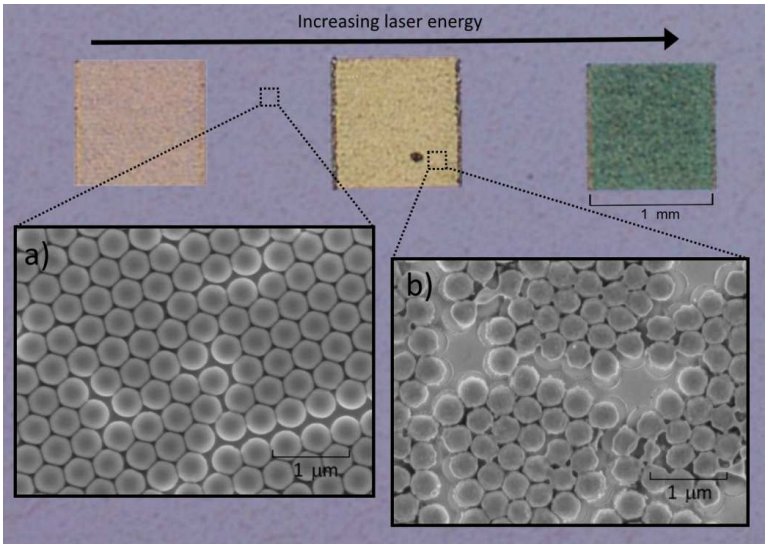

Figure 5.7. Magnified image taken by an optical microscope of the PS spheres covered with Ag. Three different areas treated with the laser are shown in terms of the laser energy. a) SEM image of the spheres without laser treatment; b) SEM image of the area treated by laser.

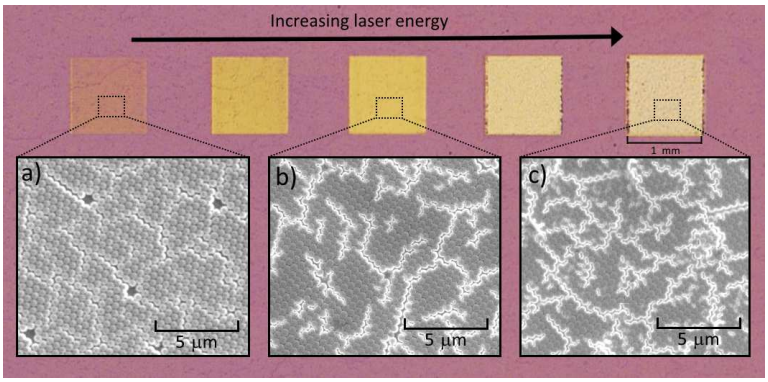

Figure 5.8. Magnified image taken by an optical microscope of the PS spheres covered with Al. Five different areas treated by the laser are shown in terms of the laser energy. a) SEM image of the spheres treated at low energy; b) SEM image of the area treated with the laser at medium energy; c) SEM image of the area treated with the laser at high energy.

The instant energy of the pulsed laser allowed heating the spheres under the beam above the melting temperature. Considering a direct excitation of the SPR with electric field confinement, the energy is concentrated in a specific region of the spheres conducting to melting and reshaping of the nanostructure. As the pulse energy increases, the amount of the metallic layer decreases, which reveals the optical response of the polystyrene spheres. The magnitude of these changes can be tuned by the laser dose in time and energy.

Finally, figure 5.9 illustrates the effect of the laser on the spheres. The laser energy was absorbed inducing the melting of part of the metallic layer. This melting caused a progressive depletion of the top metal part. Furthermore, the metal films moved from the top of the spheres getting closer, even it was possible to observe the creation of links between some particles. These changes in the morphology should affect the resonant frequency of the SPR and therefore the observed colour.

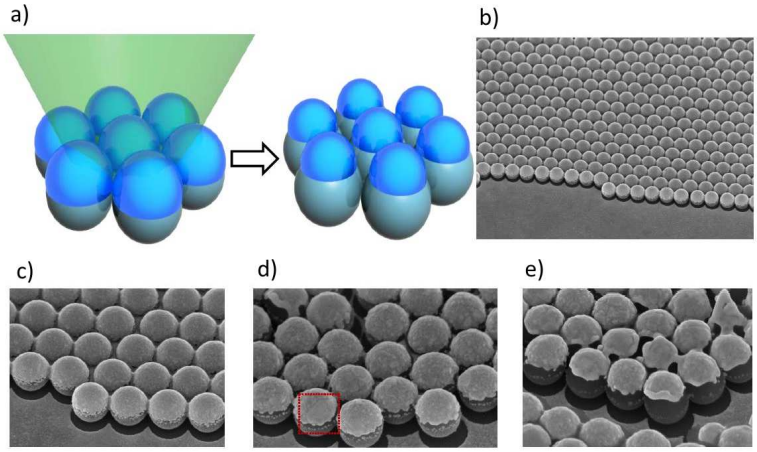

Figure 5.9. Illustration of the laser reshaping process on the spheres top layer. a) Effect on the spheres, the top metal layer decreased under the laser beam; b-e) SEM images of the progressive depletion of the metallic layer.

5.2.2. Example of application

It was possible to print images at a microscopic scale considering the scale of the changes observed. Moreover, any image can be drawn using the motorised stage and the programmable beam polariser controlled by a specific software developed to synchronise both movements. Thus, three different pictures were done on the PS spheres covered either with Al or Ag, see figure 5.10. The resolution of each pixel was around 4 µm. The images were seen using a microscope with a 0.9 NA 100x objective lens (the colours were a bit altered because of the camera software used to capture these images). On the samples covered with Al (figures 5.10.a and b) a flower and a soccer ball were printed, while the DTU university logo was printed on the spheres covered with Ag (figure 5.10.c).

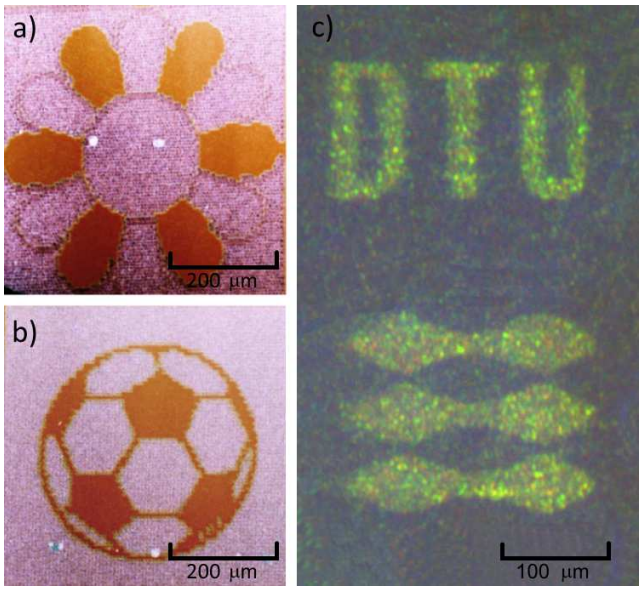

Figure 5.10. Examples of laser printing on a layer of PS spheres covered either with Al (a and b) or Ag (c) and observed under an optical microscope. The images were written in a rectangle whose biggest size was less than 500 µm. The printing process was made fully automatic.

5.2.3. Conclusions

It was introduced a fast approach creating a plasmonic surface to be later post-processed using nanosecond laser pulses. The structure consists of a pattern of PS spheres made by self-assembling being after sputtered either with Ag or Al. The laser beam was absorbed by the spheres inducing melting and reshaping processes by transient local heat generation. The intensity of these changes was determined by the amount of laser fluence deposited over the samples. Thus the final colour appearance was directly controlled by the laser intensity. Furthermore, the magnitude of the changes was in the micro-scale, so fully pictures can be done in areas less than one square millimetre.

5.3. Colour marking based on iridescence colours produced by DLIP

Direct laser interferometry patterning (DLIP) was showed in section 4.5 to micro-pattern the white-c ABS in an attempt to control its wettability. Additionally, these structures potentially behave as a diffraction grating giving rise to iridescent colours creating a hologram [5.46].

On the one hand, a diffraction grating can be defined as an optical device that exhibits a periodical variation of any parameter that affects the propagation of a light beam in such a way that the energy is scattered in several discrete directions or diffracted orders. Each of the diffracted orders depends on, among others, the periodicity of the grating and its relation to the wavelength. Therefore, a grating disperses a variety of wavelengths giving rise to a spectrum in a similar way that a prism. There are many examples in nature where the interaction of light with matter is used to produce brilliant colours for a variety of purposes [5.5], [5.6].

Consequently, the visual appearance of the microstructured material depends on the wavelength of the incident light and the period of the grating. Each wavelength is diffracted at a different angle selecting a fixed incident angle according to eq. (5.1).

$$\Lambda(n_m \sin\theta_m + n_{in} \sin\theta_{in}) = m\lambda \tag{5.1}$$

where Λ is the period of the grating, λ is the wavelength, m is the diffraction order, θ_{in} is the incident angle and θ_m is the diffraction angle for the m order, see figure 5.11. Also, the groove density (G) is defined as the inverse of the grating period ($G = 1/\Lambda$). The refraction indexes for the incident and diffractive media are n_{in} and n_m respectively, which will be equal if the propagation is in the air [5.47].

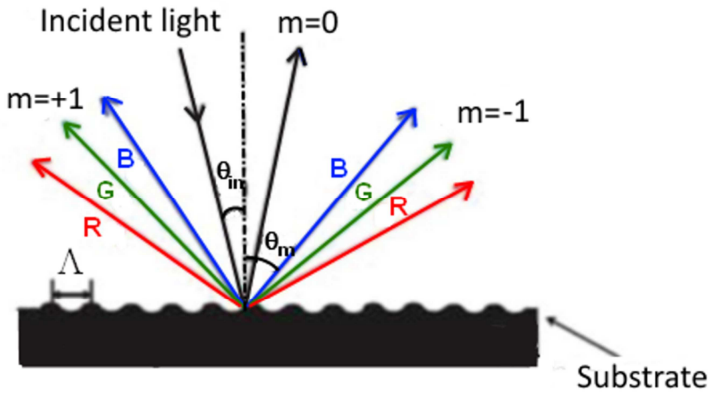

Figure 5.11. Diffraction orders and angles for a white incident light.

In addition, two more relationships between parameters of a grating are of interest for this study [5.47]:

-The maximum number of diffracted orders is determined by:

$$\left|m\lambda / \Lambda\right| < 2 \tag{5.2}$$

-The resolving power is a measurement of the grating ability to separate adjacent spectral lines $\Delta\lambda$ of an average wavelength λ, expressed as the dimensionless quantity:

$$R = \frac{\lambda}{\Delta\lambda} = mN = mGd \tag{5.3}$$

where N is the number total of grooves illuminated on the surface of the grating, G the groove density and d the distance corresponding to illuminated grooves.

On the other hand, iridescence is the optical phenomenon of a surface associated with hue changes with the angle of observation and the angle of illumination [5.2]. The iridescence colours are caused by different interference or diffractive effects such as thin-film interference or surface micro-structuring. Consequently, a diffraction grating exhibits an iridescent effect in the visible spectrum depending on its period.

So, in the same way that the micrometric pattern created in the chapter 4th affected the wettability properties of the material, it can also alter the visual appearance of the surface.

5.3.1. Iridescent colours related to the microscopic structure

The same optical set-up used to produce the wettability modification was employed in this case, see figure 4.24. The material marked was the white-c ABS. The angle between the laser beams was the same utilised in the previous chapter, 12° that according to eq. (4.12) should produce a grating with a period of around 7 µm. In this case, the interference pattern was created only in one direction. The topography produced after turning 90° the sample, as it was done in the previous chapter, did not exhibit a visible optical effect.

Two different processing speeds of the motorised stage were selected: 13 mm/s and 7 mm/s. Confocal optical images of the structure created using the fastest speed are shown in figure 5.12. The overall effect was the presence of a grating distributed along the surface. Additionally, the right image taken at 100x magnification displayed that there were some clusters of materials within the created lines.

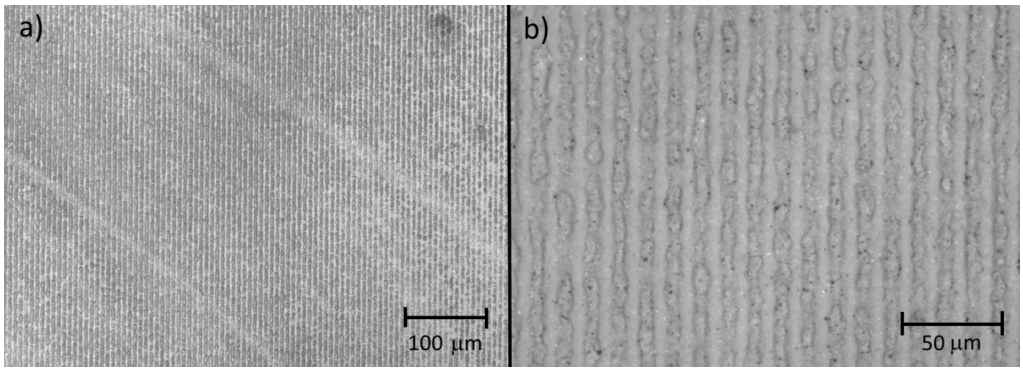

Figure 5.12. Confocal optical images of the area treated at 13 mm/s. a) Image taken at 20x magnification; b) image taken at 100x magnification.

Therefore, the structure exhibited a periodical variation in its colour, directly related to a change in their optical properties. This change affects the propagation of the light in such a way that the surface can be considered a diffraction grating. According to the eq. (5.1) each wavelength is diffracted at a different angle producing the iridescence effect. The period of the grating created was 6.7 µm. The groove density was G ≈ 149 grooves/mm. Therefore, considering that the visible ranged from 400 to 700 nm, the number of diffracted orders, determined from the eq. (5.2), was high, between 19 and 34 depending on the wavelength.

Figure 5.13 displays the white-c ABS marked at two scanning speeds, 7 mm/s and 13 mm/s, the look of the surface changed with the angle of observation. The surface had a grey colouration observed at the front view; the mark was darker in the case of the lowest speed. The observation at angles below 90° allowed distinguishing the diffractive effect and the iridescence colours. The appearance of the grating created with a scanning speed of 13 mm/s was much defined than the grating made at 7 mm/s that presented some dark areas due to a high overlapping. Furthermore, the look of the iridescent colours relied on the type of illuminant and light source used. Figure 5.13.b shows the disc under the illuminant D65 (bluish/white light). The light source was diffuse, so almost all the area covered by the grating was

illuminated. The bluish colours were more intense than those corresponding to the red part of the spectrum. The resolving power according to the eq. (5.3) (taking into account that approximate 40 mm of grooves were illuminated and the observation was done on the first diffractive order) was R = 5970. Thus, the grating was able to separate 0.1 nm of adjacent wavelengths. By contrast, figure 5.13.c showed the disc under the illuminant D50 (yellowish/white light; point source of light). In this case, the yellow/red colours dominated. The resolving power (taking into account that approximate 10 mm of grooves were illuminated and the observation was done on the first diffractive order) was R = 1493, allowing to resolve wavelengths higher than 0.5 nm.

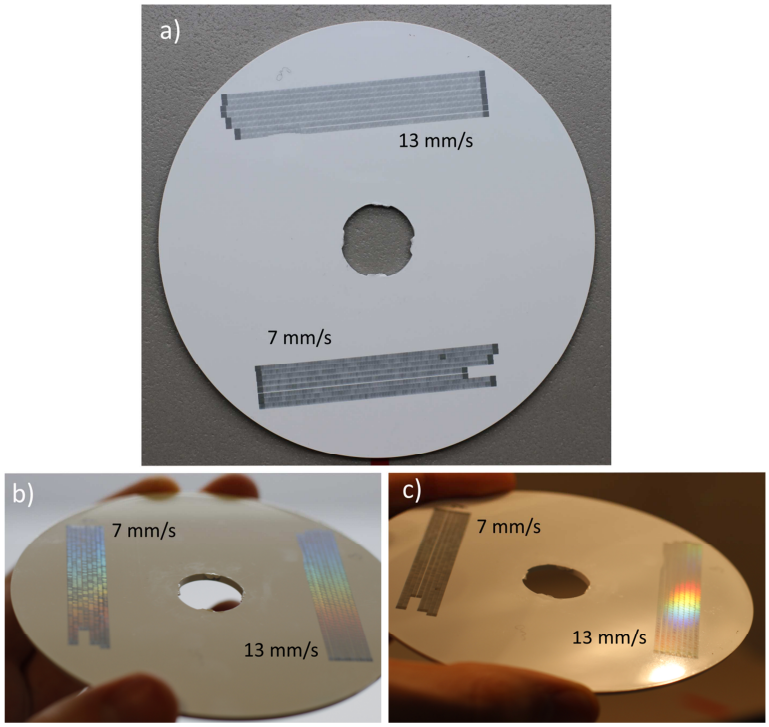

Figure 5.13. Images of the grating created on a disc of white-c ABS at two processing speeds, 13 mm/s and 7 mm/s. a) Front view of the ABS disc marked; b) Angular view of the disc illuminated with a diffuse source of light based on illuminant D65; c) Angular view of the disc illuminated with a point source of light based on illuminant D50.

Thus, the grating created allowed to observe the entire spectrum of visible light although the observation of consecutive orders depends on the angle of view and the distance between the observer, the light source and the sample. Figure 5.14 shows an example of two consecutive orders. Theoretically, the number of diffractive orders of the grating created was high. However, their intensity decreased when the m factor increased, so experimentally it was difficult to observe more than six orders. Therefore, considering the case where the sample is illuminated at an angle of 45° and six diffractive orders are visible, the observation of the diffractive phenomena will be possible for angles ranging from 55° to 16°.

Figure 5.14. Image of a grating observed at 45° under a point source of light showing two consecutive diffracted orders.

The number of diffractive orders and their observation angles can be tuned changing the angle formed by the two laser beams. For example, the increase of that angle would cause the reduction of the grating period. Thus, the number of diffracted orders would be reduced while the angle diffraction of each wavelength and the resolving power would be increased. Visually, it would not be possible to observe the entire visible spectrum on the same observer position; the viewer should move to see the colour change (always considering the same distance between the light source, the

sample and the viewer of the photographs showed before). On the opposite, the reduction of the angle between the beams would induce the increment of the grating period. This grating would present an increment of the diffractive orders since the angle between the diffracted wavelengths and the resolving power would decrease. In this case, the observation of the different diffractive orders might possible. However, since the intensity decays with each diffractive order, the angles where the iridescence colours are visible would be reduced and consequently hampering its observation.

5.3.2. Example of application

A photomask was used to overcome the limitations of the experimental setup to apply this laser marking technique. This mask was prepared by IR laser using cardboard to obtain the brand logos of Balay and Siemens. The approximate dimensions of the logos were 60x15 mm. The logos were adapted to accommodate the internal parts of the letters like the “B” or the “a” in the Balay logo. This system can be improved for example employing adhesive masks.

Therefore, both logos were marked using the interferometric system utilising the same laser parameters. Figure 5.15 displays different views of the Balay logo where it was possible to observe the diffractive effect. The iridescence colours appeared in all the extension of the logo using a diffuse light source. Thus, it was even possible to observe in some cases two consecutive diffractive orders. The observation at front view only allowed observing a grey mark typical of a conventional laser marking. Similarly, figure 5.16 shows the Siemens brand logo exhibiting the same iridescence effect. Again the use of a diffuse light source permitted to saw the visible spectrum covering almost the entire logo.

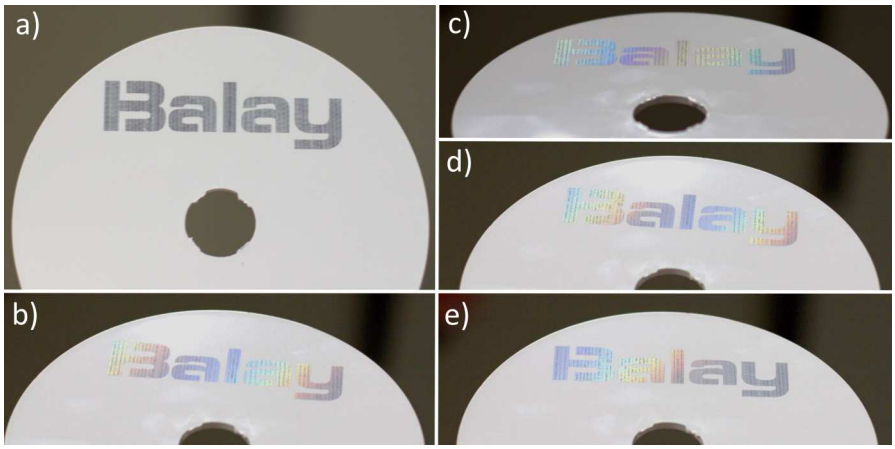

Figure 5.15. Balay brand logo seen at different positions. a) Front view; b-d) observation at different angles.

Figure 5.16. Siemens brand logos created by the holographic system.

5.3.3. Conclusions

The interferometer technique employing two laser beams was used to create a periodical modification of the visual appearance of the polymeric material due to the created diffractive grating. This microstructure gives rise to iridescence colours that were observed from different angles. Furthermore, it was possible to perform the marking process of logos (or others) with iridescent effects using a photomask. However, this technology cannot be used to marking with a specific colour. Consequently, its final purpose cannot be to replace the traditional decorative techniques but the creation of new styles of decoration based on iridescence effects.

References

[5.1] Society of dyers and colourists, "Definitions of a dye and a pigment," 2017. [Online]. Available: https://colour-index.com/definitions-of-a-dye-and-a-pigment. [Accessed: 07-Nov-2017].

[5.2] S. Kinoshita, S. Yoshioka, and J. Miyazaki, "Physics of structural colors," *Reports Prog. Phys.*, vol. 71, no. 7, p. 76401, 2008.

[5.3] Merck KGaA, "Merck presents new effect pigments for laser marking and rotomoulding," *Addit. Polym.*, vol. 2015, no. 8, pp. 1–2, Aug. 2015.

[5.4] H. Y. Zheng, D. Rosseinsky, and G. C. Lim, "Laser-evoked coloration in polymers," *Appl. Surf. Sci.*, vol. 245, no. 1–4, pp. 191–195, 2005.

[5.5] A. R. Parker and N. Martini, "Structural colour in animals—simple to complex optics," *Opt. Laser Technol.*, vol. 38, no. 4, pp. 315–322, 2006.

[5.6] M. Srinivasarao, "Nano-optics in the biological world: beetles, butterflies, birds, and moths," *Chem. Rev.*, vol. 99, no. 7, pp. 1935–1962, 1999.

[5.7] A. J. Antończak, D. Kocoń, M. Nowak, P. Kozioł, and K. M. Abramski, "Laser-induced colour marking—Sensitivity scaling for a stainless steel," *Appl. Surf. Sci.*, vol. 264, pp. 229–236, 2013.

[5.8] Z. L. Li *et al.*, "Analysis of oxide formation induced by UV laser coloration of stainless steel," *Appl. Surf. Sci.*, vol. 256, no. 5, pp. 1582–1588, 2009.

[5.9] V. Veiko *et al.*, "Development of complete color palette based on spectrophotometric measurements of steel oxidation results for enhancement of color laser marking technology," *Mater. Des.*, vol. 89, pp. 684–688, 2016.

[5.10] S. A. Maier, *Plasmonic: Fundamentals and applications*, 1st ed. New York: Springer, 2007.

[5.11] E. Højlund-Nielsen, J. Weirich, J. Nørregaard, J. Garnaes, N. A. Mortensen, and A. Kristensen, "Angle-independent structural colors of silicon," *J. Nanophotonics*, vol. 8, no. 1, p. 83988, 2014.

[5.12] X. Zhu, C. Vannahme, E. Højlund-Nielsen, N. A. Mortensen, and A. Kristensen, "Plasmonic colour laser printing," *Nat Nano*, vol. 11, no. 4, pp. 325–329, 2016.

[5.13] J. Yao *et al.*, "Selective appearance of several laser-induced periodic surface structure patterns on a metal surface using structural colors produced by femtosecond laser pulses," *Appl. Surf. Sci.*, vol. 258, no. 19, pp. 7625–7632, 2012.

[5.14] V. Veiko *et al.*, "Metal surface coloration by oxide periodic structures formed with nanosecond laser pulses," *Opt. Lasers Eng.*, vol. 96, pp. 63–67, 2017.

[5.15] O. T. Picot *et al.*, "Manufacturing of surface relief structures in moving substrates using photoembossing and pulsed-interference holography," *Macromol. Mater. Eng.*, vol. 298, no. 1, pp. 33–37, 2013.

[5.16] M. I. Stockman, "Nanoplasmonics: past, present, and glimpse into future," *Opt. Express*, vol. 19, no. 22, pp. 22029–22106, 2011.

[5.17] E. Højlund-Nielsen *et al.*, "Polarization-dependent aluminum metasurface operating at 450 nm," *Opt. Express*, vol. 23, no. 22, pp. 28829–28835, Nov. 2015.

[5.18] H. F. Ghaemi, T. Thio, D. E. Grupp, T. W. Ebbesen, and H. J. Lezec, "Surface plasmons enhance optical transmission through subwavelength holes," *Phys. Rev. B*, vol. 58, no. 11, pp. 6779–6782, Sep. 1998.

[5.19] J. Homola, S. S. Yee, and G. Gauglitz, "Surface plasmon resonance sensors: review," *Sensors Actuators B Chem.*, vol. 54, no. 1–2, pp. 3–15, 1999.

[5.20] T. W. Ebbesen, H. J. Lezec, H. F. Ghaemi, T. Thio, and P. A. Wolff, "Extraordinary optical transmission through sub-wavelength hole arrays," *Nature*, vol. 391, no. 6668, pp. 667–669, 1998.

[5.21] W. L. Barnes, A. Dereux, and T. W. Ebbesen, "Surface plasmon subwavelength optics," *Nature*, vol. 424, no. 6950, pp. 824–830, 2003.

[5.22] S. Yokogawa, S. P. Burgos, and H. A. Atwater, "Plasmonic color filters for CMOS image sensor applications," *Nano Lett.*, vol. 12, no. 8, pp. 4349–4354, 2012.

[5.23] S. Roh, T. Chung, and B. Lee, "Overview of the characteristics of micro- and nano-structured surface plasmon resonance sensors," *Sensors*, vol. 11, no. 2, pp. 1565–1588, 2011.

[5.24] F. P. de Arquer, A. Mihi, and G. Konstantatos, "Large-area plasmonic-crystal–hot-electron-based photodetectors," *ACS Photonics*, vol. 2, no. 7, pp. 950–957, 2015.

[5.25] Y. Shen, V. Rinnerbauer, I. Wang, V. Stelmakh, J. D. Joannopoulos, and M. Soljačić, "Structural colors from fano resonances," *ACS Photonics*, vol. 2, no. 1, pp. 27–32, 2015.

[5.26] J. Olson *et al.*, "Vivid, full-color aluminum plasmonic pixels," *Proc. Natl. Acad. Sci.*, vol. 111, no. 40, pp. 14348–14353, 2014.

[5.27] X. Jiang, E. S. P. Leong, Y. J. Liu, and G. Si, "Tuning plasmon resonance in depth-variant plasmonic nanostructures," *Mater. Des.*, vol. 96, pp. 64–67, 2016.

[5.28] F. Cheng, J. Gao, T. S. Luk, and X. Yang, "Structural color printing based on plasmonic metasurfaces of perfect light absorption," *Sci. Rep.*, vol. 5, p. 11045, 2015.

[5.29] J. Proust, F. Bedu, B. Gallas, I. Ozerov, and N. Bonod, "All-dielectric colored metasurfaces with silicon mie resonators," *ACS Nano*, vol. 10, no. 8, pp. 7761–7767, 2016.

[5.30] K. Kumar, H. Duan, R. S. Hegde, S. C. W. Koh, J. N. Wei, and J. K. W. Yang, "Printing colour at the optical diffraction limit," *Nat Nano*, vol. 7, no. 9, pp. 557–561, 2012.

[5.31] L. Duempelmann, A. Luu-Dinh, B. Gallinet, and L. Novotny, "Four-fold color filter based on plasmonic phase rretarder," *ACS Photonics*, vol. 3, no. 2, pp. 190–196, 2016.

[5.32] X. M. Goh *et al.*, "Three-dimensional plasmonic stereoscopic prints in full colour," *Nat. Commun.*, vol. 5, p. 5361, 2014.

[5.33] S. J. Tan *et al.*, "Plasmonic color palettes for photorealistic printing with aluminum nanostructures," *Nano Lett.*, vol. 14, no. 7, pp. 4023–4029, 2014.

[5.34] J. S. Clausen *et al.*, "Plasmonic metasurfaces for coloration of plastic consumer products," *Nano Lett.*, vol. 14, no. 8, pp. 4499–4504, 2014.

[5.35] Z. Li, W. Wang, D. Rosenmann, D. A. Czaplewski, X. Yang, and J. Gao, "All-metal structural color printing based on aluminum plasmonic metasurfaces," *Opt. Express*, vol. 24, no. 18, pp. 20472–20480, Sep. 2016.

[5.36] R. Yu *et al.*, "Structural coloring of glass using dewetted nanoparticles and ultrathin films of metals," *ACS Photonics*, vol. 3, no. 7, pp. 1194–1201, 2016.

[5.37] X. M. Goh, R. J. H. Ng, S. Wang, S. J. Tan, and J. K. W. Yang, "Comparative study of plasmonic colors from all-metal structures of posts and pits," *ACS Photonics*, vol. 3, no. 6, pp. 1000–1009, 2016.

[5.38] X. Chen, Y. Chen, M. Yan, and M. Qiu, "Nanosecond photothermal effects in plasmonic nanostructures," *ACS Nano*, vol. 6, no. 3, pp. 2550–2557, 2012.

[5.39] G. Baffou and R. Quidant, "Thermo-plasmonics: using metallic nanostructures as nano-sources of heat," *Laser Photon. Rev.*, vol. 7, no. 2, pp. 171–187, 2013.

[5.40] X. Zhu, M. Keshavarz Hedayati, S. Raza, U. Levy, N. A. Mortensen, and A. Kristensen, "Digital resonant laser printing: Bridging nanophotonic science and consumer products," *Nano Today*, 2017.

[5.41] X. Zhu, W. Yan, U. Levy, N. A. Mortensen, and A. Kristensen, "Resonant laser printing of structural colors on high-index dielectric metasurfaces," *Sci. Adv.*, vol. 3, no. 5, May 2017.

[5.42] D. Bäuerle, *Laser processing and chemistry*, 4th ed. Berlin: Springer, 2011.

[5.43] J. C. Ion, *Laser processing of engineering materials*, 1st ed. Oxford: Elsevier, 2005.

[5.44] J. Sun, C. Tang, P. Zhan, Z. Han, Z.-S. Cao, and Z.-L. Wang, "Fabrication of centimeter-sized single-domain two-dimensional colloidal crystals in a wedge-shaped cell under capillary forces," *Langmuir*, vol. 26, no. 11, pp. 7859–7864, 2010.

[5.45] L. Wang, R. J. H. Ng, S. Safari Dinachali, M. Jalali, Y. Yu, and J. K. W. Yang, "Large area plasmonic color palettes with expanded gamut using colloidal self-assembly," *ACS Photonics*, vol. 3, no. 4, pp. 627–633, 2016.

[5.46] G. Saxby, *Practical holography*, 3rd ed. Bristol: IOP Publishing, 2004.

[5.47] C. Palmer, *Diffraction grating handbook*, 5th ed. New York: Thermo RGL, 2002.

6. General conclusions

At the beginning of this thesis, two objectives were proposed. The primary goal was to study the interaction of three different laser wavelengths (1064 nm, 532 nm and 355 nm) with ABS materials to produce high-quality aesthetical marks. The results were depended on the colour pigment used on the ABS material: TiO_2 or CB.

On the one hand, the TiO_2 molecule suffered a reduction process under irradiation with the green and the UV lasers while negligible changes were detected using the IR laser. The formation of reduced species like Ti^{2+} or TiC gave rise to a black colouration in the laser treated area. More energy was needed to produce the high contrasted marks with the green wavelength than with the UV laser. This fact is directly related to the increment of the cycle time of the process. Additionally, the green laser produced a light brownish colouration of the marks, probably due to a partial polymer carbonization. Consequently, the UV laser is a better choice to produce aesthetical marking on the white ABS. Furthermore, the increment of the pigment content did not improve the marking process.

On the other hand, the ABS with CB exhibited a thermally induce foaming effect under irradiation with the green or the IR lasers leading to white marks. Again, a brownish colour was observed, probably due to polymer carbonisation, in the marks made with the green laser, while this effect was reduced using the IR laser. Furthermore, a lower DPI was needed to produce the highest contrast on each CB compound employing the IR laser than using the green laser. The UV laser produced marks by a photochemical effect although the final contrast achieved was worse than the obtained using the other two lasers. Consequently, the IR laser is the preferred option to mark the black ABS. Moreover, the increment of CB content did not improve the marking process.

As a second objective, functional marks to control the wettability of ABS samples were proposed using three different approaches. Firstly, direct laser ablation made with the UV laser was employed to create two types of topographies, one based on truncated cones and the other in a regular arrangement of holes. The minimum period achieved for these structures was 60 μm. The experimental CA can be approximate to either Wenzel or Cassie-Baxter models depending on the structure dimensions. However, no superhydrophobic or superhydrophilic surfaces stable in time were found. Better results were obtained utilising the roughness control by green laser marking. Both, superhydrophobic and superhydrophilic surfaces were obtained being also temporally stable. This wettability behaviour was related to the surface topography measured that was dependent on the laser fluence deposited on the surface. Finally, DLIP technique employing UV laser wavelength also enabled to alter the wetting behaviour. The structures created were one order of magnitude less in size than those made by direct ablation, achieving a period of around 7 μm. The Cassie-Baxter model predicted their behaviour. Nevertheless, the highest CA achieved was 99°, far from a superhydrophobic behaviour.

Finally, a preliminary study of producing colour marks, beyond the grey scale, was performed. Three different approaches were considered. The use of additives, based on diacetylenes and leucodyes activated under UV laser irradiation, together with the IML technique proved to be a solution for colour marking. However, their long-term stability to UV light and the range of colours should be improved for a commercial purpose. Other alternative proposed was the use of structures exhibiting SPR (surface plasmon resonance) on the visible spectrum. Specifically, the structures were based on self-assembled PS spheres covered with Ag and Al. A green laser was employed to induce a reshaping of their metallic layer causing a modification of their optical response The magnitude of the changes was directly related to the laser parameters like the deposited fluence. Nevertheless, the cycle time of this technology

is still low and is too complex to be scaled up. Finally, DLIP was used to create iridescence colours. However, this effect seemed to be an additional decorative technique of colour marking; it was not possible to achieve non-angle-dependent colour marks using DLIP.

As a concluding remark, during the development of this thesis aesthetic laser marking on ABS was successfully implemented on an industrial scale. At least five different factories of the BSH home appliances group around the world are now employing the laser marking on ABS (mainly on white polymer) manufacturing a total of 2.5 million of pieces. This thesis has contributed to understanding the laser/ABS interaction phenomena and humbly helping to implement this promising technology in the industrial world.

7. Conclusiones generales

Para la elaboración de esta tesis se plantearon dos objetivos principales. En primer lugar, se propuso el estudio de la interacción entre tres láseres de longitudes de onda diferentes (1064 nm, 532 nm y 355 nm) con el termoplástico ABS para producir un marcaje estético de alta calidad. Los resultados obtenidos dependieron del pigmento de color incorporado al polímero TiO_2 o CB.

Por un lado, la molécula de TiO_2 (empleada como aditivo blanqueante) sufría un proceso de reducción bajo la radiación láser verde (532 nm) y ultravioleta (355 nm) mientras que los cambios químicos observados empleando el láser infrarrojo (1064 nm) fueron despreciables. En concreto, se detectaba la formación de especies reducidas como el Ti^{2+} o el TiC que provocaban una coloración negra en el área tratada por el láser. Sin embargo, empleando el láser verde era necesario depositar mayor energía para producir el mejor contraste de color que con el láser ultravioleta, y este hecho está directamente relacionado con el incremento del tiempo de ciclo del proceso. Además, el láser verde producía marcas con una ligera coloración marrón, probablemente causada por una carbonización parcial del polímero. De este modo, se considera que el mejor láser para producir el marcaje estético en el ABS blanco es el UV. Además el incremento del porcentaje de TiO_2 no mejoraba el marcado en ningún caso.

Por otro lado, el ABS con CB (pigmento negro) presentaba un efecto de espumado cuando era irradiado por los láseres verde o IR produciéndose marcas blancas. De nuevo, el láser verde producía un efecto de carbonización en el polímero asociado a una ligera coloración marrón en las marcas, mientras que empleando el láser IR este fenómeno era muy reducido. Además, el mayor contraste en el caso del láser IR fue obtenido a valores de DPI menores que empleando el láser verde. Por el

contrario, el láser UV producía marcas por efecto fotoquímico causando una posible degradación del pigmento (blanqueamiento) aunque daba lugar a un menor contraste final que empleando los otros dos láseres. Así pues, en este caso se prefiere el uso del láser IR para conseguir las mejores marcas estéticas en el ABS negro. Del mismo modo se estudió el efecto de la cantidad de pigmento y al igual que en el caso del TiO_2, los mejores resultados se obtuvieron empleando la menor cantidad de CB de entre todas las estudiadas.

Como segundo objetivo se propuso la creación de marcas funcionales en el ABS de tal modo que se modificara la mojabilidad del material empleando tres diferentes métodos. En primer lugar, mediante ablación láser directa usando el láser UV se crearon dos tipos diferentes de topografías en la superficie, una basada en conos truncados y la otra en una distribución regular de agujeros. En ambos casos el periodo mínimo obtenido fue de 60 µm. Experimentalmente se midieron ángulos de contacto que se aproximaban o bien al model de Wenzel o al de Cassie-Baxter dependiendo de las dimensiones de la estructura creada. Sin embargo, empleando esta técnica no se consiguieron superficies que mostraran comportamientos superhidrófilos o superhidrófobos estables en el tiempo. Mejores resultados se alcanzaron utilizando el láser verde mediante el control de la rugosidad superficial. Esta técnica se basaba en realizar un calentamiento de la superficie controlado dando lugar a una topografía definida por la fluencia total laser depositada. Mediante esta técnica fue posible obtener tanto superficies superhidrófilas y como superhidrófobas estables en el tiempo. Finalmente, empleando la técnica DLIP con un láser ultravioleta se consiguió también modificar el comportamiento de mojabilidad del ABS. Las topografías creadas eran un orden de magnitud menor que aquellas hechas por ablación directa, obteniéndose estructuras con periodos de alrededor de 7 µm, prediciéndose su comportamiento de mojabilidad mediante el modelo de Cassie-Baxter. No obstante, el

mayor ángulo de contacto obtenido fue de 99°, lejos de un comportamiento superhidrófobo.

Finalmente, se exploraron de una manera preliminar diferentes aproximaciones para conseguir un marcaje en color más allá de la escala de grises utilizando la tecnología láser. En concreto se consideraron tres posibles alternativas de marcado láser en color. En primer lugar se utilizaron aditivos químicos (leucodyes y diacetylenes) que bajo la luz UV del láser y empleando la tecnología de inyección de IML (in-mould labelling) demostraron ser una solución factible para obtener marcas en color. Sin embargo, para un uso comercial se debería mejorarse su estabilidad a largo plazo a las condiciones de luz ambiental y ampliarse el rango de colores disponible. Otra de las alternativas propuestas fue el empleo de estructuras que presentaran resonancias de plasmones superficiales (SPR) en el espectro visible. En concreto, se emplearon esferas de PS auto-ensambladas cubiertas a su vez con una fina capa de aluminio o plata. Mediante un láser verde se inducía un cambio en esa capa metálica eliminando el material progresivamente de tal modo que se modificaba su respuesta óptica. La magnitud de los cambios estaba directamente relacionada con los parámetros láser como la fluencia depositada. Sin embargo, el tiempo de ciclo del procesado era lento además de ser una técnica muy compleja de ser implementada a escala industrial. Finalmente, se empleó de nuevo la técnica DLIP para crear un efecto de colores iridiscentes en el material, un fenómeno que es dependiente del ángulo de observación. Pese a ser posible conseguir este efecto para un amplio rango de ángulos, no era posible obtener colores independientes del ángulo y por lo tanto se considera una técnica complementaria para la decoración estética del material.

Como observación final, durante el desarrollo de esta tesis el marcado estético láser sobre el ABS fue implementado satisfactoriamente a escala industrial. Al menos cinco factorías del grupo BSH electrodomésticos alrededor del mundo emplean ahora el marcado láser en ABS (principalmente sobre el polímero blanco) fabricando un

total de 2.5 millones de piezas. Esta tesis ha contribuido a entender los fenómenos de interacción entre el láser y el polímero y humildemente a implementar esta prometedora tecnología en el mundo industrial.